

**ISOLATION, BIOTRANSFORMATION, CHEMICAL
MODIFICATION AND BIOACTIVITY STUDIES OF
TERPENOIDS FROM PLANT SOURCES**

THESIS SUBMITTED TO THE
SAVITRIBAI PHULE PUNE UNIVERSITY
FOR THE DEGREE OF

DOCTOR OF PHILOSOPHY
IN CHEMISTRY

BY
HARSHAL SHIVAJI PATIL

RESEARCH SUPERVISOR
DR. THULASIRAM H. V.
DIVISION OF ORGANIC CHEMISTRY
CSIR-NATIONAL CHEMICAL LABORATORY
PUNE 411008, INDIA

JUNE 2019

Dr. H. V. Thulasiram
Principal Scientist,
Chemical-Biology Unit,
Division of Organic Chemistry,
CSIR-National Chemical Laboratory
Pune-411008

Tel: +912025902478
Fax: +91 2025902629
Email: hv.thulasiram@ncl.res.in

CERTIFICATE

This is to certify that the research work presented in this thesis entitled “**Isolation, Biotransformation, Chemical Modification and Bioactivity Studies of Terpenoids from Plant Sources**” has been carried out under my supervision at CSIR-National Chemical Laboratory, Pune and is a bonafide work of Harshal Shivaji Patil. This work is original and has not been submitted for any other degree or diploma to this or any other university.

Pune-411008
June, 2019

(Dr. H. V. Thulasiram)
Research Supervisor

DECLARATION

I hereby declared that the research work presented in this thesis was carried out by me at CSIR-National Chemical Laboratory, Pune under the supervision of Dr. H. V. Thulasiram, Organic Chemistry Division, CSIR-National Chemical Laboratory, and Pune. This work is original and has not been submitted in part or full for any degree or diploma to this or any other university.

Pune -411008
June, 2019

(Harshal Shivaji Patil)
Research Fellow,
Organic Chemistry Division,
CSIR-National Chemical Laboratory,
Pune-411008

Dedicated to My Beloved Family
& Friends for their Love, Endless
Support, Encouragement &
Sacrifices

ACKNOWLEDGEMENTS

It is a delightful opportunity to express my deep sense of gratitude to all my well-wishers who have accompanied and supported in doctoral studies. Although it is the helpfulness of uncountable individuals, the following personalities are those I reckon most coming out of my instant recalling.

First and foremost, I would like to express my sincere gratitude and respect to my research supervisor Dr. Thulasiram H. V. His insightful guidance, immense support, valuable suggestions, encouragement and inspiration rendered to me during my research career. It was really a great experience to expertise, myself in the field of natural products, biocatalysis, metabolomics and biosynthesis under his caring guidance. This helped me to develop skills and knowledge in this multidisciplinary scientific domain. He gave me the creative space and freedom in the laboratory, which every researcher earnestly desires for the independent thinking, planning and execution of the research. I revere his lessons on perfection, skills and many more to germinate and grow up a researcher in me.

I am also grateful to Director, NCL, Pune, and Head, Organic Chemistry Division for giving me an opportunity to work in this institute and making all the facilities available for my research work.

I owe my earnest regards to Dr. M. Muthukrishnan, Dr. Jomon Joseph and Dr. Shinde V. S. for evaluating my progress reports and presentations. I owe my sense of gratitude to Dr. G. Kundu (NCCS-Pune), Dr. Sharanappa (University of Mysore), Dr. J. Joseph (NCCS-Pune), Dr. M. Kulkarni (NCL-Pune), Prof. Gopi (IISER-Pune), Dr. Prabhune for collaboration.

I must thank Dr. Muthukrishnan, Dr. Shinde, Dr A. Sen, Dr. D. S. Reddy, and Dr. S. Hotha for their help, guidance and kind attention to me for their help and suggestions during this research work. I really acknowledge the help from Dr. Pradeep Kumar (NCL, Pune), Jagdeesha (Mysor University), Dr. Santosh, Dr. Dhiraj, Mahadev from NCCS, Pune for teaching new area of research. Help rendered by the members of IR and microanalysis (Dr. P. L. Joshi and group), mass spectroscopy (Dr. Shanthakumari and group), NMR (Dr. Rajmohan and group) and X-ray analysis (Mr. Rajesh Gonade) for characterization of compounds is also acknowledged. I wish to thank all the divisional members and staff of SAO for the timely help I received from them. A wonderful company of Dr. Kishor, Dr. Ravi, Dr. Sathe, Dr. Manoj Chopade, Dr. Prasad Phaphle, with his brotherly support during hard times is a must mention. Great friends at

NCL will be an asset throughout life, and their company was most cherishable Dr. Manoj, Dr. Pitambar, Dr. Sachin, Dr. Prakash, Dr. Jitu their cheerful company added a lighter mode to life. I am thankful to Dr. Pitambar, Dr. Sachin, Dr. Prakash, Dr. Jitu for helping and guiding me in my PhD work in the initial years of my PhD tenure. The M.Sc. circle with great friends like Sunil Vidhate, Dr. Sambhaji, Dr. Amar, Ishwar, Dr. Govind, Dipak, Suhas, Dr. Manoj, Ravi, Jagdish, Dr. Ganesh (M.), Dr. Kailas, Dr. Rohan is indeed a wonderful academic memory of the time.

I express highly obliged to my teachers and mentors, Prof. Shingare, Prof. Mane, Prof. Lande, and Prof. Gill, who dreamt and sacrificed themselves to guide me through the path. I owe my sense of gratitude to Dr. B. Dongre sir for his moral support during a hard time.

Friends are the essential gifts of life who rise themselves up irrespective of the situation to make the life colourful. Throughout the stay in NCL, I was best owed with a bunch of buzzing friends who have made the memory of NCL unforgettable. The cheerful and rocking group of friends including Dr. Dipesh, Dr. Rakesh, Dr. Pradeep, Dr. Rupesh, Dr. Dattatray, Dr. Sneha, Dr. Shruti, Mrs. Varsha, Mrs. Tejashree, Mrs. Vijayshree, Mrs. Debabrata, Vaibhav, Dr. Ashish, Mrs. Aradhana, with whom I used to share knowledge, time, several joyful moments and sufferings of life. I heartedly thank Makarand Kulkarni and Dr. Vijay Padul for their moral support throughout and for the rest of my life.

Labmates are the closest troubleshooter in the life of a researcher, and they smoothen the arduous course of this tenure. I was highly fortunate to have Dr. Pankaj, Dr. Swati, Dr. Saikat, Dr. Prabhakar, Dr. Devdutta and Atul as my guiding seniors who fostered the feeble new comer to a competitive researcher. I especially thank my labmates Dr. Shrikant, Dr. Dipesh, Jagdeesha, Kuhoo, Ajay, Fayaj, Rohan, and Nilesh for their significant scientific contribution towards this work. I am thankful to Aarthy, Dr. Avinash, Dr. Krithika, Balaji, Rincy, Nilofer, Priya, Sonia, Debu, Ashwini, Deepti, Dr. Sreekanth, Trushna, Ashish, Rohil, Rahul, Vijayshree, Rajashree, Rani, Ajay, Shiva, Uttara, Shrikant, Sharvani, Ashish Kumar, Govinda, Nivedita, Krunal, Ashwini, Bhagyashree, (I) Jeevitha, Chitra, Nikita, Ankita, Sneha, Pruthviraj, Anurag, Rohil, Shiva, Yugendra, Jenifer, Arundhati, Bhagyashree, Ramesha, Dr. Sharanbassapa, Dr. Prasad, Dr. Anirban, Dr. Mohan, Dr. Sunil, Dr. Poojadevi, Rahul Chauhan for maintaining a cheerful ambience inside the lab and especially Dr. Sudha, for support during tough time.

It will be insufficient and injustice to document the gratitude on the small space of a paper for my parents Pramila Patil (Aai), Shivaji Gokul Patil (Abba) and their selfless sacrifice to build me what I am today. On this occasion, I am crouching down before my Aai, Abba for the endless struggle they accomplished to organize me 'brick by brick'. I would like to thank my brothers, Santosh Nikam (dada) and Rahul S. Patil (bhau), they are always my mentor and a role model from my childhood. I really appreciate the effort made by my brother Santosh Nikam to educate me and his futuristic vision that leads me up to here. I am highly grateful to Dr. Rahul S. Patil for helping me out through every aspect of life and especially for recognizing my hidden potentials. He was always there for me for solving my personal or professional problems. My, sister-in-law Mrs Manjusha (Aau) for her motherhood, support during a bad phase of life; also I really appreciate her enthusiasm for life. I must thank Mrs Priya, my sister-in-law for never-ending encouragement and support. I extend heartiest thanks to Aai (mother in law) and Abba (father in law) for their continuous support during the struggling time. I especially thank my wife, Ashwini for being with me, the closest individual of my heart with whom I have shared every aspect of life. I really appreciate her love, affection, sacrifice, encouragement and adjustment on several fronts has made it possible for me to complete this work. I am lucky to have a niece like Radhika and nephew Shlok; they are full of positive vibes, joy and curiosity. I am thankful for Digambar, Himesh and Tejshwini giving me the enthusiastic approach about life. Last but not the least, I appreciate my babies, Ved and Reva for abiding my ignorance and the patients both showed during my Ph. D. Finally, I am grateful to the eternal, omnipotent, almighty Swami Samarth, for giving me patience, strength, energy and determination to for guiding my path of life when faced with hardships.

Contents

No.	Title	Page
	List Of Research Publications/ Symposia Attended/ Poster Presentations	i
	Abbreviations	iv
	Abstract Of Thesis	v
Chapter 1 Introduction and Literature review		
1A	Introduction	1
1A.1	Terpenoids	2
1A.2	Terpenoid Biosynthesis in Plants	2
1A.3	Classification of Terpenoids	8
1A.4	Terpenoids applications	13
1B	<i>Andrographis paniculata</i>: Botanical Description, Pharmacology, Phytochemistry	
1B.1	Introduction	17
	1B.1.1 Botanical description	17
	1B.1.2 Geographical distribution	18
1B.2	Analytical Techniques	18
1B.3	Extraction and Purification of Compounds from <i>A. paniculata</i>	20
1B.4	Phytochemicals from <i>A. paniculata</i>	21
1B.5	Ethnobotany of <i>A. paniculata</i>	23
1B.6	Pharmacology	24
	(a) Anticancer Activity	24
	(b) Antimicrobial Activity	26
	(c) Insecticidal Activity	26
	(d) Anti-malarial Activity	27
1C	<i>Wedelia paludosa</i>: Botanical Description, Pharmacology, Phytochemistry	
1C.1	Introduction	31
	1C.1.2 Geographical Distribution	31

	1C.1.3 Botanical Description	31
1C.2	Extraction and Phytochemicals from <i>W. paludosa</i>	32
1C.3	Pharmacological Activities	34
1D	<i>Glochidion tomentosum</i>: Botanical description, Pharmacology, Phytochemistry	
1D.1	Introduction	39
1D. 2	Botanical Description	39
1D.3	Geographical Distribution	39
1D.4	Ethnobotany	40
1D.5	Pharmacological activities	40
1D.6	Phytochemicals	41
1E	References	47
Chapter 2		
Phytochemical Investigation of <i>Andrographis paniculata</i>		
2A	Isolation and Characterization of Terpenoids from <i>Andrographis paniculata</i>	
2A.1	Introduction	58
2A.2	Result and Discussion	
	2A.2.1. Isolation of Terpenoids from Aerial Part Powdered	59
	2A.2.2. Characterization of Terpenoids	59
	2A.2.3 Preparative Scale Isolation of Major Terpenoids and Profiling of Isolated Terpenoids	62
2A.3	Conclusion	63
2A.4	Experimental Section	
	2A.4. 1 Collection and Identification	63
	2A.4. 2 Extraction and Isolation	64
	2A.4. 3 Characterization of Terpenoids	66
2A.5	Spectral Copies	68
2B	Expedient MPLC Based Preparative Isolation and MS/MS Characterization of Labdane Diterpenoids from <i>A. paniculata</i>	
2B.1	Introduction	79
2B.2	Result and Discussion	
	2B.2.1 Fractionation of Crude Extract on Normal Phase Cartridges in MPLC	80

	2B.2.2 Purification of Diterpenoids on Reverse Phase Cartridges and Characterization of Purified Diterpenoids	81
	2B.2.3 Scale-up Studies for Separation Protocol	83
	2B.2.4 Standardization of Normalised Collision Energy	83
	2B.2.5 UPLC-ES (+)-MS and MS-MS Characterization	85
	2B.2.5.1 MS/MS Characterization of Andrographolide	86
	2A.2.5.2 MS/MS Characterization of Isoandrographolide	87
	2B.2.5.3 MS-MS Characterization of Neoandrographolide	88
	2B.2.5.4 MS-MS Characterization of 14-deoxy-11, 12-didehydroandrographolide	89
	2B.2.5.5 MS/MS-Based Identification of Diterpenoid from Leaves Extract of <i>A. Paniculata</i> .	90
2B.3	Conclusion	91
2B.4	Experimental Section	
	2B.4.1 Materials and Methods	94
	2B.4.2 Extraction of Plant Material	94
	2B.4.3 Preparative Isolation and Purification of Diterpenoids by MPLC	94
	2B.4.4 TLC and HPLC Conditions	95
	2B.4.5 UPLC–ESI (+)-MS and MS/MS Conditions	96
2B.5	HRMS Spectral Copies	97
2C	Cytotoxicity Study and Investigation of Cellular Localization of Andrographolide by Fluorescent Tagging	
2C.1	Introduction	107
2C.2	Result and Discussion	
	2C.2.1 Cell Viability Assay of Andrographolide	108
	2C.2.2 Wound Healing Assay Andrographolide	108
	2C.2.3 One Pot Labeling Protocol	109
	2C.2.4 Characterization of NBD-Andrographolide	110
	2C.2.5 Cell Imaging Studies	111
2C.3	Conclusion	112
2C.4	Experimental Section	
	2C.4.1 Cell Lines, Antibodies, and Reagents	112

	2C.4.2 Cell Viability assay (MTT)	112
	2C.4.3 Cell mobility assay (Wound Healing)	112
	2C.4.4 Instrumentation	112
	2C.4.5 One-pot Labeling Protocol	113
	2C.4.6 Synthesis of 3, 19-isopropylidene andrographolide	113
	2C.4.7 Synthesis of NBD-andrographolide	114
	2C.4.8 Confocal Microscopy	114
2C.5	Spectra Copies	115
2D	References	117
Chapter 3		
Enzymatic Modification and Formulation of Andrographolide		
3A	Regioselective and Efficient Enzymatic Synthesis of Anti-Microbial Andrographolide Derivatives	
3A.1	Introduction	121
3A.2	Result and discussion	
	3A.2.1 Screening of Lipases for Andrographolide Acylation	122
	3A.2.2 Effect of Solvents on Andrographolide Acetylation	123
	3A.2.3 Effect of Temperature on Andrographolide Acetylation	124
	3A.2.4 Time course Study of Andrographolide Acetylation	125
	3A.2.5 Operational Stability of Amano Lipase AK (<i>P. fluorescens</i>) in Andrographolide Acetylation	125
	3A.2.6 Effect of Alkyl Substituent of the Acyl Donor on Andrographolide Acylation	125
	3A.2.7 Anti-Microbial Activity of Andrographolide and Derivatives	126
	3A.2.8 Hemolytic Assay	127
	3A.2.9 Membrane Integrity Studied with Bacterial Protein Leakage Assay	127
	3A.2.10 Effect on Membrane Integrity and Cell Viability	128
	3A.2.11 Visualization of Cell Damage by using Scanning Electron Microscopy (eSEM)	128
3 A.3.	Conclusion	129
3 A.4.	Experimental Section	
	3A.4.1 General Procedure for Lipase-Catalysed Acylation of Andrographolide	130
	3A.4.2 Anti-bacterial Activity	131

	3A.4.3 Antifungal Activity	131
	3A.4.5 Hemolytic Assay	132
	3A.4.6 Fluorescent Staining for Assessing Cell Viability and Membrane Integrity	132
	3A.4.7 Bacterial Protein Leakage Assay	133
	3A.4.8 Scanning Electron Microscopy	133
	3A.4.9 Characterization Data of Monoester Derivatives of Andrographolide	134
3 A.5	Spectral Copies	136
3B	Anticancerous Nanoparticles of Andrographolide by Sophorolipid Formulation	
3B.1	Introduction	141
3B.2	Result and discussion	
	3B.2.1 Complexation of Andrographolide with Sophorolipid	143
	3B.2.2 Ultraviolet-Visible (UV) Spectrum and Photoluminescence Studies	143
	3B.2.3 Fourier Transform Infrared Spectroscopy Analysis	144
	3B.2.4 X-ray Diffraction (XRD) Analysis	145
	3B.2.5 Dynamic Light Scattering (DLS) and Zeta Potential Measurement	145
	3B.2.6 Microscopic Studies of SL(A) Andrographolide Complex	146
	3B.2.7 Cytotoxicity Study of SL(A) Andrographolide against MDA-MB-231	147
3B.3	Conclusion	148
3B.4	Experimental Section	
	3C.4.1 Synthesis of Acidic Sophorolipid-Andrographolide Complex	148
	3C.4.2 Cell Lines, Antibodies, and Reagents	149
	3C.4.3 Cell Viability Assay	149
3C	Nanoscale Assembly of Zinc oxide Nanoparticles for <i>in vitro</i> Controlled Release of Andrographolide	
3C.1	Introduction	151
3C.2	Result and Discussion	
	3C.2.1. Zinc oxide Nanoparticles Synthesis	152
	3C.2.2 Saturation Solubility Study	153
	3C.2.3 <i>in vitro</i> pH Release Study	154
	3C.2.4 Cell Viability Assay against Hella Cell Lines	154

3C.3	Conclusion	155
3C.4	Experimental Section	
	3C.4.1. Material and Methods	155
	3C.4.2 Zinc oxide Nanoparticle Synthesis Procedure	156
	3C.4.3 Synthesis Of Zinc oxide –Andrographolide Complex	156
	3C.4.4 pH Stimulated Andrographolide Release Study	157
3D	References	158
Chapter 4 Isolation, purification and characterization of terpenoids from <i>Glochidion tomentosum</i>, <i>Wedelia paludosa</i>		
4A	MPLC Based Isolation of Lupane Triterpenoids from <i>Glochidion tomentosum</i>	
4A.1	Introduction	163
4A.2	Results and discussion	
	4A.2.1 Extraction of Bark Powder	164
	4A.2.2 MPLC Based Purification of Terpenoids	165
	4A.2.3 Characterization of Terpenoids	165
4A.3	Conclusion	166
4A.4	Experimental Section	
	4A.4.1 Materials and Solvents	167
	4A.4.2 Instrumentation	168
	4A.4.3 Extraction Procedure	168
	4A.4.4 Preparative Isolation and Purification of Triterpenoids by MPLC	169
4A.5	Spectral Copies	172
4B	Self-assembly study of a renewable triterpenoid Glochidonol isolated from <i>Glochidion tomentosum</i>	
4B.1	Introduction	185
4B.2	Results and Discussion	
	4B.2.1 Glochidonol Gelation Test in Various Solvent	186
	4B.2.2 Optical Microscopic Images of Glochidonol Self-assembly	187
	4B.2.3 Scanning Electron Microscopy Images of SAFIN Self-assemblies	187
	4B.2.4 Atomic Force Microscopy (AFM) Studies	188

	4B.2.5 Gelation Temperature	189
	4B.2.6 Structural Analysis FTIR Studies	189
	4B.2.7 Rheological Study of Self-assembly	190
	4B.2.8 Adsorption of 5(6)-carboxyfluorescein in Glochidonol Fibrillar Microstructure	191
4B.3	Conclusion	187
4B.4	Experimental Section	
	4B.4.1 Glochidonol Extraction, Purification and Characterization	188
	4B.4.2 Screening of Triterpenoid Gelation	189
	4B.4.3 Glochidonol Self assembly Studies	190
	4B.4.4 Atomic Force Microscopy	190
	4B.4.5 Rheological study	191
	4B.4.6 Small Molecule Adsorption Study	191
4C	Isolation and Purification of Terpenoids from <i>Wedelia paludosa</i>	
4C.1	Introduction	196
4A.2	Results and discussion	
	4C.2.1 Isolation of Terpenoids from <i>W. paludosa</i> Powder	196
	4C.2.2. Characterization of Terpenoid	197
	4C.2.3 Synthesis of Kaurenoic Acid Derivatives	197
	4C.2.4 Glucosidase assay	198
4A.3	Conclusion	198
4A.4	Experimental Section	
	4C.3.1 Collection and Extraction and Isolation	199
	4C.3.2 General Experimental Procedures	200
	4C.3.3 Synthesis of Kaurenoic Acid Derivatives	202
	4C.3.4 Characterization Data	203
4A.5	Spectral Copies	206
4D	References	220
Chapter 5 Biocatalyst Mediated Functionalization of Terpenoids		
5A	Biotransformation of Menthol using <i>Mucor piriformis</i>	
5A.1	Introduction	224

5A.2	Results and Discussion	
	5A. 2.1 Screening of Fungal Cultures for lanceol biotransformation	225
	5A.2.2 Purification and Characterization of Metabolites	226
	5C.2.3 Antimicrobial Activity studies	227
	5C.2.4 Hemolytic activity	228
	5C.2.5 Effect on Membrane Permeability and Cell Viability	229
5A.3	Conclusion	229
5A.4	Experimental Section	
	5A.4.1 Material and Methods	232
	5A.4.2 General Biotransformation Procedure	
	(a) Screening of Fungal Cultures	232
	(b) Time Course Experiment	232
	(c) Substrate Concentration Experiment	232
	(d) Resting Cell Experiment	233
	(e) Preparative Scale Fermentation	234
	(f) Characterization of Metabolites	234
5A.5	Spectral copies	236
5B	Biotransformation of Andrographolide using <i>Mucor piriformis</i>	
5B.1	Introduction	240
5B.2	Results and Discussion	
	5B.2 1. Screening of fungal cultures	241
	5B.2.2 Substrate concentration and Time-course Experiment	241
	5A.2.3 Purification and Characterization of Metabolites	242
5B.3	Conclusion	243
5B.4	Experimental Section	
	5B.4.1 Chemical, reagents, and biological materials	244
	5B.4.2 General Biotransformation Procedure	244
	(a) Screening of Fungal Cultures	245
	(b) Time Course Experiment	245
	(c) Substrate Concentration Experiment	245
	(d) Resting Cell Experiment	246
	(e) Preparative Scale Fermentation	246

	(f) Characterization of metabolites	246
5B.5	Spectral Copies	247
5C	Biotransformation of Lanceol by <i>Cunninghamella echinulata</i>	
5C.1	Introduction	249
5C.2	Results and Discussion	
	5C. 2.1 Screening of Fungal Cultures for lanceol biotransformation	250
	5C.2.2 Purification and Characterization of Metabolites	251
	5C2.3 Antimicrobial Activity	252
5C.3	Conclusion	253
5C.4	Experimental Section	
	5A.4.1 Material and Methods	253
	5A.4.2 General Biotransformation Procedure	
	(a) Screening of Fungal Cultures	254
	(b) Time Course Experiment	255
	(c) Substrate Concentration Experiment	255
	(d) Resting Cell Experiment	255
	(e) Preparative Scale Fermentation	255
	(f) Characterization of Metabolites	256
5C.5	Spectral copies	259
5D	References	262

Research Publications

1. Regioselective and efficient enzymatic synthesis of antimicrobial andrographolide derivatives; **H.S.Patil**, Ajay Paul, H. V. Thulasiram, *Bioorg. Med. Chem. Lett.*, **2018**, 18, 1134-1141.
2. Lipase-catalyzed synthesis of antimicrobial andrographolide derivative **H.S.Patil**, Ajay Paul, H. V. Thulasiram, *Data in Brief*, **2018**, 18, 1134-1141.
3. Fungal mediated kinetic resolution of racemic acetates to (R)-alcohols using *Fusarium proliferatum*, D. D. Jadhav, **H.S.Patil**, Patil S. Chaya, H. V. Thulasiram, *Tetrahedron Lett.*, **2016**, 57, 4563–4567
4. Notch1-MAPK signalling axis regulates CD133D cancer stem cell-mediated melanoma growth and angiogenesis D. Kumar, S. Kumar, **H.S.Patil**, Nalukurthi N.V. Radharani, Totakura V.S. Kumar, T. V. Patil, H. V. Thulasiram and G.C. Kundu, *J. Invest.Dermatol.* **2016**, 136, 2462-2474.
5. One-Pot Fluorescent Labeling Protocol for Complex Hydroxylated Bioactive Natural Products. Saikat Haldar; **H.S.Patil**; H. V. Thulasiram, *J. Org.Chem.*, **2013**, 3, 2941.
6. Proteome-wide reduction in AGE modification in streptozotocin induced diabetic mice by hydralazine mediated transglycation. S. K. Kesavan, A. B. Deshmukh, **H.S.Patil**, M. L. Shaikh, H. V. Thulasiram, R. Boppana & M. h J. Kulkarni, *Nat. Sci. Rep.*, **2013**, 78, 10192-1.
7. Andrographolide inhibits osteopontin expression and breast tumor Santosh Sharma, **H.S.Patil**, P. Sharma, D. Kumar, S. Dasari, V.G. Puranik, H.V. Thulasiram and G.C. Kundu. *Curr. Molecul. Med.*, **2012**, 12, 952-966.
8. Anticancerous Nanoparticles of Andrographolide by Sophorolipid Formulation; **H. S. Patil**, P. K. Singh, D. D. Jadhav, A. A. Prabhune, H. V. Thulasiram (*Manuscript under preparation*)
9. Expedient MPLC Based preparative isolation and MS/MS characterization of labdane diterpenoids from *Andrographis paniculata*; **H. S. Patil**, H. V. Thulasiram (*Manuscript under preparation*)
10. Bioconversion of lanceol by *Cunning hamella*, antimicrobial metabolites; **H. S. Patil**, K. Barao, H. V. Thulasiram (*Manuscript under preparation*)
11. Regio- and stereoselective hydroxylation of (-) Menthol by *Mucor Piriformis* and antibacterial activity of metabolites; **H. S. Patil**, P. P. Daramwar, H. V.

Thulasiram (*Manuscript under preparation*)

12. Self-assembly study of a renewable triterpenoid Glochidonol isolated from *Glochidion tomentosum*; **H. S. Patil**, K. S. Jagadeesh, Sudha Ramkumar, P. Sharanappa, H. V. Thulasiram (*Manuscript under preparation*)

Symposia and Presentation

1. Agnimitra Memorial Best Poster Award (Feb. 2012), National Science Day in CSIR-National Chemical Laboratory, Pune.
2. Indo-Mexico conference on biotechnology: beyond borders held by CSIR - National Chemical Laboratory, Pune.
3. International Symposium on Proteomics IDs and 4th Annual Meeting of Proteomics Society (INDIA).
4. International symposium “Next Two Decades of Chemical Sciences & Technology.”
5. Science day poster presentation (Feb. 2014) in National Chemical Laboratory, Pune.
6. Special training on chemical analysis of honey at CBRTI, Pune.

Abbreviations

UPLC	Ultra Pressure Liquid Chromatography	EtOAc	Ethyl Acetate
ESI	Electrospray Ionization	FBS	Fetal Bovine Serum
MS	Mass Spectrometry	AcOH	Acetic Acid
HRMS	High-Resolution Mass Spectrometry	TMS	Tetramethylsilane
MPLC	Medium Pressure Liquid Chromatography	DCM	Dichloromethane
HPLC	High-Pressure Liquid Chromatography	δ	Chemical Shift
APCI	Atmospheric Pressure Chemical Ionization	g	Gram
UV	Ultraviolet	TEA	Triethylamine
NMR	Nuclear Magnetic Resonance	nM	Nanomolar
TLC	Thin Layer Chromatography	ppm	Parts per million
PTLC	Preparative Thin Layer Chromatography	$^{\circ}\text{C}$	Degree Celsius
NCE	Normalized Collision Energy	m/z	Mass to charge ratio
LC	Liquid Chromatography	R_t	Retention Time
SFC	Supercritical Fluid Chromatography	R_f	Retention Factor
HMBC	Heteronuclear Multiple Bond Coherence	MHz	Megahertz
DAPI	4',6-Diamidino-2-Phenylindole	L	Litre
MTT	3-(4,5-Dimethylthiazol-2-yl)-2,5-Diphenyltetrazolium Bromide	Kg	Kilogram
rpm	Revolutions per minute	h	Hour
EDC	1-Ethyl-3-(3-dimethylaminopropyl) carbodiimide	min	Minute
DCC	N,N'-Dicyclohexylcarbodiimide	μL	Microlitre
TBAF	Tetra-n-butylammonium fluoride	mg	Milligram
DEPT	Distortionless Enhancement by Polarization Transfer	nm	Nanometre
COSY	Correlation Spectroscopy	mbar	Millibar
NOESY	Nuclear Overhauser Effect Spectroscopy	mmol	Millimole
HSQC	Heteronuclear Single Quantum Coherence	fmol	Femtomole
MIC	Minimum Inhibitory Concentration	mm	Millimetre
IC_{50}	50 % Inhibitory concentration	μg	Microgram
TBDMS	Tert-butyldimethylsilyl	cm	Centimetre
DMF	N, N-Dimethylformamide	μm	Micron
NBD	7-Nitrobenzo-2-oxa-1,3-diazole	ng	Nanogram
DMAP	4-(Dimethylamino)pyridine	mL	Millilitre
CDCl_3	Deuterated chloroform	μM	Micromolar
PBS	Phosphate buffered saline	M	Molar
TBAI	Tetra-n-butylammonium iodide	μA	Microampere
		KV	Kilovolt

Abstract of the Thesis

The thesis entitled “**Isolation, Biotransformation, Chemical Modification and Bioactivity Studies of Terpenoids from Plant sources**” consists of five chapters. The introduction is an overview of terpenoids, and plants *viz.* *A. paniculata*, *W. paludosa* *G. tomentosum*. Chapter second deals with the rapid isolation of diterpenoids from *A. paniculata* on preparative-scale was developed by using automated medium pressure liquid chromatography (MPLC) based technique and diterpenoids characterizations by ESI (+)-quadrupole/orbitrap-MS/MS and structure fragmentation pathway of daughter ions. Cytotoxicity of andrographolide was evaluated against MDA-MB-231, MCF-7 and studies 4-nitro-1,2,3-benzoxadiazole (NBD)-tag andrographolide internalization and localization in cancer cells. In chapter third C-14 ester analogues of andrographolide were synthesised through Amano lipase AK (*P.fluorescens*) catalysed acylation using various acyl donors. These monoesters tested for anti-microbial, hemolytic activity and investigated the mechanism of action by triple staining assay. Sophorolipid was used in order to enhance aqueous solubility and bioavailability of andrographolide and tested the cytotoxicity against MDA-MB-231. Zinc oxide nanoparticles were used as carriers for control pH release of andrographolide. Chapter fourth consists of isolation of lupane triterpenoids from the bark of *Glochidion tomentosum* on a preparative scale by medium automated pressure chromatographic technique. Self-assembly of glochidonol was investigated in different solvents and systematically studied by using advanced characterization techniques. The fibrillar microstructures of glochidonol have been utilised for the entrapping small molecule. Terpenoids were isolated from *W. paludosa* and kaurenoic acids derivatised were synthesised, which are evaluated for the glucosidase inhibitor activity. In Chapter four, whole-cell biotransformation of monoterpenoid (menthol), sesquiterpenoids (*Z*-lanceol) and diterpenoids (andrographolide) were systematically studied by using *Mucor piriformis* and *Cunninghamella echinulata*. Metabolites were tested for antimicrobial activity and evaluated the site of action by triple staining assay.

Chapter 1

Introduction and Literature Review

Introduction: Terpenoids

Isoprenoids are the most ancient and diverse class of “natural products” having over 80,000 individual structures with a diverse array of carbon skeleton and functional groups. Isoprenoids exhibiting a vast array of chemical structures are majorly found in plants. Word “terpenes” was originated from turpentine, whereas the terpenoids are the modified derivatives of terpenes skeleton. Biosynthesis of all terpenoids begins with isopentenyl diphosphate (IPP) and dimethylallyl diphosphate (DMAPP). In all eukaryotes (mammals, fungi, plants), archaea and some eubacteria, IPP and DMAPP are synthesized by the mevalonate (MVA) or HMG-CoA reductase pathway and 2-C-methyl-D-erythritol-4-phosphate (MEP) exist in eubacteria, cyanobacteria, apicomplast-type protozoa, and plants. Terpenoids are mainly involved in plant defense mechanism, adaptation, reproduction, and chemical signalling, in order to ensure survival under different conditions. Terpenoids possess several potent pharmacological activities such as anti-microbial, anti-inflammatory, anti-allergic, anti-parasitic, anti-cancer, antidiabetic, insecticidal, anti-plasmodic etc. Two such commercially successful anticancer drug taxol and antimalarial drug artemisinin are terpene derivative from *Taxus brevifolia* and *Artemisia annua* respectively. Recently, terpenoids have emerged as a biofuel due to the chain, branched or ring hydrocarbons, isopentanol and farnesene potential alternatives for gasoline. The skeletal complexity in the terpenes leading to the formation of such a diverse structure is justified with an understanding of the terpenoids biosynthesis.

B: *Andrographis paniculata*: Botanical Description, Pharmacology, Phytochemistry

Andrographis paniculata (Burm f.) Nees is herb associated with family *Acanthaceae*. It mainly distributed in India, Taiwan, Srilanka, Pakistan, Indonesia, Java, and Mainland China. *Andrographis*, which consisting of 40 species but only a few are of medicinal importance out of that *A. Paniculata* is a well known medicinal plant compared to the others. In Asian countries, it is a source to treat disorders such as respiratory tract infections, sore throat, fevers, and gastric infections. In Ayurvedic texts and pharmacopoeia, *A. paniculata* was the constituent of sixteen ayurvedic preparations. Earlier reports suggested that *Andrographis paniculata* extracts exhibited various

pharmacological activities such as an anti-diabetic, anti-cancer, anti-inflammatory and anti-microbial etc. It is a rich source of terpenoids mainly distributed in aerial part (leaves, stems).

C: *Wedelia paludosa*: Botanical Description, Pharmacology, Phytochemistry.

Wedelia paludosa DC belongs to genus *Wedelia* consisting of 60 species; it is a genus of flowering plant in the sunflower family. It has small flowers, herbaceous, a creeping plant used for medicinal as well as a decorative purpose. It is utilized as a conventional herbal medicine throughout the world. The earlier report suggested that it possess antipyretic-analgesic, molluscicidal, hepatoprotective, and bactericidal activity.

D: *Glochidion tomentosum*: Botanical description, Pharmacology, Phytochemistry

Glochidion tomentosum Dalz. belonging to the family *Phyllanthaceae* and tribe *Heliantheae*. It is a medium size evergreen medicinal tree endemic to Western Ghats region of Southern India, tropical semi-evergreen forests. It is a native Indian plant distributed in Karnataka, Tamil Nadu. Plants from this genus are commonly used as a traditional medicinal system for treatment of dyspepsia, wounds, rheumatoid arthritis, dysentery, stomachache. An earlier report on the phytochemical investigation of *Glochidion* species suggested the presence of alkaloids, terpenoids, steroids, terpenoid glycosides, saponins, lignans, and flavonoids. Until now, no literature is available on the phytochemical investigation from *G. tomentosum*, although several species of this genus are described to have medicinal value.

Chapter 2

Phytochemical Investigation of *Andrographis paniculata*

Section A: Isolation and Characterization of Terpenoids from *Andrographis paniculata*

A. paniculata various solvents extracts of *A. paniculata* reported to exhibits several pharmacological activities. Hence, there is a need to purify the bioactive constituent from the extract in order to find the pharmacophore. Extraction *A. paniculata* aerial parts powder followed by purification resulted in five labdane diterpenoid and two steroids. Purified terpenoids were characterized by the analyses spectrometric data as andrographolide, 14-deoxyandrographolide, 11,12-didehydro-14-deoxyandrographolide, neoandrographolide, and isoandrographolide (Figure 1).

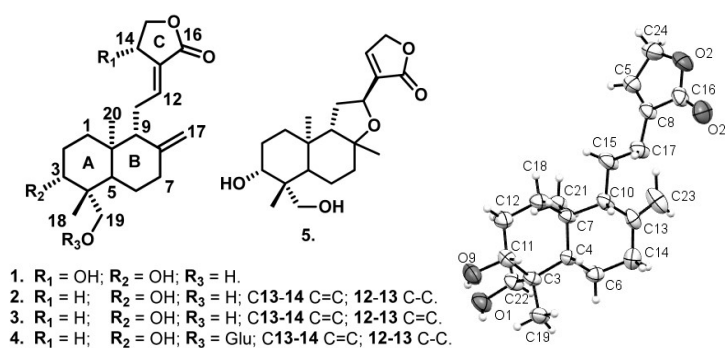
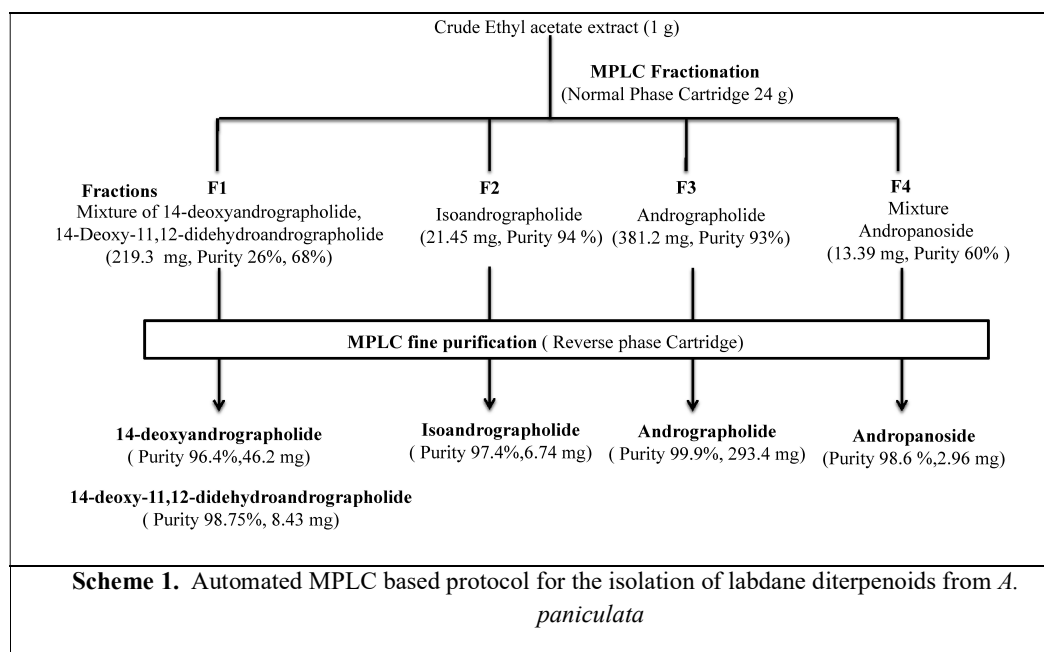


Figure 1. Structures of isolated diterpenoids from *A. paniculata* and ORTEP diagram of 14-deoxy-11,12-didehydroandrographolide (ellipsoids are drawn at 50 % probability)

Section: B Expedient MPLC Based Preparative Isolation and MS/MS Characterization of Labdane Diterpenoids from *A. paniculata*

Rapid isolation of diterpenoids with high purity on preparative-scale from *A. paniculata* was developed by using automated MPLC based technique (Scheme 1). UPLC-ESI(+)-quadrupole/orbitrap-MS/MS-based characterised the isolated labdane diterpenoids. Structure fragmentation correlation and MS/MS signature spectra of the daughter ion generated from isolated diterpenoids were studied with standardised HRMS parameters.



The developed technique was validated by the identification of compounds from leaf extract by UPLC-ESI (+)-MS/MS using data-dependent inclusion mode. Structure fragmentation correlation and MS/MS signature spectra of the daughter ion generated from isolated diterpenoids were studied with standardised HRMS parameters.

Section C: Cytotoxicity Study and Investigation of Cellular Localization of Andrographolide by Fluorescent Tagging

Andrographolide cytotoxicity was examined against human breast carcinoma (MDA-MB-231, MCF-7) and controlled NIH-3T3 mouse fibroblast used as a normal cell line (Figure 2). Andrographolide (20 μM) displayed significant inhibition of viability on both MDA-MB-231 and MCF-7 cells. Andrographolide is non-toxic to normal cells NIH-3T3 mouse fibroblast up to 50- 100 μM .

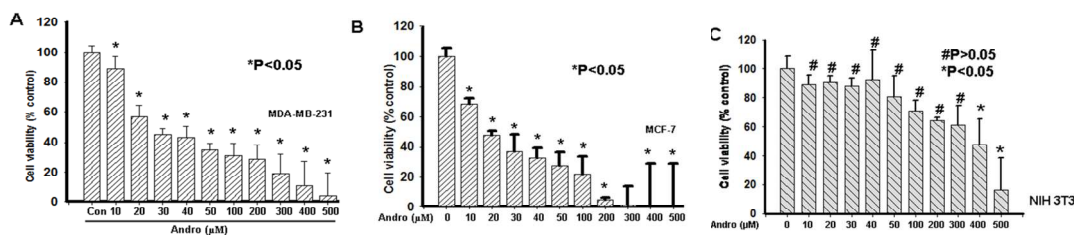


Figure 2. Andrographolide was tested for anticancer activity against MDA-MB-231, MCF-7; and NIH-3T3.

Wound healing assays suggested that andrographolide inhibits cell growth. Further simple and highly efficient one-pot methodology for the NBD based fluorescent labelling andrographolide was developed. NBD-andrographolide was used to track its mode of action through fluorescence cell imaging. The internalisation and localisation of those probes were imaged successfully inside the cancer cells and found to be localised in the endoplasmic reticulum (Figure 3).

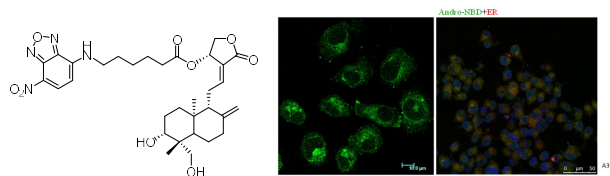


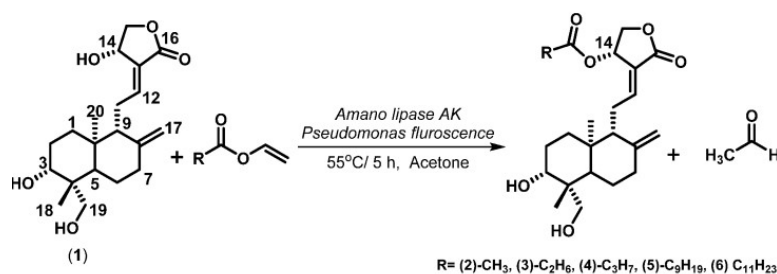
Figure 3 NBD-andrographolide confocal microscopy images of HeLa cells treated with NBD-andro and colocalization

Chapter 3

Chemo-enzymatic Modification of Andrographolide

Section A: Regioselective and Efficient Enzymatic Synthesis of Anti-microbial Andrographolide Derivatives

C-14 ester analogues of andrographolide were synthesised through Amano lipase AK (*P. fluorescens*) catalysed acylation using various acyl donors (Scheme 2). The products were obtained in high yield and with excellent regioselectivity under mild reaction conditions.



Scheme 2. Amano lipase AK (*P. fluorescens*) lipase-catalysed acylation of andrographolide with acyl donors

andrographolide-14-acetate, andrographolide-14-propionate, andrographolide-14-butanoate, andrographolide-14-caproate and andrographolide-14-laurate showed promising anti-microbial activities than andrographolide. These monoesters showed anti-microbial activity, which significantly changed with a chain length of alkyl substitution. Andrographolide-14-acetate was found to be effective against gram-negative *Pseudomonas fluorescens* and *Staphylococcus aureus* at 4 µg/mL and 16 µg/mL concentrations respectively. *E. coli* cells treated with MIC concentrations of andrographolide-14-propionate and andrographolide-14-butanoate were subsequently stained with fluorescent dyes DAPI, FITC and PI. Fluorescent microscopy image of control was not shown to uptake FITC and PI, whereas *E. coli* cells treated with derivatives showed FITC and PI uptake.

Section B: Anticancerous Nanoparticles of Andrographolide by Sophorolipid Formulation

Co-sonication of andrographolide with acidic sophorolipid SL(A) forms an acidic sophorolipid-andrographolide complex, which reduced the size of andrographolide from micro to the nanoscale is due to encapsulation with SL(A). Complex physical and chemical properties were studied by advanced techniques such as DLS, Zeta-potential, microscopic, and eSEM images (Figure 4). Andrographolide, SL(A) and complex tested for cytotoxicity against MDA-MB-231 (Figure 5). Enhanced in the anticancer activity of andrographolide observed, may be due to its increased bioavailability by complexation with acidic sophorolipid.

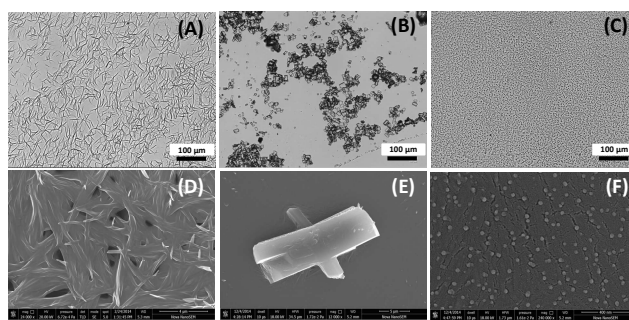


Figure 4. Microscopic and Scanning Electron Microscopic images of (A,D) SL(A); (B,E) Andrographolide; (C,F)

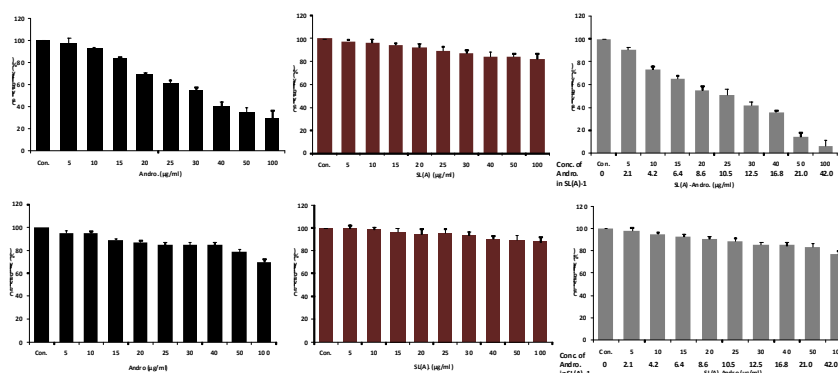


Figure 5. Cytotoxicity study of SL(A); Andrographolide; SL(A)+I by MTT assay against (A) MDA-MB-231 and (B) HEG-293 cells.

Section C: Nanoscale Assembly of ZnO Nanoparticles for *in vitro* Controlled Release of Andrographolide

Zinc oxide nanoparticles were synthesised by using a simple, facile method. The IR, UV-spectra, and elemental analysis suggested the non-covalent interaction of andrographolide with zinc oxide nanoparticles. pH trigger release of andrographolide

from zinc-oxide nanoparticles was studied. Andrographolide release with a change in pH is significant because the cancerous cells have a lower pH compared to the normal cells (Figure 6a). Cytotoxicity of zinc-oxide nanoparticles, andrographolide and complex studied against HeLa cell lines (Figure 6b)., the result indicated that the cell viability is decreased by the presence of ZnO nanoassemblies. Andrographolide release with a change in pH is significant because the cancerous cells have lower pH compared to the normal cells.

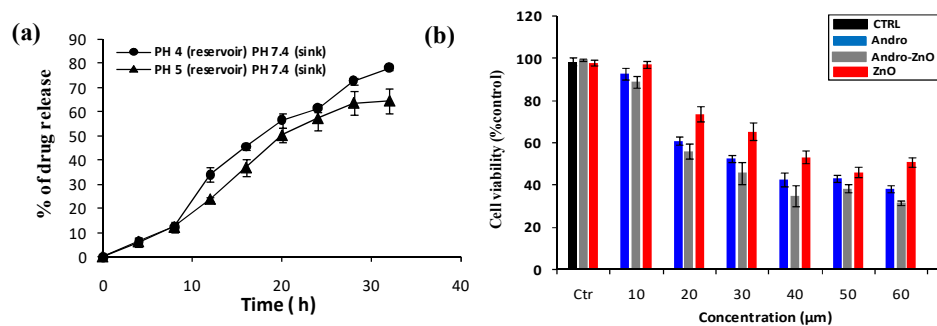


Figure 6. (a) *in vitro* pH release of andrographolide from the complex (b). MTT assay of zinc oxide nanoparticles, andrographolide and complex against HeLa cell line

Chapter 4

Isolation, Purification and Characterization of Terpenoids from *Glochidion tomentosum*, *Wedelia paludosa*

Section A: MPLC Based Isolation of Lupane Triterpenoids from *Glochidion tomentosum*

Glochidion tomentosum, a medium size evergreen medicinal tree endemic to Western Ghats region of Southern India. It is used in traditional medicinal systems e.g. leaves of the tree will be used in the treatment of wounds by applying a grounded paste of the leaves. Till now no literature was available on phytochemical studies of this tree, although several species of this genus are described to have medicinal values. Lupane triterpenoids from the bark of *Glochidion tomentosum* were isolated first time by automated Medium pressure chromatographic (MPLC) technique. Compounds were isolated on a preparative scale and characterized by spectroscopic techniques like NMR's and mass (Figure 10). Glochidone, Epilupeol, Lupeol, Glochidonol, Lup-20(29)-ene-3 α ,23-diol, Glochidiol and Lup-20(29)-ene-1 β ,3 β -diol (Figure 7).

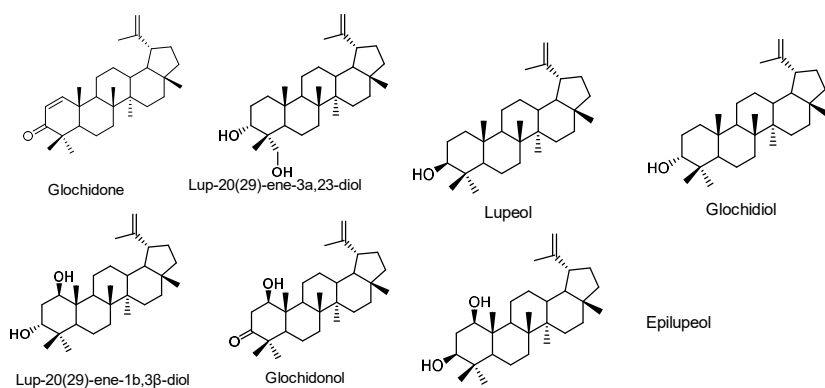


Figure 7. Structure of purified triterpenoids from *G. tomentosum*

Section B: Self-Assembly Study of a Renewable Triterpenoid Glochidonol Isolated from *Glochidion tomentosum*

Glochidonol, a lupane pentacyclic (6-6-6-6-5) triterpenoid isolated from *G. tomentosum*. Glochidonol was found to be excellent gelator compared to the screened

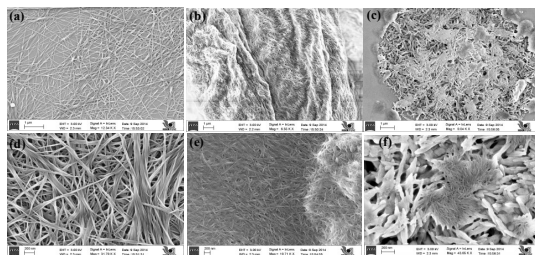


Figure 8. Scanning electron microscopic images of glochidonol xerogel, gel in (a,d) butanol (b,e) toluene (c,f) carbon tetrachloride

lupane and oleanane-type triterpenoids. We reported the first time the glochidonol self-assembly in various liquids. The molecule gets self-assembled and formed a gel in the entire screened aromatic liquids. Physical properties and structure of Glochidonol self-assembly were studied by using optical microscopy, scanning electron microscopy (Figure 8), atomic force microscopy, and Fourier-Transform Infrared Spectroscopy. The Glochidonol self-assembled fibrillar network (SAFIN) has been utilized in order to entrap the 5(6)carboxyfluorescein fluorophore as a model drug.

Epifluorescence images suggested that the fluorescence was adsorbed in the self-assembly (Figure 9), and dispersed after triton-X treatment suggested that the glochidonol self-assembly entrap the fluorophore.

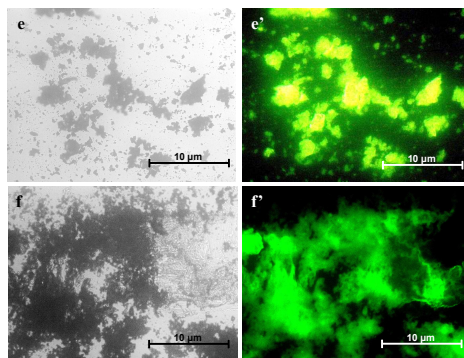


Figure 9. Optical and epifluorescence microscopic images of (e, e') **1** gel in 1,4-dioxane containing CF entrap; Release of CF (f, f'), from **1** gel

Section C: Terpenoids Isolation from *Wedelia paludosa* and Chemical Modification for Its Function as Glucosidase Inhibitors

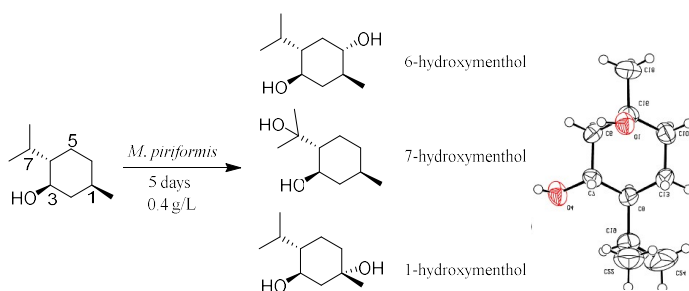
Wedelia paludosa is a small flowering, a creeping plant belonging to a family, *Acmela brasiliensis* (*Asteraceae*). It is being used as an ornamental plant also, it has significant medicinal properties. It is found in many regions of Brazil, especially in the states of Pernambuco, Bahia, Minas Gerais, São Paulo and Santa Catarina. In traditional medicine, the whole plant used for the treatment of respiratory, infectious and dolorous conditions. Its crude extract assessed by markers of liver damage and oxidative stress-related parameters. *W. paludosa* possess hepatoprotective, antipyretic-analgesic, bactericidal and antidiabetics activities. Terpenoids were isolated from *Wedelia paludosa* aerial parts by normal column chromatographic technique. Purified terpenoids were characterised by various spectroscopic techniques. Kaurenoic acid is a major constituent of *W. paludosa*, which was derivatives have been synthesized using chemical agents, further Kaurenoic acids along with its derivatives were tested as glucosidase inhibitors. Results suggested enhanced in glucosidase inhibition activity of Kaurenoic acid due to derivatization

Chapter 5

Biocatalyst Mediated Functionalization of Terpenoids

Section A: Biotransformation of Menthol using *Mucor piriformis*

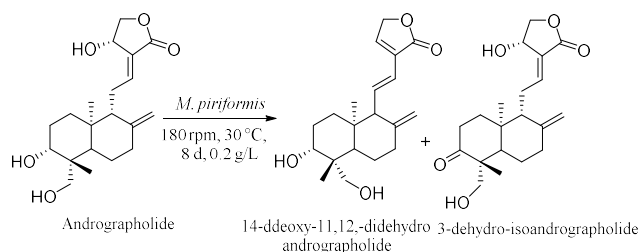
Regio- and stereoselective hydroxylation of menthol was explored with fungal strain *M. piriformis* (Scheme 3). Metabolites were characterized by various spectroscopic and advance crystallographic techniques. 1 was oxidized to 6-hydroxymenthol as major and 1-hydroxymenthol, 8-hydroxymenthol as minor metabolites. Menthol showed antimicrobial activity MIC at higher concentration compared to its metabolites against gram-positive, gram-negative bacteria and yeast with MIC as low as 8 $\mu\text{g/mL}$. Hemolytic activity of menthol and metabolites were low at their respective MIC values. Systematic investigation of biotransformation and antimicrobial activity of menthol and metabolites can be helpful to be developed as natural cheap, effective antibacterial agents.



Scheme 3. biotransformation pathway of Menthol with *Mucor piriformis*

Section B: Biotransformation of Andrographolide using *Mucor piriformis*

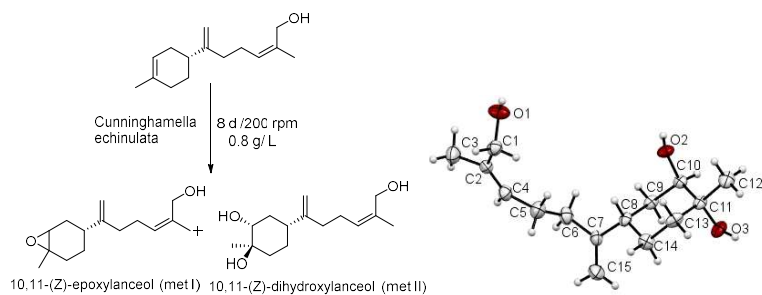
Andrographolide biotransformation investigated the first time by using *M. piriformis* after substrate concentration, time course, and large-scale studies were performed (Scheme 4). Metabolites were isolated from crude extract were purified and characterized by various spectroscopic methods 3-dehydroandrographolide and 14-deoxyandrographolide.



Scheme 4. Biotransformation pathway of andrographolide by *M. piriformis*

Section C: Biotransformation of Lanceol by *Cunninghamella echinulata*

(*Z*)-Lanceol biotransformation investigated the first time by using *Cunninghamella echinulata*. Metabolites were characterized by various spectroscopic techniques (Scheme 5). Lanceol oxidized by *C. echinulata* into new metabolites, 10, 11-(*Z*)-epoxylanceol and 10, 11-(*Z*)-dihydroxylanceol. Lanceol has antimicrobial activity at high minimum inhibitory concentration (MIC) value, but its oxidized derivatives are exhibited antimicrobial activity against gram positive, gram negative bacteria and yeast with MIC as low as 16 µg/mL. Antibacterial activity varies spontaneously with hydroxyl functionality.



Scheme 5. Biotransformation of Lanceol by *Cunninghamella echinulata*
ORTEP diagram of Lanceol-10,11-diol (ellipsoids are drawn at 50 % probability)

Chapter 1

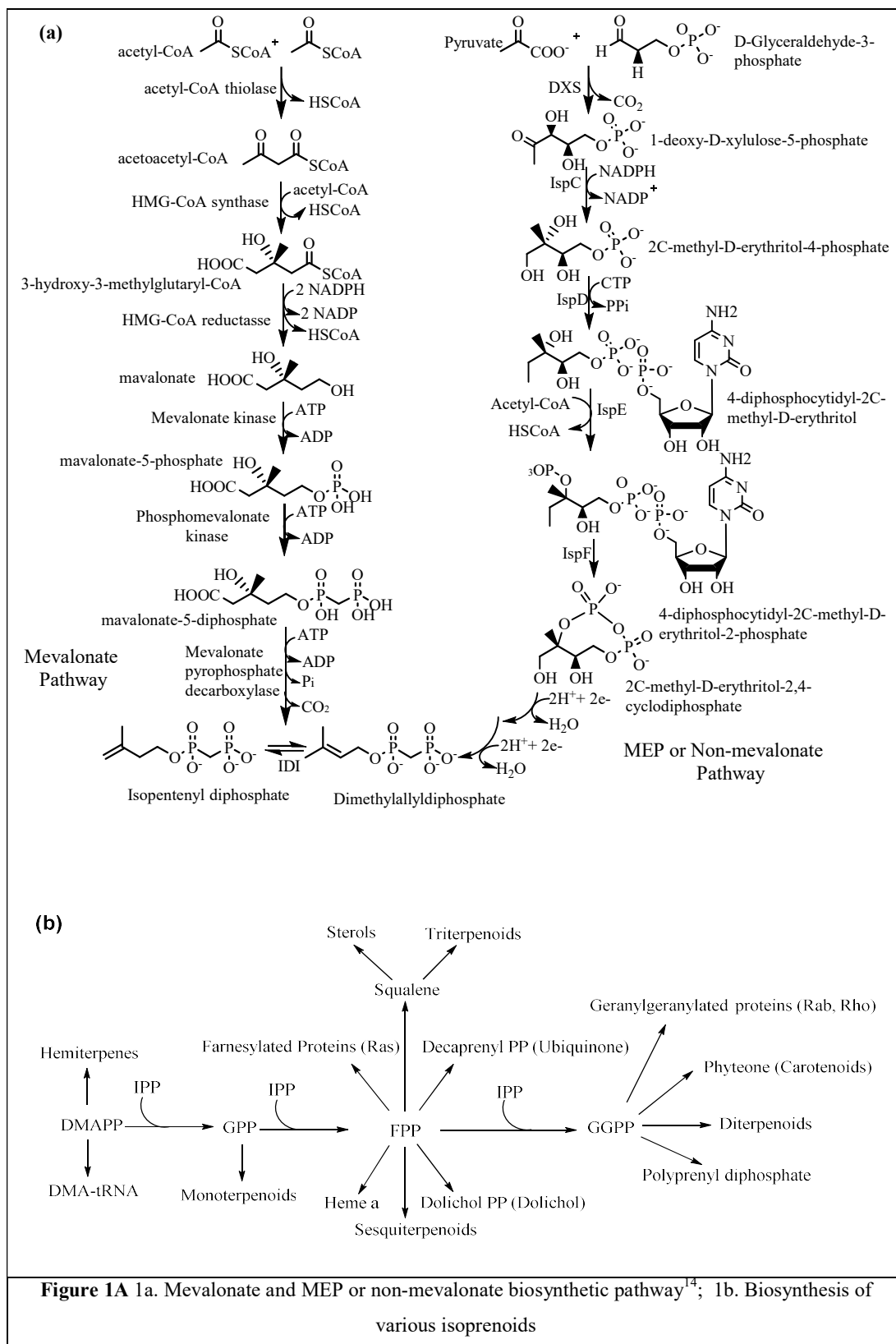
Introduction

1A.1 Terpenoids

Isoprenoids are the most ancient and diverse class of “natural products” having over 80,000 individual structures with a diverse array of carbon skeleton and functional groups.^{1,2} Isoprenoids exhibiting a vast array of chemical structures are majorly found in plants. It ranges from universal primary metabolites, such as sterols (as essential components of bio-membrane), carotenoids and chlorophyll (as photosynthetic pigments), ubiquinones, vitamins and hormones (involve in plant defense, communication) to secondary metabolites including terpenoids.^{3,4} Word “terpene” was originated from turpentine, which is a semi-fluids oleoresins extracted from coniferous trees.⁵ Terpenoids are the modified derivatives of terpene skeleton, which are formed by chain elongation and cyclization with the inclusion of functional groups on hydrocarbon skeleton. Terpenoids are mainly involved in plant defense mechanism, adaptation, reproduction, and chemical signalling, in order to ensure survival under different conditions.^{6,4} Terpenoids possess several potent pharmacological activities such as anti-microbial, anti-inflammatory, anti-allergic, anti-parasitic, anti-cancer, antidiabetic, insecticidal, anti-plasmodic etc.^{7,8,9} Two such commercially successful anticancer drug taxol and antimalarial drug artemisinin are terpene derivative from *Taxus brevifolia* and *Artemisia annua* respectively.^{10,11} Recently, terpenoids have emerged as a biofuel due to the chain, branched or ring hydrocarbons, isopentanol and farnesene potential alternatives for gasoline.¹² The skeletal complexity in the terpenes leading to the formation of such a diverse structure is justified with an understanding of the terpenoids biosynthesis.

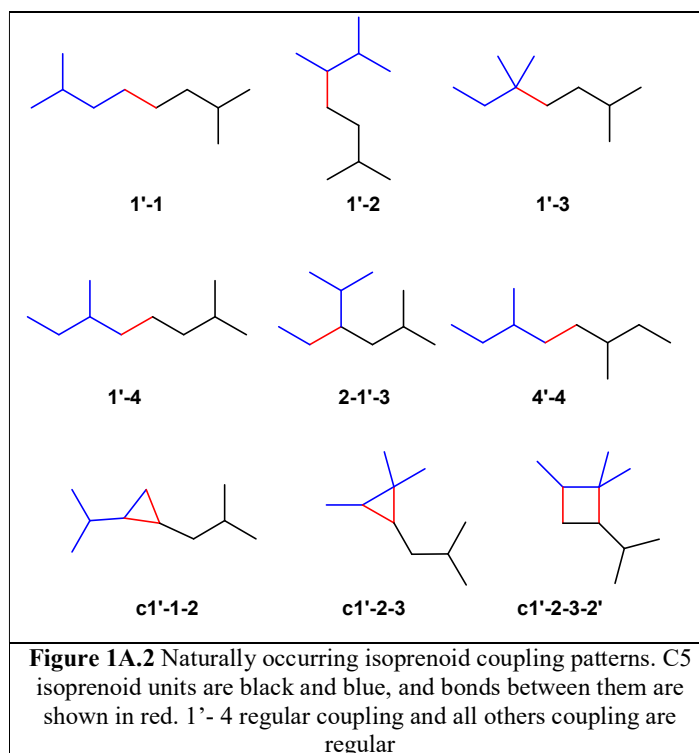
1A.2 Terpenoid Biosynthesis in Plants

Biosynthesis of all isoprenoids begins with two simple five-carbon building blocks, isopentenyl diphosphate (IPP) and dimethylallyl diphosphate (DMAPP). They are classified by the number of five carbon units present in the core structure (hemi-, mono-, sesqui-, di-, ses-, tri-, tetra-, poly-terpenes).¹³ In all eukaryotes (mammals, fungi, plants), archaea and some eubacteria, IPP and DMAPP are synthesized from three molecules of acetyl-CoA in seven steps by the mevalonate (MVA) or HMG-CoA reductase pathway, which operates in the cytosol and mitochondria (Figure 1A. 1a).¹⁴

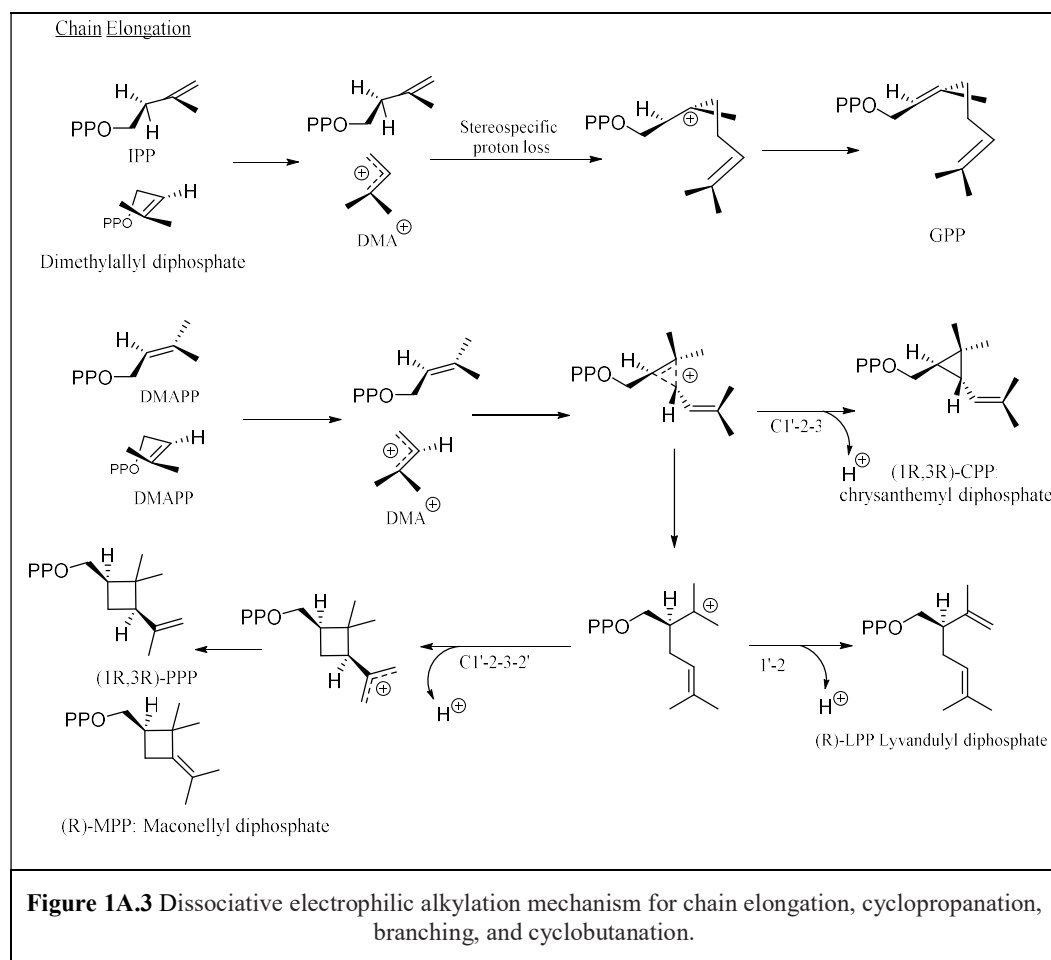


Before the 1990s it was believed that isoprenes are only synthesized by the MVA pathway. In the mid-1990s, Rohmer and Arigoni's discovered the existence of a second pathway for IPP and DMAPP biosynthesis, which occurs in eubacteria, cyanobacteria, apicoplast-type protozoa, and plants is now firmly established. This pathway starts with pyruvic acid, glyceraldehydes-3-phosphate (GAP), leading to the formation of IPP and DMAPP in seven enzymatic steps (Figure 1A.1a). In this biosynthesis, the first pathway-specific intermediate is 2-C-methyl-D-erythritol-4-phosphate (MEP), from which the pathway derives its name.¹⁵ In addition to isoprenoids synthesis, deoxy-xylulose phosphate (DXP) is the precursor for the biosynthesis of thiamin (vitamin B₁) and pyridoxol (vitamin B₆) hence the pathway also known as 1-deoxy-D-xylulose 5-phosphate (DOXP) pathway.¹⁶

The MVA and MEP pathways converge at DMAPP, beyond which the enzymes involved leading to the formation of multitude metabolites in nature are similar in all organisms (Figure 1A.1b).¹⁷ Hemiterpenes are the smallest known terpenes produced by most of the plants, and the first terpenes formed from DMAPP or IPP. The basic reaction in the isoprenoid pathway is chain elongation, where the allylic carbocation formed from isoprenoid allylic diphosphate such as DMAPP, geranyl diphosphate (GPP), farnesyl diphosphates (FPP) is added to the double bond in IPP (Figure 1A.4) to form a growing allylic diphosphate chain products. The chain elongation or head-to-tail or 1'-4 linkage is by far most common and occurs in all organisms.¹⁸ Terpenes are biosynthesized from isoprene units by four fundamental reactions: chain elongation, cyclopropanation, branching, and cyclobutanation (Figure 1A. 3). Chain elongation is the basic reaction in the terpene biosynthesis. Molecules generated by these reactions have head to tail or regular carbon skeletons. Other three reactions produce irregular carbon skeletons. Cyclopropanation (c1'-2-3) reaction is the first pathway-specific reaction in the biosynthesis of triterpenoids, steroids which are formed through the cyclopropyl intermediate, pre-squalene (C30) and carotene compounds through pre-phytoene (C40) found in Archaea, some bacteria and all Eukaryotes.¹⁹ Mealybug mating pheromones such as planococyl & maconelliol are formed through irregular cyclobutation reaction.²⁰



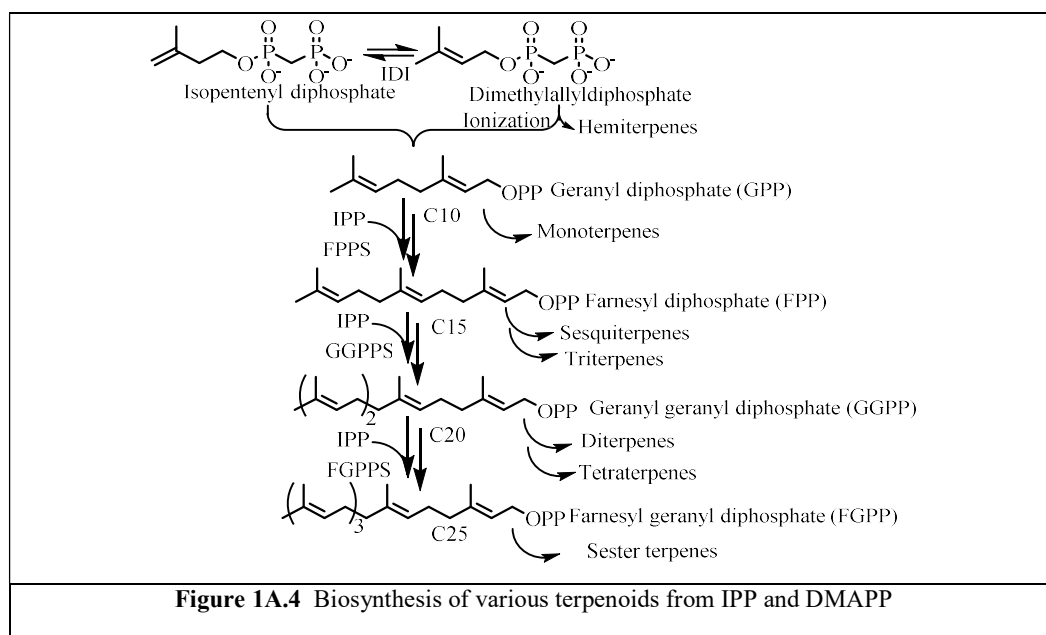
3-methyl-1-butyl is the basic unit of isoprenoid carbon skeletons, which are joined in nine different patterns (Figure 1A.2).^{1,21} The four structures followed combination in which, C1' of one unit (blue) formed a bond (red) with the single carbon of another unit (black) (1'-1, 1'-2, 1'-3, and 1'-4). C1' is joined to the other unit in a cyclic structure (c1'-1-2, c1'-2-3, and c1'-2-3-2') this pattern showed in three structures and one structure C1' is inserted between atoms in the other unit (2-1'-3). Only in one structure which follows 4'-4 combining pattern does not involve C1'. Regular terpenes possess most commonly 1'-4 linkage in the isoprene units. Other attachment patterns are designated as non-head-to-tail or irregular terpenes. Four of the basic isoprenoid structures (1'-2, 1'-4, c1'-2-3, and c1'-2-3-2') are synthesized by joining simpler units, whereas the other four (1'-1, 1'-3, 2-1'-3, and c1'-1-2) are produced by rearrangement of 1'-2-3 structures. In isoprenoid biosynthesis pathway, all the isoprenoid skeletons are formed before the modification reactions that are required to the synthesized specific natural product, except the 4'-4 attachment pattern.



The mechanism for four fundamental steps involved in terpenes biosynthesis is studied using deuterium isotope to trace the key rearrangement and elimination steps reported by Thulasiram *et al.*²² In chain elongation, reaction first step is the formation of dimethylallyl cation (DMA^+) from DMAPP. Further, the reaction proceeds by dissociative electrophilic alkylation of IPP double bond by the cation (Figure 1A.3). Stereospecific deprotonation of intermediate carbocation generates GPP. Chrysanthemyl cation (C^+) a protonated cyclopropane intermediate formed by the dissociative electrophilic alkylation of the double bond DMAPP by dimethyl allyl cation (DMA^+) in C 1',4-addition. Further pro-S hydrogen lost from C1 position of intermediate lead to chrysanthemyl diphosphate (CPP). The rearrangement reaction in chrysanthemyl cation (C^+) form lanvandulyl cation (L^+), in the branching step, which can be deprotonated to generate lavandulyl diphosphate (LPP). Cyclobutanation of the lanvandulyl cation (L^+)

generates a protonated cyclobutyl carbinyl cation intermediate. Deprotection of the intermediate cation leads to Maconellyl diphosphate (MPP).

Monoterpenoids are acyclic (linalool, myrcene and ocimene), or monocyclic (limonene, carveol and carvone) or bicyclic (camphene, sabinene and pinene) compounds synthesized from GPP catalyzed by monoterpene synthases. GPP binds to the active site of monoterpene synthases as a complex with the divalent metal ion. GPP undergoes ionization to form linalyl cation which undergoes further isomerization and cyclization to form diverse monoterpenes. In plants, monoterpenoids are synthesized through the MEP pathway.



Farnesyl diphosphate (FPP), which lies at the juncture of terpene pathway, branched into sesquiterpenes, squalene, farnesylated proteins (Ras), decaprenyl PP ubiquinones), heme a, and dolichol PP (dolichol). Sesquiterpenes are generated by ionization followed by intermolecular cyclization of FPP. Squalene synthase catalyzes 2 FPP condensation to form squalene, which further oxidized to the (3*S*)-oxidosqualene/2,3-oxido squalene in the pathway and it is the common substrate for biosynthesis of all the triterpenoids. Triterpenoids are synthesized by cyclization of oxido squalene in which the first step is a 2,3-peroxide bond cationic attack, which generates cyclic carbocation. 1,2-proton and methyl shifts of cation intermediates lead to the formation of different triterpenes. In plants, triterpenoids are stored in glycosylated form, or saponins. Modification of

lanosterol and cycloartenol produces steroids and hormones. Lanosterol syntheses are present in animals and fungi for steroids synthesis, and whereas cycloartenol synthase involved in plants, protozoa and microalgae steroid biosynthesis.

Diterpenoids are biosynthesized from GGPP, forms by cyclization followed by several skeletal modifications. Most of the diterpenoids are secondary metabolites and limited to some specific plant taxonomy as a signature metabolites. Head-to-head condensation of two GGPP molecules forms phytoene, which used as a precursor for tetraterpenoids. Polyrenoids are the linear polymers produced from isoprene (6-100) with primary alcohol at a terminal. The reduction of a double bond at α -residue gives rise to dolichols. Dolichols are polyrenoids produced by bacterial and plants are involved in N-glycosylation of proteins. Quinones are one of the important groups in polyrenoids, containing polar head group and non-polar isoprenoid side chain. These quinones are involved in the electron transport chain. Rhoquinone (RQ), the ubiquinone derivative with amino group substituting one of a methoxy group, present in purple bacteria Rhodospirillaceae family.

1A.3 Classification of Terpenoids

Terpenoids are classified according to the number of isoprene units present in it, e.g. hemiterpenes, monoterpenes, sesquiterpenes, diterpenes, sesterterpenes, triterpenes, polyterpenes (Table 1A.1).²³ But in some cases, there are violations of isoprene rule, e.g. cryptone (**2**) and lavandulol (**3**).²⁴ The carbons contain in cryptone, a naturally occurring ketonic terpenoid, carbons are not a multiple of five, and it contains only nine carbons. Lavandulol is composed of two isoprene units but linked through exceptional C3 and C4 (3,4-linkage). Hemiterpenes are the smallest and simplest terpene consisting of five-carbon single isoprene unit; it has low occurrence in nature with no significant bioactivities e.g methyl butanol (**5**).²⁵ Monoterpenes are reclassified based on rings present in it structure as acyclic (citral (**7**), citronellol (**8**)), monocyclic e.g menthol (**9**), α -terpineol, and bicyclic. Bicyclic monoterpenes are further reclassified into three classes according to the second ring size such as 6+3 (carane) (**10**), 6+4 (pinane) (**11**), 6+5 (camphane) (**12**).²⁶ Sesquiterpenoids are classified according to the number of rings present in its acyclic (farnesol (**14**)), monocyclic (bisabolene (**15**)), bicyclic (cadinene (**16**)), and tricyclic (cedrol (**17**)).²⁷ The diterpenes are the diversified class of terpenoid,

biosynthesised by the combination of four isoprenoid units. Diterpenoids are classified according to the number of the rings present in the structure acyclic (phytol (**18**)), monocyclic (vitamin-A(**19**)), bicyclic (agathic acid (**20**)), tricyclic (abietic acid (**21**)),²⁸

Table 1A.1 Classification of Terpene²⁹

Terpenes	Number of isoprene units	Number of carbons
Hemiterpenes	1	5
Monoterpenes	2	10
Sesquiterpenes	3	15
Diterpenes	4	20
Sesterterpenes	5	25
Triterpenes	6	30
Tetraterpenes	8	40
Polyterpenes	>8	>40

Diterpenoids are further subdivided according to the specific skeletal structures like labdanes (**4a**), *ent*-kaurans (**4b**), halimanes, clerodanes, pimaranes, abeitanes. Labdane is a bicyclic diterpenoid; the name originated from the labdanum a resin derived from the *gum rockrose*. *ent*-kauran is a bioactive class of tetracyclic diterpenoids. Five isoprene containing sesterterpenes are rare compounds, which are mainly isolated from marine sponges. Triterpenes are biosynthesised from six isoprene units and biologically important class of terpene. It classified into acyclic (squalene (**23**)), tricyclic (ambrein(**24**)), and tricyclic (lanosterol (**26**)). Tetraterpenes contain eight isoprene units and are classified into acyclic (lycopen (**27**)), bicyclic (lutein (**28**)).

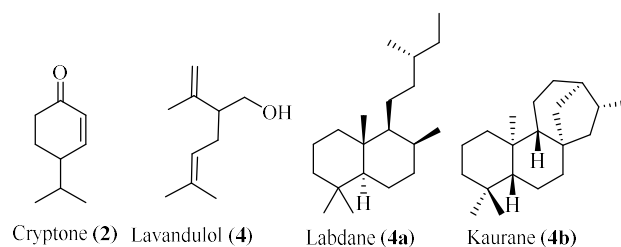
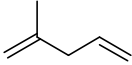
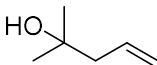
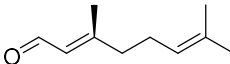
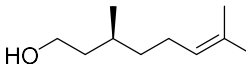
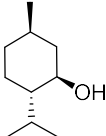
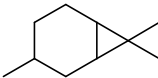
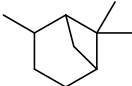
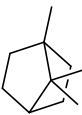
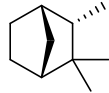
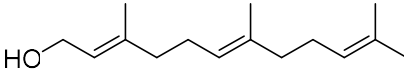
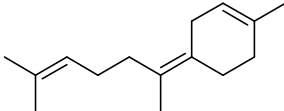
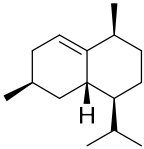
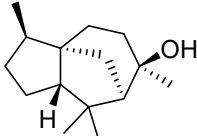
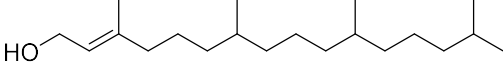
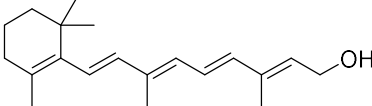
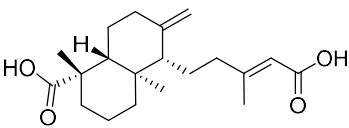
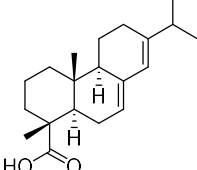
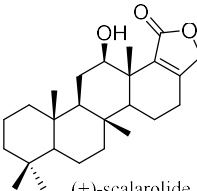


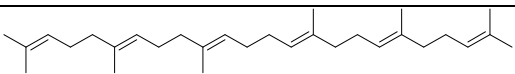
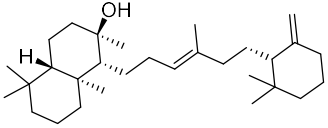
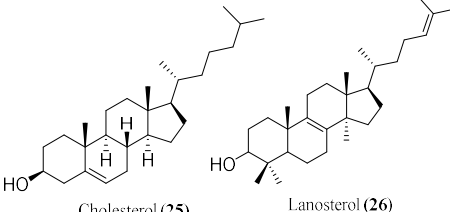
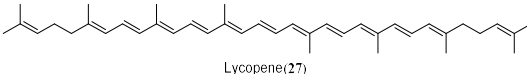
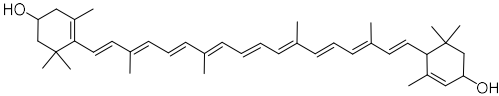
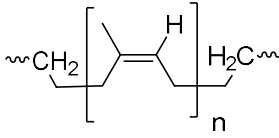
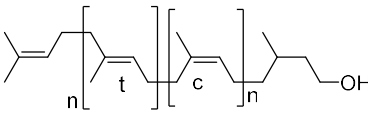
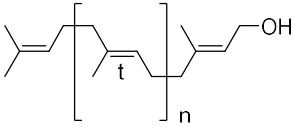
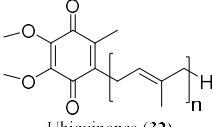
Figure 1A.5 Structure of Terpenoids

Carotenoids pigments are the important cyclic class of tetraterpenes used as a natural food additive and in pharmaceutical industries. Xanthophylls pigments are the other broadly distributed class of tetraterpenes, responsible for flowers, vegetable and fruit colouring.³⁰ Polyterpenes is the polymer of isoprene units (6-100) with the hydroxyl group at the terminal. Rubber (**29**) is extensively used polyterpene for several applications by humans. It is present in several plants in the latex form, e.g. *Hevea brasiliensis* (Rubber tree). It classified into di-*trans*-poly-*cis* (dolichols), tri-*trans*-poly-*trans* (solanosol (**31**)). Quinones are one of the important groups in polyprenoids, containing polar head group and non-polar isoprenoid side chain.

Table. 1A.2 Terpenes classification and chemical structures

Hemiterpene			
		Isoprene (5)	Methyl butanol (6)
Monoterpenes	Acyclic		
		Citral (7)	Citronellol (8)
	Monocyclic		
		Menthol (9)	
	Bicyclic	6+3-membered rings	
			Carane(10)
		6+4-membered rings	
			Pinane (11)
		6+5-membered rings Borane derivative	
			Camphane (12)

		norbornane derivative	
Sesquiterpenoids	Acyclic		Isocamphane (13)  Farnesol (14)
	Monocyclic		 Bisabolene (15)
	Bicyclic		 Cadinene (16)
	Tricyclic		 Cedrol (17)
Diterpenes	Acyclic		 Phytol (18)
	Monoicyclic		 Vitamin A (19)
	Dicyclic		 Agathic acid (20)
	Tricyclic		 Abietic acid (21)
Sesterterpenes			 (+)-scalarolide (22)

Triterpenoid	Acyclic	
	Tricyclic	
	Tetracyclic	
Tetraterpenes	Acyclic	
	Bicyclic	
Polycyclic		
	di- <i>trans</i> -poly- <i>cis</i>	
	tri- <i>trans</i> -poly- <i>trans</i>	
	Quinones	

1A.4 Terpenoids applications

Terpenoids represent diverse class molecules with complex structure and functionalities that provide great opportunities to solve many human social and health issues. Presently

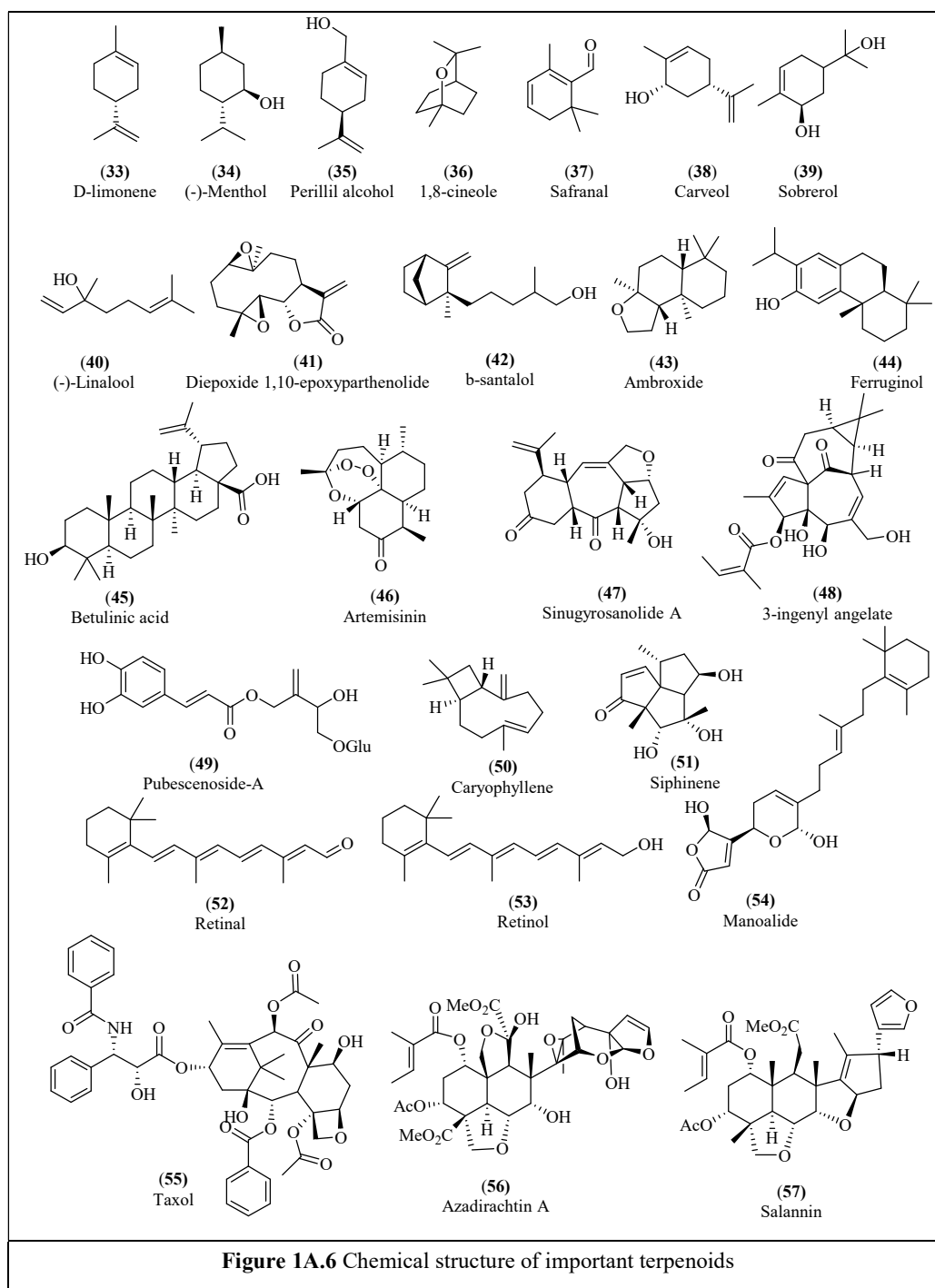
terpenoids are utilised for numerous purpose in agriculture, food, perfumery, and pharmaceutical industries etc.^{31,32} Terpenes viz. ambroxides and santalol play an essential role in fragrance industries in perfumery essential oils (Figure 1A.6).³³ Terpenoids have pharmacological properties including anticancer, antimicrobial, antiallergenic, antihyperglycemic, antispasmodic, anti-inflammatory properties.^{34,35}

Hemiterpenes are the smallest terpene with no significant bioactivities. Pubescenoside-A, a hemiterpene glycoside isolated from *Ilex pubescens* is reported to exhibit anti-platelet aggregation activity.³⁶ Monoterpenes produced in the plants act as a chemical defense against herbivores, as fragrances in order to attract pollinators and also as phytotoxins to the other plants.³⁷ Limonene at a concentration (10 μ M) acts on the microtubules leading to membrane leakage in the transgenic *Arabidopsis thaliana* weed..^{38,39} Limonoids from *Meliaceae* family trees are used for pest management due to its antifeedant and insecticidal properties.⁴⁰ In food industries terpenoids are used as a colour, flavour and fragrance enhancers. 1-menthol (**34**) is one of the most important flavouring agents in pharmaceuticals, cosmetics, toothpaste, chewing gum, and other toiletries as well as in cigarettes.³² 1,8-cineole (**36**) is commonly used in flavouring and fragrance industries due to its pleasant taste and spicy aroma.^{41,42,43} Cineole based eucalyptus oil is used as a flavouring agent at low levels (0.002 %) in various products, including baked goods, confectionery, meat products and beverages.⁴³ Safranal, (**37**) biosynthesised from carotenoids degradation pathway is one of the most expensive spice flavour compound present in Saffron (*Crocus sativus* L.).⁴⁴ D-limonene (**33**) and perillyl alcohol (**35**) are known to inhibit the development of carcinomas in liver, mammary, skin, lung, colon, prostate, and pancreas.^{45,46} Monoterpenes such as carveol (**38**), sobrerol (**39**) have shown activity against mammary carcinomas.⁴⁷ Menthol, exhibited a bacterial activity against *S. aureus* and *E. coli*.⁴⁸ Sesquiterpenes are less volatile compared to hemiterpenes, monoterpenes and function as semiochemicals in plant and insect.⁴⁹ It has several pharmacological activities such as anti-inflammatory, bactericidal, antioxidant, and antitumor activities etc.⁵⁰ β -caryophyllene sesquiterpenes are first known “dietary cannabinoid” present in spices and got generally recognized as safe status from FDA as a common component of food. β -caryophyllene in cancerous cell line stimulates the apoptosis and suppresses the tumorgrowth.⁵¹ Silphinenes and its

derivatives exhibited insect antifeedant activity against *aphid*, and *Leptinotarsa decemlineata* species.⁵²

Sinugyrosanolide-A is *trans*-neoclerodane type diterpenes and psychoactive drug, ferruginol (**44**) have been reported to possess anti-mycobacterial activity.^{53,7} 3-ingenyl angelate (**48**), a hydrophobic diterpene ester isolated from *Euphorbia peplus* is reported to be used as a topical chemotherapeutic agent for skin cancer.⁵⁴ Sesterterpenes exist rare in nature compared to other terpenes, and a maximum of it was isolated from marine fungi. Manoalide (**54**) a bioactive sesterterpene isolated from *Luffarella variabilis* sponge. It showed various bioactivities such as antihypertensive (calcium channel blocker), anti-inflammatory, antimicrobial, and analgesic.⁵⁵ Betulinic acid (**45**) shown to induce apoptosis of several human tumorcells, including melanoma and glioma. It is used as an inhibitor for the NF- κ B pathway.^{56,57} Triterpene glycoside glycyrrhizin and glycyrrhetic acid act via the P13K/Akt/GSK3- β to reduce the cytoline production hence investigated for their therapeutic potential for asthma treatment.⁵⁸ The natural rubber is the isoprene polymer, which is extensively used for several applications either alone or in combination with other material.⁵⁹

As discussed above, the terpenoids are bioactive molecules with structural and chemical diversity, which give the opportunities to find out the new drug leads.^{60,61} In nature, the plants are the major sources of terpenoids. In folk or traditional medicine, the medicinal plant parts powder or crude extracts were used for therapeutic and experimental purpose, but the use of these crude preparations has several disadvantages like the quantity of bioactive constituents varies, raw material collection, storage and preparation.^{62,63} Isolation and purification of the crude extracts helps for characterization of the bioactive constituent, which may help further for the synthesis in large quantity and derivative formation, determine the mechanism of action, formulation as a drug, derivatisation. Also, bioassays can be developed for pure bioactive molecules; this is important for screening it for various bioactivities quality control in therapeutic formulation for consumption as a drug.⁶⁴



Plant extraction protocols majority plays the most important role in the isolation and characterization of bioactive terpenoids. The earlier extraction protocol was solely focused on analytical scale isolation with few targeted compounds; hence alternative technique is required, which facilitates the easy availability of these compounds in

large scale.^{65,66} MPLC is a robust automated technique for developing an effective, rapid and reproducible protocol for preparative scale isolation of natural products. Ultra performance liquid chromatography coupled with high-resolution mass spectrometry is a technique to recognise the expected metabolites in the complex plants or biological mixtures even at a minor concentration (nm-pm range) with low sample requirement, high sensitivity, rapidity and high accuracy.^{67,68} However, terpenoid bioactive compounds were not explored efficiently due to their low bioavailability, which affects their bioactivities greatly.^{69, 70} Application of surfactant to enhance the solubility of hydrophobic bioactive terpenoids in water due to their amphiphilic behaviour, which tends to reduce drugs surface tension is one of the strategies to improve the bioavailability.⁷¹ Biotransformation is a green approach is used to expand the chemical diversity of terpenoids at mild reaction conditions.^{72,73,74}

1B.1 *Andrographis paniculata*

Andrographis paniculata (Burm f.) Nees is a medicinal herb associated with family *Acanthaceae* (Table 1B.1).⁷⁵ It possesses extremely bitter taste hence also called as “king of bitters” in English.⁷⁶ The name *A. paniculata* refers genus *Graphis* is from family *Graphidaceae*, which means pencil and *paniculata* means panicles in Latin means inflorescence of the plant.⁷⁷

Table 1B.1 Taxonomic hierarchy of *Andrographis paniculata*

Subkingdom	<i>Tracheobionta</i>
Superdivision	<i>Spermatophyta</i>
Division	<i>Angiosperm</i>
Class	<i>Dicotyledonae</i>
Subclass	<i>Gamopetalae</i>
Series	<i>Bicarpellatae</i>
Order	<i>Personales</i>
Family	<i>Acanthaceae</i>
Subfamily	<i>Acanthoideae</i>
Tribe	<i>Justiciae</i>
Subtribe	<i>Andrographideae</i>
Genus	<i>Andrographis</i>
Species	<i>A. paniculata</i>

1B.1.1 Botanical Description

A. paniculata is a branched, medium size herbaceous plant grown up to 30-110 cm in height. The stem is quadrangular dark green, brittle, branched, length with on the angle longitudinal furrows (30 -100 cm) and the diameter of 2-6 mm. Leaves are simple, green, glabrous, opposite with lanceolate arrangement, pinnate with acute apex, entire margin and length of about 2-12 cm, the width of 1-3 cm (Figure. 1B. 1).⁷⁸ Size of the flower is around 2.5 -10 mm, terminal panicles spreading auxiliary. Flowers are white with a rose-purple spot on the petals. In *A. paniculata* fibrous or adventitious root system is present with 0.5-1 m height and of 2-6 mm diameter. Seeds are small, yellowish brown, and numerous in numbers.⁷⁹ *A. paniculata* is gregarious, mostly found along the roadside, in shady, moist and dry regions. It is commercial cultivation face problem of seed dormancy hence the modern techniques like tissue culture is used to improve plantlets production within short duration along with the increase in

phytochemical constituents.^{77,80}

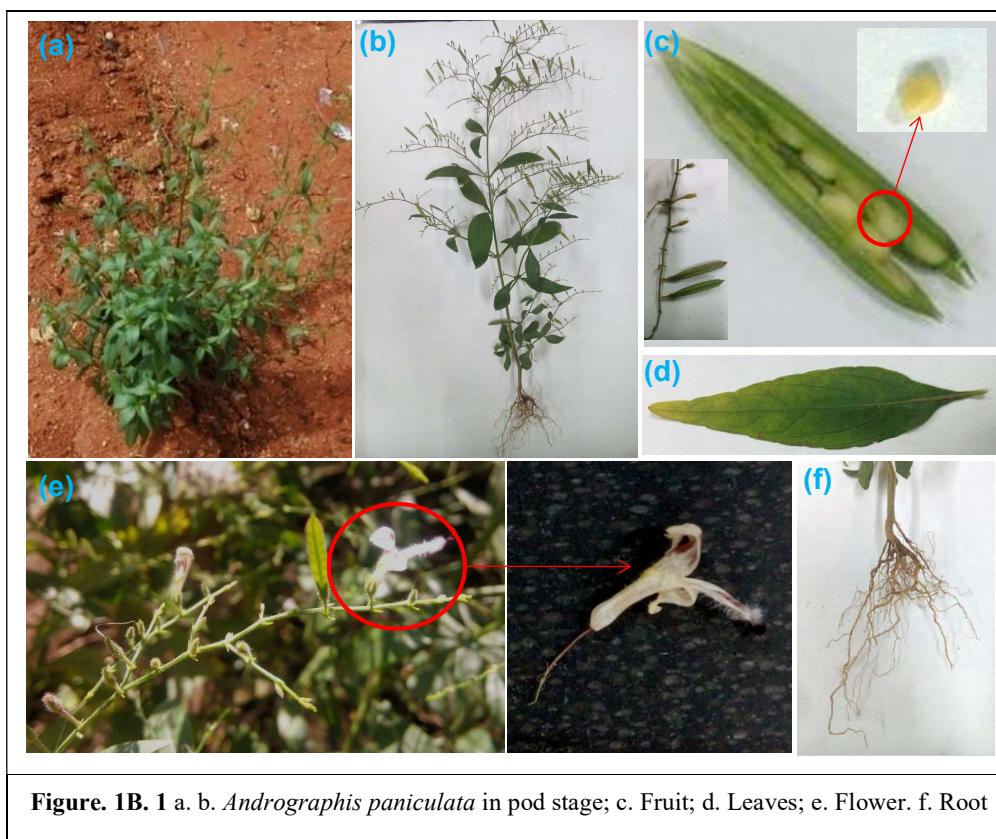


Figure. 1B. 1 a. b. *Andrographis paniculata* in pod stage; c. Fruit; d. Leaves; e. Flower. f. Root

1B.1.2 Geographical Distribution

In Southern and Southeastern Asian countries *A. paniculata* is abundantly found and spread over an enormous eco-geographical range.⁷⁶ It mainly is distributed in India, Taiwan, Srilanka, Pakistan, Indonesia, Java, and Mainland China. Native populations occur in Srilanka and India, which is the centre of diversity and origin of the species. Because of popularity, economic feasibility and medicinal use, farmers are cultivating *A. paniculata* in Jamaica, Nigeria, Malaysia, China, Indonesia, and Thailand.⁸¹

1B.2 Separation and Quantification Techniques for *A. paniculata* Terpenoids

Qualitative and quantitative analysis of phytochemicals from medicinal plants is an important aspect in term of their extraction, purification and pharmacological activities. The best analytical method for isolation and purification of phytochemicals should be simple, rapid, sensitive, and accurate. Simultaneous determination of dehydroandrographolide and andrographolide from *A. paniculata* was developed using

developed microemulsion electrokinetic chromatography (MEEKC), whereas silver ion reversed-phase high-performance liquid chromatography (Ag[I]-HPLC) one of the sensitive and rapid methods was reported for simultaneous determination 14-deoxyandrographolide, neoandrographolide, andrographolide and 14-deoxy-11,12-didehydroandrographolid.^{82,83} In Ag[I]-HPLC compounds are baseline separated in a novel way due to non-covalent interaction between compound Ag(I) ions.⁸⁴ Phytochemical analysis of *A. paniculata* using various solvents suggested that the chloroform was the efficient solvent, which contained higher phytochemicals as compared to acetone and petroleum ether.⁸⁵

Table 1B.2 *Andrographis paniculata* vernacular names.⁸⁶

Language	Name	Language	Name
Sanskrit	Kalmegha, Bhunimba and Yavatikta	Spanish	Andrografis
Marathi	Oli-kiryata	Turkish	Acılar Kralı, Acı Pas, a, Acı Bey
Kannada	Nelaberu	Philippines	Aluy, Lekha and Sinta
Malayalam	Kiriyattu	Malay	Hempedu Bumi
Gujarati	Kariyat	Russian	Andrografis
Bengali	Kalmegh	Scandinavian	Green Chiratta
Telugu	Nilavembu	Thai	Fa-Talai-Jorn, Fah-talai-jon (jone)
Hindi	Kirayat	Japanese	Senshinren
Tamil	Nilavembu	Arabic	Quasabhuvu
Oriya	Bhuinimba	English	The Creat, King of Bitters
Burmese	Se-ga-gyi	French	Chirette verte, Roi des amers
Chinese	Chuan Xin Lian	Persian	Nain-e Havandi
Azerbaijani	Acılar S,ahı, Acılar Xanı (kham)	Indonesian	Sambiloto

High-performance liquid chromatography (HPLC) method (at a lower limit of detection 0.001 % w/w) with photodiode array was developed for determination of 14-deoxy-11,12-didehydroandrographolide neoandrographolide, andrographolide.⁸⁷ Another group reported *A. paniculata* chemical fingerprinting by using HPLC with liquid chromatography-electrospray ionization mass spectrometry (LC-ESI-MS).⁸⁸ Differential pulse voltammetry (DPV) having various advantages such as high

sensitivity, low cost, environment-friendly over other techniques was used to detect andrographolide, the key component from *A. paniculata*.⁸⁹ Proton nuclear magnetic resonance, a quantitative analysis technique was used for detection labdane diterpenoid from *A. paniculata*. This technique was reported to possess disadvantages like the high instrument cost, high sample quantity and complicated sample preparation.⁸⁹ Dynamic microwave-assisted extraction (DMAE) technique in a recirculating system connected with HPLC, with advantages of high extraction yield, ultrasonic extraction with rapid analysis, and reproducibility was used to isolate andrographolide and dehydroandrographolide.⁹⁰ Kumoro and coworkers have developed the mathematical model for the determination or estimation of andrographolide extraction yield in Soxhlet extractor.⁹¹ Same group also reported the supercritical carbon dioxide extraction method for andrographolide from leaves. However, this method has limitations like high instrumental cost, and more time required for separation.⁹²

1B.3 Extraction and Purification of Compounds from *A. paniculata*

Phytochemical extraction methods play an essential role in order to preserve active constituents and their pharmacological activity.⁹³ Depending on active constituents of interest; the best extraction protocol can be selected. Extraction protocol should be simple, rapid, reproducible maintaining the active constituent in its natural form. Industrial scale extraction of the dihydroxy-6,8-dimethoxy-xanthone active constituents requires the processes to be economical, sensitive, rapid and the most importantly the processes developed could be automated.⁹⁴ Several conventional extraction procedures are reported earlier for extraction of bioactive constituents such as Soxhlet extraction, maceration, and ultrasonic extraction.⁹⁵ Besides, these conventional methods new extraction technique such as supercritical carbon dioxide, micellar extraction, vacuum-assisted (VAE) and microwave-assisted extraction were growing important area of research in the past decade.^{96,97}

Supercritical carbon dioxide extraction of andrographolide from leaves powder resulted in yield of 0.0174/ g tissue.⁹² Temperature and pressure effect on supercritical carbon dioxide extraction of andrographolide was indicated that an increase in the operating temperature, increases the rate of extraction and yield by 10 %.^{98,92} Another andrographolide extraction technique, gas anti-solvent (GAS) uses carbon dioxide as an anti-solvent with other organic solvents. (ref) In this process, andrographolide was

precipitated from acetone, dimethylformamide (DMF), methanol, and ethanol extracts. The optimized extraction was obtained using acetone at a flow rate of 5 mL /min at 35 °C resulting in the yield of 1.24 g / 100 g of the plant tissue.⁹⁹ Andrographolide, neoandrographolide, and andrograpanine extracted by supercritical fluid extraction, it has advantages over conventional solid-liquid extraction in terms of minimum solvents requirement and elimination of undesirable components, reduced sample degradation. Heat reflux extraction method was used for andrographolide extraction from the *A. paniculata* stem but it is time-consuming method and required an ample amount of hazardous solvents.⁹⁸ Vacuum-assisted quantitative extraction technique of andrographolide and 14-deoxyandrographolide from leaves at a lower temperature is a better method than heat reflux extraction.⁹⁷ Aqueous two-phase flotation (ATPF) technique was used for andrographolide extraction which has advantages in term of energy consumption and extraction.¹⁰⁰

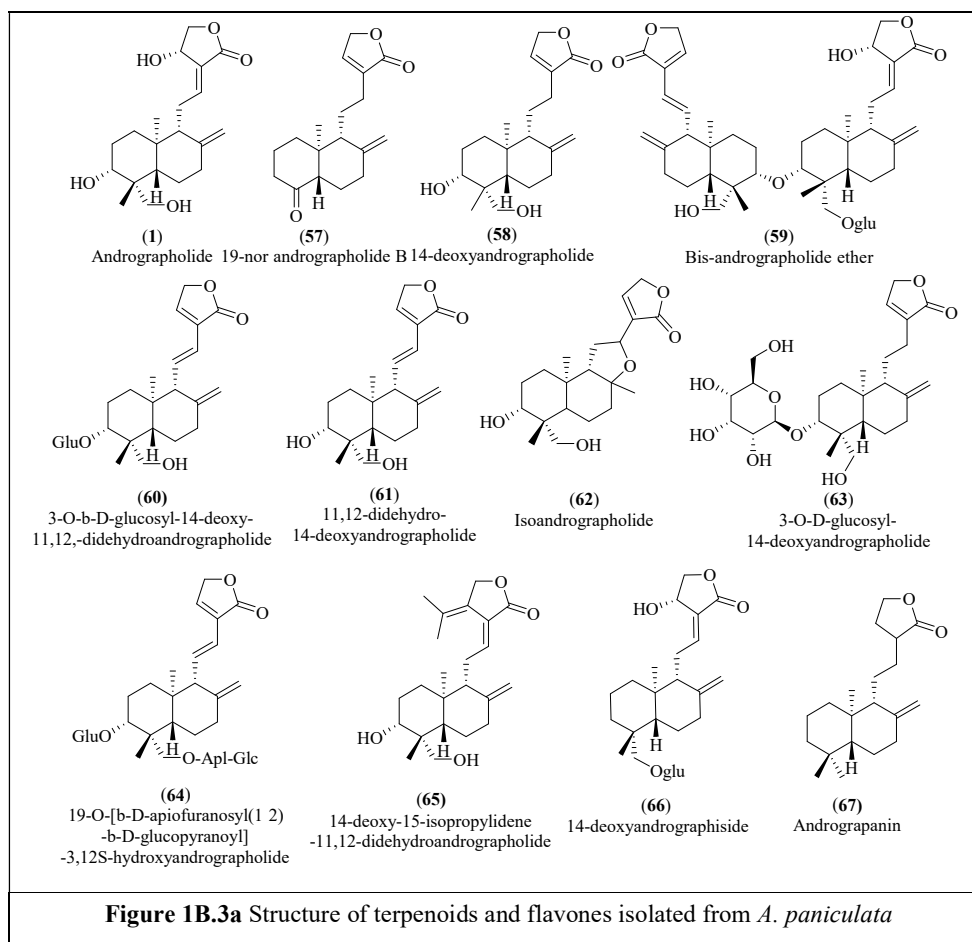
1B.4 Phytochemicals from *Andrographis paniculata*

A. paniculata is a rich source of terpenoids, which are mainly distributed in plant aerial part. Flavonoids are the major constituents present in *A. paniculata* roots, but it is also present in leaves and stem⁸⁶ Xanthonenes, noriridoids, quinic acid derivatives are also reported to be present in *A. paniculata*. Labdane diterpenoid lactone from *A. paniculata* was first time reported by Boorsma, which was named Andrographolide (**57**) by Gorter Kleipool.¹⁰¹ Flavonoids 5-hydroxy-7,8-dimethoxyflavanone (**68**) and 5-hydroxy-7,8,2', 5'-tetramethoxyflavone (**69**) was isolated from petroleum root extract of *A. paniculata* along with known flavonoid 5-hydroxy-2',7,8-dimethoxyflavone (**70**) (Figure 1B.2).¹⁰² Isolation of a novel diterpenoid lactone and flavones from *A. paniculata* had reported by Reddy and coworkers.¹⁰³ Terpenoid and flavonoid are characterised as 14-deoxy-15-isopropylidene-11,12-didehydroandrographolide (**65**) and (2S)-5,2β-dihydroxy-7,8-dimethoxyflavone (**71**) respectively. Along with novel compounds, known flavonoids were also isolated and characterised as 7-O-methyl dihydrowogonin, 7-O-methylwogonin (**72**), skullcap flavone 2'-methyl ether, 7-O-methylwogonin-5-O-glucoside, Dihydroskullcapflavone (**73**).¹⁰³ Isolation of *p*-hydroxybenzoic esters (ethyl, methyl) using HPLC was reported by Li and coworkers.¹⁰⁴ A phytochemical investigation of chloroform fraction of methanolic *A. paniculata* root extract resulted

into the isolation of 5,7,2',3'-tetramethoxyflavanone (**75**) and 5-hydroxy-2',5,8-trimethoxyflavone, along with andrographolide and polyphenols.⁸⁷ Novel terpenoids, along with other known diterpenoids are isolated from *A. paniculata* from methanolic extract of the aerial part. The chemical investigation suggested 22-carbon diterpenoid, which was characterized as bis-andrographolide ether (**59**).¹⁰⁵ Two new labdane diterpenoids andrograpanin (**67**) and isoandrographolide (**62**) were isolated from the leaf methanolic extract by HPLC. Isolation followed by HPLC purification of water and methanolic *A. paniculata* extract after chloroform extraction resulted in two new flavones andropaniculosin-A and andropaniculoside.¹⁰⁶ Two new flavonoid glycosides along with one diterpenoid 5-hydroxy-7,8-dimethoxy (2*R*)-flavanone-5-*O*- β -D-glucopyranoside and 5-hydroxy-7,8,2',5'-tetramethoxy-flavone-5-*O*- β -D-glucopyranoside and andrograpanin, respectively from the whole plant methanolic extract was reported.¹⁰⁷ Silica gel column purification of ethyl acetate aerial crude extract of *A. paniculata* resulted in the isolation of a new labdane diterpenoid 3-*O*-acetyl-14-deoxy-11,12-didehydroandrographolide (Figure 1B.3).¹⁰⁸ Four flavones from ethyl acetate and hexane partition of ethanolic root and leaves extracts resulted in isolation and characterization of flavonoids viz., 5,7,4'-trihydroxyflavone, 5-hydroxy-7,8-dimethoxyflavone, 5-hydroxy-7,8,2',-tetramethoxyflavone, and 5,4'-dihydroxy-7,8,2',3'-tetramethoxyflavone (**69**), one flavanone (5-hydroxy-7,8-dimethoxyflavone (**68**)).¹⁰⁹ Polysaccharide (galactose, mannose, fructose, arabinose and rhamnose; 15.4:2.5:4.3:1.5:1.6) was isolated from the *A. paniculata* in 2012 year.¹¹⁰ Balmain and coworkers have isolated labdane type diterpenoid 14-deoxy-11,12-didehydroandrographolide (**61**) together with 14-deoxyandrographolide (**58**), 14-deoxyandrographiside, and andrographiside.¹¹¹ Six labdane diterpenoids were isolated from acetone extract of aerial part, which are 3-*O*- β -D-glucopyranosyl-14-andrographolide, 14-deoxyandrographolide, andrographatoside, 3-*O*- α -D-glucopyranosyl-14,19-dideoxyandrographolide, 19-*O*-[β -D-apiofuranosyl(1-2)- β -D-glucopyranoyl]-3,12*S*-hydroxyandrographolide (**64**), and 14-deoxy-17-hydroxyandrographolide.¹¹² Diterpenoids andropanoside and isoandrographolide from methanolic extract were isolated and characterized for the first time.¹¹³ Purification of ethyl acetate fraction lead to the isolation of a new labdane diterpenoid 19-*O*-acetyl-14-deoxy-11, 12-didehydroandrographolide.¹¹⁴

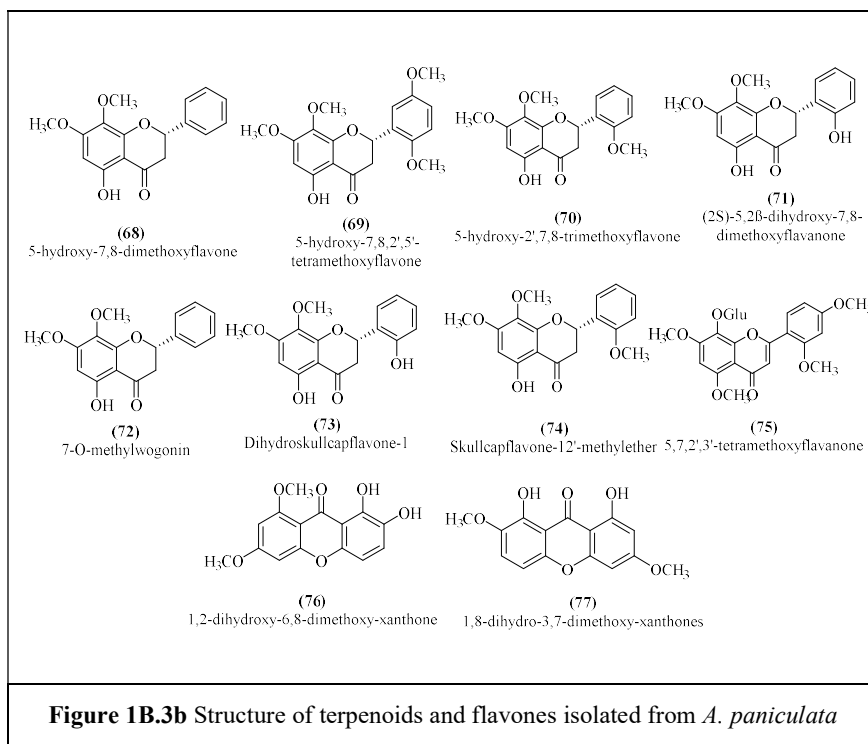
1B.5 Ethnobotany of *A. paniculata*

In Asian countries, *A. paniculata* is a source to treat disorders such as respiratory tract infections, sore throat, fevers, and gastric infections.^{77,115} In Ayurvedic texts and pharmacopoeia, *A. paniculata* is one of the constituents of many ayurvedic preparations.



The whole plant is applied locally or orally for treating a body heat; it also used as an antidote for insects poisons and against snakebite (Cobra, Russell's viper, Banded Krait).¹¹⁶ The leaves aqueous extract is used as a common household remedy for loss of appetite, flatulence, griping, and diarrhoea. It is also used as a tonic in order to eliminate intestinal worms. The tribals from eastern India kheria, khatra region, West Bengal use an infusion of the whole plant to cure fever. Moreover, *A. paniculata* was reported to arrest the progress of the Influenza epidemic in India around 1919. In Chinese traditional medicine, the plant is used for the common cold, fever, inflammation infection,

diarrhoea. In Malaysian traditional medicine, the decoction of leaves has been used in order to treat antidiabetic and antihypertensive disorders.^{117,118,119}



1B.6 Pharmacology

(a) Anticancer Activity

A. paniculata extracts and isolated terpenoids, flavonoids and their synthetic derivatives are reported to exhibit promising cytotoxicity against several cancer cell lines. Cytotoxic activity of diterpenoids isolated from *A. paniculata* against different cancer cell lines has been listed in (Table 1B.3). Andrographolide, the key lead metabolite exhibited potent anticancer activity against several cancer cell line compared to the other diterpenoids from *A. paniculata*.

Table 1B.3 Cytotoxic activity of compounds from *A. paniculata* against cancer cell lines

Compounds	Cancer cell	Cytotoxic potency
Andrographolide	MCF-7/ADR	IC ₅₀ = 15 μM
	NCI/ADR-RES	IC ₅₀ = 15 μM
	M14	IC ₅₀ = 11 μM
	U251	IC ₅₀ = 10 μM
	SKOV3	IC ₅₀ = 18 μM
	SW620	IC ₅₀ = 11 μM
	KB	IC ₅₀ = 16 μM
	DU145	IC ₅₀ = 12 μM
	P388	IC ₅₀ = 28 μM
	T-47D	EC ₅₀ = 13.3 μg/mL
	Caov-3	EC ₅₀ = 23.6 μg/mL
	HepG2	EC ₅₀ = 29.4 μg/mL
	NCI-H23	EC ₅₀ = 9.9 μg/mL
	Hs-578T	EC ₅₀ = 17.3 μg/mL
	NCI/ADR-RES	IC ₅₀ = >100 μM
14-deoxyandrographolide	U251	IC ₅₀ = >100 μM
	SW620 H522	IC ₅₀ = >100 μM
	M14	IC ₅₀ = >100 μM
	SKOV3	IC ₅₀ = >100 μM
	DU145	IC ₅₀ = >100 μM
	A498	IC ₅₀ = >100 μM
	T-47D	EC ₅₀ = 2.8 μg/mL
	HepG2	EC ₅₀ = 28.3 μg/mL
	NCI/ADR-RES	IC ₅₀ = >30 μM
	NCI-H23	EC ₅₀ = 26.4 μg/mL
14-deoxy-11, 12-didehydro andrographolide	U251	IC ₅₀ = >100 μM
	SW620 H522	IC ₅₀ = >100 μM

	SW620 H522	IC ₅₀ => 80 μM
	M14	IC ₅₀ => 60 μM
	SKOV3	IC ₅₀ =>100 μM
	DU145	IC ₅₀ =>100 μM
	A498	IC ₅₀ => 40 μM
Neoandrographolide	T-47D	EC ₅₀ = 18.1 μg/mL
	Caov-3	ND
	HepG2	ND
	NCI-H23	ND
	Hs-578T	ND
Andrographiside	T-47D	ND
	Caov-3	ND
	HepG2	ND
	NCI-H23	ND
	Hs-578T	ND

† IC₅₀ (50 % growth inhibitory concentration), ED₅₀ (50 % Effective dose), ND: Not determined, values of the compound may be higher than maximum concentration tested, no inhibition or positive growth.

Andrographolide exhibited anticancer activity against different tumor cell lines of various types of cancers.¹²⁰ Antiproliferative activities of xanthenes isolated from *A. paniculata* were found to be cytotoxic with IC₅₀ > 32 μg/mL against mammalian cells in comparison to 1, 2-dihydroxy-6,8-dimethoxy-xanthone which resulted to be non-cytotoxic¹¹⁸. Its antiproliferative potential against colon-205 cells was reported with an IC₅₀ of 0.05 mM.¹²¹ In another study, among flavonoids, flavones and labdane diterpenoid from *A. paniculata*, 14-deoxy-14,15-didehydroandrographolide exhibited potent cytotoxic effect due to increase in the proportion G₀/G₁ phase of the cell, and decrease in the percentage of cells those in the S phase.¹²² Andrographolide showed significant anticancer activity compared to other isolated diterpenoids from *A. paniculata* against leukaemia cells of mouse myeloid by inducing cell differentiation.¹²³ In another report, andrographolide exhibited cytotoxicity against human colorectal carcinoma LoVo cells by inhibiting the cell cycle progression.¹²⁴ (ref) Cytotoxicity

studies using andrographolide against promyelocytic leukemic cells (HL-60, NB4) suggested that andrographolide inhibited the growth by apoptosis and inducing cell differentiation.¹²⁵ (ref) Furthermore, metastasis and angiogenesis inhibition studies revealed that andrographolide inhibits Janus tyrosine kinases-signal transducers, activators of NF-kappa β signalling pathways, phosphatidylinositol 3-kinase, cyclin-dependent kinases, and metalloproteinases, proinflammatory cytokines, IL-2, with induction of tumor suppressor proteins p53 and p21.^{126,120} It is reported that andrographolide down-regulates PI3 kinase/Akt activation leading to inhibition of proangiogenic molecules such as OPN, and VEGF.^{127,128} Inhibition of *in vivo* tumor growth by andrographolide is mediated by stimulation of cytotoxic T-lymphocyte production through enhance secretion of IL-2 and IFN-c by T cells. Furthermore, studies reveal that andrographolide delays tumor growth by improving the sensitization of cells to radiation therapy.^{129,130,127} Andrographolide, 14-deoxy-11,12-didehydroandrographolide and 14-deoxyandrographolide showed enhanced proliferation and IL-2 induction in cells human peripheral blood lymphocytes.¹³¹

(b) Antimicrobial Activity

A. paniculata leaf methanolic extract exhibits antibacterial activity against *S. aureus*, *E. faecalis* and *S. aureus* BHU with a zone of inhibition diameter, being 26 mm, 24 mm, and 18 mm respectively (Table 1B.4).¹³² Chloroform and its mixture with HCl (1 M, at 2 mL/ 100 mL) extract of *A. paniculata* showed antimicrobial activity against gram-negative bacteria *Escherichia coli*, *Pseudomonas aeruginosa*, *Klebsiella pneumoniae* and gram-positive bacteria *Bacillus subtilis*, *Enterobacter faecalis*, *Staphylococcus epidermis*. Crude powdered *Andrographis paniculata* is effective against *Salmonella*, *E.coli*, and *Streptococci*.¹³³ Chloroform extract is more active compared to the chloroform with HCL. Chloroform extracts (250 μ g/ μ L) showed antimicrobial activity against *S. typhimurium*, *S. epidermidis*, *E. coli*, *P. aeruginosa*, and *E. faecalis* with a zone of inhibition diameter, being 18 mm, 20 mm, 28 mm and 35 mm respectively.¹³⁴ The ethanolic extract showed potent antibacterial activity against *Enterohemorrhagic* strains of *E.coli*.¹³⁵

Table 1B.4 Antibacterial potential of 75 % methanol extract of *A. paniculata* leaves against different bacteria

Bacteria	Zone of inhibition diameter (mm) at the well content (3.0 mg)	Zone of inhibition with Streptomycin (10/300 µg)
<i>S. aureus</i> ATCC 25923 18	26	20 (10 µg)
<i>S. aureus</i> BHU	18	27 (300 µg)
<i>E. faecalis</i>	24	20 (300 µg)
<i>P. aeruginosa</i> ATCC 27853	ND*	17 (10 µg)
<i>P. vulgaris</i>	ND	18 (10 µg)
<i>E. coli</i> ATCC 35218	ND	20 (10 µg)

* ND: Not detected.

Andrographis paniculata leaf extracts in various solvents like water, acetone, ethanol, and chloroform were tested against bacteria (*P. aeruginosa*, *B. subtilis*, *S. aureus*, fungal strains like *A. niger* and *P. chrysogenum*). Acetone and ethanol extracts were found to be most effective against *S. aureus* and *B. subtilis*.¹³⁶ Anti-microbial activities of chloroform extracts of *A. paniculata* root and stem at a concentration of 100 µg/ mL indicated that stem extract, chloroform stem extract showed significant activity, but root extract showed moderate activity compared to the benzylpenicillin. Both the extract exhibits moderate antifungal activities compared to fluconazole.¹³⁷ Singha *et al.* reported antimicrobial activity of aqueous extract of *A. paniculata*, andrographolide and arabinogalactan proteins (Table 1B.4) isolated from the same.¹³⁸ Aqueous extract exhibited significant antimicrobial activity compared to arabinogalactan proteins. Whole plant and leaves of *A. paniculata* extracted in cold and hot methanol were evaluated for antibacterial activity. Cold methanolic whole plant extracts showed moderate antibacterial (MTCC-452), while hot methanol leave extract exhibited significant antibacterial activity against both the bacteria.⁸¹ MIC values for both isolated compounds ranged from 15.6-250 µg/mL. Andrographolide exerted the highest MIC value against *P. aeruginosa* (250 µg/mL) while the lowest was exerted against *S.aureus* (15.6 µg/mL). Antibacterial activity indexes (AbI) in mm of *A. paniculata* MeOH extract of the whole plant was found against Gram-positive *S.aureus*, *M. luteus*, *S. pyogenes* (13.9 µg/mL) Gram-negative *P.mirabilis*, *P.seruginosa*.^{132,138} DCM and methanol extracts of *A. paniculata* showed potent anti-fungal activities. DCM extract exhibited MIC value of 100 µg/ mL against *Candida albicans*, *Microsporum canis* and

Candida tropicalis, whereas it exhibited MIC value 250 µg/mL against *A. niger*. Antifungal activity with a MIC value of 150 µg/mL was exhibited by ethanolic extracts of the whole plant against *A. niger* and *C. tropicalis*. Potent antiviral activities are reported by *A. paniculata* crude extracts and andrographolide. The ethanolic extract and andrographolide inhibits the expression of epestei-Bar virus (EBV) lytic proteins Rta, zta, and EAD. *Andrographis paniculata* showed antiviral activity against DENV infected Vero E6 cell.¹³⁹ Andrographolide exhibited antiviral activity against herpes simplex virus.¹⁴⁰

Table 1B.5 Antibacterial and antifungal activity of *A. paniculata* fractions¹³⁸

Microorganism	Zone of inhibition diameter (mm), 10 mg/ disc					
	<i>A. paniculata</i> extract	Andro. ^a	Arabinogalactan ^a	Streptomycin*	Gentamycin*	Nystatin*
<i>B. subtilis</i>	16.3 ± 0.58	13.3 ± 1.00	14.0 ± 1.00	20.0 ± 1.00	---	---
<i>S. aureus</i>	₋ ^b	₋ ^b	₋ ^b	20.0 ± 1.00	---	---
<i>E. coli</i>	18.3 ± 0.33	₋ ^b	16.0 ± 1.00	---	22.0 ± 1.00	---
<i>P. aeruginosa</i>	19.3 ± 0.33	₋ ^b	17.6 ± 0.34	---	24.0 ± 1.00	---
<i>C. albicans</i>	18.3 ± 0.33	14.6 ± 0.34	15.6 ± 0.34	---	---	19.0 ± 1.00

*Positive control (100 µg/ disc)^a. Results are mean ± SD values of three replicates, 10 mg/disc; ^b No activity (diameter of inhibition zone is less than 10 mm)

(c) Insecticidal Activity

Insecticidal activity of various solvent extracts from *A. paniculata* aerial part was tested against *Cowpea weevil* (*Collosobruchus chinensis* L.). Methanolic extract is the most potent than ethyl acetate, acetone extracts with 72.01 % adult's mortality with lowest total egg count.¹⁴¹ *A. paniculata* leaf extract in hexane, methanol, chloroform, and benzene, showed larvicidal along with ovicidal activities against *Culex quinquefasciatus*. Whereas methanol and ethyl acetate extracts exhibited ovicidal activity against *C. quinquefasciatus* and *Aedes aegypti*.¹⁴² Elango *et al.* reported the effect of hexane extract of *A. paniculata* against *Culex tritaeniorhynchus* and *Aedes aegypti* and found to be a potent repellent.¹⁴³

(d) Anti-malarial Activity

Antiprotozoal activities are reported by various extracts of *A. paniculata*.¹⁴⁴ The chloroform and methanol extract inhibited malarial parasite completely within 24 hr at a concentration of 0.05 mg/mL and 0.25 mg/mL, respectively.¹⁴⁵ Ethanolic extract of *A. paniculata* showed inhibited *Plasmodium falciparum* activity with an IC₅₀ of 7.2 µg/mL. (ref)¹⁴⁰ Another study reported the antimalarial activity of four xanthenes isolated from *A. paniculata* roots. Dihydroxy-6,8-dimethoxy-xanthone exhibited an IC₅₀ value of 4 µg/mL (Table 1B.6).¹⁴⁶ The antimalarial activity of *Andrographis paniculata* is due to reactivation of the antioxidant enzyme superoxide dismutase.

Table 1B.6 *in vitro* antiplasmodial activity Xanthenes isolated from *A. paniculata*

Compound	Activity (IC ₅₀ µg/mL)		
	<i>T. cruzi</i>	<i>T. b. brucei</i>	<i>L. infantum</i>
1,8-dihydroxy-3,7-dimethoxy xanthone	4	>32	>32
4,8-dihydroxy-2,7-dimethoxy xanthone	>32	>32	>32
1,2-dihydroxy-6,8-dimethoxy xanthone	31	4.6	8.0
3,7,8-trimethoxy-1- xanthone	>32	>32	>32
Nifurtimox	--	0.29	--
Stibogluconate	--	--	7.13
Suramin*	0.092	--	--

IC₅₀ µg > 32 = nontoxic

1C.1 *Wedelia paludosa*

W. paludosa DC, a flowering plant belongs to genus *Wedelia* consisting of 60 species. It is a small, herbaceous, creeping plant used for medicinal as well as a decorative purpose.¹⁴⁷ *W. paludosa*, an ornamental plant

Order	<i>Asterales</i>
Family	<i>Asteraceae</i>
Subfamily	<i>Asteroideae</i>
Tribe	<i>Heliantheae</i>
Subtribe	<i>Ecliptinae</i>
Genus	<i>Wedelia</i>

commonly known as creeping daisy, creeping-oxeye, and yellow dots, Singapore daisy, in English trailing daisy is reclassified as *Acmela brasiliensis* belonging to family *Asteraceae* (sunflower) and tribe *Heliantheae*. In Brazil, it is popularly known as “pseudo-arnica”, “pingo-de-our” or

“margaridilo”.^{148,149} It is listed in the IUCN's “List of the world's 100 invasive species”.

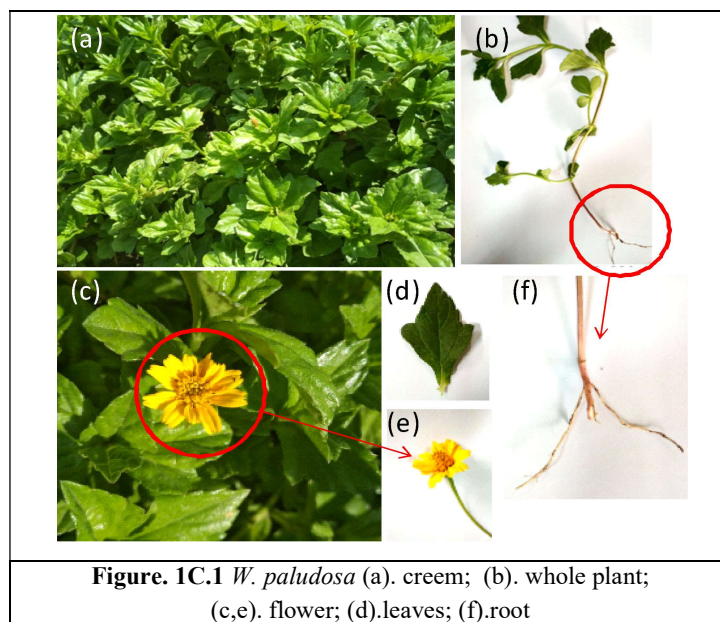
It is commonly known as.

1C.1.2 Geographical Distribution

W. paludosa is distributed around the warm, tropical, temperate regions and countries like India, Japan, Burma, Brazil, and Ceylon. It is also distributed on South Africa, Hong Kong, Pacific Islands, Indonesia, and Sri Lanka.¹⁴⁹

1C.1.3 Botanical Description

Wedelia paludosa is a creeping evergreen perennial herb with roots at nodes. Branches are spread widely over ground up to 30 cm in height form mat, under the tree. The stem is rounded faint green, brittle, branched, rooting at nodes. The stem is 10-30 cm long, and new plants formed when stem touches the soil, flower portion is ascending. Leaves are simple, opposite to sub-opposite, hairy, dark green above and lighter green at the bottom.¹⁵⁰ It is fleshy ovate with three lobes, usually with pairs of lateral lobes. Leaf has bowed and brochidodrome venation and chaffy bracts are lanceolate, rigid. Length is about 4-9 cm; the width is 2-5 cm, 3-10 cm long peduncles of the margin with a short petiole.¹⁴⁷ The flowers which grow in the axils of the leaf up to 10 cm height with the hemispherical pedicel varying 3-10 cm are bright yellow, solitary, daisy-like with 1 inch and available throughout the year (Figure. 1C.1).^{151,152} The seeds of *W. paludosa* are 4-5 mm long and mostly non-fertile hence showed vegetative propagation.



1C.2 Phytochemicals from *W. paludosa*

Very few reports are available on the extraction and purification of compounds from *W. paludosa*. Iso-kaurenoic acids from *W. paludosa* plant powder ethanolic extract first time isolated by Batista *et al.* The ethanol extract was fractionated over the column, chromatographic separation yield mixture of three compounds. Further purification yield pure compounds, which were characterized as grandiflorenic acid, kaurenoic acid, and iso-kaurenoic acid. In another report, Batista *et al.* reported the isolation of diterpenoids from the aerial part ethanolic extract of *W. paludosa*. Isolated compounds were characterized as kaurenoic acid (**78**), grandiflorenic acid (**79**), 3 α -tigloyloxykaur-16-*en*-19-oic acid (**86**) and (22-E)-stigmasta-5,22-dien-3 β -ol, β -amyrin (**84**), friedelan-3 β -ol, *ent*-kaur-16 α -ol-19-oic acid (Table 1C.1).^{153,154}

Table 1C.1 Structure of compounds isolated from *W. paludosa*.

no	Name/ Molecular formula	Structure	no	Name/ Molecular formula	Structure
1.	Kaurenoic acid $C_{20}H_{30}O_2$ (78)		8.	Iso-kaurenoic acid $C_{20}H_{30}O_2$ (85)	
2.	Grandiflorenic acid $C_{20}H_{28}O_2$ (79)		9..	3 α - tigloyloxykaur- 16- <i>en</i> -19-oic acid $C_{25}H_{36}O_4$ (86)	
3.	3 α - cinnamoyloxykaur- 16- <i>en</i> -19-oic acid, $C_{29}H_{36}O_4$ (80)		10..	Luteolin $C_{15}H_{10}O_6$ (87)	
4.	Paludolactone $C_{23}H_{32}O_9$ (81)		11.	Eudesmanolide $C_{23}H_{32}O_9$ (88)	
5.	Eudesmanolide lactones A $C_{23}H_{32}O_9$ (82)		12.	Eudesmanolide lactones B $C_{23}H_{32}O_9$ (89)	
6.	Amyrin acetate $C_{32}H_{52}O_2$ (83)		13.	Oleanic acid $C_{30}H_{48}O_2$ (90)	
7.	Amyrine $C_{30}H_{50}O$ (84)		14.	α -sitosterol $C_{29}H_{50}O$ (91)	

W. paludosa aerial dried part and root are extracted in various solvents such as dichloromethane, ethyl acetate, butanol, and hexane. Kaurenoic acid was obtained as a significant constituent after column chromatographic purification of hexane extract, whereas luteolin was obtained after dichloromethane fraction purification.¹⁵⁵ The volatile compounds from the essential oil of leaves of *W. paludosa* and *W. trilobata* were characterized.¹⁵⁶ *W. paludosa* essential oil majorly constitute terpenoids along with the aliphatic alcohols as a minor constituent. Sesquiterpenoid eudesmanolide lactones A (**82**) from *W. paludosa* flowers ethanolic extract was isolated first time by Ferreira.¹⁵⁷ The flowers were dry, soaked in 95 % ethanol and extracted at room temperature. The extract obtained was concentrated, dissolved in methanol: water and extracted with petrol further chromatographed on florisil (magnesium-silicate) column.¹⁵⁸ Novel eudesmanolide lactone along with other compounds were isolated from *W. paludosa* ethanolic extract. Compounds were characterized as paludolactone a novel eudesmanolide lactone B (**89**) along with known compounds eudesmanolide, kaurenoic, stigmasterol, and oleanone.¹⁵⁸

1C.4 Pharmacological Activities

The earlier report suggested that *W. paludosa solvent* extracts and compounds isolated from it exhibited several pharmacological activities such as antimicrobial, anti-inflammatory, antidiabetic, and anticancerous etc. Many plants of this genus are also utilized as a conventional herbal medicine throughout the world. In Brazil, rural communities use the plant for herbal preparations in order to treat various diseases such as fever, inflammation, and respiratory tract diseases treatment.

Table 1C.1 Effect of *W. paludosa*, acetyl salicylic acid, dipyrene indomethacin, and acetaminophen, hydroalcoholic extract Acetic acid-induced abdominal constrictions in mice

Treatment	Dose (mg/ kg)	Number of writhes	% Inhibition
Fraction n-Hexane	3	19.4 ± 7	55
Fraction dichloromethane	3	12.2 ± 6	72
Fraction ethyl acetate	3	23.9 ± 6	45
Fraction n-butanol	3	23.9 ± 5	45
Dipyrene	10	29.1 ± 8	33
Indomethacin	10	27.0 ± 4	38
Acetaminophen	10	28.3 ± 1	35
Acetyl salicylic acid	10	27.0 ± 2	38
Control	---	43.5 ± 3	00

W. paludosa, various solvent extracts along with the pure compounds kaurenoic acid, luteolin were studied for antinociceptive effect. Kaurenoic acid and luteolin showed antinociceptive activity against acetic acid-induced constrictions in mice as compared to the analgesic drugs, e.g. acetaminophen, indomethacin (Table 1C.1).¹⁵⁵ In another study for the screening of compounds for trypanosomicidal activity from *W. paludosa*, 3 α -angeloi-loxy-ent-kaur-16-en-19-oic acid showed activity at the lowest concentration of 0.68 mg/mL, whereas (22-E)-stigmasta-5-22-dien-3 β -ol, β -amyirin acetate and friedelan-3 β -ol-ent-kaur-16- α -ol-19-oic acid, were inactive (Table 1C. 2).¹⁵⁹ The study conducted for screening *W. paludosa* flower extracts along with kaurenoic acid and luteolin for its antifungal activity resulted it to be effective against *T. metagrophytes*. The hexane and DCM extract exhibited an MIC 500, 250 μ g/mL respectively (Table 1C.3). Kaurenoic acid is most active against *T. rubrum* and *E. floccosum* with MIC of 100 μ g/mL and 50 μ g/mL, respectively as compared to other fractions and luteolin. Luteolin is inactive against other screened fungi but exhibits antifungal activity against *T. rubrum* with MIC 125 μ g/mL and *E. floccosum* at MIC of 250 μ g/mL.¹⁶⁰ Kaurenoic acid exhibited hypoglycemic effect in alloxan-induced diabetic rats rapidly compared to the glibenclamide used as reference drugs (Table 1C.4).¹⁶¹

Table 1C.2 *in vitro* effect of compounds against *Tryptosoma cruzi* trypomastigotes.

Compounds	Concentration (mg/mL)		
	2.73	1.36	0.68
<i>ent</i> -kaur-16-en-19-oic acid	-(TL)	-(TL)	+
friedelan-3 β -ol	++	++	++
<i>ent</i> -kaur-16 α -ol-19-oic acid	++	++	++
β -amyirin acetate	++	++	++
<i>ent</i> -kaur-9(11),16(17)-dien-19-oic acid	-(TL)	-(TL)	-(TL)
(22E)-stigmasta-5,22-dien-3 β -ol	++	++	++
3 α -angeloi-loxy- <i>ent</i> -kaur-16-en-19-oic acid	-(L)	-(L)	-(L)
Control			
DMSO	++	++	++
Gentian violet	-	-	-

TL: Total lysis of erythrocytes; L: Partial lysis of erythrocytes; - : Absence of *T. cruzi* (active); +: Number of *T. cruzi* trypomastigotes smaller than in control; ++: Number of *T. cruzi* trypomastigotes equal to the control;

Table 1C.3 Minimal inhibitory concentrations (MICs in mg/mL) of different fractions and two pure compounds, kaurenoic acid (1) and luteolin (2), of flowers from *Wedelia paludosa*

Fractions	Ca	Ct	Cn	Sc	Afu	Afl	An	Mc	Mg	Ef
Hexane	1000	>1000	>100 0	>100 0	>100 0	>100 0	>100 0	>100 0	>100 0	>1000
Dichlorome thane	>1000	>1000	>100 0	>100 0	>100 0	>100 0	>100 0	1000	>100 0	1000
Ethyl acetate	>1000	>1000	>100 0	>100 0	>100 0	>100 0	>100 0	1000	>100 0	>1000
Butanol	>1000	>1000	>100 0	>100 0	>100 0	>100 0	>100 0	1000	>100 0	>1000
Kaurenoic acid	>250	>250	>250	>250	>250	>250	>250	>250	>250	>250
Luteolin	>250	>250	>250	>250	>250	>250	>250	>250	>250	>250

Candida albicans (Ca); *Candida tropicalis* (Ct); *Cryptococcus neoformans* (Cn); *Saccharomyces cerevisiae* (Sc); *Aspergillus fumigatus* (Afu); *Aspergillus flavus* (Afl); *Aspergillus niger* (An); *Microsporium canis* (Mc);

Table 1C.4 Effect of kaurenoic acid (1), saline (control), or glibenclamide on blood glucose levels in alloxan-induced diabetic rats.

	Basal value	1 h	2 h	4 h	6 h
Normal control (n=9)	64.02 ± 13.58	126.92 ± 28.43**	113.29 ± 13.21**	113.28 23.92**	78.15 ± 14.02
Hyperglycemic contro (n=6)	1325.33 ± 80.9	448.11 ± 91.8	502.59 ±124.4*	539.58 ± 122.28*	577.4 ± 139.03**
Glibenclamide (40 mg/kg) (n=6)	256.56 ± 38.59	470.52 ± 100.75**	434.3 ± 99.08**	365.53 ± 53.95	332.03 ± 69.93
Kaurenoic acid (10 mg/kg) (n=5)	316.92 ± 130.05	587.58 ± 78.27**	413.26 ± 131.33	421.92 ± 112.99	296.75 ± 78.09

* p < 0.05; ** p < 0.01 (Dunnett test).

Toxicity studies of aerial part hydroalcoholic extract from *W. paludosa* in Swiss mice resulted in a lethal dose to be higher than 4000 mg/ Kg in case of the acute model. Moreover, the treatment did not affect haematological parameters and corporal weight in the subacute model (Table 1C.5). No change in hepatic enzymes was seen, except for the changes in liver weight occurred suggesting that *W. paludosa* did not alter liver function.¹⁶²

Table 1C.5 Hematological parameters after 15 days of treatment with the *W. paludosa* extract.

Parameter	Control	1000 mg/kg	4000 mg/kg
Red blood cell (mm ³)	9.043 ± 0.370	8.095 ± 0.451	8.81 ± 0.129
Hematocrit (%)	46.1 ± 4.63	44.1 ± 1.524	47.049 ± 2.63
Leukocyte (x106/mL)	7.550 ± 2.192	8.730 ± 2.493	7.14 ± 1.689

Values are the mean of 10 animals ± S.D. (Dunnett's test). No significant difference was observed in any parameter.

In another study effect of kaurenoic acid containing ointments for its topical anti-inflammatory activity suggested that kaurenoic acid exhibits more significant anti-inflammatory effect compared to the positive control. Lanette is anionic cream having permeation agents like bisabolol, isopropyl myristate, urea. Kaurenoic acid (100 µg/g) was added from the stock solution of propylene glycol (1 mg/mL) in the various cream formulations (Table 1C.6).¹⁶³

Table 1C.6 Formulations of a cream containing KA and permeation enhancers.

Ingredients	Composition (%)				
	LO*	LA*	LU*	LUA*	LML*
Anionic Wax	15	15	15	15	15
Preservatives	0.2	0.2	0.2	0.2	0.2
Propylene glycol	5.0	5.0	5.0	5.0	5.0
EDTA	0.1	0.1	0.1	0.1	0.1
BHT	0.01	0.01	0.01	0.01	0.01
Water	qsp	qsp	qsp	qsp	qsp
bisabolol	--	1.0	--	1.0	--
Isodecyl oleate	5.0	--	--	--	--
Urea	--	--	10	10	--
Isopropyl myristate	--	--	--	--	1.0
Soy lecithin	--	--	--	--	0.5

*LO – cream containing isodecyl oleate; LA – cream containing alpha bisabolol; LU - cream containing urea; LUA – cream containing urea and alpha bisabolol; LML – cream containing isopropyl myristate and soy lecithin.

Cytotoxicity of *W. paludosa* dichloromethane, water, hydromethanol fractions along with the kaurenoic acid and grandiflorenic acid were evaluated by using the brine shrimp lethality bioassay (BSLB). Kaurenoic acid exhibited an LC₅₀ of 15.9 µg/ mL and is more cytotoxic in comparison compared to grandiflorenic acid, which showed an

LC₅₀ of 29.8 µg/mL. The crude hydromethanolic and DCM extracts exhibited , LC₅₀ of 980.1 µg/mL, 140.6 µg/mL, respectively with water extract to be inactive (Table 1C.7).¹⁶⁴

Table 1C.7 Cytotoxicity of *W. paludosa* fractions, kaurenoic acid, and Grandiflorenic acid.

	LC ₅₀ (µg/mL)	95 % confidence interval (µg/mL)
Hydromethanolic extract	980.1	707.3- 1800.1
Water	>> 1000 ^a	---
Dichloromethane	140.6	127.9-154.6
Kaurenoic acid	15.9	13.5 -20.6
Grandiflorenic acid	29.8	27.2-32.4
Lapachol	68.1	57.2 -79.1

^a 100 % of survivors at maximum assayed WF concentration (1000 µg/mL) *Microsporium gypseum* (Mg); *Epidermophyton floccosum* (Ef); *Trichophyton rubrum* (Tr); *Trichophyton metagrophytes* (Tm)

1D.1 *Glochidion tomentosum*

Glochidion tomentosum Dalz. *Phyllanthaceae* family and tribe *Heliantheae* is a a medium size evergreen medicinal tree endemic to Western Ghats region of Southern

Class	<i>Magnoliopsida</i>
Order	<i>Malpighiales</i>
Family	<i>Phyllanthaceae</i>
Tribe	<i>Heliantheae</i>
Genus	<i>Glochidion</i>
Species	<i>tomentosum</i>



India, tropical semi-evergreen forests. The vernacular name in Kannada is niru chelle, in Malayalam Nellikkapuli, Pageri in Andhra Pradesh.¹⁶⁵

1D. 2 Botanical Description

G. tomentosum is a small tree to 10 m high, with the branchlets and pink-red blaze, covered with densely matted hair, i.e. tomentose. *G. tomentosum* is dicotyledonous plant and flowering, fruiting from March to May.¹⁶⁶

Leaves are simple, alternate, 2-8 mm long petiole, with lateral green stipules rounded or acute at base. Leaves are sometime suborbicular, cordate, base oblique, round, glabrous above and

tomentose inside.¹⁶⁷ Flowers are unisexual yellow with 8-10 mm long adnate peduncle to the stem supra-axillary umbels. Male flowers connate by their connective in a column with 3+2-3, 1.5-3 x 1-2.5 mm tepals, 5-10 mm pedicel. Whereas, female flowers are triangular oblong, ovate to connate and with 2-4 mm capsular, 2- 7 mm long pedicel. Flowers have superior ovary with 2 ovules in each cell, columnar with 4-6 triangular lobes, 4 -6 locular, subulate or oblong. Fruits are subglobose, angled, capsuled, hispid.

1D.3 Geographical Distribution

Glochidion genus habitat is deciduous and evergreen forests and are also found in the grasslands. The genus comprises of 300 species that are spread from Madagascar to the Pacific Islands but mainly in tropical Asia.¹⁶⁸ It is a native Indian plant distributed in Karnataka, Tamil Nadu. The species has been collected only rarely from sites at medium elevation in southern Karnataka locality: Dakshina Kannada, Hassan, Kodagu, and Mysore etc.¹⁶⁹

1D.4 Ethnobotany

Plants from this genus are commonly used in traditional medicinal for the treatment of dyspepsia, wounds, rheumatoid arthritis, dysentery, stomachache.¹⁷⁰ In Bangladesh leaves and root extract of the *Glochidion multilocular* are used for the treatment of diarrhoea in the cow.¹⁷¹ Nicobarese tribe used *Glochidion calocarpum* Kurz leaf paste to treat skin disease by applying on the skin, and 2-3 teaspoon of leaves juice taken for an intestinal disorder.¹⁷² In hilly track area of East Godavari district in Andhra Pradesh, *G. tomentosum* is used in traditional medicinal systems, e.g. turmeric powder along with the grounded leaves paste is applied on cuts and wounds and used as an external ointment.¹⁷³

1D.5 Pharmacological activities

Glochidion velutinum ethanolic extract showed hypoglycemic activity against streptozotocin-nicotinamide induced type II diabetic rats. Ethanolic extract of leaves was administered to the mouse which resulted in blood glucose levels reduction ($P < 0.05$) as compared to the diabetic control rats.¹⁷⁴ *Glochidion velutinum* dried leaves methanolic extract showed antiurolithiatic activity against induced urolithiasis model in rats. Ethylene glycol and ammonium chloride induced urolithiasis rats were treated with *G. velutinum* methanolic whole extract (Table 1D.1). After 24 h the stone forming constituents calcium, phosphorus, oxalate level, creatinine and uric acid in the kidney and urine of calculogenic rats were reduced.¹⁷⁵

Table 1D.1 Analysis of EG induced urolithiasis rats urine for stone-forming constituents

Group no.#	Treatment	Levels in urine*		
		Calcium	Phosphate	Oxalate
I	Control	1.307 ± 0.011	3.658 ± 0.008	0.387 ± 0.007
II	Positive control	4.608 ± 0.006a	7.292 ± 0.022a	3.735 ± 0.005a
III	Standard	1.527 ± 0.010b	3.892 ± 0.008b	0.533 ± 0.008b
IV	Test 1(250mg/kg)	2.122 ± 0.005b	4.342 ± 0.005b	1.303 ± 0.018b
V	Test 2(500mg/kg)	1.917 ± 0.005b	4.160 ± 0.007b	0.973 ± 0.005b

#Each group consist of six animals, *Data presented in mean ± SEM; ^a $P < 0.05$ as compared to the vehicle-treated group; ^b $P < 0.05$ as compared to vehicle + EG treated group

Lupane triterpenoids were isolated and characterized from roots and stem wood of *G. sphaerogynum* and *G. eriocarpum*. Further compounds were tested for anticancer

activity against MCF-7, NCI-H-460 and SF-268 cancer cell lines (Table 1D.2).¹⁷⁶ Results suggested that only two compounds inhibited cell growth significantly. Glochidonol inhibited the growth of NCI-H-460, SF-268 and MCF-7, at IC₅₀ values of $17.9 \pm 1.1 \mu\text{M}$, $17.9 \pm 0.5 \mu\text{M}$ and $12.7 \pm 3.7 \mu\text{M}$ respectively. Similarly, glochidiol inhibited growth at GI₅₀ values 7.5 ± 0.5 , $9.7 \pm 0.3.3$ and 6.63 ± 0.7 . In-depth, the study suggested that the antiproliferative activity of glochidonol is through the involvement in apoptosis.

Table 1D.2 Effect of triterpenes on the growth of three human tumorcell lines ^a

Compound	IC ₅₀ (μM)		
	MCF-7 (breast)	NCI-H460 (lung)	SF-268(CNS)
Lupenone	75.6 ± 11.7	86.1 ± 12.4	80.9 ± 2.6
3-epi-lupeol	12.7 ± 1.6	17.9 ± 1.1	17.9 ± 0.5
Glochidone	> 100	> 100	> 100
Glochidonol	9.0 ± 3.7	4.9 ± 0.2	9.8 ± 0.5
Glochidiol	6.6 ± 0.7	7.5 ± 0.5	9.7 ± 0.3
Lup-20(29)-ene-1-β,3-β-diol	79.2 ± 2.4	> 100	> 100
Doxorubicinb	42.8 ± 8.2	94.0 ± 8.7	93.0 ± 7.0

Results are expressed as IC₅₀ (concentrations of compounds that cause 50 % inhibition of cell growth). Compounds were tested at a maximum concentration of 100 μM. Results are the mean ± SEM of 6 independent experiments performed in duplicate. ^b Data from the positive control doxorubicin are expressed in nM.

In another study on screening of olean-type triterpenoid saponins isolated from *Glochidion eriocarpum* for its anticancer potential against HL-60 and HCT-116 cells, the antiproliferative effects were seen. Compounds exhibited cytotoxicity against HCT-116 cell lines with IC₅₀ values ranging from 0.41~1.16 μM (Table 1D.3).

Table 1D.3. Triterpenoids cytotoxic effect against the growth of human cancer cells

Compounds	IC ₅₀ (μM)	
	HL-60 (Leukemia)	HCT-116 (colon)
1	5.50 ± 0.12	1.16 ± 0.08
2	4.51 ± 0.07	0.41 ± 0.01
3	5.07 ± 0.05	0.94 ± 0.07
4	6.33 ± 0.16	0.73 ± 0.04
MX*	8.40 ± 0.21	7.23 ± 0.35

IC₅₀: concentration that inhibits 50% of cell growth. Compounds were tested at a maximum concentration of 100 μM. MX (Mitoxantrone)* was used as a positive control. Data are presented as the mean of experiments performed in triplicate

The detailed investigation suggested that the pro-apoptotic effects were mediated through the activation of ERK and p38 in HCT-116 cells.¹⁷⁷ Another study reported the effect of saponins isolated from *G. glomerulatum* Glomerulosides A-F against HT-29, MCF-7, OVCAR and A-549 cancer cell lines. Glomerulosides A showed cytotoxicity against OVCAR and HT-29 with IC₅₀ 6.6 and 7.3 μ M, respectively (Table 1D.4). Glomerulosides C and Glomerulosides E inhibited the growth of HT-29, MCF-7, OVCAR and A-549 significantly with IC₅₀ values (5.9 μ M to 9.8 μ M).¹⁷⁸

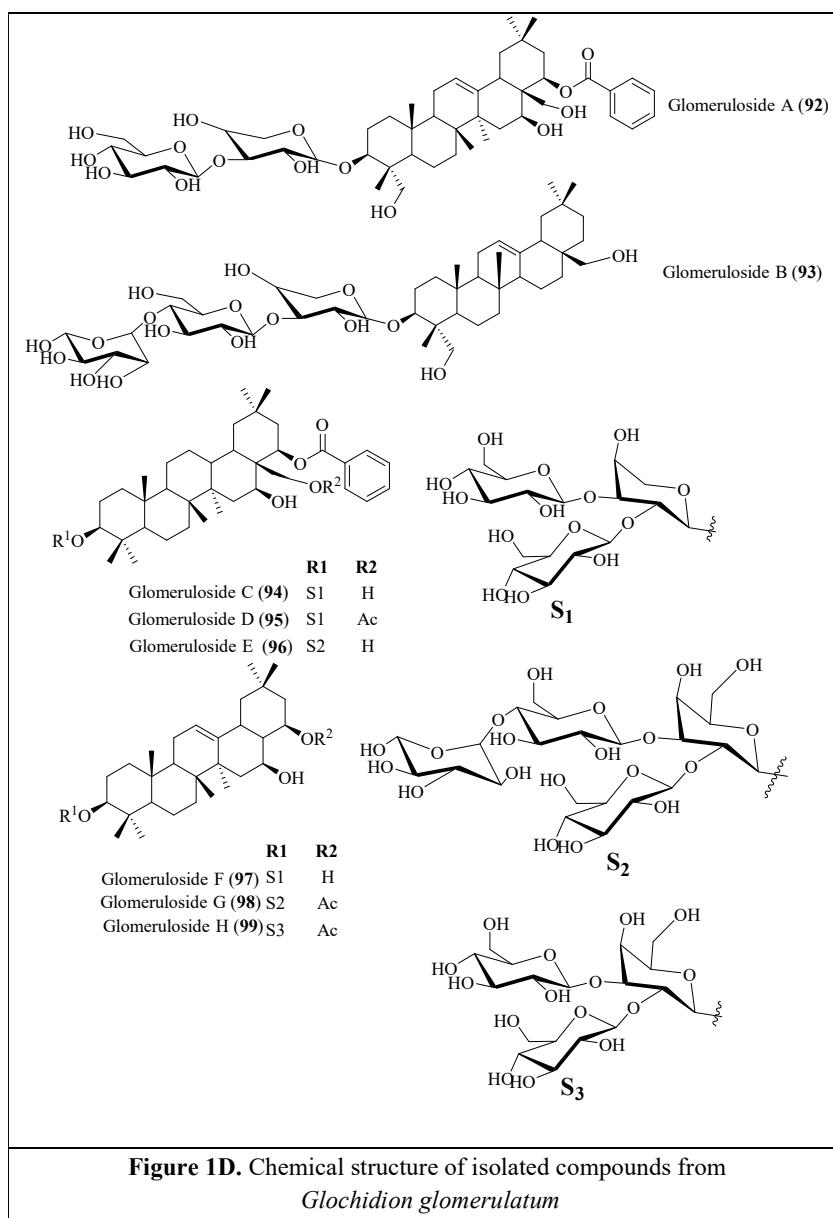
Table 1D.4 Cytotoxicity effect of glomerulosides A-F on human cancer cell lines

Compounds	IC ₅₀ μ M			
	A-549	HT-29	OVCAR	MCF-7
Glomerulosides-A	41.0 \pm 3.5	7.3 \pm 1.4	6.6 \pm 0.7	58.4 \pm 3.7
Glomerulosides-B	9.7 \pm 1.2	7.5 \pm 1.7	41.5 \pm 3.1	60.7 \pm 5.2
Glomerulosides-C	7.9 \pm 0.8	5.9 \pm 0.5	9.8 \pm 2.1	42.8 \pm 5.2
Glomerulosides-D	58.2 \pm 2.4	49.3 \pm 3.1	59.4 \pm 6.8	69.3 \pm 5.2
Glomerulosides-E	8.2 \pm 1.0	5.9 \pm 0.7	8.6 \pm 3.1	63.5 \pm 3.6
Glomerulosides-F	94.9 \pm 4.1	45.0 \pm 2.4	34.1 \pm 3.4	86.3 \pm 5.2
^a Mitoxantrone	7.2 \pm 0.5	3.1 \pm 0.3	8.4 \pm 0.9	10.3 \pm 1.2

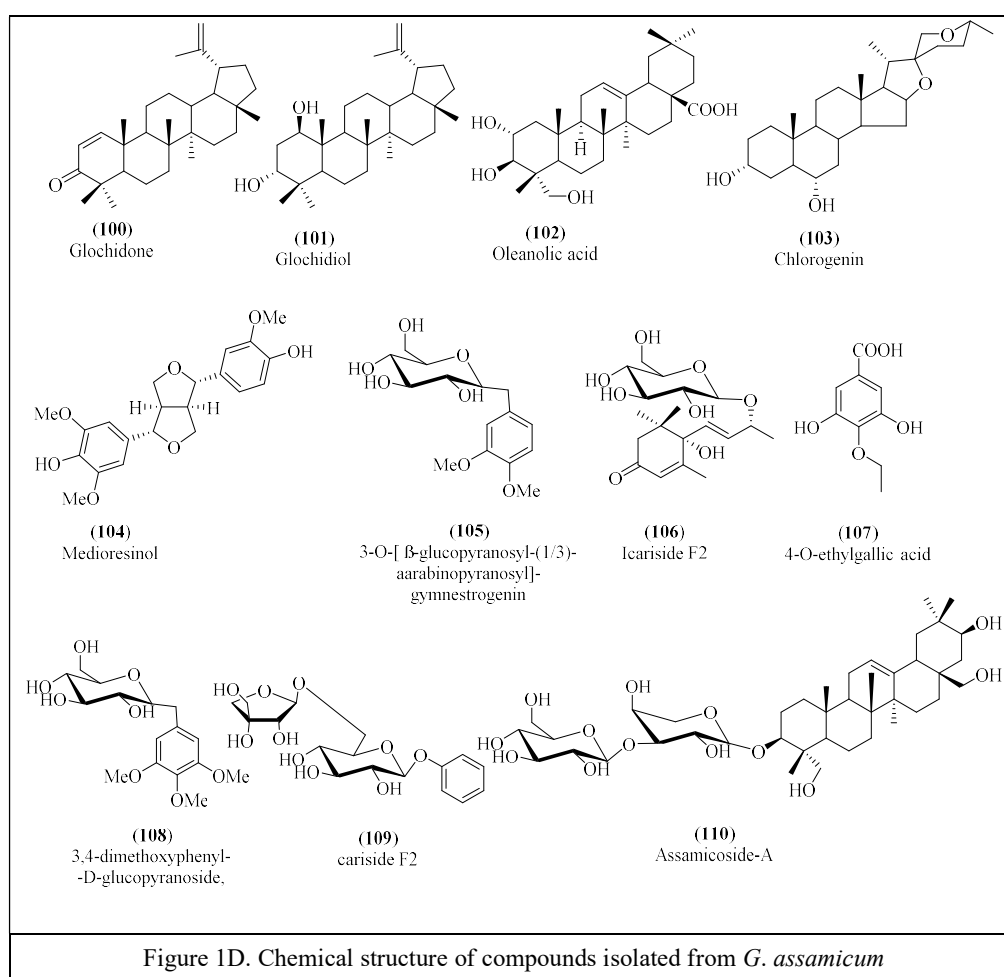
^aMitoxantrone was used as a positive control.

1D.6 Phytochemicals

Until now, no reports are available on the phytochemical investigation from *Glochidion tomentosum*. although several species of this genus are described to have terpenoids as major metabolites along with other metabolites *viz.* alkaloids, steroids, saponins, lignans, and flavonoids. Oleanane-type saponins were isolated from the leaf methanolic extract of *G. glomerulatum* named as glomeruloside A to glomeruloside F (92- 97).¹⁷⁹



Eleven compounds were isolated and characterized from the aerial part of *Glochidion assamicum* new triterpenoids saponin 3-O-[β -glucopyranosyl-(1-3)- α -arabinopyranosyl]-gymnestrogenin or assamicoside A (**110**), were isolated along with the ten known compounds. For the first time, C27 type steroid spirostane were isolated from *G. assamicum*, which can be used for differentiating this species from others. These are the known isolated compounds glochidone (**100**), glochidiol (**101**), arjunolic acid, chlorogenin (**103**), medioresinol (**104**), 4-O-ethylgallic acid, 3-O-[β -glucopyranosyl-(1/3)- α -arabinopyranosyl]-gymnestrogenin, 3,4-dimethoxyphenyl- β -D-glucopyranoside (**108**), icariside F2 (**106**).¹⁸⁰



Ethnobotanical and pharmacological studies of *A. paniculata*, *W. paludosa* and *G. tomentosum* suggested that these plants were used in traditional medicine and exhibited a wide range of pharmaceutically relevant bioactivities.¹⁸¹ Phytochemical analysis of *A. paniculata*, *Wedelia paludosa* and the plants belong to genus *Glochidion* were reported to have terpenoids as major secondary metabolites.^{182,179}

With this introduction about *A. paniculata*, though many reports are available on bioactive terpenoids purification, there is no rapid, automated and robust technique, which is the need. Andrographolide exhibits cytotoxicity against several cancerous cell lines, but no studies are reported on fluorescent probe formation and the localization studies. Moreover, there is a need to improve the aqueous solubility of andrographolide by formulation with the eco-friendly agent for better bioavailability. The literature study indicated that *G. tomentosum* is the active medicinal plant, but it is not explored for the phytochemical analysis. No reports were available on glochidonol gelation properties and utilization for small molecule trapping. Kaurenoic acid is bioactive constituent isolated from *W. paludosa* and acts as a potent antidiabetic agent, but very few reports were available on the derivatisation and gaining the mechanistic insight for the hypoglycemic activity. Terpenoids chemical derivatisation in search of more bioactive analogue is not economical, eco-friendly method, hence there is a need for an alternative greener approach, e.g. microbial biotransformation. Based on this, the objectives of the current study are the development of robust, automated purification and characterizations techniques for terpenoids. Evaluation of terpenoids for bioactivities, and the study the site of action with a mechanism. Enzymatic, chemical modification and formulation of terpenoids in order to improve its bioavailability and bioactivity. Use of microorganisms for biotransformation of bioactive terpenoids to form more bioactive derivatives.

Rapid isolation of diterpenoids from *A. paniculata* on preparative-scale was developed by using automated medium pressure liquid chromatography (MPLC) based technique. Diterpenoids were characterized by ESI (+)-quadrupole/orbitrap-MS/MS and structure fragmentation pathway of daughter ions were predicted based on high-resolution MS/MS data. Cytotoxicity of andrographolide was evaluated against MDA-MB-231, MCF-7. Further simple and highly efficient one-pot methodology were developed for

the NBD based fluorescent labelling of andrographolide. The internalisation and localisation of NBD-andrographolide were imaged successfully inside the cancer cells. C-14 ester analogues of andrographolide were synthesised through Amano lipase AK (*P.fluorescens*) catalysed acylation using various acyl donors. These monoesters tested for anti-microbial and hemolytic activity. Investigated the mechanism of action of potent antimicrobial derivatives by triple staining assay. Sophorolipid was used for the andrographolide in order to enhance aqueous solubility and bioavailability. Cytotoxicity of andrographolide, Sophorolipid (SL-A)-andrographolide was tested against MDA-MB-231. Zinc oxide nanoparticles were synthesised by using a simple, facile method and formed a complex with andrographolide. pH release of andrographolide from zinc oxide nanoparticles was studied. Lupane triterpenoids from the bark of *Glochidion tomentosum* were isolated on a preparative scale by Medium automated pressure chromatographic (MPLC) technique. Self-assembly of glochidonol was investigated in different solvents and systematically studied by using advanced characterization techniques. The fibrillar microstructures of glochidonol have been utilised for the entrapping small molecule by the epifluorescence experiment. Biotransformation of menthol was systematically studied by using *Mucor piriformis*, metabolites were purified and characterized. Menthol and metabolites were tested for antimicrobial activity and evaluated the site of action by triple staining assay. Whole-cell biocatalysis approach for andrographolide biotransformation was developed and characterized metabolites. (*Z*)-lanceol was oxidised regio- and stereo-selectively into two new metabolites by using *Cunninghamella echinulata*. (*Z*)-lanceol and metabolites were screened for antimicrobial activity.

1E. References

- 1 D. W. Christianson, *Chem. Rev.*, 2017, **117**, 11570–11648.
- 2 P. N. Blank, S. A. Shinsky and D. W. Christianson, *ACS Chem. Biol.*, 2019, **4**, 1011–1019.
- 3 D. J. McGarvey and R. Croteau, *Plant Cell*, 2007, **7**, 1015.
- 4 Y.-B. Mao, X.-Y. Chen, L.-J. Wang, A.-X. Cheng, S. Lu and Y.-G. Lou, *J. Integr. Plant Biol.*, 2007, **49**, 179–186.
- 5 J. C. Harman, in *Veterinary Herbal Medicine*, eds. S. G. Wynn and B. J. Fougère, Mosby, Saint Louis, 2007, pp. 411–439.
- 6 E. Vranová, D. Coman and W. Gruissem, *Mol. Plant*, 2012, **5**, 318–333.
- 7 M. T. and J. F. Roman Paduch1, Martyna Kandefer–Szerszeń1, *Arch. Immunol. Ther. Exp.*, 2007, **55**, 315.
- 8 A. Salminen, M. Lehtonen, T. Suuronen, K. Kaarniranta and J. Huuskonen, *Cell. Mol. Life Sci.*, 2008, **65**, 2979–2999.
- 9 E. Enan, *Comp. Biochem. Physiol. Part C Toxicol. Pharmacol.*, 2001, **130**, 325–337.
- 10 B. Monsarrat, E. Mariel, S. Cros, M. Garès, D. Guénard, F. Guéritte-Voegelein and M. Wright, *Drug Metab. Dispos.*, 1990, **18**, 895–901.
- 11 F. Lévesque and P. H. Seeberger, *Angew. Chemie Int. Ed.*, 2012, **51**, 1706–1709.
- 12 P. P. Peralta-Yahya, F. Zhang, S. B. del Cardayre and J. D. Keasling, *Nature*, 2012, **488**, 320–328.
- 13 J. Bohlmann and C. I. Keeling, *Plant J.*, 2008, **3**, 656–669.
- 14 T. Kuzuyama, *Biosci. Biotechnol. Biochem.*, 2003, **66**, 1619–1627.
- 15 L. Zhao, W. Chang, Y. Xiao, H. Liu and P. Liu, *Annu. Rev. Biochem.*, 2013, **82**, 497–530.
- 16 G. A. Sprenger, U. Schörken, T. Wiegert, S. Grolle, A. A. de Graaf, S. V Taylor, T. P. Begley, S. Bringer-Meyer and H. Sahn, *Proc. Natl. Acad. Sci.*, 1997, **94**, 12857 LP-12862.
- 17 T. Kuzuyama and H. Seto, *B. Phys. Biol. Sci.*, 2012, **88**, 41–52.
- 18 H. V. Thulasiram, H. K. Erickson and C. D. Poulter, *J. Am. Chem. Soc.*, 2008, **130**, 1966–1971.
- 19 R. Raja, S. Hemaiswarya and R. Rengasamy, *Appl. Microbiol. Biotechnol.*, 2007, **74**, 517–523.
- 20 Y. Zou and J. G. Millar, *Nat. Prod. Rep.*, 2015, **32**, 1067–1113.
- 21 C. Dale Poulter, *Acc. Chem. Res.*, 1990, **23**, 70–77.
- 22 H. V. Thulasiram, H. K. Erickson and C. D. Poulter, *Science*, 2007, **73**, 73–77.
- 23 Z. Katerova, D. Todorova, K. Tasheva and I. Sergiev, *Genet. Plant Physiol.*, 2012, **2**,

- 113–144.
- 24 H. V Thulasiram, H. K. Erickson and C. D. Poulter, *Science*, 2007, **316**, 73–76.
- 25 I. I. Abdallah and W. J. Quax, *KnE Life Sci.*, 2017, **3**, 81–98.
- 26 N. Yadav, R. Yadav and A. Goyal, *Int. J. Pharm. Sci. Rev. Res.*, 2009, **27**, 272–278.
- 27 G. Rubulotta and E. A. Quadrelli, in *Horizons in Sustainable Industrial Chemistry and Catalysis*, eds. S. Albonetti, S. Perathoner and E. A. Quadrelli, Elsevier, 2019, vol. 178, pp. 215–229.
- 28 J. R. Hanson, *Nat. Prod. Rep.*, 2009, **26**, 1156–1171.
- 29 A. Ludwiczuk, K. Skalicka-Woźniak and M. I. Georgiev, in *Pharmacognosy*, eds. S. Badal and R. Delgoda, Academic Press, Boston, 2017, pp. 233–266.
- 30 J. Nagarajan, R. N. Ramanan, M. E. Raghunandan, C. M. Galanakis and N. P. Krishnamurthy, in *Nutraceutical and Functional Food Components*, ed. C. M. Galanakis, Academic Press, 2017, pp. 259–296.
- 31 H. N. Kamel and M. Slattery, *Pharm. Biol.*, 2005, **43**, 253–269.
- 32 L. Caputi and E. Aprea, *Recent Patents Food, Nutr. Agric.*, 2012, **3**, 9–16.
- 33 C. Fehr, I. Magpantay, J. Arpagaus, X. Marquet and M. Vuagnoux, *Angew. Chemie - Int. Ed.*, 2009, **48**, 7221–7223.
- 34 T. G. Tolstikova, I. V. Sorokina, G. A. Tolstikov, A. G. Tolstikov and O. B. Flekhter, *Russ. J. Bioorganic Chem.*, 2006, **32**, 261–276.
- 35 H. Gross and G. M. König, *Phytochem. Rev.*, 2006, **5**, 115–141.
- 36 Z.-H. Jiang, J.-R. Wang, M. Li, Z.-Q. Liu, K.-Y. Chau, C. Zhao and L. Liu, *J. Nat. Prod.*, 2005, **68**, 397–399.
- 37 B. Singh and R. A. Sharma, *Biotech.*, 2015, **5**, 129–151.
- 38 T. Vuorinen, G. V. P. Reddy, A. M. Nerg and J. K. Holopainen, *Atmos. Environ.*, 2004, **38**, 675–682.
- 39 M. E. Litvak and R. K. Monson, *Oecologia*, 1998, **114**, 531–540.
- 40 M. C. Carpinella, M. T. Defago, G. Valladares and S. M. Palacios, *J. Agric. Food Chem.*, 2003, **51**, 369–374.
- 41 R. Chauhan, K. M. Ruby and J. Dwivedi, *Int. J. Pharm. Pharm. Sci.*, 2013, **5**, 9–16.
- 42 W. Kehrl, U. Sonnemann and U. Dethlefsen, *Laryngoscope*, 2004, **114**, 738–742.
- 43 A. Sarkic and I. Stappen, *Cosmetics*, 2018, **5**, 11.
- 44 M. Carmona, A. Zalacain, M. R. Salinas and G. L. Alonso, *J. Agric. Food Chem.*, 2006, **54**, 6825–6834.
- 45 P. L. Crowell, A. S. Ayoubi and Y. D. Burke, in *Dietary Phytochemicals in Cancer Prevention and Treatment*, Springer US, Boston, MA, 1996, pp. 131–136.
- 46 P. L. Crowell, *Symp. Phytochem. Biochem. Physiol.*, 1999, 775–778.

- 47 P. L. Crowell, W. S. Kennan, J. D. Haag, S. Ahmad, E. Vedejs and M. N. Gould, *Carcinogenesis*, 1992, **13**, 1261-.
- 48 M. Karapinar and Ş. Esen Aktuğ, *Int. J. Food Microbiol.*, 1987, **4**, 161–166.
- 49 S. Pattnaik, V. R. Subramanyam, M. Bapaji and C. R. Kole, *Microbios*, 1997, **89**, 39–46.
- 50 T. J. Brocksom, K. T. de Oliveira and A. L. Desideri, *J. Braz. Chem. Soc.*, 2017, **28**, 933–942.
- 51 J. Gertsch, M. Leonti, S. Raduner, I. Racz, J.-Z. Chen, X.-Q. Xie, K.-H. Altmann, M. Karsak and A. Zimmer, *Proc. Natl. Acad. Sci.*, 2008, **105**, 9099–9104.
- 52 A. González-Coloma, F. Valencia, N. Martín, J. J. Hoffmann, L. Hutter, J. A. Marco and M. Reina, *J. Chem. Ecol.*, 2002, **28**, 117–129.
- 53 E. C. J. Smith, E. M. Williamson, N. Wareham, G. W. Kaatz and S. Gibbons, *Phytochemistry*, 2007, **68**, 210–217.
- 54 M. Lebwohl and A. Sohn, *Expert Rev. Dermatol.*, 2012, **7**, 121–128.
- 55 A. Gauvin-Bialecki, M. Akinin and J. Smadja, *Molecules*, 2008, **13**, 3184–3191.
- 56 E. Pisha, H. Chai, I. S. Lee, T. E. Chagwedera, N. R. Farnsworth, G. A. Cordell, C. W. W. Beecher, H. H. S. Fong, A. D. Kinghorn, D. M. Brown, M. C. Wani, M. E. Wall, T. J. Hieken, T. K. D. Gupta and J. M. Pezzuto, *Nat. Med.*, 1995, **1**, 80–84.
- 57 S. Fulda and G. Kroemer, *Drug Discov. Today*, 2009, **14**, 885–890.
- 58 T.-C. Kao, M.-H. Shyu and G.-C. Yen, *J. Agric. Food Chem.*, 2010, **58**, 8623–8629.
- 59 M. Abdelmouleh, S. Boufi, M. N. Belgacem and A. Dufresne, *Compos. Sci. Technol.*, 2007, **67**, 1627–1639.
- 60 J. D. McChesney, S. K. Venkataraman and J. T. Henri, *Phytochemistry*, 2007, **68**, 2015–2022.
- 61 K. H. Lee, *J. Nat. Prod.*, 2004, **67**, 273–283.
- 62 S. M. K. Rates, *Toxicon*, 2001, 603–613.
- 63 J. L. Ríos and M. C. Recio, *J. Ethnopharmacol.*, 2005, 80–84.
- 64 H. Yuan, Q. Ma, L. Ye and G. Piao, *Molecules*, 2016, **21**, 1–16.
- 65 S. D. Sarker, Z. Latif and A. I. Gray, in *Natural Products Isolation*, eds. S. D. Sarker, Z. Latif and A. I. Gray, Humana Press, Totowa, NJ, 2005, pp. 1–25.
- 66 M. D. Luque De Castro, M. M. Jiménez-Carmona and V. Fernández-Pérez, *TrAC - Trends Anal. Chem.*, 1999, **18**, 708–716.
- 67 S. Haldar, P. B. Phapale, S. P. Kolet and H. V. Thulasiram, *Anal. Methods*, 2013, **5**, 5386–5391.
- 68 S. Haldar, F. A. Mulani, T. Aarthy, D. S. Dandekar and H. V. Thulasiram, *J. Chromatogr. A*, 2014, **1366**, 1–14.
- 69 W. Guo, W. Liu, G. Chen, S. Hong, C. Qian, N. Xie, X. Yang, Y. Sun and Q. Xu, *Int. Immunopharmacol.*, 2012, **14**, 613–619.

-
- 70 Y. Shahzad, S. N. H. Shah, M. T. Ansari, R. Riaz, A. Safdar, T. Hussain and M. Malik, *Chinese Sci. Bull.*, 2012, **57**, 1685–1692.
- 71 P. K. Singh, K. Wani, R. Kaul-Ghanekar, A. Prabhune and S. Ogale, *RSC Adv.*, 2014, **4**, 60334–60341.
- 72 P. P. Daramwar, P. L. Srivastava, S. P. Kolet and H. V. Thulasiram, *Org. Biomol. Chem.*, 2014, **12**, 1048–1051.
- 73 S. P. Kolet, S. Niloferjahan, S. Haldar, R. Gonnade and H. V. Thulasiram, *Steroids*, 2013, **78**, 1152–1158.
- 74 S. Haldar, S. P. Kolet and H. V. Thulasiram, *Green Chem.*, 2013, **15**, 1311–1317.
- 75 H.-W. Chen, C.-S. Huang, P.-F. Liu, C.-C. Li, C.-T. Chen, C.-T. Liu, J.-R. Chiang, H.-T. Yao and C.-K. Lii, *Evidence-Based Complement. Altern. Med.*, 2013, **2013**, 1–11.
- 76 M. Sanower Hossain, Z. Urbi, A. Sule and K. M. Hafizur Rahman, *Sci. World J.*, 2014, **2014**, 1–28.
- 77 A. Valdiani, M. A. Kadir, S. G. Tan, D. Talei, M. P. Abdullah and S. Nikzad, *Mol. Biol. Rep.*, 2012, **39**, 5409–5424.
- 78 R. Subramanian, M. Z. Asmawi and A. Sadikun, *Phytochem. Rev.*, 2012, **11**, 39–75.
- 79 A. Niranjana, S. K. Tewari and A. Lehri, *Indian J. Nat. Prod. Resour.*, 2010, **1**, 125–135.
- 80 Shirisha K and Mastan M, *Pharmacophore*, 2013, **4**, 212.
- 81 M. Sivananthan and M. Elamaran, *Int. J. Biomol. and Biomed.*, 2013, **3**, 1–12.
- 82 Z. Yanfang, L. Xingping, Z. Zongde, C. Liren and L. Yongmin, *J. Pharm. Biomed. Anal.*, 2006, **40**, 157–161.
- 83 T. Xu, J. Pan and L. Zhao, *J. Chromatogr. Sci.*, 2008, **46**, 747–750.
- 84 F. fang Xu, S. jun Fu, S. pan Gu, Z. min Wang, Z. zhong Wang, X. He and W. Xiao, *J. Chromatogr. B Anal. Technol. Biomed. Life Sci.*, 2015, **990**, 125–131.
- 85 S. Nv, Komathi S, Rajalakshmi G, Queen J and Bharathi D, *Eur. J. Biotechnol. Biosci. Online*, 2016, **4**, 2321–9122.
- 86 M. Sanower Hossain, Z. Urbi, A. Sule and K. M. Hafizur Rahman, *Sci. World J.*, 2014, **2014**, 1–28.
- 87 W. Li, Y. Sun, J. Joseph, J. F. Fitzloff, H. H. S. Fong and R. B. Van Breemen, *J. Agric. Food Chem.*, 2003, **51**, 524–529.
- 88 H. J. Dong, Z. J. Zhang, J. Yu, Y. Liu and F. G. Xu, *J. Chromatogr. Sci.*, 2009, **47**, 931–935.
- 89 D. M. Stanković, A. Samphao, D. Kuzmanović and K. Kalcher, *Microchem. J.*, 2015, **122**, 16–19.
- 90 L. Chen, H. Jin, L. Ding, H. Zhang, X. Wang, Z. Wang, J. Li, C. Qu, Y. Wang and H. Zhang, *J. Chromatogr. A*, 2007, **1140**, 71–77.
- 91 A. C. Kumoro and M. Hasan, *Chem. Eng. Commun.*, 2008, **195**, 72–80.
-

-
- 92 A. C. Kumoro and M. Hasan, *Chinese J. Chem. Eng.*, 2007, **15**, 877–883.
- 93 A. Altemimi, N. Lakhssassi, A. Baharlouei, D. Watson and D. Lightfoot, *Plants*, 2017, **6**, 42.
- 94 A. Nn, *Med. Aromat. Plants*, 2015, **04**, 3–8.
- 95 T. Dhanani, S. Shah, N. A. Gajbhiye and S. Kumar, *Arab. J. Chem.*, 2017, **10**, S1193–S1199.
- 96 K. Y. Khaw, M. O. Parat, P. N. Shaw and J. R. Falconer, *Molecules*, 2017, **22**, 1186.
- 97 Y. Q. Wang, Z. F. Wu, G. Ke and M. Yang, *Molecules*, 2015, **20**, 430–445.
- 98 S. Kumar, T. Dhanani and S. Shah, *J. Chromatogr. Sci.*, 2014, **52**, 1043–1050.
- 99 M. Charoenchaitrakool, W. Trisilanun and P. Srinopakhun, *Korean J. Chem. Eng.*, 2010, **27**, 950–954.
- 100 W. Yi, C. Yau, P. Zhi and V. A. L. Sagindharan, *Chem. Eng. Trans.*, 2015, **45**, 1075–1080.
- 101 R. J. C. Kleipool and D. G. F. R. Kostermans, *Recl. des Trav. Chim. des Pays-Bas*, 1951, **70**, 1085–1088.
- 102 K. L. D. and C. K. A. K K Gupta, S C Taneja, *Phytochemistry*, 1983, **22**, 314–315.
- 103 M. K. Reddy, M. V. B. Reddy, D. Gunasekar, M. M. Murthy, C. Caux and B. Bodo, *Phytochemistry*, 2003, **62**, 1271–1275.
- 104 L. W., S. Y., J. J., F. J.F., F. H.H.S. and V. B. R.B., *J. Agric. Food Chem.*, 2003, **51**, 524–529.
- 105 V. L. N. Reddy, S. M. Reddy, V. Ravikanth, P. Krishnaiah, T. V. Goud, T. P. Rao, T. S. Ram, R. G. Gonnade, M. Bhadbhade and Y. Venkateswarlu, *Nat. Prod. Res.*, 2005, **19**, 223–230.
- 106 T. S. Wu, H. J. Chern, A. G. Damu, P. C. Kuo, C. R. Su, E. J. Lee and C. M. Teng, *J. Asian Nat. Prod. Res.*, 2008, **10**, 17–24.
- 107 L. I. Wenkui, X. U. Xudong, H. Z. Hang, M. A. Cuiying and H. F. Ong, 2007, **55**, 455–458.
- 108 W. W. Chao and B. F. Lin, *Chin. Med.*, 2010, **5**, 1–15.
- 109 R. Kotewong, P. Duangkaew, E. Srisook, S. Sarapusit and P. Rongnoparut, *Parasitol. Res.*, 2014, **113**, 3381–3392.
- 110 Y. Zou, H. Xiong, H. Xiong, T. Lu, F. Zhu, Z. Luo, X. Yuan and Y. Wang, *Tumor Biol.*, 2015, **36**, 5179–5186.
- 111 Q. Du, G. Jerz and P. Winterhalter, *J. Chromatogr. A*, 2003, **984**, 147–151.
- 112 O. Sareer, S. Ahmad and S. Umar, *Nat. Prod. Res.*, 2014, **28**, 2081–2101.
- 113 S. Pramanick, S. Banerjee, B. Achari, B. Das, A. K. Sen, S. Mukhopadhyay, A. Neuman and T. Prangé, *J. Nat. Prod.*, 2006, **69**, 403–405.
- 114 W. W. Chao, Y. H. Kuo and B. I. F. Lin, *J. Agric. Food Chem.*, 2010, **58**, 2505–2512.
-

-
- 115 S. Ignacimuthu, M. Ayyanar and S. Sivaraman K., *J. Ethnobiol. Ethnomed.*, 2006, **2**, 1–7.
- 116 A. Garg, L. Agrawal, R. C. Misra, S. Sharma and S. Ghosh, *BMC Genomics*, 2015, **16**, 1–16.
- 117 M. M. M. Abdul Manaf Ali, *Antiviral and Cytotoxic Activities of Some Plants Used in Malaysian Indigenous Medicine Colorectal Adenocarcinoma Cells View project Herbal and Medicinal Plant View project*, 1996, vol. 19.
- 118 H. L. Wong, R. Bendayan, A. M. Rauth, Y. Li and X. Y. Wu, *Adv. Drug Deliv. Rev.*, 2007, **59**, 491–504.
- 119 J. C. Bertoglio, M. Baumgartner, R. Palma, E. Ciampi, C. Carcamo, D. D. Cáceres, G. Acosta-Jamett, J. L. Hancke and R. A. Burgos, *BMC Neurol.*, 2016, **16**, 1–8.
- 120 and R. R. Sriram Rajagopal, R. Ajaya kumar, Dhanvanthri S. Deevi, Chitkala Satyanarayana, *J. Exp. Ther. Oncol.*, 2014, **3**, 1–2.
- 121 S. R. Jada, G. S. Subur, C. Matthews, A. S. Hamzah, N. H. Lajis, M. S. Saad, M. F. G. Stevens and J. Stanslas, *Phytochemistry*, 2007, **68**, 904–912.
- 122 T. L. Yen, W. H. Hsu, S. K. H. Huang, W. J. Lu, C. C. Chang, L. M. Lien, G. Hsiao, J. R. Sheu and K. H. Lin, *Pharm. Biol.*, 2013, **51**, 1150–1157.
- 123 T. Matsuda, M. Kuroyanagi, S. Sugiyama, K. Umehara, A. Ueno and K. Nishi, *Chem. Pharm. Bull. (Tokyo)*, 1994, **42**, 12161–1225.
- 124 Y. Tung, H.-L. Chen, H. Tsai, S. Yang, Y. Chang and C. Chen, *Evidence-Based Complement. Altern. Med.*, 2013, **12**, 1–8.
- 125 S. T. Manikam and J. Stanslas, *J. Pharm. Pharmacol.*, 2009, **61**, 69–78.
- 126 J. C. W. Lim, T. K. Chan, D. S. Ng, S. R. Sagineedu, J. Stanslas and W. F. Wong, *Clin. Exp. Pharmacol. Physiol.*, 2012, **39**, 300–310.
- 127 S. Kumar, H. S. Patil, P. Sharma, D. Kumar, S. Dasari, V. G. Puranik, H. V. Thulasiram and G. C. Kundu, *Curr. Mol. Med.*, 2012, **12**, 952–966.
- 128 S. Nanduri, V. K. Nyavanandi, S. Sanjeeva Rao Thunuguntla, S. Kasu, M. K. Pallerla, P. Sai Ram, S. Rajagopal, R. Ajaya Kumar, R. Ramanujam, J. Moses Babu, K. Vyas, A. Sivalakshmi Devi, G. Om Reddy and V. Akella, *Bioorganic Med. Chem. Lett.*, 2004, **14**, 4711–4717.
- 129 K. Sheeja and G. Kuttan, *Immunopharmacol. Immunotoxicol.*, 2007, **1**, 81–93.
- 130 K. Sheeja, C. Guruvayoorappan and G. Kuttan, *Int. Immunopharmacol.*, 2007, **2**, 211–221.
- 131 Y. Zhang, G. Hu, H. Lin, S. Hong, Y. Deng, J. Tang, S. W. Seto, Y. Kwan, M. M. Waye, Y. Wang and S. M. Lee, *J. Ethnopharmacol.*, 2004, **92**, 291–295.
- 132 P. K. Singha, S. Roy and S. Dey, *J. Ethnopharmacol.*, 2007, **111**, 13–21.
- 133 A. Leelarasamee, S. Trakulsomboon and N. Sittisomwong, *J. Med. Assoc. Thai.*, 1990, **73**, 299–304.
-

-
- 134 S. Roy, K. Rao, C. Bhuvaneswari, A. Giri and L. N. Mangamoori, *World J. Microbiol. Biotechnol.*, 2010, **26**, 85–91.
- 135 R. Moghimi, L. Ghaderi, H. Rafati, A. Aliahmadi and D. Julian, *Food Chem.*, 2016, **194**, 410–415.
- 136 R. Premanath and L. Nanjaiah, *J. Appl. Pharm. Sci.*, 2015, **5**, 069–076.
- 137 R. Parvataneni and R. Lakshmi, *Int. Res. J. Microbiol.*, 2010, **1**, 37–39.
- 138 P. K. Singha, S. Roy and S. Dey, *Fitoterapia*, 2003, **74**, 692–694.
- 139 T.-P. Lin, S.-Y. Chen, P.-D. Duh, L.-K. Chang and Y.-N. Liu, *Biol. Pharm. Bull.*, 2008, **31**, 2018–2023.
- 140 N. Dey, K. Mishra and A. P. Dash, *J. Trop. Med.*, 2011, **3**, 1–7.
- 141 A. A. Bright, A. Babu, S. Ignacimuthu and S. Dorn, *Indian J. Exp. Biol.*, 2001, **39**, 715–718.
- 142 M. Govindarajan, *Asian Pac. J. Trop. Med.*, 2011, **4**, 176–181.
- 143 G. Elango, A. A. Rahuman, A. Bagavan, C. Kamaraj, A. A. Zahir and C. Venkatesan, *Parasitol. Res.*, 2009, **104**, 1381–1388.
- 144 Y. Zhang, G. Hu, H. Lin, S. Hong, Y. Deng, J. Tang, S. W. Seto, Y. Kwan, M. M. Waye, Y. Wang and S. M. Lee, *Phyther. Res.*, 2009, **23**, 126–128.
- 145 C. Wiart, K. Kumar, M. Y. Yusof, H. Hamimah, Z. M. Fauzi and M. Sulaiman, 2005, **1070**, 1069–1070.
- 146 V. K. Dua, V. P. Ojha, R. Roy, B. C. Joshi, N. Valecha, C. U. Devi, M. C. Bhatnagar, V. P. Sharma and S. K. Subbarao, *J. Ethnopharmacol.*, 2004, **95**, 247–251.
- 147 T. T. Quang, J. Jossang, A. Jossang, P. P. N. Kim and G. Jaureguiberry, *J. Org. Chem.*, 2007, **72**, 7102–7105.
- 148 L. F. V. Bresciani, V. Cechinel-Filho and R. A. Yunes, *Nat. Prod. Lett.*, 2000, **14**, 247–254.
- 149 N. Balekar, T. Nakpheng and T. Srichana, *Chiang Mai J. Sci.*, 2014, **41**, 590–605.
- 150 F. Bohlmann, C. Zdero, R. M. Kinct and H. Rosrnsont, *Phylochemisfry*, 1982, **21**, 2329–2333.
- 151 N. Balekar, N. G. Katkam, T. Nakpheng, K. Jehtae and T. Srichana, *J. Ethnopharmacol.*, 2012, **141**, 817–824.
- 152 R. Batista, P. A. García, M. Á. Castro, J. M. M. Del Corral, A. S. Feliciano and A. B. de Oliveira, *An. Acad. Bras. Cienc.*, 2010, **82**, 823–31.
- 153 P. A. García, A. B. De Oliveira and R. Batista, *Molecules*, 2007, **12**, 455–483.
- 154 R. Batista, F. C. Braga and A. B. Oliveira, *Rev. Bras. Farmacogn.*, 2008, **15**, 119–125.
- 155 M. M. de S. a Luciana C. Block a , Adair R.S. Santos a, C. S. A, R. A. Y. B, F. D. M. d , Ma'rio Alves Santos c and V. C. F. A, *J. Ethnopharmacol.*, 1998, **61**, 85–9.
- 156 N. Balekar, T. Nakpheng and T. Srichana, *Chiang Mai J. Sci.*
-

- 157 B. C. Cavalcanti, J. R. O. Ferreira, D. J. Moura, R. M. Rosa, G. V. Furtado, R. R. Burbano, E. R. Silveira, M. A. S. Lima, C. A. G. Camara, J. Saffi, J. A. P. Henriques, V. S. N. Rao, L. V. Costa-Lotufo, M. O. Moraes and C. Pessoa, *Mutat. Res. - Genet. Toxicol. Environ. Mutagen.*, 2010, **701**, 153–163.
- 158 D. Ferreira, A. LevoRato, T. De Faria, M. De Carvalho and R. Braz-Filho, *Nat. Prod. Lett.*, 1994, **4**, 1–7.
- 159 R. Batista, E. Chiari and A. de Oliveira, *Planta Med.*, 2007, **66**, 283–284.
- 160 M. R. K. Sartori, J. B. Pretto, A. B. Cruz, L. F. V. Bresciani, R. A. Yunes, M. Sortino, S. A. Zacchino and V. C. Filho, *Pharmazie*, 2003, **58**, 567–569.
- 161 L. F. V. Bresciani, R. A. Yunes, C. Bürger, L. E. De Oliveira, K. L. Bóf and V. Cechinel-Filho, *Zeitschrift fur Naturforsch. - Sect. C J. Biosci.*, 2004, **59**, 229–232.
- 162 C. Bürger, D. R. Fischer, D. A. Cordenunzi, A. P. de Borba Batschauer, V. C. Filho and A. R. dos Santos Soares, *J. Pharm. Pharm. Sci.*, 2005, **8**, 370–373.
- 163 R. B. G. De Carli, P. R. A. Siqueira, M. L. Kaiser, R. A. Freitas, M. M. De Souza, V. Cechinel-Filho and R. M. Lucinda-Silva, *Lat. Am. J. Pharm.*, 2009, **28**, 594–598.
- 164 R. Batista, G. C. Brandão, F. C. Braga and A. B. Oliveira, *Brazilian J. Pharmacogn.*, 2009, **19**, 36–40.
- 165 B. R. P. Rao and B. Swetha, *Pleione*, 2013, **7**, 94–100.
- 166 M. Kato, A. Takimura and A. Kawakita, *Proc. Natl. Acad. Sci.*, 2003, **100**, 5264–5267.
- 167 E. Ekanayake, D. Wijesundara and G. Perera, *J. Sci. Biol. Sci.*, 2014, **42**, 55–70.
- 168 V. M. Meher-Homji, *Bull. Torrey Bot. Club*, 2006, **94**, 230–242.
- 169 O. P. Tripathi, K. UPADHAYA, R. S. Tripathi and H. N. Pandey, *Res. J. Environ. Earth Sci.*, 2010, **2**, 97–105.
- 170 Y. Ratna Raju, P. Yugandhar and N. Savithramma, *Int. J. Pharm. Pharm. Sci.*, 2014, **6**, 369–374.
- 171 M. Z. Uddin, M. A. Hassan and M. Sultana, *Bangladesh J. Plant Taxon.*, 2009, **13**, 63–68.
- 172 M. Fariya, A. Jain, V. Dhawan, S. Shah and M. S. Nagarsenker, *Adv. Pharm. Bull.*, 2014, **4**, 483–491.
- 173 C. Pattanaik, C. S. Reddy and K. N. Reddy, *Our Nat.*, 2010, **7**, 122–128.
- 174 P. C. Are, R. Ram, R. Adidala and G. Puchchakayala, *Eur. J. Biol. Sci.*, 2011, **3**, 126–130.
- 175 R. N. Thatikonda Vijaya, Nallani Venkata Rama Rao, A Narendra Babu, M Sathish Kumar, P Sharmila Nirojini, B Srinivasa Reddy, *Int. J. Biol. Pharm. Res.*, 2013, **4**, 878–884.
- 176 P. Puapairoj, W. Naengchomnong, A. Kijjoa, M. M. Pinto, M. Pedro, M. S. J. Nascimento, A. M. S. Silva and W. Herz, *Planta Med.*, 2005, **71**, 208–213.
- 177 N. X. Nhiem, V. K. Thu, P. Van Kiem, C. Van Minh, B. H. Tai, T. H. Quang, N. X.

- Cuong, P. H. Yen, H. J. Boo, J. Il Kang, H. K. Kang and Y. H. Kim, *Arch. Pharm. Res.*, 2012, **35**, 19–26.
- 178 V. K. Thu, N. Van Thang, N. X. Nhiem, H. L. T. Anh, P. H. Yen, C. Van Minh, P. Van Kiem, N. Y. Kim, S. J. Park and S. H. Kim, *Nat. Prod. Commun.*, 2015, **10**, 875–876.
- 179 V. K. Thu, N. Van Thang, N. X. Nhiem, B. H. Tai, N. H. Nam, P. Van Kiem, C. Van Minh, H. Le Tuan Anh, N. Kim, S. Park and S. H. Kim, *Phytochemistry*, 2015, **116**, 213–220.
- 180 J. M. Tian, X. Y. Fu, Q. Zhang, H. P. He, J. M. Gao and X. J. Hao, *Biochem. Syst. Ecol.*, 2013, **48**, 288–292.
- 181 A. Okhwarobo, J. Ehizogie Falodun, O. Erharuyi, V. Imieje, A. Falodun and P. Langer, *Asian Pacific J. Trop. Dis.*, 2014, **4**, 213–222.
- 182 X. Q. Liu, H. L. Huang, M. J. Yao, G. T. Han, N. Liu, J. C. Yuan and C. S. Yuan, *Helv. Chim. Acta*, 2011, **94**, 2264–2271.

Chapter 2
Phytochemical Investigation of
Andrographis paniculata

Chapter 2: Section A

Isolation and Characterization of Terpenoids from *Andrographis paniculata*

2A.1 Introduction

Andrographis paniculata is a medicinal herb; native populations occur in Srilanka and India, which is the centre of diversity and origin of the species, it is also distributed in Southern and Southeastern Asian countries.¹ It is used for 26 efficient Ayurvedic formulations as per the standard set by Indian pharmacopoeia commission and used in Chinese traditional medicine. *A. paniculata* crude preparations are used for treatment of disorders such as respiratory tract infections, sore throat, fevers, and gastric infections.² *A. paniculata* solvents extracts were reported to exhibit several promising pharmacological activities such as antimicrobial, anti-inflammatory, antidiabetic, anticancer, and antimalarial etc.^{3,4} Earlier reports on *A. paniculata* phytochemical investigation suggested that the terpenoids are the major secondary metabolites present in it. Terpenoids from plant sources are effective and selective bioactive agents in order to prevent and treat various diseases.^{5,6} Isolation of bioactive natural products from the plants has several advantages. The structural determination of bioactive molecule is possible after purification and characterization, which may use for bioassays development, synthesis in large quantity and derivatization.^{7,8} In the present study, we have isolated terpenoids from *A. paniculata* aerial part powder on an analytical scale by using maceration in acetone, followed by purification on flash chromatography. Isolated compounds were characterized by various spectroscopic techniques (NMR, HRMS) as an 11,12-didehydro-14-deoxyandrographolide, andrographolide, 14-deoxyandrographolide, isoandrographolide and neoandrographolide. Stereochemistry of andrographolide, and 11,12-didehydro-14-deoxyandrographolide was determined by 2-D NMR and crystallographic study. Two major labdane diterpenoid andrographolide and 14-deoxyandrographolide are separated on a gram scale by rapid isolation protocol.

2A.2 Result and Discussion

2A.2.1. Isolation of Terpenoids from Aerial Part

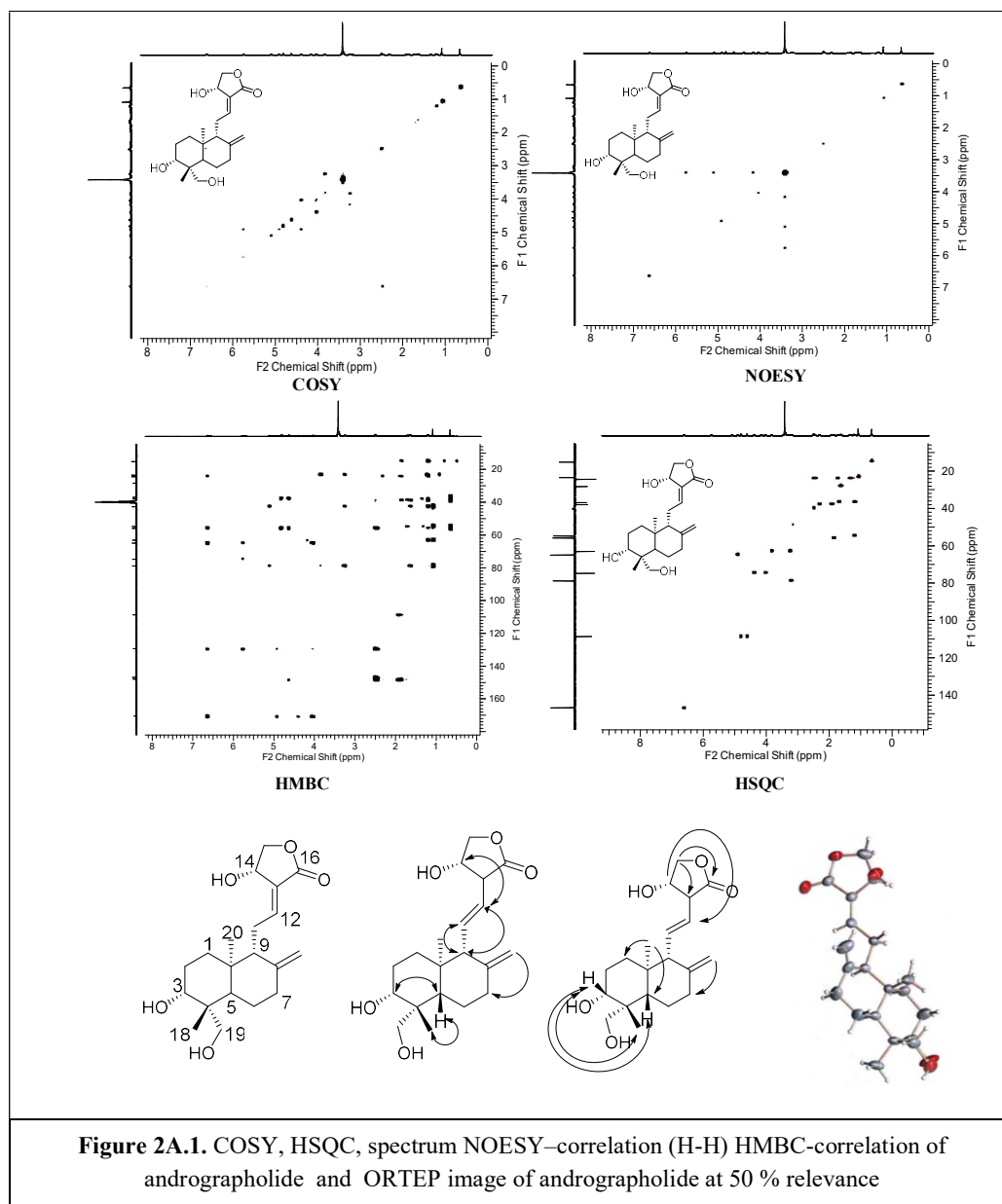
Extraction of *A. paniculata* aerial part powder followed by purification resulted in five labdane diterpenoid, two steroids and flavone (Scheme 2A.1). Out of five terpenoids, two are major diterpenoids (andrographolide, 14-deoxyandrographolide) and three are minor diterpenoids (11,12-didehydro-14-deoxyandrographolide, neoandrographolide,

isoandrographolide). Two steroids were characterised as β -sitosterol, stigmasterol. The acetone extract from aerial part fractionated by using flash column chromatographic techniques with methanol: DCM as eluent. Fractioned obtained were further purified by repeated flash chromatography with fine silica gel resulted in six pure compounds. The green residue obtained after extraction with the acetone was soaked in methanol. Methanolic extract was subjected for successive column chromatographic purification resulted in three compounds. Purification of minor terpenoids was achieved by repeated chromatographic techniques including semi-preparative reverse-phase HPLC-UV. The purity as determine by HPLC of andrographolide, 14-deoxyandrographolide-11,12-didehydro-14-deoxyandrographolide, and neoandrographolide was 99.4 %, 98.2 %, 98.5 %, 95.46 % and 96.4 % respectively.

2A.2.2. Characterization of Terpenoids

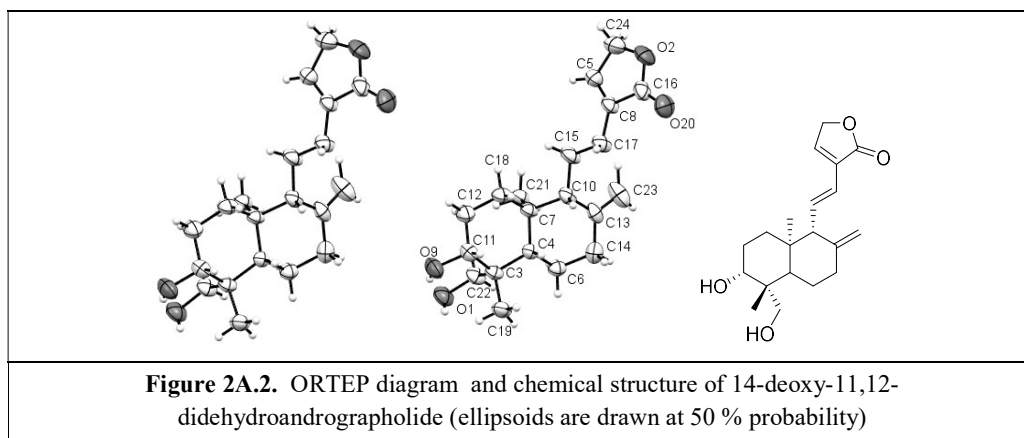
Purified terpenoids were characterized by the analyses of NMR spectrometric and HR-ESI(+)-MS data. Compound 1 was obtained as white crystalline solid. HRMS spectra showed protonated peak $[M + H]^+$ and sodiated peak m/z 351 $[M + Na]^+$ at m/z 373, with suggested molecular formula $C_{20}H_{30}O_5$. The molecular formula suggested it was diterpenoid and six degrees of unsaturation. In IR spectrum stretching frequency at 1720 cm^{-1} suggested the presence of α,β -unsaturated lactone, stretching frequency at 1673 cm^{-1} suggested alkyl double bond and peak at $3299, 3400\text{ cm}^{-1}$ indicated the presence of the hydroxyl group. ^{13}C -NMR, DEPT NMR spectrums peak at δ 147.66, 146.44, 129.02 and 108.33 suggested the presence of four alkenes carbon out of which two are quaternary carbon, one is secondary, and one is primary. DEPT showed eight methylene carbon, two methyl carbon, five quaternary carbons and five methine carbon. 1D-NMR results were in combination with 2D-NMR shift correlated ^{13}C with ^1H in HMBC spectroscopic data. HSQC and HMBC correlations observed between H-19 (δ 1.98 and 2.32) with C-20 at δ 89.36 and H-20 (δ 1.98 and 2.32) with C-11 at δ 89.36 confirmed the stereochemistry. HMBC Correlation observed of H-5 (δ 1.98) and H-6 (δ 1.98) with C-18 δ 89.36 confirmed position; lactone H-14 was confirmed based on HSQC and HMBC spectra (Figure 2A.1). The signal at δ H 5.94 (d, $J=5.52\text{ Hz}$) was assigned to H-14 according to the correlations of H-14 with C-12 (δ C 150.6), C-13 (δ C 123.8) and C-16 (δ C 169.1) in the HMBC spectrum. NOESY and COSY correlation suggested the position of hydrogen. Recrystallization of compound-1 in methanol was performed,

colourless crystals formed was then subjected for single X-ray diffraction. X-ray analysis confirmed the assigned stereochemistry in the molecule. Data analysis compared to earlier reports suggested that the compound-1 was andrographolide (Figure 2A.1).⁹



Compound-2 was obtained as colourless crystalline solid. HRMS showed peak at $[M+Na]^+$; m/z 357.2042 and suggested molecular formula $C_{20}H_{30}O_4$. Decrease in 16 amu molecular mass compared to compound-1 suggested a loss of hydroxyl

functionality. Six degrees degree of unsaturation in the molecule, which was calculated from a molecular formula. In IR spectrum a stretching frequency at 1734 cm^{-1} suggested the presence of α , β -unsaturated ester, the stretching frequency at 1663 cm^{-1} suggested alkenes double bond. IR-peak at $3299, 3400\text{ cm}^{-1}$ indicated the presence of the hydroxyl group. Comparison of $^1\text{H-NMR}$ and $^{13}\text{C-NMR}$ data of compound-2 with andrographolide suggested that except the peak at C-12, C-13 and C-14 carbons all carbon peaks are matches. Mass and spectroscopic data compared with reported analysis data suggested that the compound-2 is 14-deoxyandrographolide. Compound-3 was obtained as colourless crystalline solid. HRMS showed $[\text{M} + \text{Na}]^+$ at $m/z\ 355.1885$ and suggested molecular formula $\text{C}_{20}\text{H}_{28}\text{O}_4$ with seven degrees of unsaturation. Decrease in 18 amu molecular mass compared to compound-1 suggested a loss of hydroxyl group and hydrogens. IR spectrum showed a stretching frequency at 1734 cm^{-1} indicated the presence of α , β -unsaturated ester, the stretching frequency at 1663 cm^{-1} suggested alkenes double bond. The presence of the hydroxyl group suggested by IR-peak at $3299, 3400\text{ cm}^{-1}$. Comparison of $^1\text{H-NMR}$ and $^{13}\text{C-NMR}$ data of compound-3 with compound-1 suggested the similarity in all skeletal carbons except C-11, C-12, C-13 and C-14. Recrystallization of compound-1 in methanol was performed, colourless crystals formed was then subjected for single X-ray diffraction. X-ray analysis confirmed the assigned stereochemistry in the molecule. Further data analysis earlier reports suggested that the compound-3 is 14-deoxy-11,12-didehydroandrographolide. (Figure 2A.2, Table 2A.1).

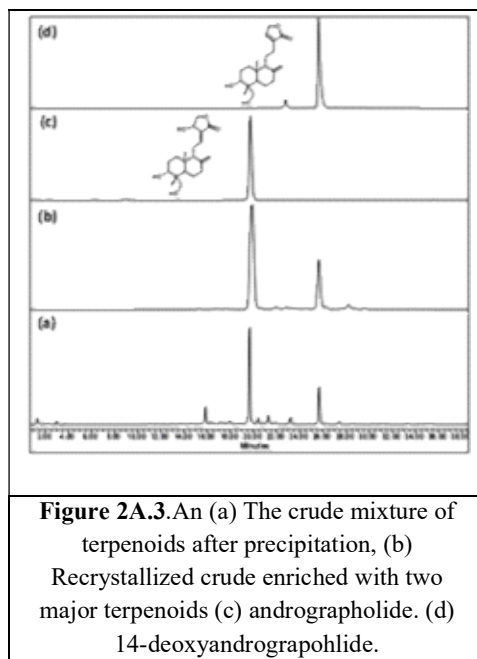


Compound-5 was obtained as a colourless solid; HRMS peak at $m/z\ 351.2117\ [\text{M}+\text{H}]^+$, suggested molecular formula $\text{C}_{20}\text{H}_{31}\text{O}_5$ with six degrees of unsaturation. IR spectrum showed a stretching frequency at 1734 cm^{-1} indicating the presence of lactone, stretching frequency at 1663 cm^{-1} suggested alkenes double bond, stretching at $3325,$

3400 cm^{-1} showed the presence of hydroxyl group along with a peak at 1260 cm^{-1} indicated presence the cyclic ether in the molecule. ^{13}C , DEPT NMR spectrums peak at δ 143.32, 138.15 showed the presence of two alkenes carbon. DEPT analysis revealed seven methylene carbon, two methyl carbon, four quaternary carbons and seven methines. Spectroscopic data obtained was superimposed on the reported data to confirm the structure, the compound-5 was identified as isoandrographolide. ref Similarly the structural data analysis of all the compounds was performed further compared with the reported data and characterised compounds.¹⁰

2A.2.3 Preparative Scale Isolation of Major Terpenoids

In acetone leave extract crude (5 g) dissolved in dichloromethane resulted in the precipitation (565.1 mg). The precipitate was



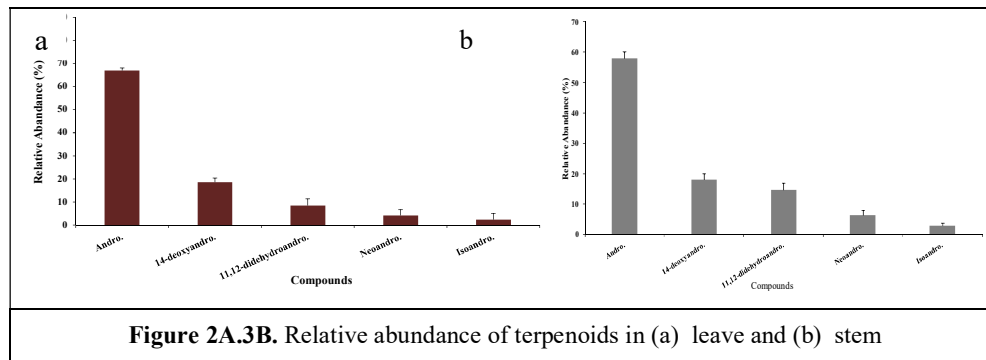
then filtered in order to remove the solvent and residue was then treated with charcoal to remove colour pigments. Recrystallization resulted into a mixture of compounds (289.6 mg) (Figure 2A.3). The mixture contains major of andrographolide (180.3 mg) and 14-deoxyandrographolide (64 mg) in minor quantity along with the other compounds in trace amount. Flash chromatographic separation of mixture resulted in pure compounds. The protocol used for the separation of andrographolide and 14-deoxyandrographolide is useful for preparative

scale separation because it is rapid and economic required a low amount of solvents.

2A.2.4 Relative Profiling of Isolated Terpenoids

The relative levels of individual five terpenoids were determined in stem and leave per gram of tissue (Figure 2A.3b). The powered part was extracted in various organic solvents methanol was found to be the best because it contained a higher concentration of phytochemicals compared other solvents. Tissue-specific profiling of five terpenoids revealed that andrographolide concentration is major in both stem and leaves

comparative concentration than the other terpenoids. 14-deoxyandrographolide was the second major component stem and 11,12-didehydro-14-deoxyandrographolide in leaves. Isoandrographolide and neoandrographolide concentration are almost same in the stem.



2A.3 Conclusion

Terpenoids from *A. paniculata* aerial part were isolated on an analytical scale and purified over silica gel flash chromatography. Isolated compounds were characterized by spectroscopic techniques (NMR, HRMS) as andrographolide, isoandrographolide, 14-deoxyandrographolide, 14-deoxy-11,12-didehydroandrographolide, and neoandrographolide. Further andrographolide and 14-deoxyandrographolide were isolated.

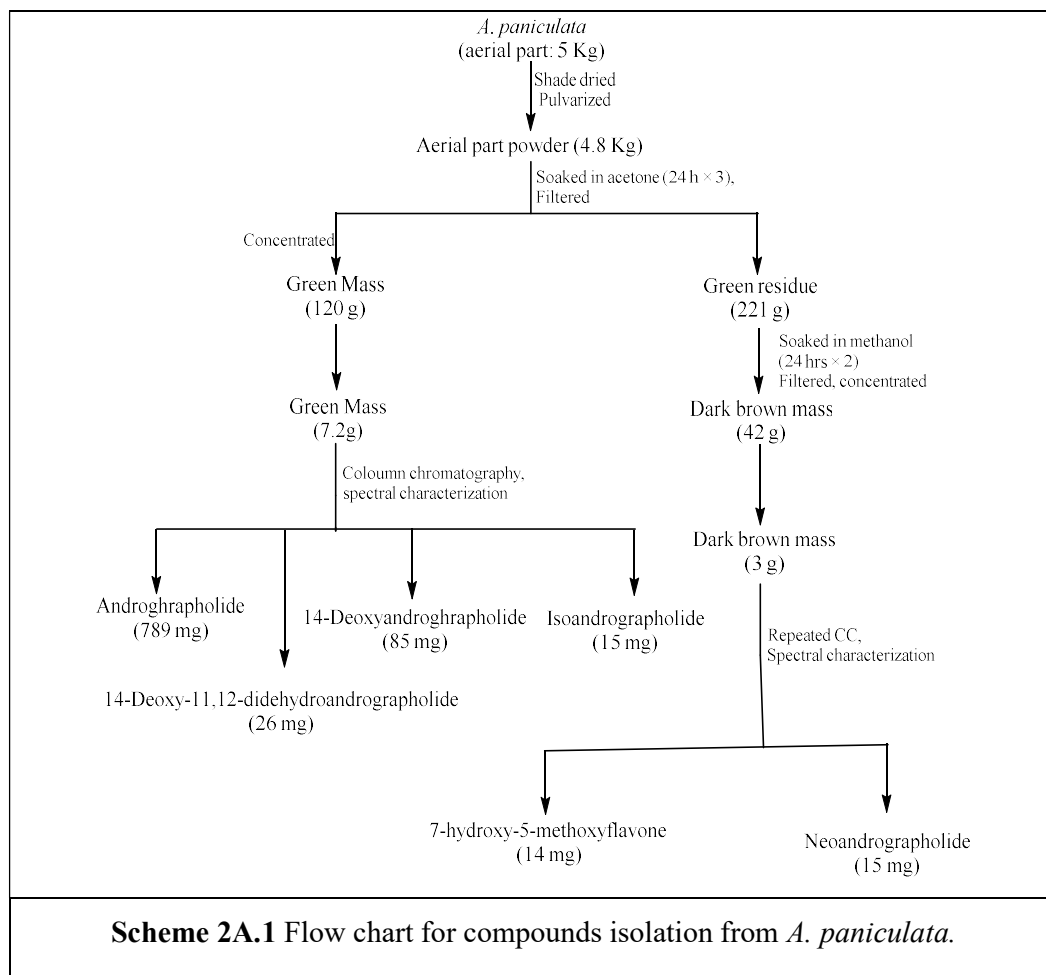
2A.4 Experimental Section

2A.4.1 Collection and Identification

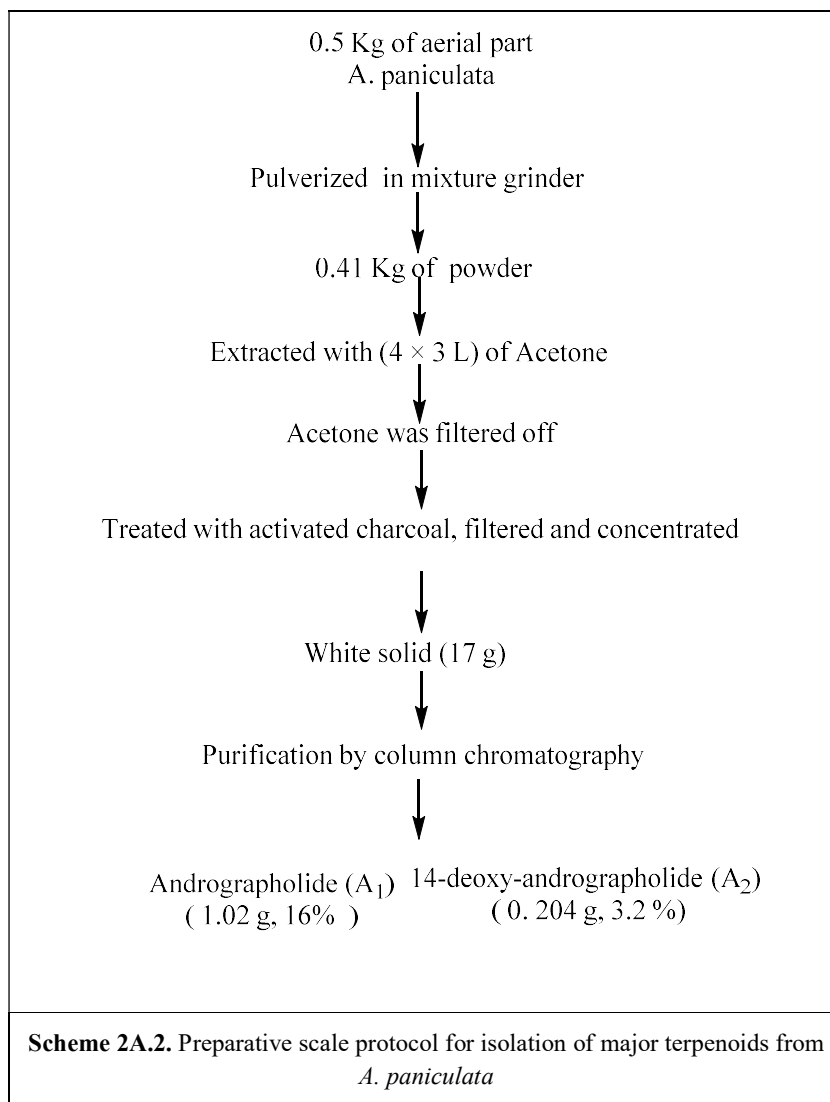
Whole plants, in the flowering stage, were collected from Eastern India, during 12 September 2011. Herbarium deposited in Research Institute (ARI Sp. No. THV-1), Pune, India identified and authenticated as *Andrographis paniculata*.

2A.4.2 Extraction and Isolation

The collected plant material was shade dried and cleaned off to remove unwanted plant material and the adhering dust. Aerial parts, roots were separated and pulverised in mixture grinder powder obtained has been stored in dry place absence of sunlight.



Aerial part powder (5 Kg) was soaked in acetone (5 L), stir using homogenizer at room temperature. After 24 h extract had filtrated using filter paper, obtained residue again soaked in an equal volume of acetone, and the same protocol had repeated for three times. Acetone extract (221 gm) was soaked in methanol (1000 ml) and macerated in homogeniser at room temperature. After 24 h the soaked material was filtered and concentrated; a similar procedure was repeated for three times for maximum extraction. Filtrates were combined and concentrated at 50 °C under reduced pressure yield a dark green extract (120 g, 2.4 % based on dry plant weight). The acetone extract was separated and purified by flash column chromatography in methanol: dichloromethane (MeOH: DCM) gradient. Fifty-five gram of the acetone extract of enriched with labdane terpenoids mixture was fractionated on to a silica gel column (14 cm × 6 cm).



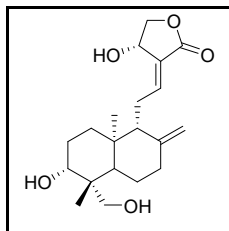
Silica gel was first equilibrated with DCM and further eluted with gradient solvent system provided 11 fractions (AP-1 to AP-11). Fraction AP3 (136 g) from the first column purified using a gradient solvent system 0.1 to 2 % (methanol: DCM) yielded a total of twenty (AP3a-w) fractions. Fractions with similar R_f on TLC were pulled together into the round bottom flask and concentrated. After concentrating the fractions white crystalline solid was obtained, which was recrystallized in methanol provided pure needle-like crystals of compound-2 (85 mg). Fraction-AP4 (60 mg) was subject to CC in 0.2 to 0.5 % methanol in DCM to collect 10 fractions (AP4 a-j). Fractions having a similar spot on TLC were pulled together and concentrated, which was gave pure solid compound-3 (22 mg). Successive CC of

fraction-AP5 (89 mg) in gradient methanol:DCM (0.2 to 0.5 %) yielded white colour solid compound-5 (22 mg). First, major column fraction-AP6 (1.6 g) was purified on silica gel 240-400 mesh using 1 to 2 % (methanol: DCM), sixty fractions were collected. Crystals were obtained after concentration of combined fractions, which was further recrystallized in methanol yielded compound-1 (789 mg). The crude methanol extract (42 g) obtained out of which dark extract (3 g) was fractionated on silica gel CC in methanol: DCM. for CC separation which yielded six fractions. Fraction 2 (76 mg) was subjected to successive CC in methanol in DCM resulted in compound 5 (15 mg).

2A.4. 3 Characterization of Terpenoids

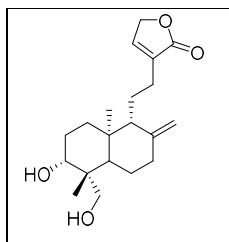
Andrographolide

White crystalline solid; m.p. 218-222 °C; IR (CHCl₃, cm⁻¹) ν_{\max} = 908, 1673, 1738, 3299, 3400 cm⁻¹; UV (methanol): 235 nm; HRMS (ESI) m/z : [M+Na]⁺ Calcd for C₂₀H₃₀O₅Na, 373.1991; found, 373.20. ¹H NMR (400 MHz, , DMSO-d₆, ppm) :



¹H NMR (400 MHz, CDCl₃, ppm): δ 6.63-6.60 (td, J = 6.84, 1.72 Hz, 1H), 5.74-5.76 (d, J = 5.81, 1H), 5.08-5.10 (d, J = 5.81, 1H), 4.91 (m, 1H), 4.81 (s, 1H), 4.62 (s, 1H), 4.37-4.41 (m, 1H), 4.16-4.17 (m, 1H), 4.05-4.02 (dd, J = 1.51, 9.79, Hz 1H), 3.82-3.85 (d, J = 10.54 Hz, 1H), 3.23-3.28 (m, 3H), 2.30-2.33 (m, 1H), 1.75-1.98 (m, 2H), 1.62-1.71 (m, 5H), 1.33-1.36 (m, 1H), 1.18-1.21 (m, 2H), 1.08 (s, 3H), 0.65 (s, 3H). ¹³C NMR (100 MHz, DMSO-d₆, ppm): δ 170.07, 147.66, 146.44, 129.02, 108.33, 78.51, 74.42, 64.58, 62.72, 55.54, 54.41, 42.32, 39.93, 39.09, 38.88, 37.56, 27.94, 24.04, 23.13, 14.81.

14-deoxyandrographolide

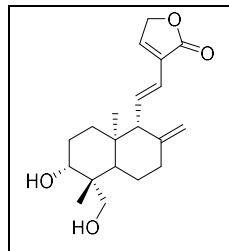


White solid; m.p. 170-173 °C; IR (CHCl₃, cm⁻¹) ν_{\max} = 904, 1663, 1734, 2900, 3325, 3400 cm⁻¹; UV (methanol): 238 nm; HRMS (ESI) m/z : [M]⁺ [M+Na]⁺ Calcd for C₂₀H₃₀O₄Na, 357.2042; found, 373.2024. ¹H NMR (400 MHz, CD₃OD, ppm): 7.10-7.12 (td, J = 1.52, 2.91 Hz, 1H), 4.83-4.88 (t, J = 1.64, 3.54 Hz, 1H), 4.78 (s, 1H), 4.59 (s, 1H), 4.16- 4.19 (d, J = 10.79 Hz, 1H), 3.42- 3.47 (t, 1H), 3.28- 3.35 (m, 3H), 2.40- 2.43 (m, 2H), 2.10- 2.13 (m, 2H), 1.91- 1.96 (m, 1H), 1.75- 1.80 (m, 6H), 1.58 (s, 2H), 1.17- 1.25 (m, 6H), 0.64 (s, 3H).

^{13}C NMR (100 MHz, CD_3OD_4 , ppm): 174.42, 146.74, 144.15, 134.52, 107.27, 80.37, 70.14, 64.12, 55.94, 55.18, 42.69, 38.94, 38.09, 36.77, 28.09, 24.43, 23.90, 22.69, 22.63, 21.83, 15.17.

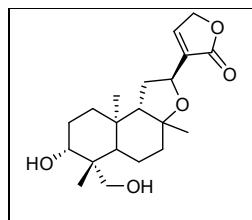
11, 12-Didehydro-14-deoxyandrographolide

White crystal; m.p. 204-206 °C; IR (CHCl_3 , cm^{-1}) ν_{max} = 904, 1663, 1734, 2900, 3325, 3400 cm^{-1} ; UV (methanol): 252 nm; HRMS (ESI) m/z : $[\text{M}+\text{Na}]^+$ Calcd for $\text{C}_{20}\text{H}_{28}\text{O}_4\text{Na}$,



355.1885; found, 373.1874. ^1H NMR (400 MHz, CDCl_3 , ppm) : 7.12-7.13 (td, J = 1.83, 3.66 Hz, 1H), 6.79-6.86 (d, dd, J = 10.07, 5.50 Hz, 1H), 6.5-6.9 (d, J = 16.03 Hz, 1H), 4.77- 4.79 (m, 2H), 4.74- 4.75 (m, 1H), 4.16- 4.19 (d, J = 11.45 Hz, 1H), 3.32- 3.45 (m, 2H), 2.39- 2.43 (m, 1H), 2.26- 2.28 (d, 1H), 1.96- 2.04 (m , 1H), 1.67- 1.78 (m, 1H), 1.46- 1.49 (m, 1H), 1.27- 1.33 (m, 1H), 1.21- 1.23 (m, 3H), 1.09- 1.20 (m, 2H), 0.77 (s, 1H). ^{13}C NMR (100 MHz, CDCl_3 , ppm): 172.15, 147.82, 139.55, 136.59, 134.84, 122.60, 107.81, 81.14, 72.22, 65.12, 62.94, 47.21, 43.81, 40.29, 38.17, 34.82, 29.20, 25.54, 23.26, 15.84.

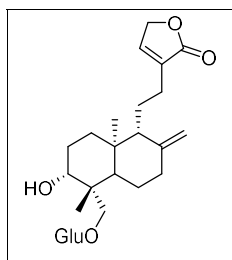
Isoandrographolide



White solid; m.p. 204-206 °C; IR (CHCl_3 , cm^{-1}) ν_{max} = 904, 1260, 1663, 1734, 2900, 3325, 3400 cm^{-1} ; UV (methanol): 252 nm; HRMS (ESI) m/z : $[\text{M}+\text{H}]^+$ Calcd for $\text{C}_{20}\text{H}_{31}\text{O}_5$, 351.2171; found, 373.2163. ^1H NMR (400 MHz, CDCl_3 , ppm) : 7.22-7.23 (td, J = 6.84, 1.72 Hz, 1H), 4.74 (s, 1H), 4.58-4.62 (t, J = 7.58, 8.07Hz, 1H), 4.16-4.19 (d, J = 11.0 Hz, 1H), 3.55 (s, 1H), 3.34-3.37 (d, J = 10.27 Hz, 1H), 3.26-3.29 (d, 11.0 Hz, 1H), 2.32-2.35 (m, 1H), 2.09-2.13 (m, 1H), 1.95-1.97 (m, 1H), 1.66-1.69 (m, 1H), 1.47-1.45 (m, 2H), 1.33-1.41 (m, 2H), 1.17 (s, 3H), 1.03 (m, 3H), 0.87 (s, 3H). ^{13}C NMR (100 MHz, CDCl_3 , ppm): 172.61, 143.32, 138.15, 82.61, 80.56, 72.93, 70.50, 64.05, 57.82, 52.47, 42.21, 38.87, 36.04, 35.49, 32.73, 31.41, 27.20, 22.69, 18.02, 16.31.

Neoandrographolide

Amorphous powder; m.p. 200-202 °C; IR (CHCl₃, cm⁻¹) ν_{\max} = 904, 1458, 1674, 1731, 2934, 3307, 3400 cm⁻¹; UV (methanol): 230 nm; HRMS (ESI) m/z : [M+Na]⁺ Calcd for



C₂₆H₄₂O₉Na, 519.2643; found, 519.2641. ¹H NMR (400 MHz, CD₃OD, ppm) : 7.34- 7.36 (td, J = 1.53, 2.75, 1H), 4.82-4.83 (d, J = 1.83, 1H), 4.63 (s, 1H), 4.16- 4.18 (d, J = 7.63, 1H), 4.08- 4.10 (d, J = 9.46 Hz, 1H), 3.84-3.87 (dd, J = 2.44, 1H), 3.66- 3.69 (m, 1H), 3.33 -3.35 (d, J = 8.85 Hz, 1H), 3.28-3.30 (m, 2H), 3.21-3.25 (m, 2H), 3.13-3.18 (m, 1H), 2.46-2.44 (m, 2H), 2.08-2.13 (m, 1H), 1.94-2.00 (m, 2H), 1.85-1.89 (m, 1H), 1.75-1.81 (m, 3H), 1.59-1.69 (m, 4H), 1.45-1.48 (m, 1H), 1.34-1.43 (m, 2H), 1.25-1.28 (m, 1H), 1.19-1.23 (m, 1H), 1.05-1.11 (m, 2H), 1.03 (s, 4H), 0.91-0.99 (m, 2H), 0.71 (s, 3H). ¹³C NMR (100 MHz, CD₃OD, ppm): 177.14, 149.36, 147.76, 134.96, 107.42, 105.21, 78.37, 77.88, 75.40, 73.58, 72.23, 62.88, 57.98, 57.83, 48.64, 40.36, 39.82, 39.51, 37.33, 28.46, 25.76, 25.59, 20.20, 16.00.

2A.5 Spectral Copies

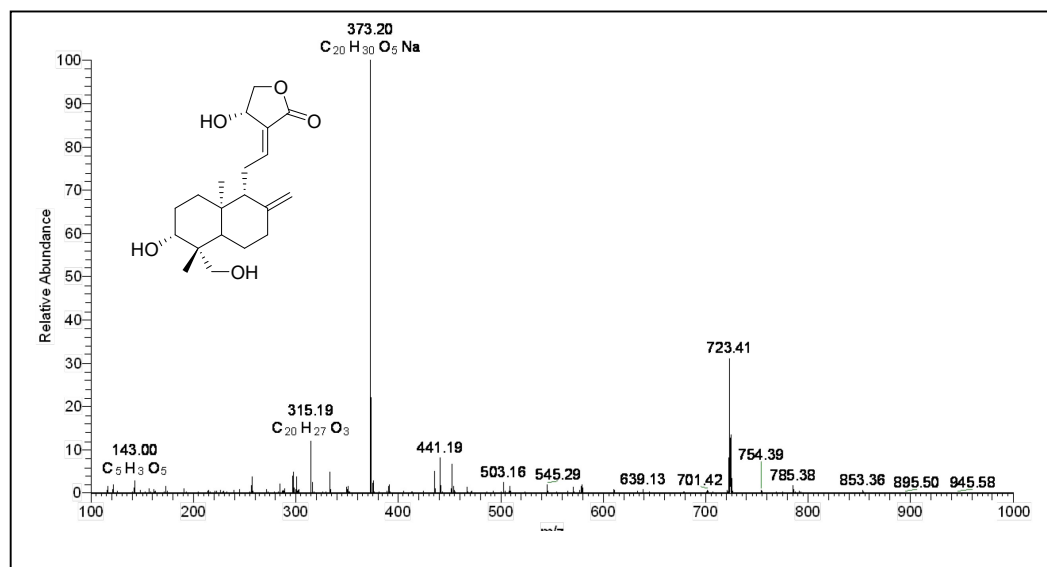
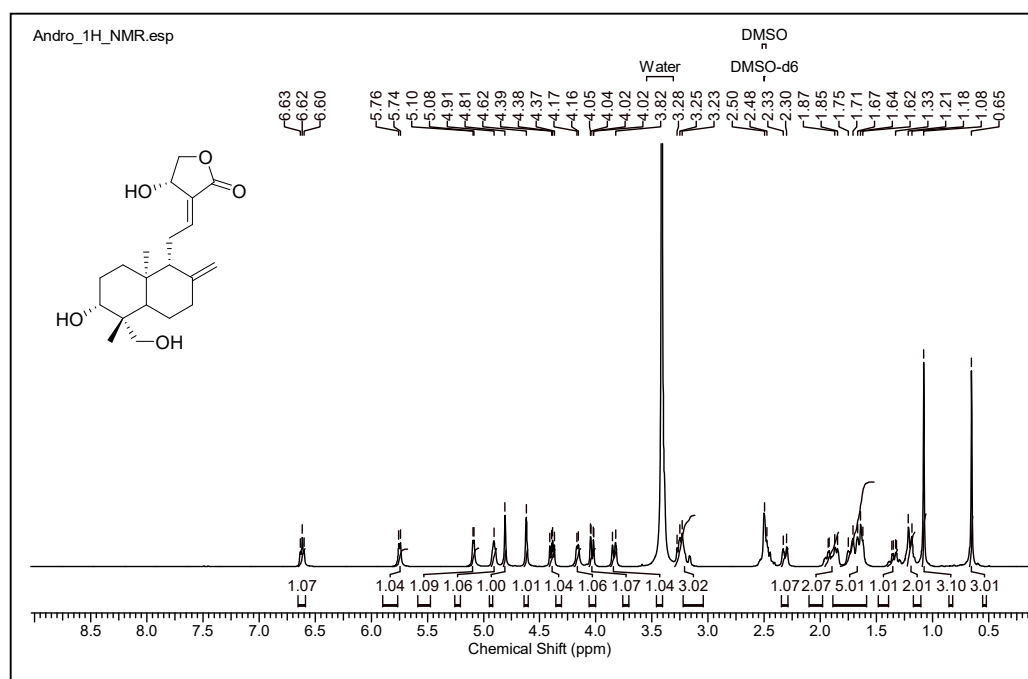


Figure 2A.4a. LC-ESI (+)-HRMS of andrographolide

Figure 2A.4b. 1H NMR spectrum (DMSO- d_6 , 400 MHz) of andrographolide

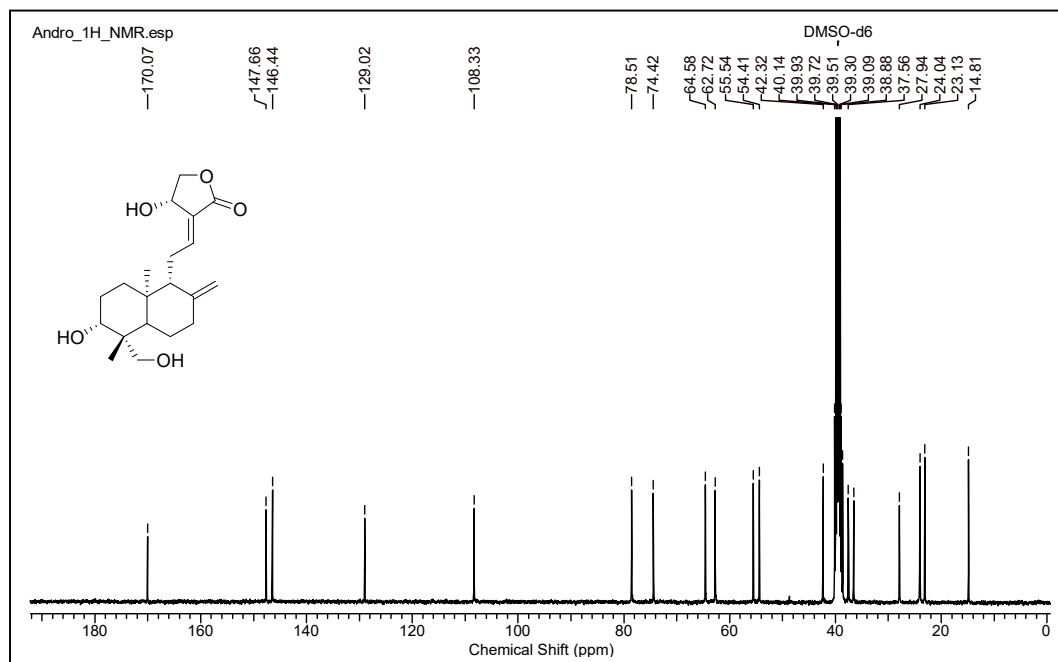


Figure 2A.4c. ^{13}C NMR spectrum (DMSO- d_6) of Andrographolide

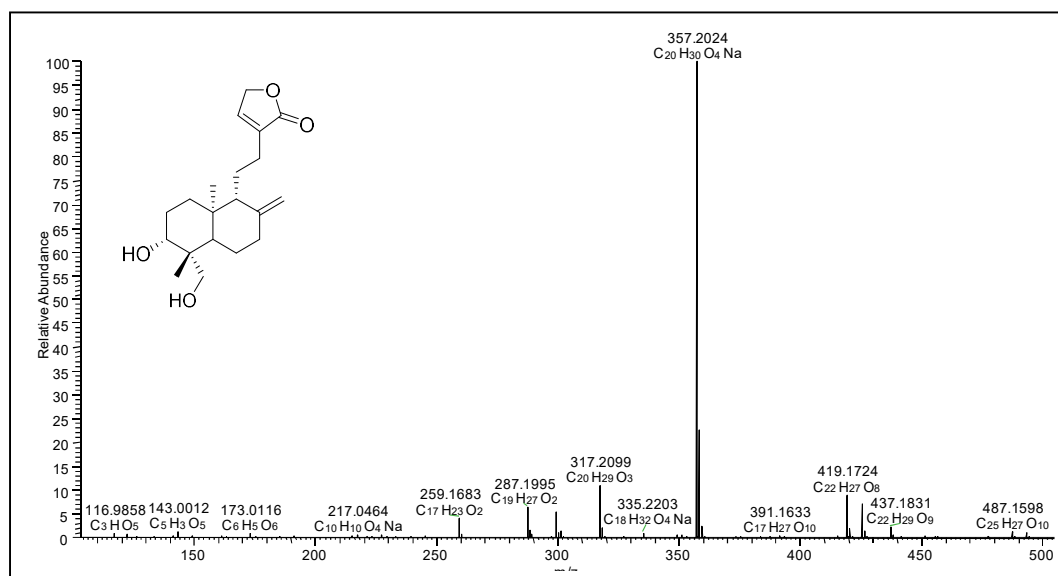


Figure 2A.5a. LC-ESI (+)-HRMS of 14-deoxyandrographolide

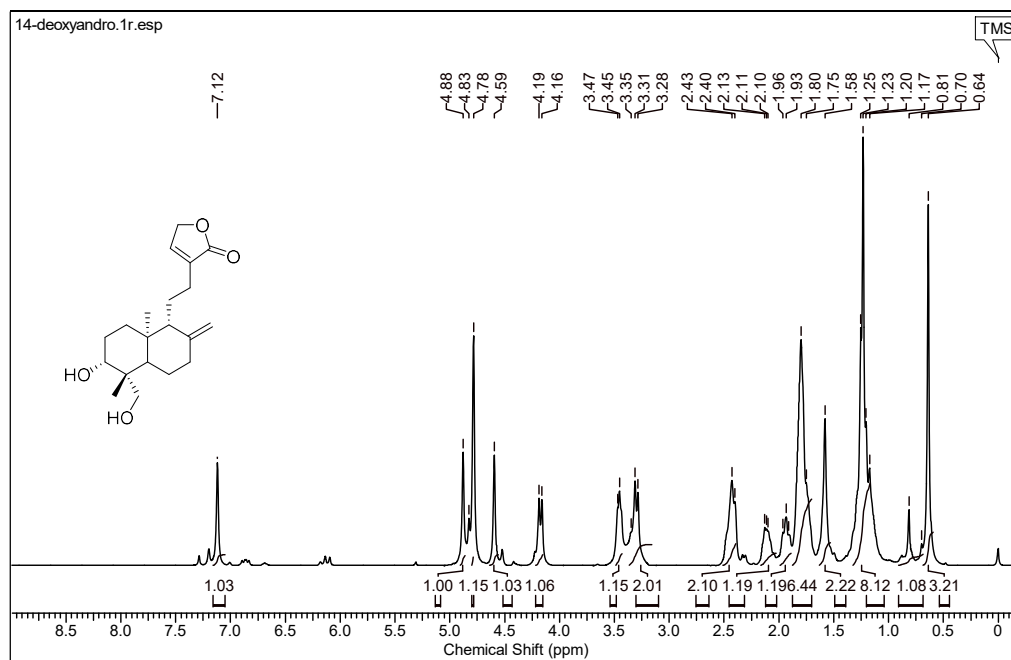


Figure 2A.5b. ^1H -NMR spectrum (CD_3OD) of 14-deoxyandrographolide

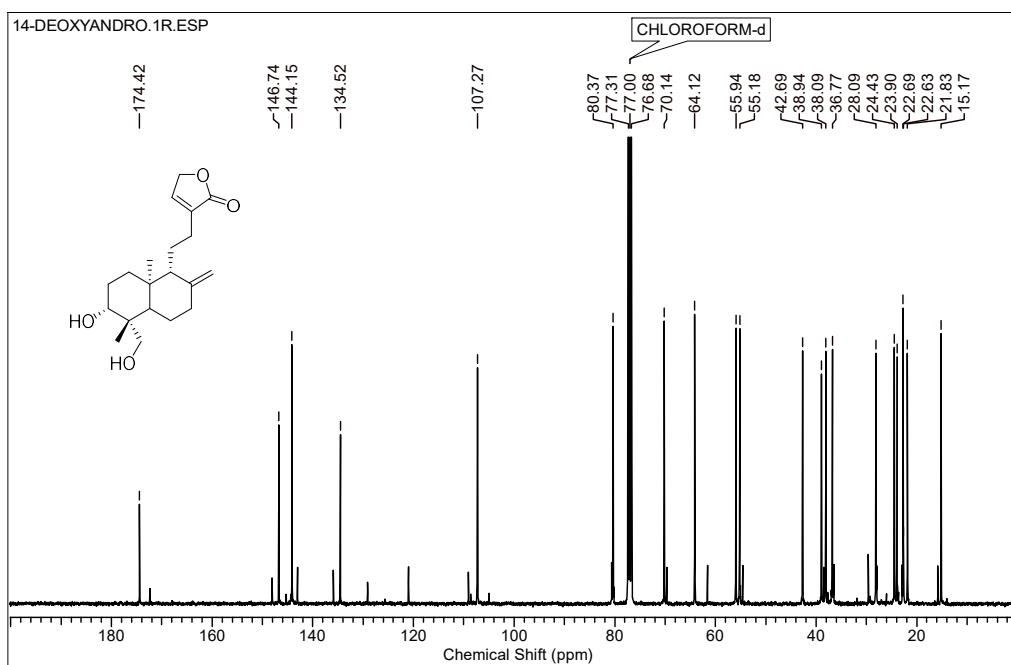


Figure 2A.5c. ^{13}C -NMR spectrum (DMSO-d_6) of 14-deoxyandrographolide

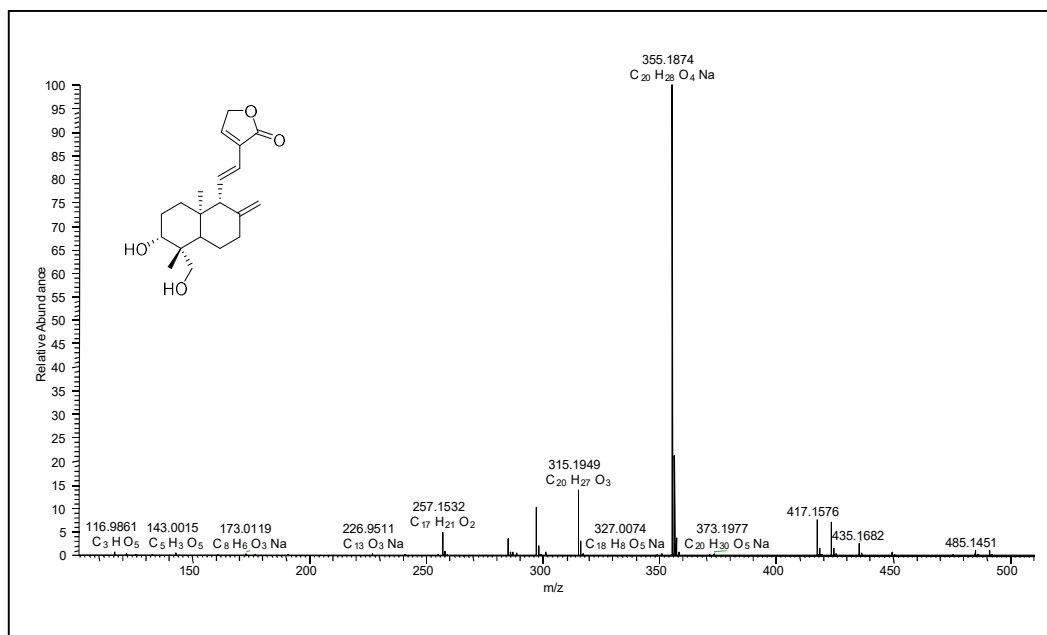


Figure 2A.6a. LC-ESI (+)-HRMS of 14-deoxy-11, 12-didehydroandrographolide

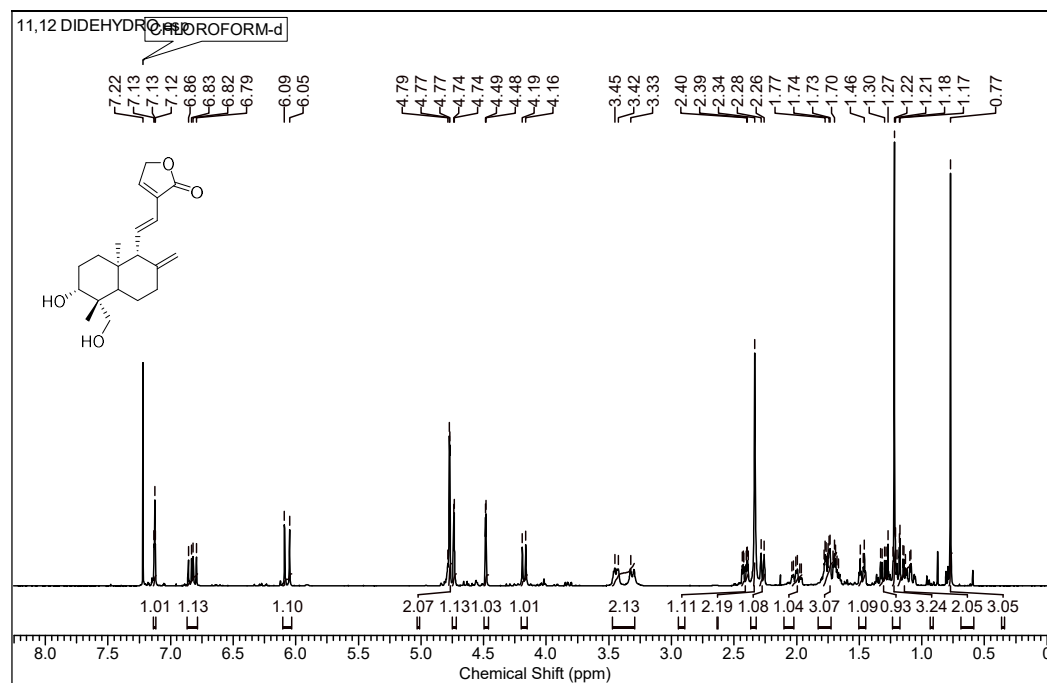


Figure 2A.6b. ¹H-NMR spectrum (CD₃OD) of 14-deoxy-11,12-didehydroandrographolide

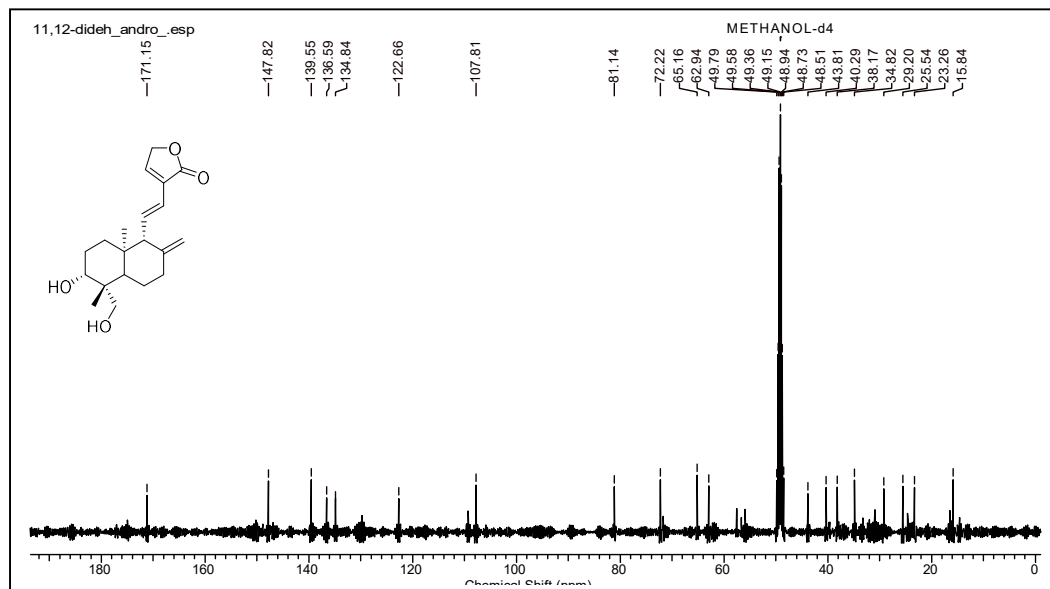


Figure 2A.6c. ^{13}C -NMR spectrum (CD_3OD) of 14-deoxy-11,12-didehydroandrographolide

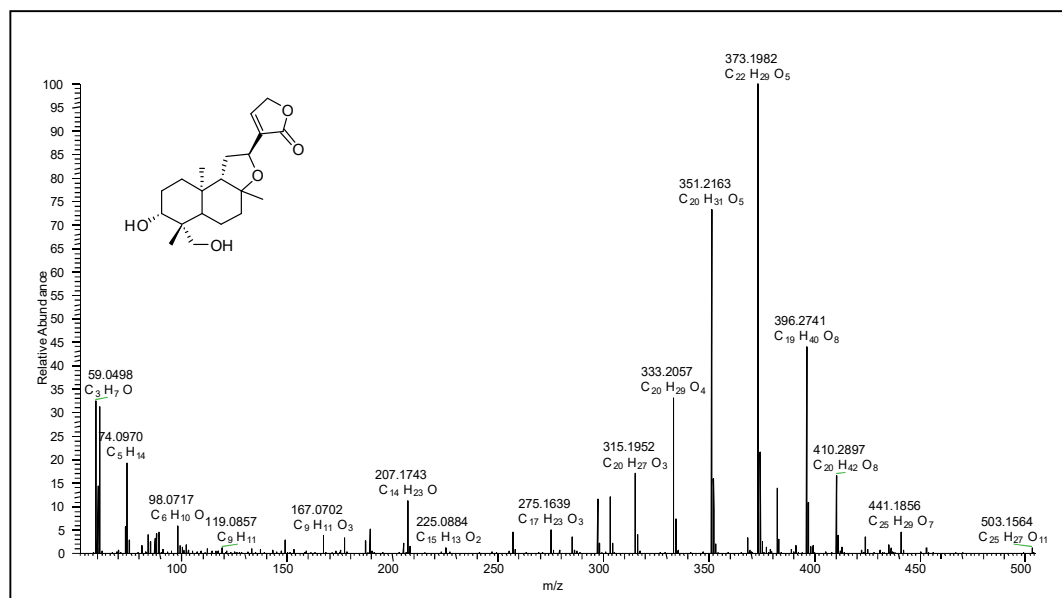


Figure 2A.7a. LC-ESI (+)-HRMS of Isoandrographolide

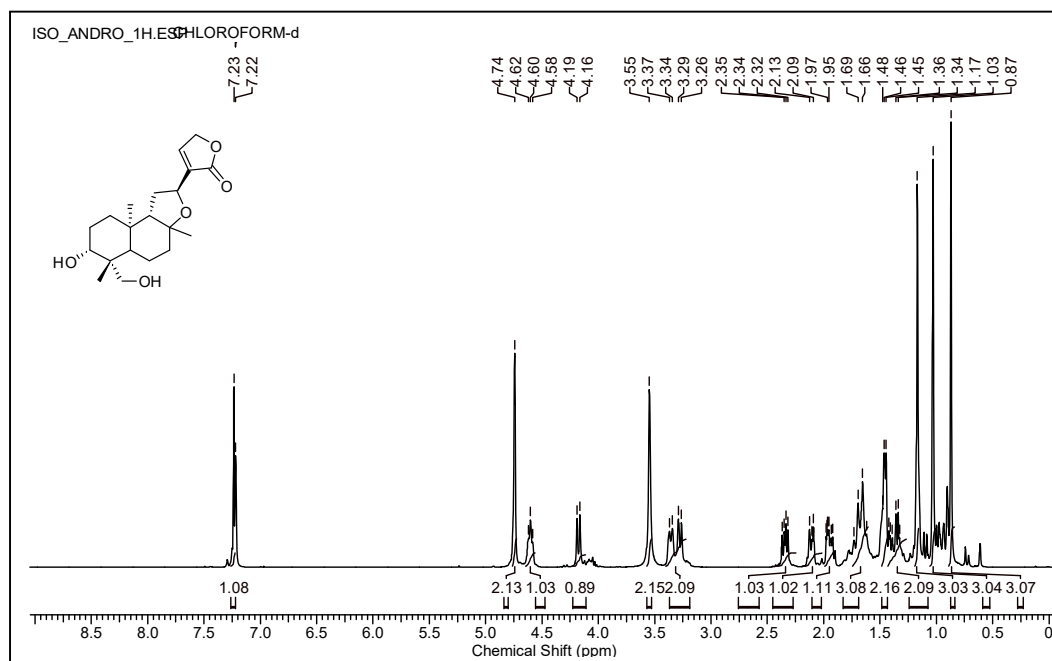


Figure 2A.7b. ^1H -NMR spectrum (CDCl_3) of Isoandrographolide

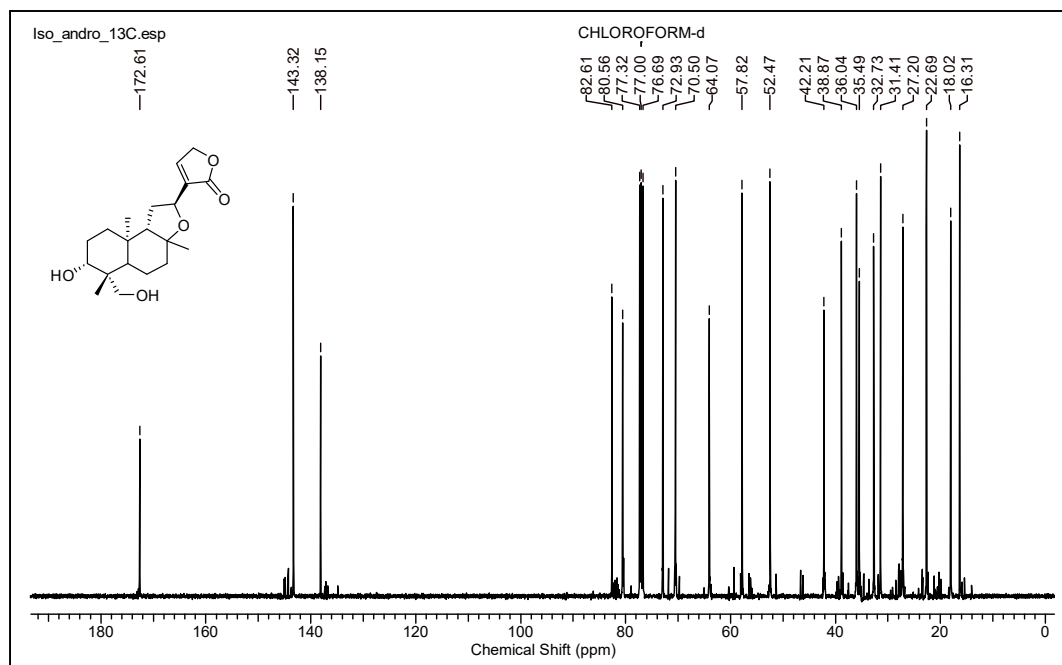


Figure 2A.7c. ^{13}C -NMR spectrum (CDCl_3) of Isoandrographolide

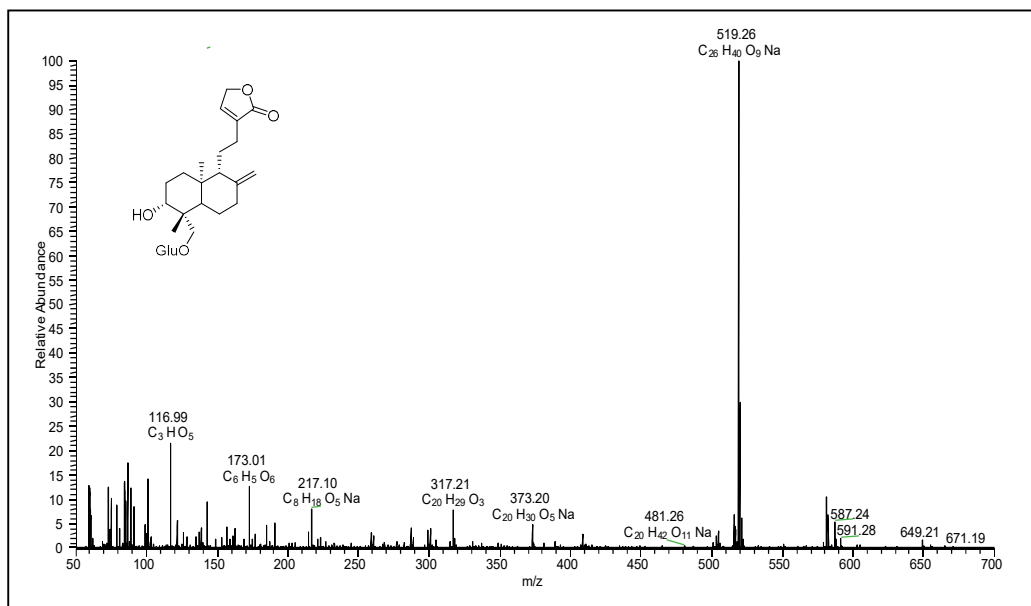


Figure 2A.8a. LC-ESI (+)-HRMS of Neoandrographolide

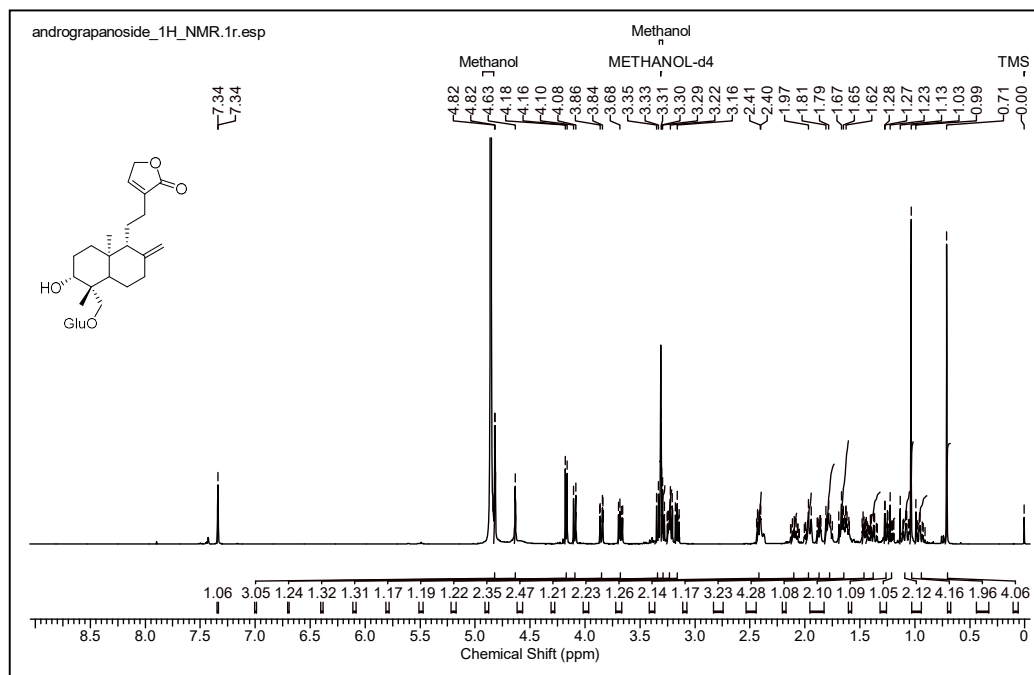


Figure 2A.8b. ¹H-NMR spectrum (CD₃OD) of Neoandrographolide

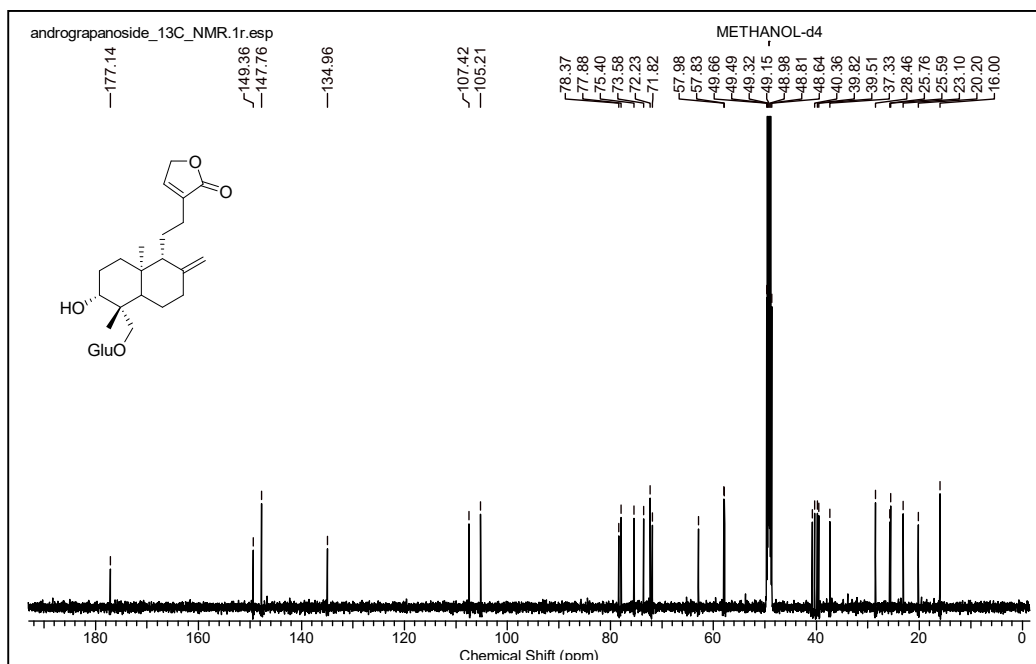


Figure 2A.8c. ^{13}C - NMR spectrum (CD_3OD) of Neoandrographolide

Table 2A.1 X-ray data for 14-deoxy-11, 12-didehydroandrographolide

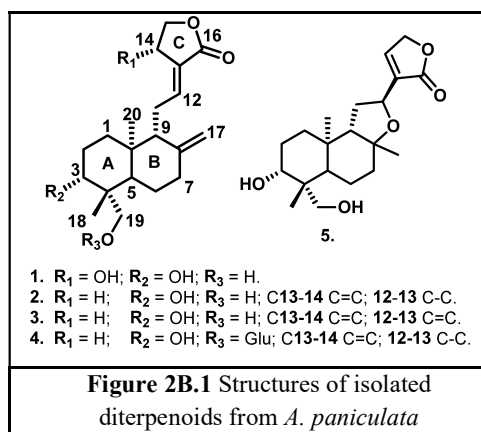
Parameter	Value
Temperature	295 K
Wavelength	1.54056 Å
Space group	$P 2_1$
Unit cell length	a. 6.7598 (4) Å b. 9486 (4) Å c. 19.3815 (12) Å
Cell angles	α . 90 β . 93.234 (5) γ . 90
Volume	908.925 Å ³

Chapter 2: Section B

**Expedient MPLC Based Preparative Isolation and
MS/MS Characterization of Labdane Diterpenoids
from *A. paniculata***

2B.1 Introduction

A. paniculata is a rich source of labdane diterpenoids having a similar skeleton like andrographolide. These diterpenoids are well known for its range of significant bioactivities including anti-inflammatory, antibacterial, anti-cancer, anti-diabetic.^{11,12,13,14} Significant bioactivities value of these diterpenoids created the need to access these terpenoids on the preparative scale for detail investigation of their bioactivities, mode of action and structural modifications aiming at more potent



analogue.^{15,16,17,18} These diterpenoids bear high structural similarities among themselves; thus making it troublesome to resolve them through chromatographic separation techniques.¹⁹ Also, these diterpenoids are featured by a complex structure, numerous stereocenters and sensitive functionality on the skeleton.^{20,21}

These associated obstacles make the synthetic chemical approach ineffective to synthesise these molecules. Therefore, there is a need to develop a useful, rapid and reproducible technique for isolation, which facilitates the easy availability of diterpenoids in large scale. Separation protocols from *Andrographis paniculata* reported earlier solely focused on analytical scale isolation with few targeted compounds.²² Preparative scale isolation of natural products by using medium pressure liquid chromatography (MPLC) has advantages such a rapid, efficient, robust technique, and reproducible.²³ In the previous reports from our group, the MPLC based protocol was developed for the isolation of significant triterpenoids from Neem fruits and Neem oil.^{24,25} In this study, we have developed a preparative scale procedure for the isolation of five major diterpenoids with purity > 95 % by successive application of normal phase and reverse phase cartridges. By using HPLC evaluated the effectiveness of the process and purity of the isolated compounds.²⁶

Ultra performance liquid chromatography coupled with high-resolution mass spectrometry is a technique to recognise the expected metabolites in the complex plants or biological mixtures even at a minor concentration (nM-pM range) with low

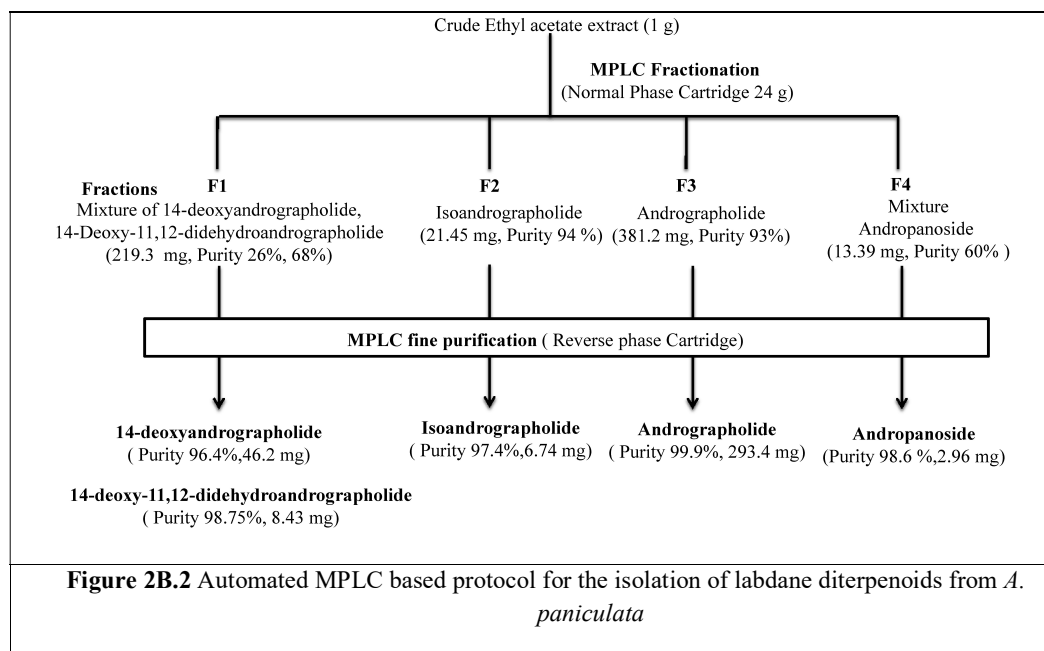
sample requirement, high sensitivity, rapidity, and high accuracy.^{27,28} Signature MS-MS spectra along with structure-fragmentation relationship can further be applicable for the novel metabolites searching with the similar skeleton, screening from various plant sources and investigating the metabolism, biosynthesis, and degradation related to the bioactive molecules having diterpenoid skeleton quantitatively and qualitatively.^{25,29,30} Detection of the individual metabolite in less quantity from the complex phytochemical extract required the reference standard which may not be available commercially, difficult for isolation or also for synthesis. ESI-MS spectrum of the compound is not that much reliable for the identification as it provides only the molecular mass and corresponding chemical formula. In such a situation, the LC system with high-resolution mass spectrometry (LC-HRMS) is a more sensitive and rapid technique used for the analysis of the metabolite from the phytochemical extract.³¹ This technique has a higher condense limit so that metabolite structural information can be extracted through tandem fragmentations of the desired ion.³²

Herein, we report UPLC-ESI(+)-quadrupole/orbitrap-MS/MS-based characterization of isolated diterpenoids of andrographolide skeleton. Also, the structure-fragment relations were predicted based on daughter ions and corresponding chemical formula obtained with high accuracy. The developed technique was validated by the identification of compounds from leaf extract by UPLC-ESI (+)-MS/MS using data-dependent inclusion mode. Lower fragments were generated with carbon-carbon bond breaking, rearrangement. To build skeleton fragment high- and low-mass fragments are essential. Low-mass fragments gave information about the skeleton and high mass fragments formed due to functional group around the basic skeleton.

2B.2 Results and Discussion

2B.2.1 Fractionation of Crude Extract on Normal Phase Cartridges in MPLC

Crude terpenoid extract was fractionated by MPLC into four fractions, (F1 to F4) and each of the fractions contained a mixture of compounds (Figure 2B.2). The eluted fractions and the purity of the isolated diterpenoids were evaluated by HPLC-UV (Figure 2B.3) Purity (or abundance) of the individual components in the HPLC profiles was determined by area (%) under the respective peaks. TLC of all the collected fractions was taken, the analysis showed that fractions which were eluted in 30-35 % acetone in pet ether at 24 min and contained a mixture of compounds with two major compounds with proximity, these fractions were combined, concentrated and named it as fraction-1. Further analysis of the fraction-1 in HPLC, showed it contained two significant peaks of diterpenoids along with some minor impurities with an abundance of compounds in 68 % and other 26 %.

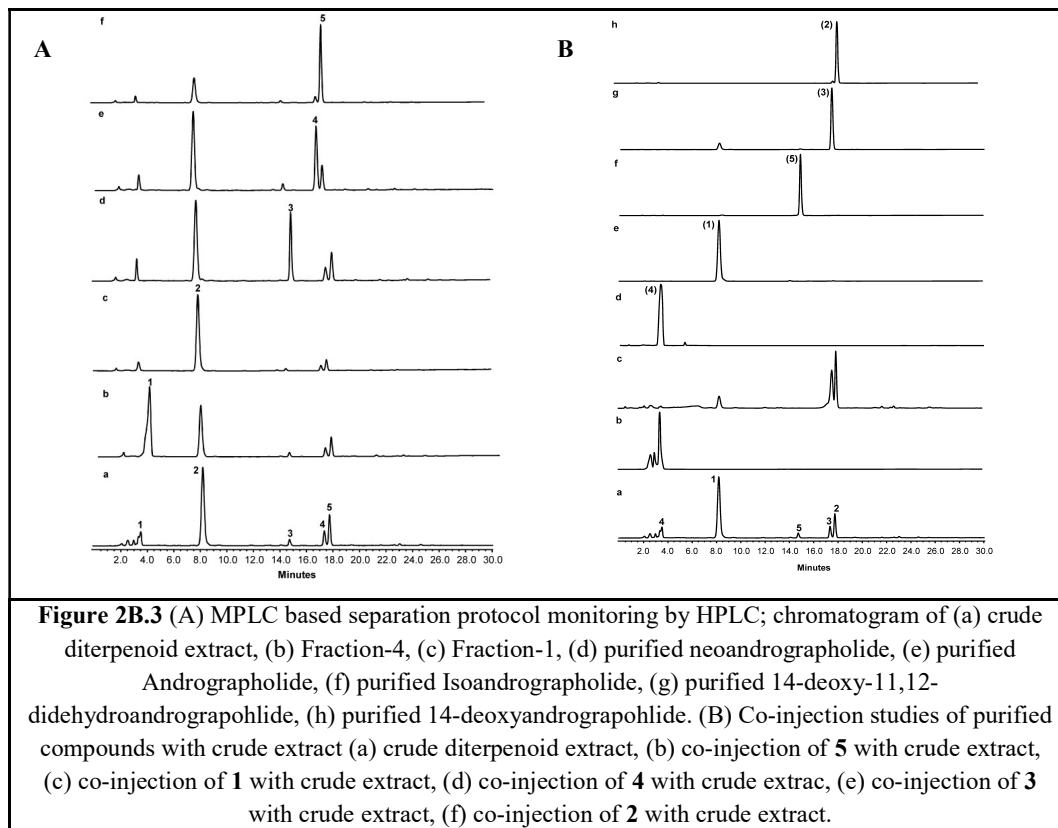


Fractions collected which were eluted in 40-45 % acetone in pet ether into fractions (46-48) showed one major spot on the TLC along with some minor spots which were combined and concentrated was fraction-2. HPLC analysis of fraction-2 showed the presence of one major diterpenoid which was more than >90 % along with some

minor impurities. Single spot on TLC was showed in fraction obtained with 50-60 % (acetone/ hexane) into the fraction (54-68), which were combined and concentrated, considered as a fraction-3. Fraction-3 contained one major diterpenoid with the purity of >93 % revealed from HPLC analysis. Another fraction collected which were eluted at 73-79 % (acetone/ hexane) showed the two major spot on the TLC along with some minor spots which were combined and concentrated was the fraction-4. It was fraction contained impurities; major was one present in > 55 % showed by HPLC analysis. It is a polar metabolite compared to earlier. As these fractions obtained were showed good separation on reverse phase HPLC all these fractions were subjected for purification of the individual compounds on reverse phase cartridges in MPLC.

2B.2.2 Purification of Diterpenoids on Reverse Phase Cartridges and Characterization of Purified Diterpenoids

Fractions obtained after normal phase purification were further purified by reverse phase silica gel prepacked cartridges to get five purified diterpenoids with high purity. The protocol developed for purification was schematically shown in (Figure 2B.2). Fraction-1 was loaded on ciliate and purified by using reverse phase cartridge; the first diterpenoid was eluted in 40-45 % (methanol in water) followed the second was eluted in 50-55 % (methanol in water) respectively both the diterpenoids showed purity > 95 %. Characterization revealed that one is 14-deoxy-11, 12-didehydro- andrographolide (R_t -18.0, R_f -0.8, 8.43 mg, purity 98.75 %) and 14-deoxyandrographolide (R_t : 17.68, R_f :0.75, 46.2 mg, purity 96.4 %) respectively. Fraction-2 after purification on reverse phase got >94.8 % pure diterpenoid revealed from HPLC chromatogram in fraction (40-50% of methanol/ water). Further, it was characterized by NMR and ESI (+) HRMS data as isoandrographolide (R_t - 15.06, R_f - 0.5, 6.74 mg, purity 97.04 %). Fraction-3, purification eluted major metabolite with purity of > 93 % , within fraction 29 to 39 (30-35 % of methanol/ water). From NMR and HRMS data it was confirmed that the diterpenoid as andrographolide (R_t - 8.2, R_f - 0.5, 293.4 gm, purity 99.9 %). Fraction-4 was subjected to reverse phase silica-gel cartridge purification eluted in 20-25% (methanol in water) diterpenoids with > 60 % purity. Isolated molecules were characterized by using spectral data as Neoandrographolide (R_t - 3.04, R_f - 0.2, 2.96 mg, purity 98.6 %).



Reproducibility of the protocol was confirmed by repeating the isolation protocol for two times. The developed protocol is highly effective in the sense of purity (>95%) of diterpenoids. The MPLC based protocol involved automation which reduced the human error and made it expedient, easy for repeatability. Diterpenoids which were having narrow chromatographic resolution were separated by utilisation of normal and reverse phase stationary phase successively. Repeatability, simplicity, automation, and rapidity made this protocol as an effective technique compares to the conventional separation/ identification methods such as HPLC or countercurrent chromatography.

2B.2.3 Scale-Up Studies for Separation Protocol

Standardisation of the scale-up isolation of terpenoids from the crude extracts we have used Redisep- R_f cartridge of various size according to its capacity. Parameter required for the better separation was mentioned into (Table. 2B.1, Table. 2B.2). MPLC protocol is effective, economical and time-saving to purify the terpenoids

compared to the used of flash column chromatography. The purity of the compound was more than > 98 %.

Table 2B.1 Scale-up studies for separation protocol

Crude-extract (g)	RediSep-R _f cartridge (g)	Flow rate (mL/min)	Yield of Fractions (mg)			
			F-I	F-II	F-III	F-IV
0.5	12	7	130	65	175	50
1	24	20	260	130	350	100
2	40	25	520	260	700	200
3	80	40	780	390	1350	300

* Solvent program: 0-3 min 5 % EtOAc, 6 min 10 % EtOAc, 3 min hold, 12 min 15 % EtOAc, 3 min hold, 18 min 20 % EtOAc, 3 min hold, 24 min 25 % EtOAc, 3 min hold, 30 min 30 % EtOAc, 6 min hold, 39 min 35 % EtOAc, 6 min hold, 48 min 40 % EtOAc, 6 min hold.

2B.2.4 Standardization of Normalised Collision Energy (NCE)

As the collision energy normalisation, required to optimised the distribution of mass fragments intensities. Andrographolide has the typical skeleton in the isolated hence it was taken as a representative molecule for standardisation with a range of NCE (10, 20, 30, 40, 50 and 60 %) (Figure 2B.4). At lower NCE value higher- mass fragments with high intensity were generated, were as at higher NCE formed lower mass fragment with high intensity. The variation in abundance of the lower and higher mass fragments with changing NCE collision energy has been shown in Figure 2B.3 30 % NCE was found most effective to get mass fragments pattern with significant intensity; hence 30 % NCE was preferred to use for fragmentation of other diterpenoids.

Table 2B.2 Scale-up Studies for Separation Protocol

Crude extract (mg)	RediSep-R _f cartridge (g)	Flow rate (mL/min)	Yield of Fractions (mg)	
			14-deoxyandrographolide	14-deoxy-11,12-didehydroandrographolide
260	12	7	130	57
520	24	17	260	114

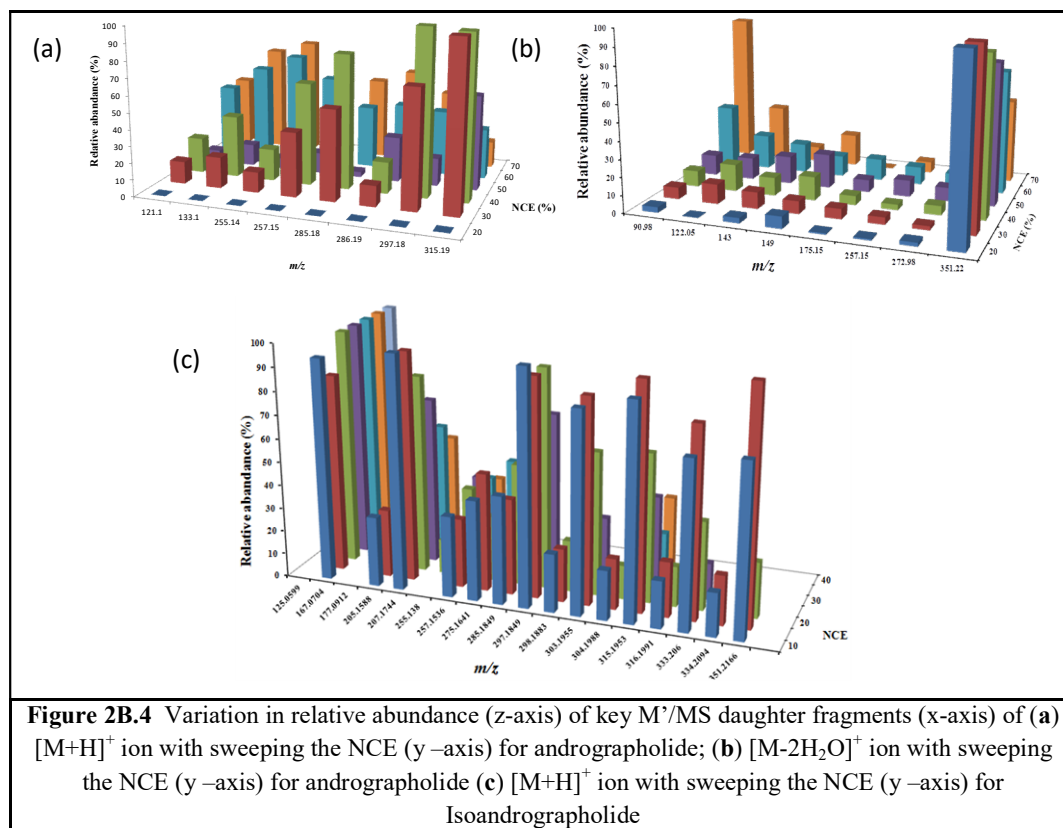
Crude-extract (mg)	RediSep R _f cartridge (g)	Flow rate (mL/min)	Yield of Fractions (mg)
			Isoandrographolide
130	12	7	8
260	24	17	16

* Solvent program: 0-3 min 5 % EtOAc, 6 min 10 % EtOAc, 3 min hold, 12 min 15 % EtOAc, 3 min hold, 18 min 20 % EtOAc, 3 min hold, 24 min 25 % EtOAc, 3 min hold, 30 min 30 % EtOAc, 6 min hold, 39 min 35 % EtOAc, 6 min hold, 48 min 40 % EtOAc, 6 min hold.

2B.2.5 UPLC-ES (+)-MS and MS-MS Characterization

Structure fragmentation correlation and MS/MS signature spectra of the daughter ion generated from five isolated diterpenoids were studied with standardised HRMS parameters. The mass fragments, molecular formula, and intensity of five diterpenoids at 30% NCE value were documented in (Table 2B.2). Correlation of structure with the fragmentation established based on a chemical formula and further predicted the probable fragmentation pathway. Mass fragments of the diterpenoids at lower NCE were generated primarily with the loss of functionalities as neutral molecules, e.g. H₂O, CO, and AcOH from the basic

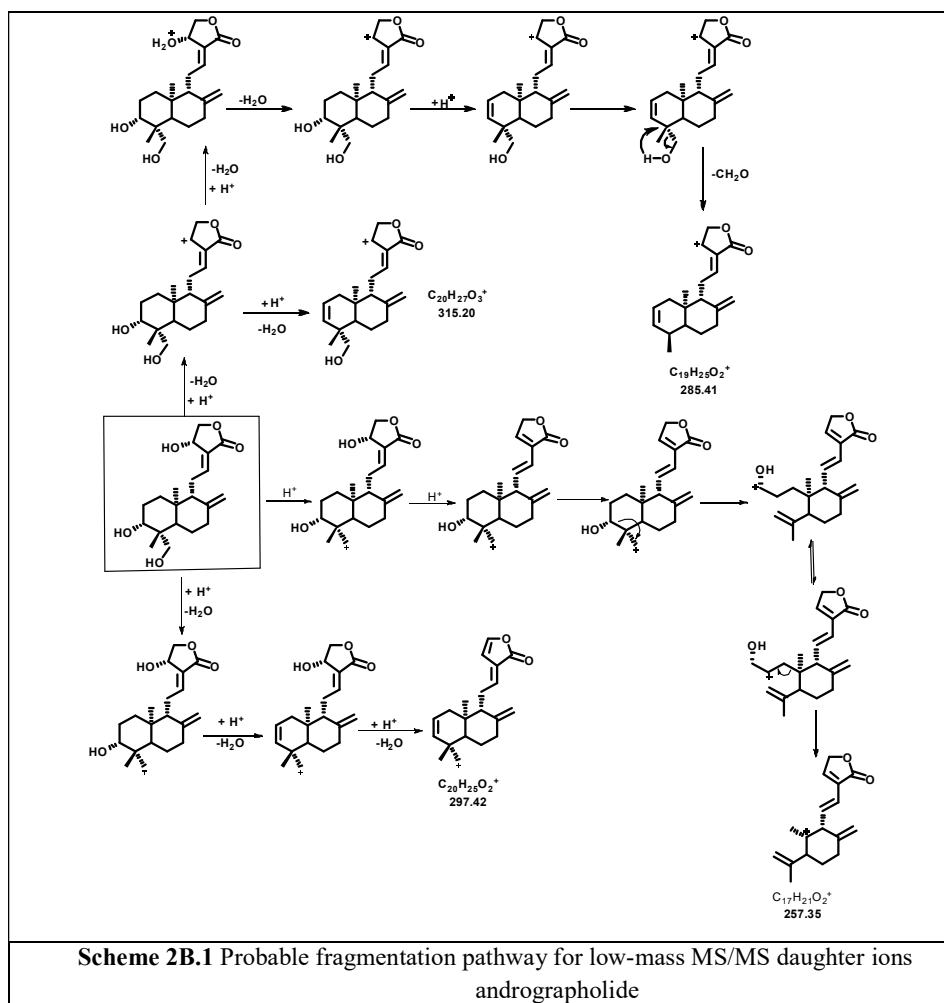
diterpenoid skeleton. Loss of functionalities like CH_2O , $\text{C}_3\text{H}_3\text{O}$ also generate due to basic skeleton rearrangement at higher collision energy. Fragments obtained were given valuable information regarding the functionalization and skeleton.



2B.2.5.1 MS/MS Characterization of Andrographolide (1)

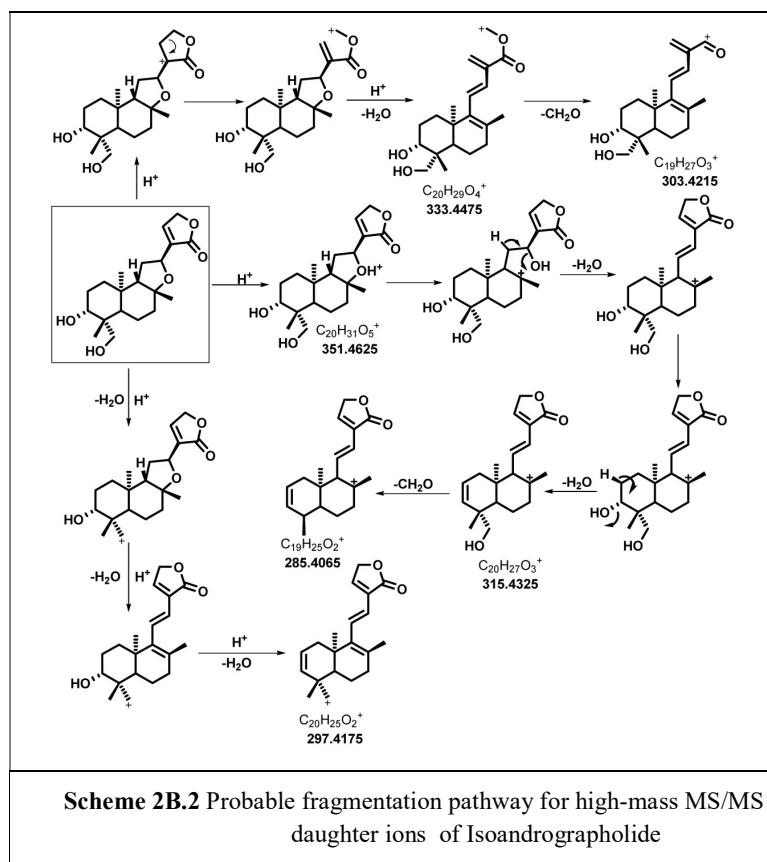
The precursor ion of andrographolide and the generate daughter ions with possible fragmentation pathway schematically shown (Scheme 2B.1). Loss of two molecules by protonation at hydroxy at C-14 and C-3 followed by subsequent H_2O loss may generate the molecular fragment at m/z 315 ($\text{C}_{20}\text{H}_{27}\text{O}_3^+$). The loss of third H_2O molecules may generate the molecular fragment at m/z 297 ($\text{C}_{20}\text{H}_{25}\text{O}_2^+$). Plausible fragmentation involved first protonation of primary hydroxy and loss of H_2O ($\text{C}_{20}\text{H}_{30}\text{O}_4$), further protonation of secondary hydroxy at C-3, C-14 and progressive loss of two H_2O . Daughter ions of mass at m/z 285.40 ($\text{C}_{19}\text{H}_{25}\text{O}_2$) generation pathway may involve the protonation of hydroxyl at C-14 of lactone ring because of the loss of the H_2O molecule given stable allylic carbocation. Further loss of another

molecule of H₂O may be from C-3 on ring-A, formed a cyclic double bond. 1, 3-hydride shift, loss the neutral fragment of formaldehyde from C-19 formed the desired ion. Mass fragment m/z 257 (C₁₇H₂₁O₂) was further might be formed by loss of two H₂O molecules from C-3 and C-14 followed the rearrangement and breaking of ring-A with loss of a molecular fragment of mass m/z -C₃H₃O. To demonstrate, **1** generated the diagnostic peaks at m/z 351.1174 [M+H]⁺, 333.4475 [M+H - H₂O]⁺, 315.1945 [M+H - 2H₂O]⁺, 297.1841 [M+H - 3H₂O]⁺, 285.1841 [M - 3H₂O - C + H]⁺, 257.153 [M - 3H₂O - 2C + H. Molecular fragments with a mass at m/z 333, 315, 297, 285 and 257 are present among four isolated diterpenoids except for Neoandrographolide since it showed that they were generated from the common skeletal region.



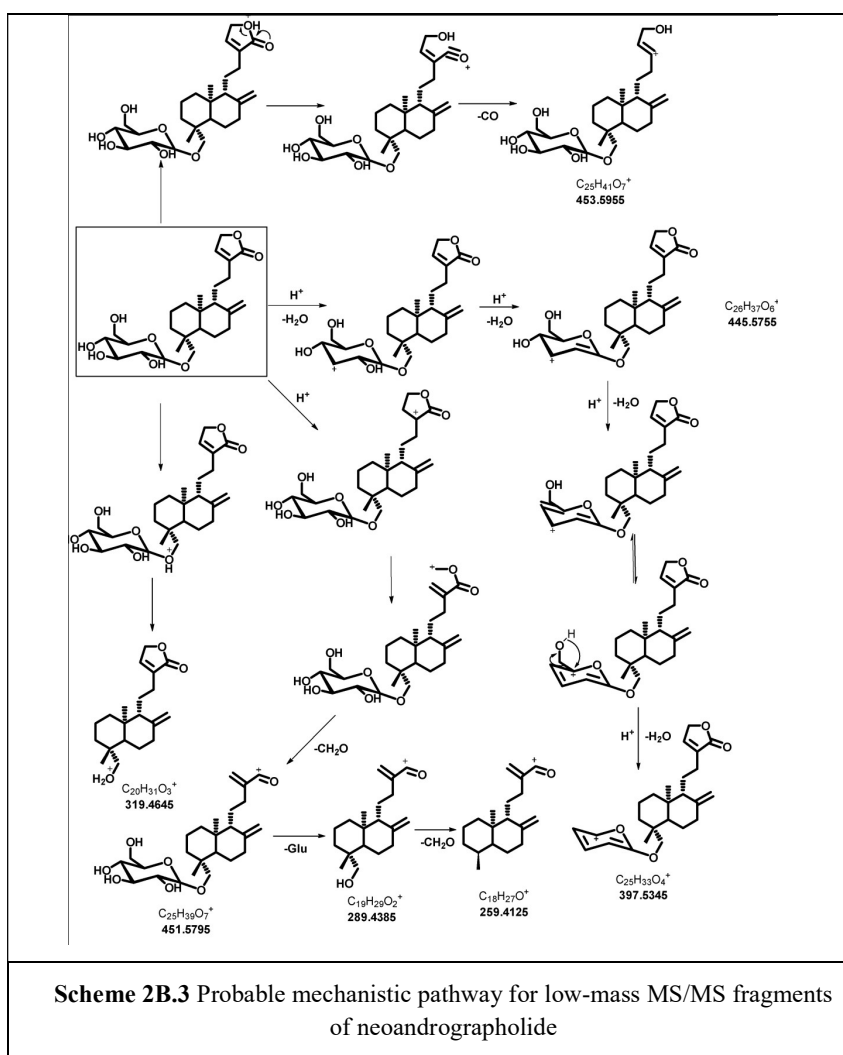
2A.2.5.2 MS/MS Characterization of Isoandrographolide

Isoandrographolide contained an additional five-member cyclic ether ring, unsaturation at C-12, -13 positions in andrographolide shifted to C-13, -14 with the removal of the hydroxyl group from C-14 position. MS/MS spectrum of isoandrographolide showed the presence of at m/z 351.2093 ($C_{20}H_{17}O_3$) has the sTable ion with the highest intensity with abundance (100%) fragment in along with the other fragments, generated by the loss of another molecule H_2O from above fragment daughter ion 333.2051 ($C_{20}H_{29}O_4$). This fragment involved in the fragmentation pathway of 5 (scheme 2B.2).



The formation of daughter ions and probable fragmentation pathway $[M+H]^+$ from the precursor ion of 5 has represented in m/z 297.41 ($C_{20}H_{25}O_2$) daughter ion generated with 56.66 % of NCE from the precursor ion, possible generation pathway involved protonation of primary hydroxy leading to loss of H_2O molecule. The second step may be the protonation and cleavage of ether ring with loss of H_2O molecule, further loss of other H_2O from ring-A to formed the daughter ion at m/z

297.41 ($C_{20}H_{25}O_2$). Daughter ion leading at m/z 285.40 ($C_{20}H_{25}O_2$) fragmentation pathway involved may be firstly protonated the ether ring with loss of H_2O molecule to generate stable tertiary carbocation on ring-B. In next step protonation and loss of Another H_2O molecule from ring-A gave daughter ion of mass at m/z 319.20 ($C_{20}H_{29}O_4$). Finally, loss of formaldehyde molecule generates at m/z 315.19 ($C_{20}H_{27}O_3$). Plausible fragmentation pathway for generating the daughter ion of mass at m/z 303.42 ($C_{19}H_{27}O_3$) involved carbocation formation on C-14 by protonation successive breaking C14- C-15 bond. Finally, the loss of methanol generated the required daughter ion.

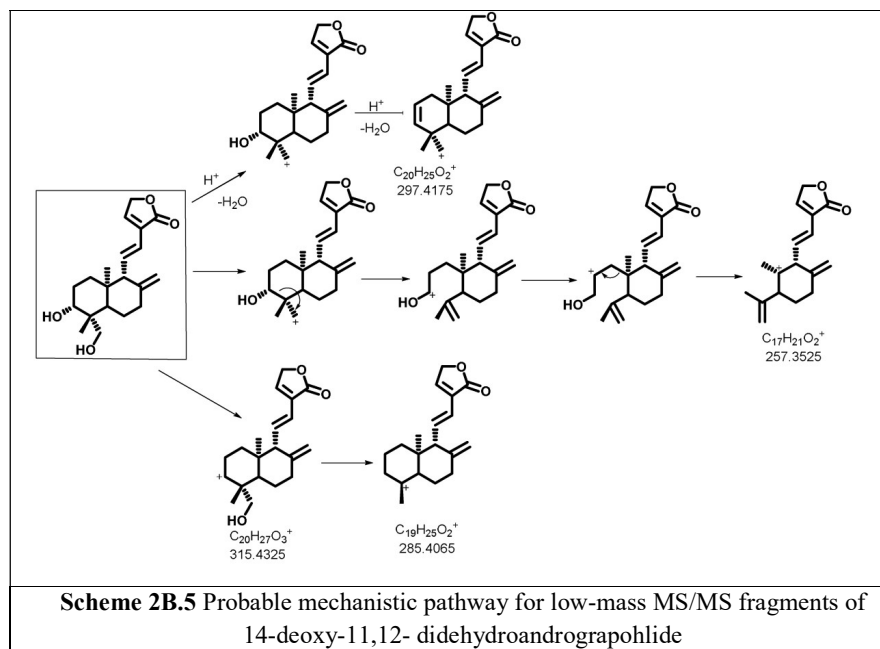


2B.2.5.3 MS-MS Characterization of Neoandrographolide

Neoandrographolide is the modified analogue of andrographolide isolated from *Andrographis paniculata*. Removals of hydroxy from C-14 position with unsaturation, hydroxy get substituted by glucose at the C-19 position. Its MS-MS fragmentation showed key mass fragment was generated at m/z 317.2267 ($C_{20}H_{29}O_3$), with high intensity of 100%, may be involved the protonation of pi bond to form carbocation at C-14, removal of water molecule from ring-A and further cleavage of ethereal (C-O) bond between primary hydroxyl of diterpenoids skeleton attached to anomeric carbon of glucose. Daughter ion at mass m/z 451.2634 ($C_{25}H_{39}O_7$) generated by the loss of neutral carbon monoxide with the loss of water molecules from ring-A. Further the daughter ion at mass at m/z 335.2371 ($C_{20}H_{31}O_4$) generated by the loss of glucose moiety with the 1, 3-hydride shift to loss of formaldehyde. Other mass fragments including 261.1530 ($C_{17}H_{25}O_2$), 287.2202 ($C_{19}H_{27}O_2$) and their possible fragmentation pathway was showed in (Scheme 2B.3).

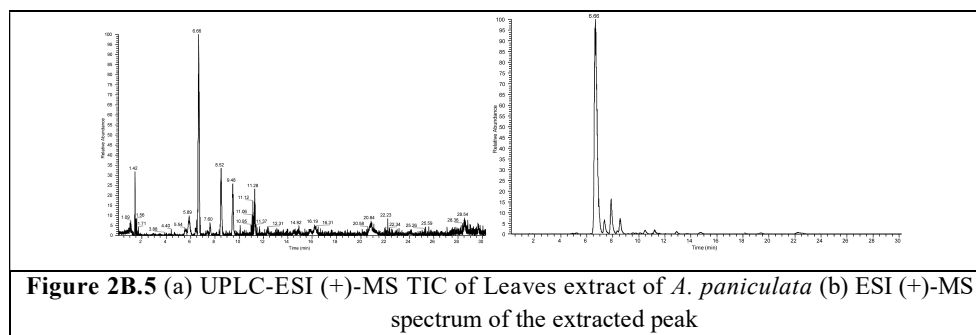
2B.2.5.4 MS-MS Characterization of 14-deoxy-11, 12-didehydroandrographolide

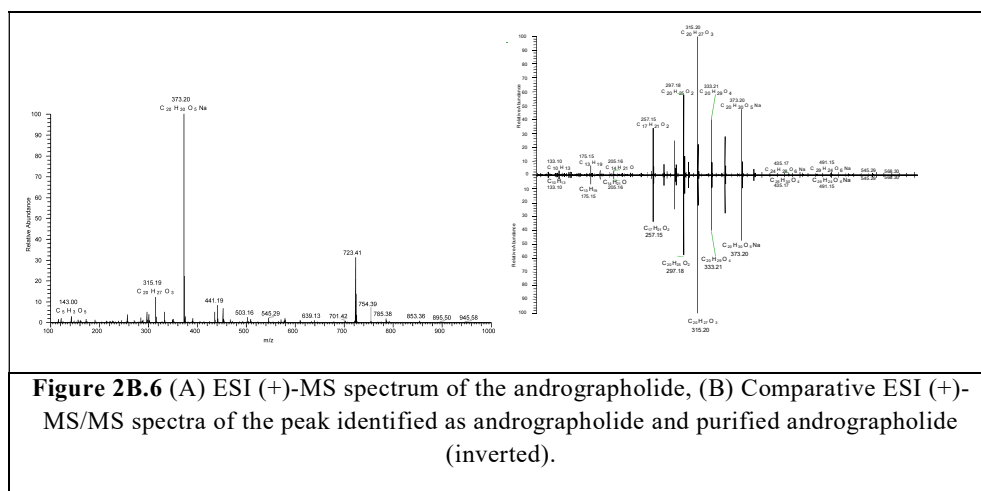
Both these are the derived structurally differ from andrographolide concerning a functional group at C-12, C-13, and C-14. Fragmentation pattern of both is same for the daughter ion for 14-deoxy-11,12-didehydroandrographolide 297.4175 ($C_{20}H_{25}O_2$), 285.4065 ($C_{19}H_{25}O_2$), 315.4325 ($C_{20}H_{27}O_3$), 257.3525 ($C_{17}H_{21}O_2$) and 14-deoxyandrographolide 299.4335 ($C_{20}H_{27}O_2$), 317.4485 ($C_{20}H_{29}O_3$), 259.3685 ($C_{17}H_{23}O_2$), 287.4225 ($C_{19}H_{27}O_2$). The daughter ion generates at mass 317.4485 ($C_{20}H_{29}O_3$) from loss of H_2O molecule further removal of other H_2O molecule gave 299.4335 ($C_{20}H_{27}O_2$) and mass at 287.4225 ($C_{19}H_{27}O_2$) formed by loss of formaldehyde from the ion of mass 317.4485 ($C_{20}H_{29}O_3$). Fragmentation pathway of daughter ion at 259.3685 ($C_{17}H_{23}O_2$) involved loss of H_2O molecule followed by a shift of carbocation from C-3 to C-2 and rearrangement. In case of 14-deoxyandrographolide 257.3965 ($C_{18}H_{25}O$) Fragmented ion obtained by protonation of the pi bond to form carbocation at C-13, loss of H_2O molecule from ring-A and loss of formaldehyde by 1, 3 hydride shift. The last step was the shifting of a carbocation from C-13 to C-15 followed by the loss of formaldehyde gave desired daughter ion (Scheme 2B.5).



2B.2.5.5 MS/MS-Based Identification of Diterpenoid from Leaves Extract of *A. paniculata*.

An MS/MS spectrum of purified andrographolide obtained was utilized for the identification of andrographolide in leaves extract. ESI-(+)-MS spectra with a retention time of pure andrographolide present in intricate leaves mixture were investigated in UPLC-ESI (+)-MS, TIC (total ion chromatogram) (Figure 2B.5). The Peak at retention time 11.83 min in TIC leaves extract protonated molecular ion peak $[M+H]^+$ at 351 (Figure 2B. 6) corresponding to the retention time and $[M+H]^+$ ion of purified andrographolide. The retention time in ESI (+) MS chromatogram and mass fragmentation pattern of the diterpenoid was a well agreement with that of purified andrographolide confirmed its presence in leave extract

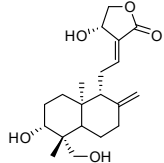
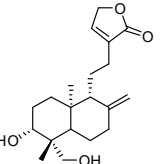
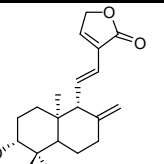
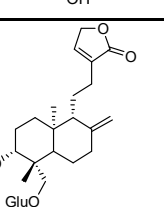
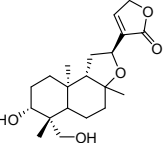
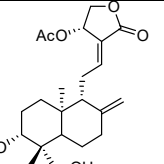


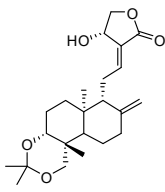
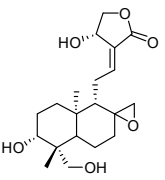
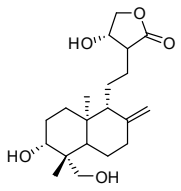
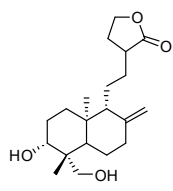


2B.3 Conclusion

Rapid isolation of five diterpenoids with high purity on preparative-scale from *A. paniculata* was developed by using automated MPLC based technique. ESI-(+)-quadrupole/orbitrap-MS/MS technique was used for diterpenoids characterization, and daughter ions structure fragmentation pathway was predicted by using high-resolution MS/MS data. Hence the preparative scale isolation with expeditious identification and characterization of labdane diterpenoid will be helpful for exploration of unknown diterpenoid in complex extracts and investigation of their properties. Further, it is essential to have these terpenoids in large quantities for exploring their bioactivities.

Table 2B.2 Structure, precursor ion, MS/MS daughter ions, their corresponding chemical formula and intensity in 30 % NCE for diterpenoids

Structure	Precursor ion (<i>m/z</i>)	Daughter ion (<i>m/z</i>), formula, intensity at 30%
	[M+2H ₂ O] ⁺ 315.1952	257.1534 (C ₁₇ H ₂₁ O ₂ , 49.34), 271.1691(C ₁₈ H ₂₃ O: 12.31), 285.1848 (C ₁₉ H ₂₅ O ₂ , 7.4), 297.1841 (C ₂₀ H ₂₅ O: 5.99), 298.1879 (C ₂₀ H ₂₆ O ₂ , 18.43), 315.1952 (C ₂₀ H ₂₇ O: 18.43).
	[M+H] ⁺ 335.2144	257.1530 (C ₁₇ H ₂₁ O ₂ , 39.76), 285.1851 (C ₁₉ H ₂₅ O: 68.12), 297.1883 (C ₂₀ H ₂₅ O ₂ , 70.50), 315.193 (C ₂₀ H ₂₇ O ₃ , 34.14), 334.1978 (C ₂₀ H ₃₀ O ₄ , 33.07, 335.1843 (C ₂₀ H ₃₁ O ₄ , 100).
	[M+H] ⁺ 333.2057	257.1530 (C ₁₇ H ₂₁ O ₂ , 81.59), 285.1842 (C ₁₉ H ₂₅ O: 65.84), 297.1847 (C ₂₀ H ₂₅ O ₂ , 85.15), 303.206 (C ₁₉ H ₂₇ O ₃ , 25.24), 315.1946 (C ₂₀ H ₂₇ O ₃ , 66.97, 332.1958 (C ₂₀ H ₂₈ O ₄ , 27.73), 333.1771 (C ₂₀ H ₂₉ O ₄ , 100).
	[M+H] ⁺ 497.3065	261.1530 (C ₁₇ H ₂₅ O ₂ , 4.05), 287.2202 (C ₁₉ H ₂₇ O ₂ , 25.27, 303.2162 (C ₁₉ H ₂₇ O ₃ , 44.23), 317.2267 (C ₂₀ H ₂₉ O ₃ , 100, 335.2371 (C ₂₀ H ₃₁ O ₄ , 5.50), 451.2634 (C ₂₅ H ₃₉ O: 13.11), 497.3064 (C ₂₆ H ₄₂ O ₉ , 5.24)
	[M+H] ⁺ 351.2163	257.1535 (C ₁₇ H ₂₁ O ₂ , 29.53), 285.1847 (C ₁₉ H ₂₅ O ₂ , 42.7, 297.1846 (C ₂₀ H ₂₅ O ₂ , 93.19), 303.1953 (C ₁₉ H ₂₇ O: 87.46), 315.1952 (C ₂₀ H ₂₇ O ₃ , 96.41), 333.2058 (C ₂ H ₂₉ O ₄ , 81.28), 351.2166 (C ₂₀ H ₃₁ O ₅ , 100).
	[M+H] ⁺ 393.2199	111.0806 (C ₇ H ₁₁ O, 9.79), 177.0908 (C ₁₁ H ₁₃ O ₂ , 12.38), 203.1063 (C ₁₃ H ₁₅ O ₂ , 9.54), 227.1063 (C ₁₅ H ₁₅ O ₂ , 12.53), 241.1219 (C ₁₆ H ₁₇ O ₂ , 10.19), 255.1375 (C ₁₇ H ₁₉ O ₂ , 11.99), 257.1531 (C ₁₇ H ₂₁ O ₂ , 39.67), 285.1843 (C ₁₉ H ₂₅ O ₂ , 58.12), 86.1876 (C ₁₉ H ₂₆ O ₂ , 12.77), 297.1843 (C ₂₀ H ₂₅ O ₂ , 66.48), 298.1874 (C ₂₀ H ₂₆ O ₂ , 18.13), 315.1948 (C ₂₀ H ₂₇ O ₃ , 100), 316.1982 (C ₂₀ H ₂₈ O ₃ , 18.44).

Structure	Precursor ion (m/z)	Daughter ion m/z (formula, % intensity at 30%)
	[M+H] ⁺ 391.2406	(C ₁₅ H ₁₅ O ₂ , 12.53), 241.1219 (C ₁₆ H ₁₇ O ₂ , 10.19), 255.1375 (C ₁₇ H ₁₉ O ₂ , 11.99), 257.1531 (C ₁₇ H ₂₁ O ₂ , 39.67), 285.1843 (C ₁₉ H ₂₅ O ₂ , 58.12), 86.1876 (C ₁₉ H ₂₆ O ₂ , 12.77), 297.1843 (C ₂₀ H ₂₅ O ₂ , 66.48), 298.1874 (C ₂₀ H ₂₆ O ₂ , 18.13), 315.1948 (C ₂₀ H ₂₇ O ₃ , 100), 316.1982 (C ₂₀ H ₂₈ O ₃ , 16.7).
	[M+H] ⁺ 367.2042	111.0815 (C ₇ H ₁₁ O, 61.13), 175.1493 (C ₁₃ H ₁₉ , 25.54), 185.1338 (C ₁₄ H ₁₇ , 23.82), 187.1494 (C ₁₄ H ₁₉ , 22.48), 203.0539 (C ₈ H ₁₁ O ₆ , 30.23), 247.1709 (C ₁₆ H ₂₃ O ₂ , 52.07), 335.1871 (C ₁₉ H ₂₇ O ₅ , 41.39), 347.1873 (C ₂₀ H ₂₇ O ₅ , 55.19), 365.1978 (C ₂₀ H ₂₉ O ₆ , 100), 367.2134 (C ₂₀ H ₃₁ O ₆ , 98.17)
	[M+H] ⁺ 353.2250	209.1165 (C ₁₂ H ₁₇ O ₃ , 22.8), 223.1321 (C ₁₃ H ₁₉ O ₃ , 10.18), 261.1838 (C ₁₇ H ₂₅ O ₂ , 11.28), 277.1788 (C ₁₇ H ₂₅ O ₃ , 8.840), 289.215 (C ₁₉ H ₂₉ O ₂ , 11.310), 307.2255 (C ₁₉ H ₃₁ O ₃ , 18.67), 319.2254 (C ₂₀ H ₃₁ O ₃ , 100), 320.2288 (C ₂₀ H ₃₂ O ₃ , 23.95), 337.2359 (C ₂₀ H ₃₃ O ₄ , 51.63), 338.2393 (C ₂₀ H ₃₄ O ₄ , 13.3).
	[M+H] ⁺ 337.2301	59.05 (C ₃ H ₇ O, 12.14), 61.03 (C ₂ H ₅ O ₂ , 14.88), 73.07 (C ₄ H ₉ O, 7.01), 87.08 (C ₅ H ₁₁ O, 13.05), 100.08 (C ₆ H ₁₂ O, 7.32), 277.18 (C ₁₇ H ₂₅ O ₃ , 5.16), 279.2 (C ₁₇ H ₂₇ O ₃ , 4.76), 305.21 (C ₁₉ H ₂₉ O ₃ , 4.18), 317.21 (C ₂₀ H ₂₉ O ₃ , 5.77), 319.23 (C ₂₀ H ₃₁ O ₃ , 34.22), 335.22 (C ₂₀ H ₃₁ O ₄ , 15.91), 337.24 (C ₂₀ H ₃₃ O ₄ , 100)

2B.4 Experimental section

2B.4.1 Materials and Methods

Herb was collected from eastern India and identified from the Agharkar Research Institute (ARI) Pune as *Andrographis paniculata*. Extraction solvents for plant material were a technical grade (Spectrochem) and distilled before use. MPLC and HPLC solvents were purchased from Sigma (St. Louis, MO, USA). For LC-ESI (+)-MS experiments, solvents were procured from JT Baker (PA, USA). Teledyne, Isco (Combi-flash Rf 200) MPLC system with PDA detector was used for the normal and reverse phase purification. Waters HPLC system (Delta 600 pump and controller) coupled with Waters 2489 UV/Visible detector. Q Exactive Orbitrap (Thermo Scientific) for mass and MS/MS experiments. NMR's data were recorded on Bruker spectrophotometer (^1H on 200, 400, 500 MHz; ^{13}C on 100 MHz) in methanol- d_4 and CDCl_3 or TMS as the reference.

2B.4.2 Extraction of Plant Material

The collected plants were air dried, roots were separated, and the aerial part was powdered in the grinder. One kilogram aerial part powdered was soaked in methanol and stir with a homogeniser (4 L, 24 h) at room temperature. The mixture was filtrated on filter paper, the remaining residue was again soaked in an equal amount of methanol, and a similar procedure was repeated for twice. The obtained methanol extract was concentrated at 50 °C under reduced pressure to obtain dark green mass (76 g) which was further partitioned between ethyl acetate (750 mL) and water (750 mL). The organic layer after concentration under similar conditions furnished 33.5 g of a green crude mixture of diterpenoids.

2B.4.3 Preparative Isolation and Purification of Diterpenoids by MPLC

One gram ethyl acetate extract was adsorbed on normal silica gel (w/w, 1:3) loaded in the empty cartridge. Normal phase silica RediSep cartridge (24 g) was used for the fractionation with a flow rate of 20 mL min^{-1} and monitoring by a UV detector at 235 and 254 nm. For fractionation gradient solvent program of 120 min with increasing percentage of acetone in hexane was employed as the eluent (0–5 min, 0–5 % acetone, 5 min hold, 10–15 min, 5–10 % acetone, 5 min hold, 20–25 min, 10–

20 % acetone, 5 min hold, 25–30 min 20-30 % acetone, 5 min hold, 30-40 min 30-40 % acetone, 5 min hold, 50-60 min 40-50 % acetone, 5 min hold, 70-80 min 50-60 % acetone, 5 min hold, 90-95 min 60-70 % acetone, 5 min hold, 100-105 min 70-80% acetone, 5 min hold, 110-115 min 80-90 % acetone, 5 min hold). Total of 145 fractions was collected in a test tube (25 mL) by the automated, integrated fraction collector. By using TLC analysed all these fractions, the fractions having a similar spot on TLC were pooled together; four fractions were obtained. These fractions were further purified on reverse phase silica prepacked cartridge. Fractions were adsorbed on celite (w/w, 1:3), RediSep®pre-packed reverse (C18) phase cartridge (26 g) with a flow rate 20 mL/ min and monitoring by a UV detector at 235 and 254 nm. For purification of the all four fractions common gradient solvent programme (65 min) was used, with increasing percentage of methanol in water (10 % MeOH 0- 5 min, 10-20 % MeOH 5-10 min, 5 min hold, 20-30 % MeOH 15-20 min, 5 min hold, 30-40 % MeOH 25-30 min, 5 min hold, 40-50 % MeOH 35-40 min, 5 min hold, 50-60 % MeOH 45-50 min, 5 min hold, 60-70 % MeOH 55-60 min, 5 min hold). Fractions obtained were analysed by TLC and HPLC, a fraction having the similar spots were pooled together and concentrated. Purified diterpenoids were analysed by HPLC.

2B.4.4 TLC and HPLC Conditions

Thin layer chromatogram (TLC) was developed on silica gel G pre-coated plates (Merck, 0.25 mm) with 10% methanol in chloroform (twice) as the mobile phase. Spots were visualised in a solution of 3.0 % anisaldehyde, 2.8 % H₂SO₄, 2 % acetic acid in ethanol. Samples were filtered and diluted in HPLC grade methanol prior to injection. HPLC runs were performed on analytical XBridge C-18 column (4.6 × 250 mm, 5 μm), UV detection at 225 and 254 nm. Gradient solvent programme of Acetonitrile in water 30 min (0-5 min, 30% ACN/ water, 5-6 min, 30-40 % ACN/ water, 6-10 min, 60 % ACN/ water, 10-11 min, 50 % ACN/ water, 11-15 min, 50 % ACN/ water, 15-16 min, 40 % ACN/ water, 16-20 min, 40 % ACN/ water, 20-21 min, 30 % ACN/ water, 21-25 min, 30 % ACN/ water, 25-30 min, 70 % ACN/ water) with a flow rate of 1 mL/min and 15 μL samples was injected.

2B.4.5 UPLC–ESI (+)-MS and MS/MS Conditions

All the samples were centrifuged and diluted in methanol (0.1 mg/mL), and 5 μ L of each was injected. Reverse phase Thermo Hypersil gold column (2.1 mm \times 200 mm, 1.9 μ m) used for MS and MS/MS analysis. MS and MS/MS runs were carried out using the tune method: flow rate 10 units auxiliary gas (nitrogen), flow rate 45 units sheath gas (nitrogen), spray voltage 3.60 |kV|, heater temperature 350°C, capillary temperature 320 °C, s-lens RF level 50, flow rate 2 units sweep gas (nitrogen), spray current 3.70 μ A. ESI-MS and MS/MS data were recorded within the mass range m/z 100–1000 in ESI (+) mode. Diterpenoids in the leaves extract, was resolved on reverse phase (C-18) UPLC column (2.1 \times 100 mm, particle size 1.7 μ m), gradient solvent programme of methanol in water (30 min) with 0.3 mL/min of a flow rate, 0.1% LC-MS grade formic acid was added to water ESI (+)-MS/MS experiments were performed on data dependent

2B.5 HRMS Spectral Copies

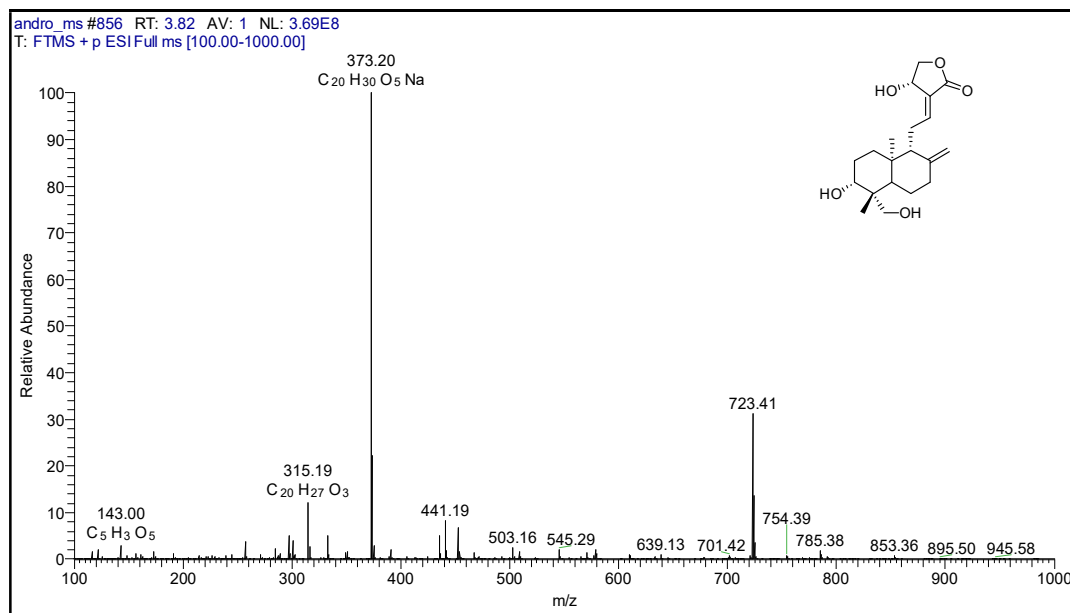
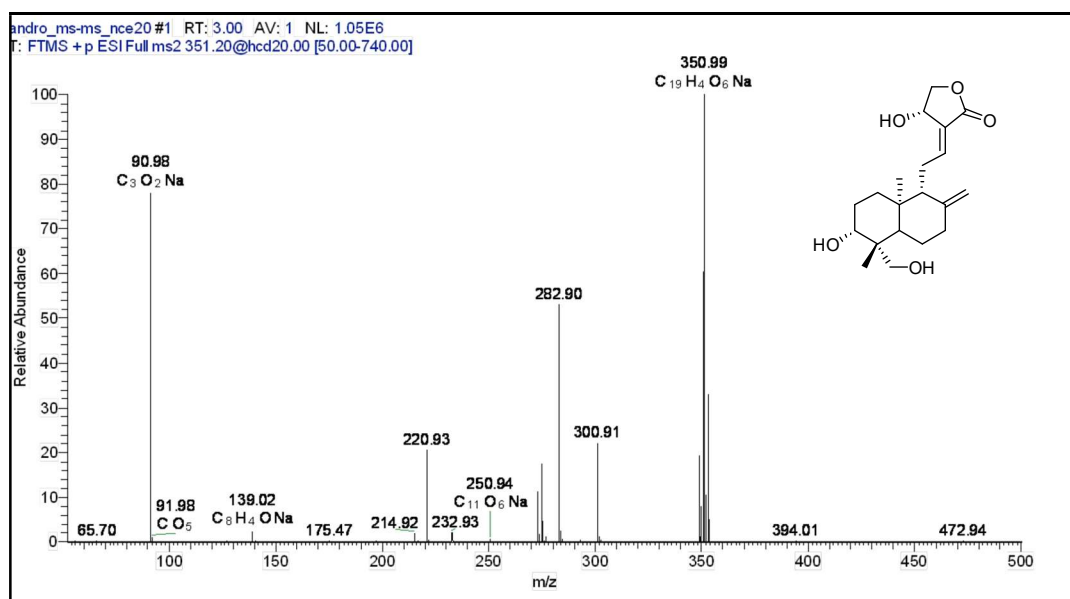


Figure 2B.7a. LC-ESI(+)-HRMS of andrographolide

Figure 2B.7b. ESI(+)-MS/MS spectrum of andrographolide in NCE 20 % (precursor ion $[M-2H_2O]^+$ m/z 315.19)

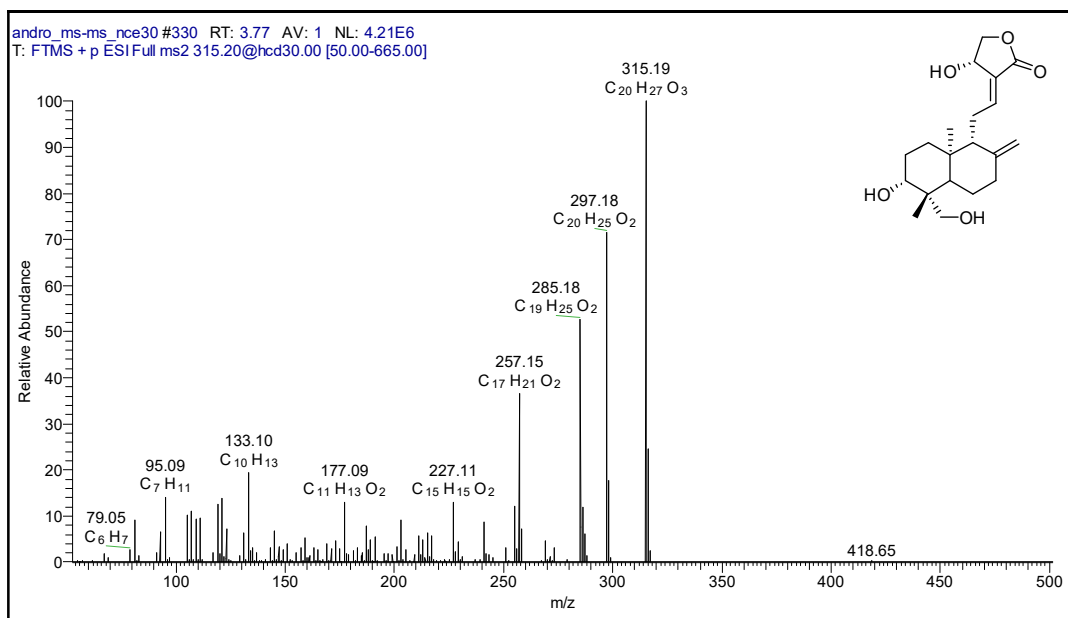


Figure 2B.7c. ESI(+)-MS/MS spectrum of andrographolide in NCE 30 % (precursor ion $[M-2H_2O]^+$ 315.19)

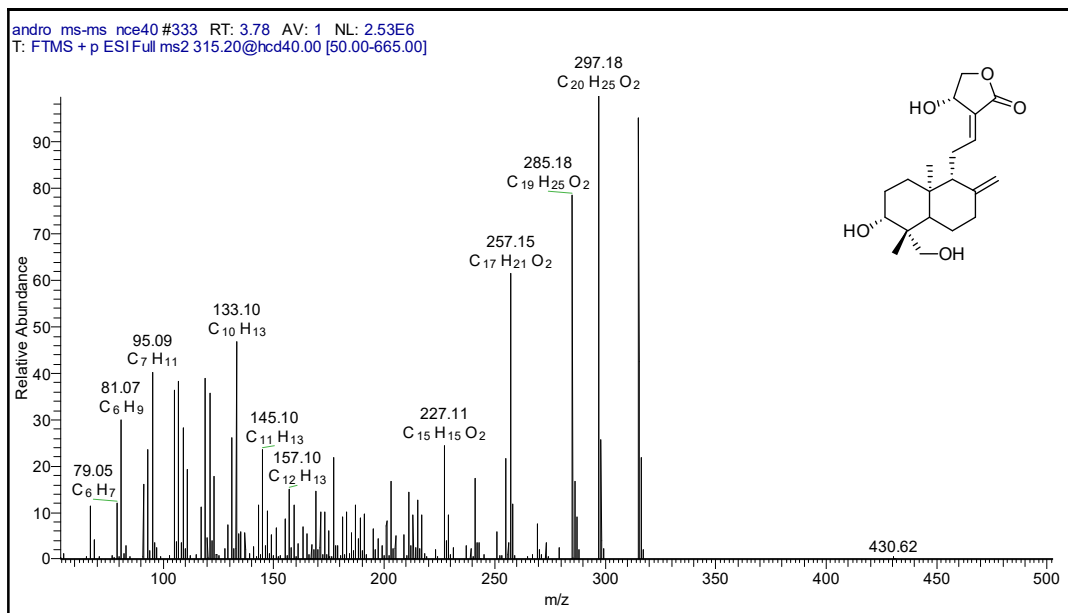


Figure 2B.7d. ESI(+)-MS/MS spectrum of andrographolide in NCE 40 % (precursor ion $[M-2H_2O]^+$ m/z 315.19)

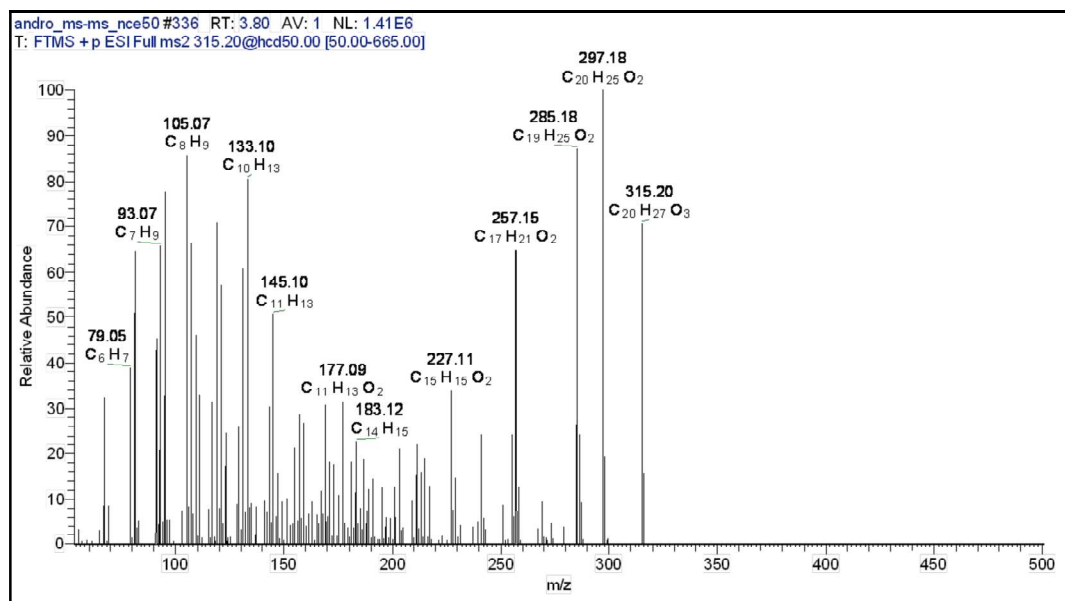


Figure 2B.7e. ESI(+)-MS/MS spectrum of andrographolide in NCE 50% (precursor ion $[M-2H_2O]^+$ m/z 315.19)

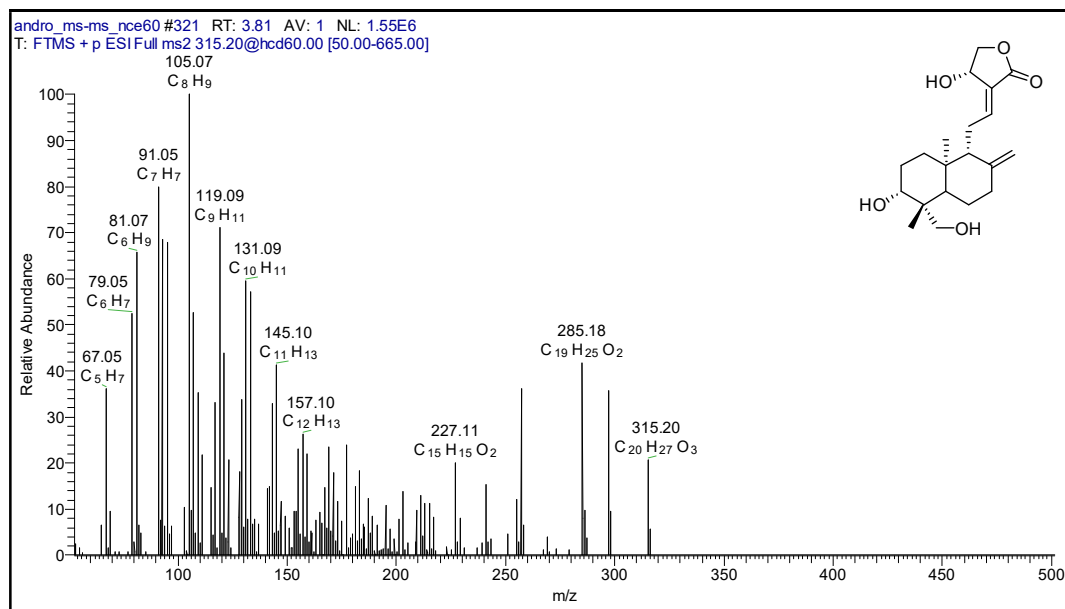


Figure 2B.7f. ESI(+)-MS/MS spectrum of andrographolide in NCE 60 % (precursor ion $[M-2H_2O]^+$ m/z 315.19)

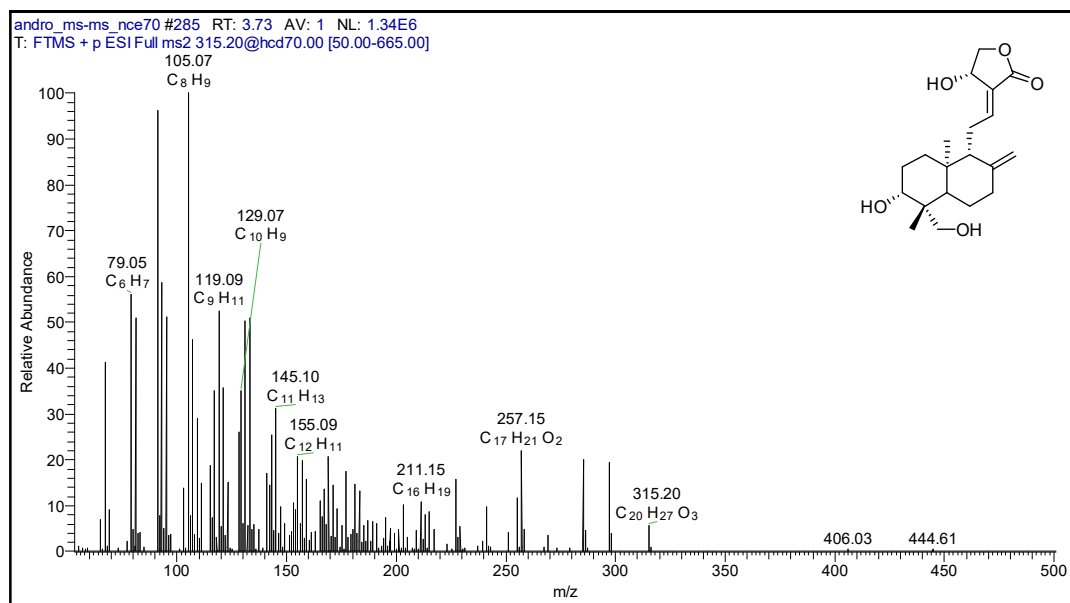


Figure 2B.7g. ESI(+)-MS/MS spectrum of andrographolide in NCE 70% (precursor ion $[M-2H_2O]^+$ m/z 315.19)

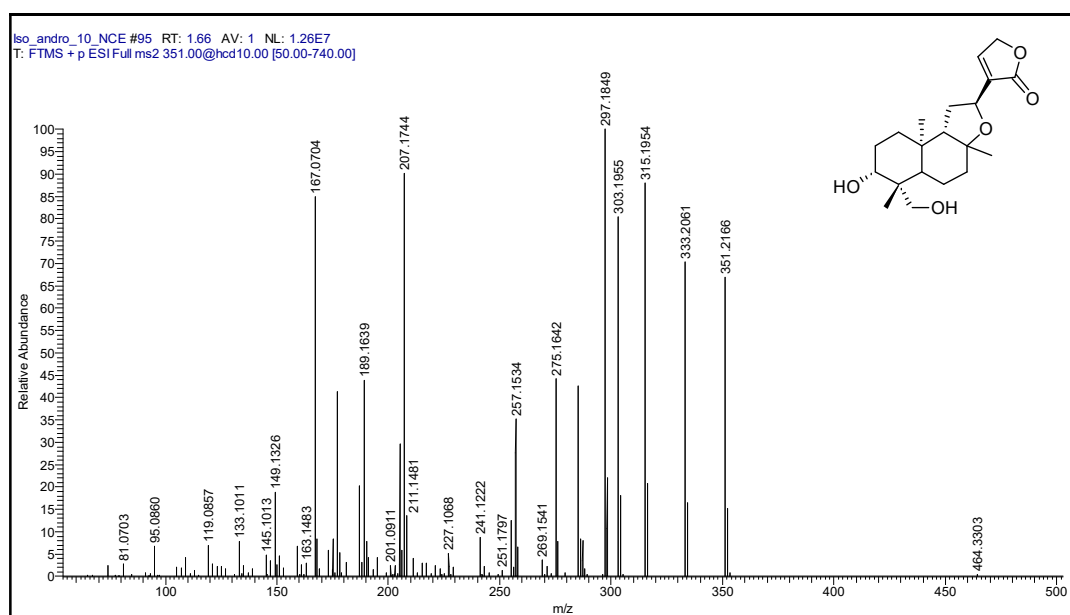


Figure 2B.8a. ESI(+)-MS/MS spectrum of Isoandrographolide in NCE 10% (precursor ion $[M-H_2O]^+$ m/z 351.21)

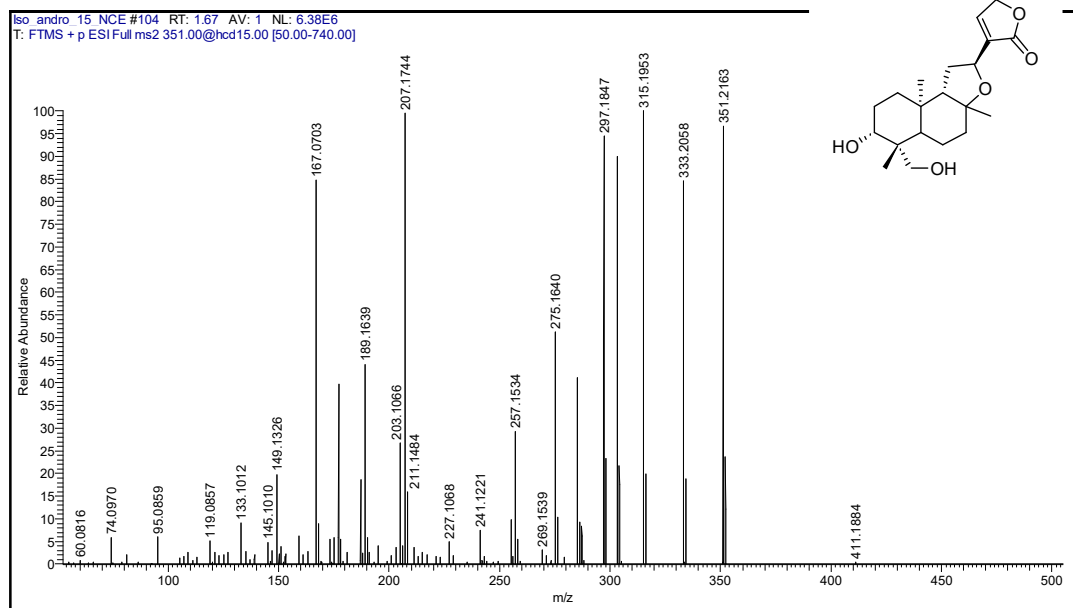


Figure 2B.8b. ESI(+)-MS/MS spectrum of Isoandrographolide in NCE 15 % (precursor ion $[M-H_2O]^+$ m/z 351.21)

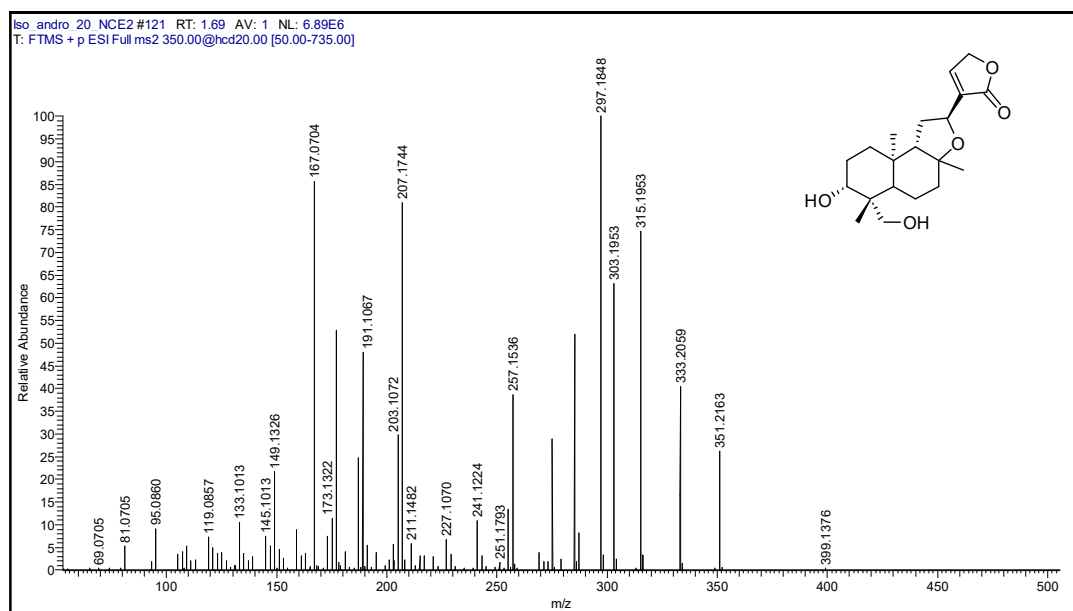


Figure 2B.8c. ESI(+)-MS/MS spectrum of Isoandrographolide in NCE 20 % (precursor ion $[M-H_2O]^+$ m/z 351.21)

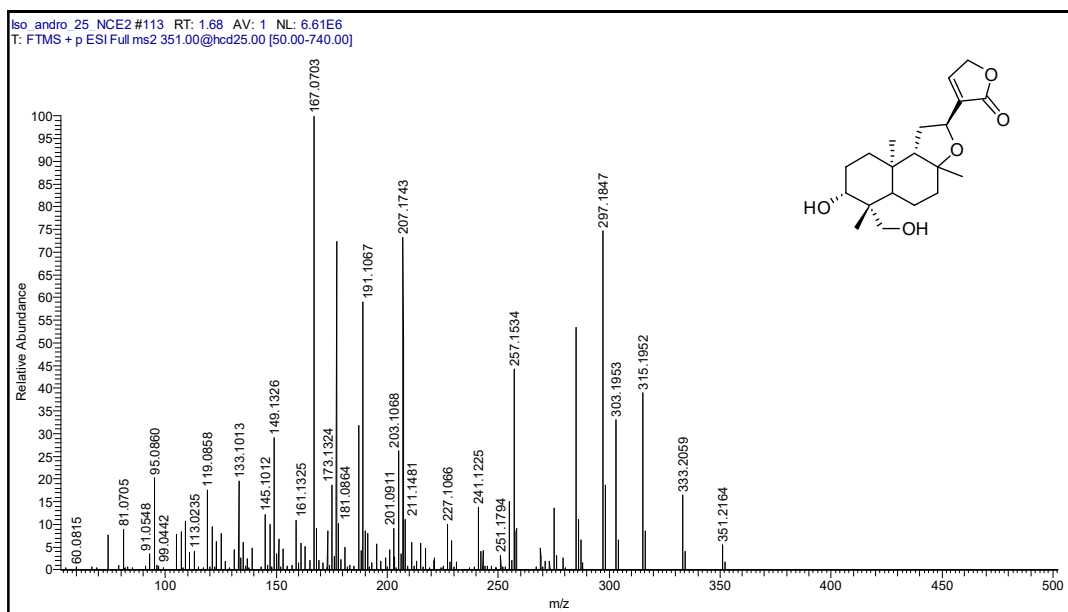


Figure 2B.8d. ESI(+)-MS/MS spectrum of Isoandrographolide in NCE 25 % (precursor ion $[M-H_2O]^+$ m/z 351.21)

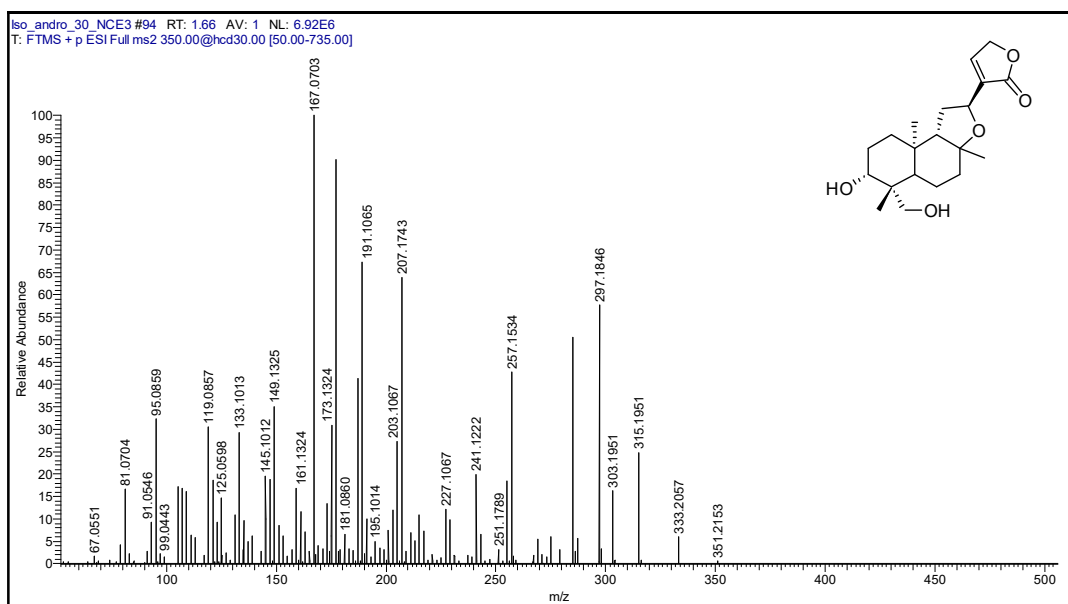


Figure 2B.8e. ESI(+)-MS/MS spectrum of Isoandrographolide in NCE 30 % (precursor ion $[M-H_2O]^+$ m/z 351.21)

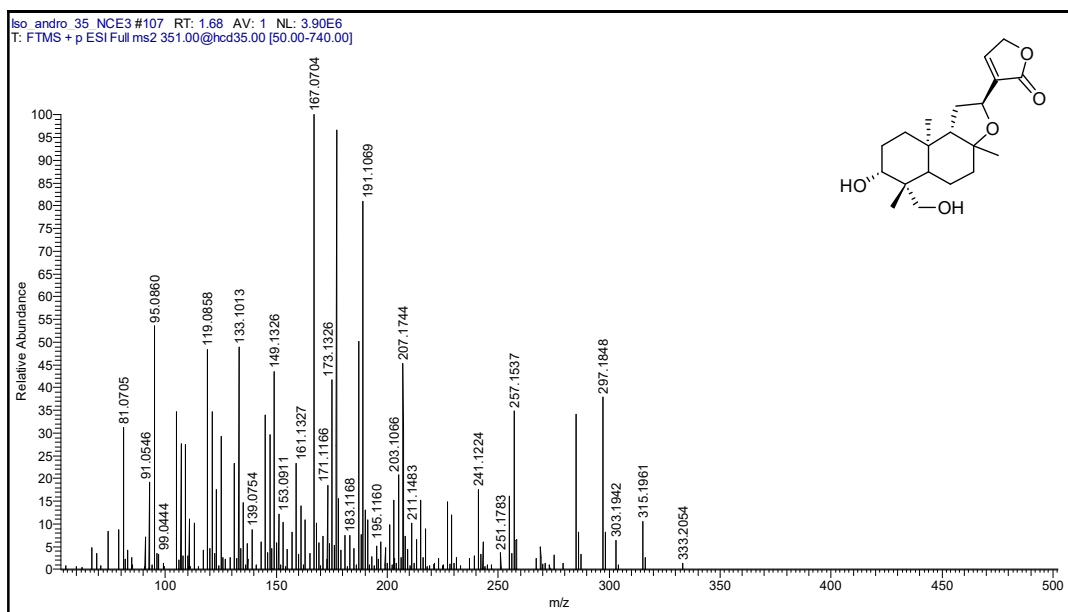


Figure 2B.8f. ESI(+)-MS/MS spectrum of Isoandrographolide in NCE 35 % (precursor ion $[M-H_2O]^+$ m/z 351.21)

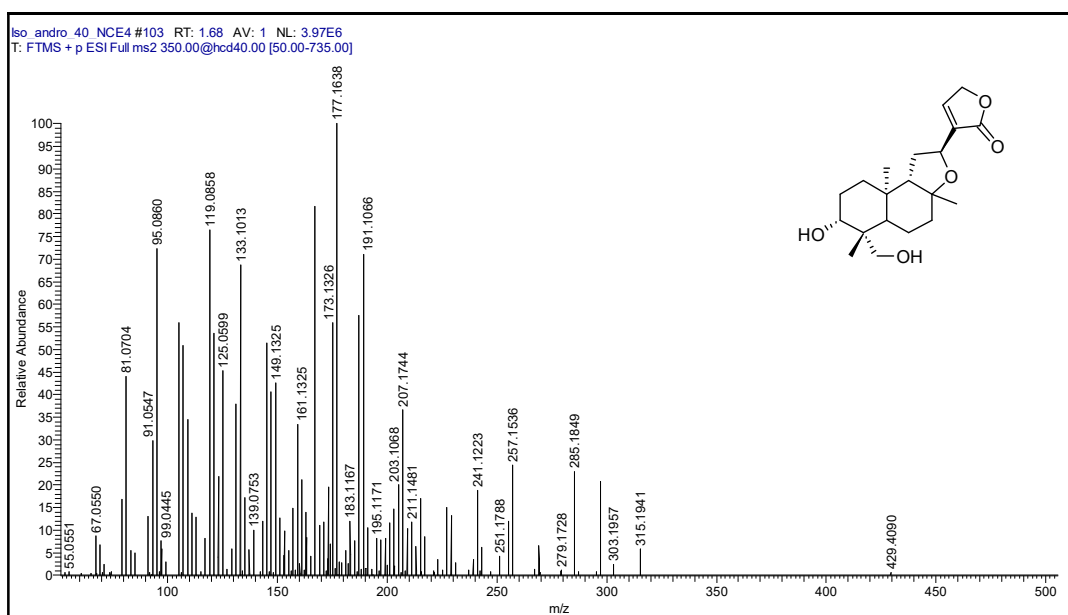


Figure 2B.8g. ESI(+)-MS/MS spectrum of Isoandrographolide in NCE 40 % (precursor ion $[M-H_2O]^+$ m/z 351.21)

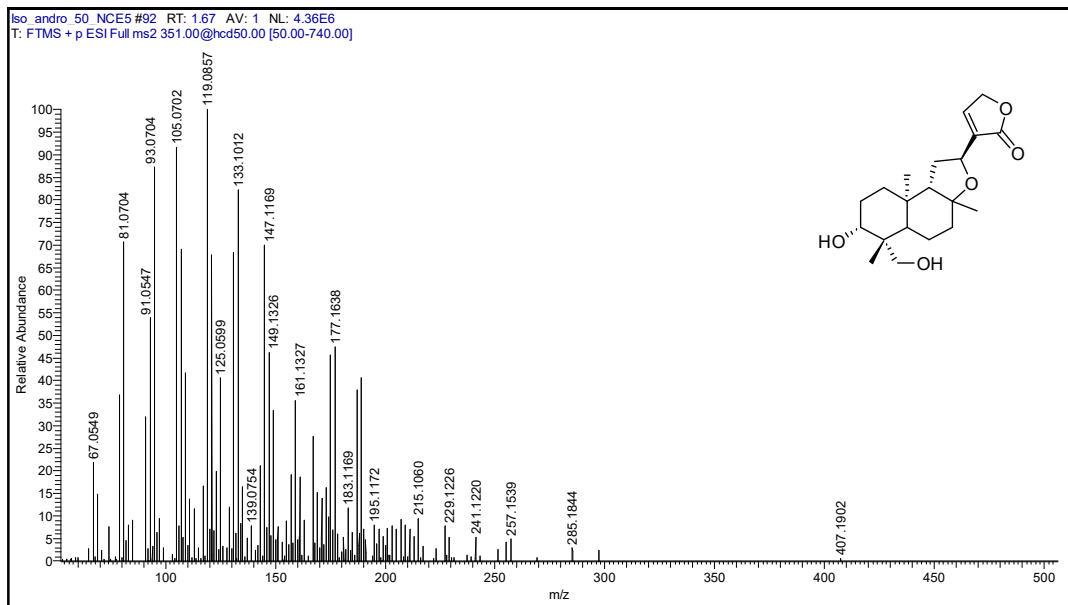


Figure 2B.8h. ESI(+)-MS/MS spectrum of Isoandrographolide in NCE 50% (precursor ion $[M-H_2O]^+$ m/z 351.21)

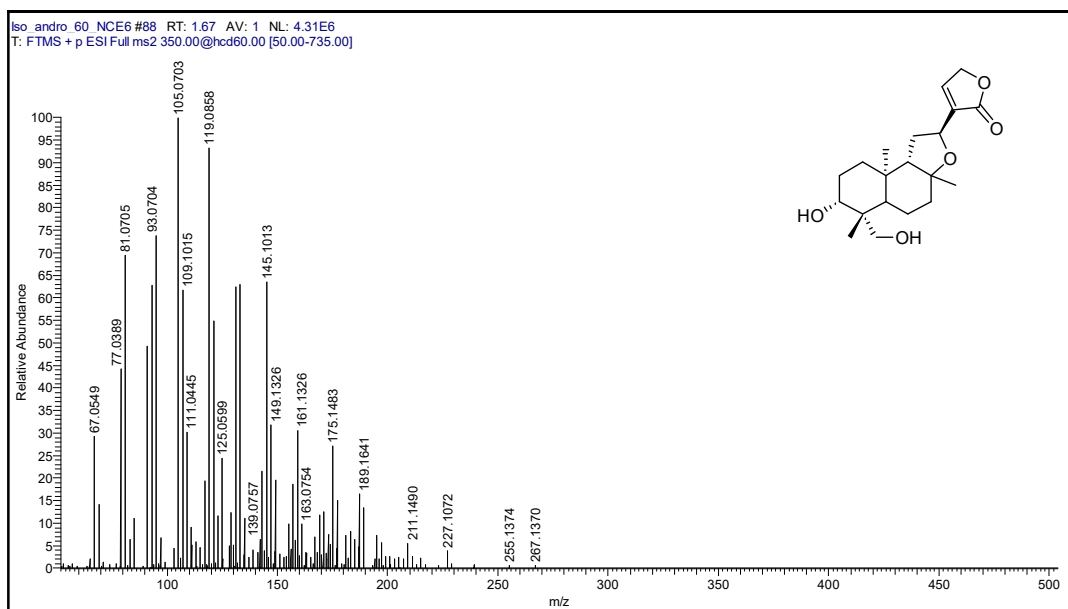


Figure 2B.8i. ESI(+)-MS/MS spectrum of Isoandrographolide in NCE 60 % (precursor ion $[M-H_2O]^+$ m/z 351.21)

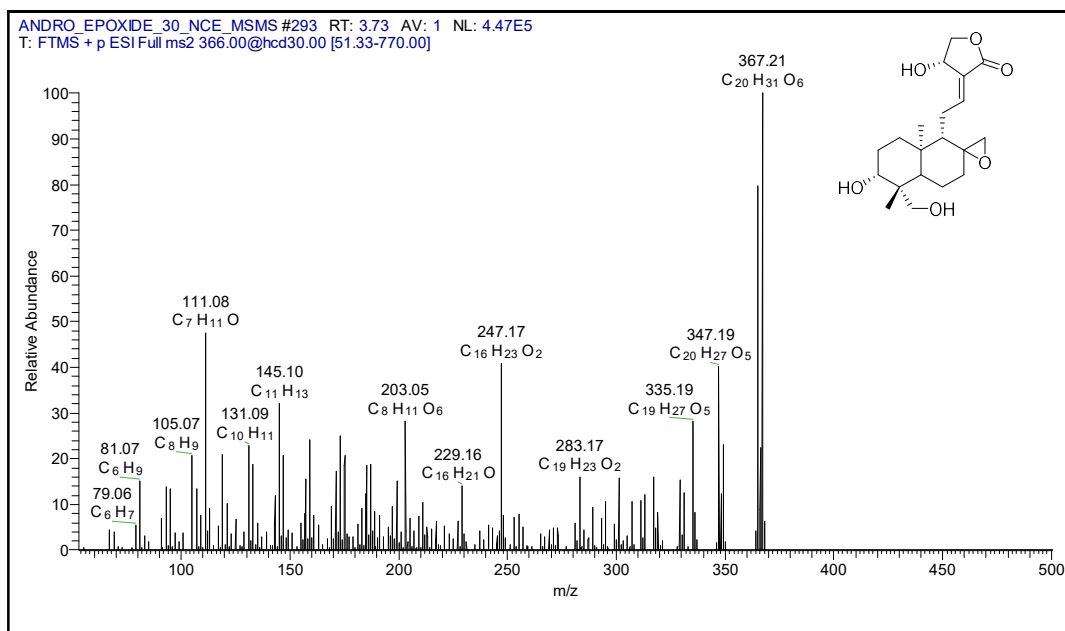


Figure 2B.9. ESI(+)-MS/MS spectrum of andrographolide-8,17-epoxide in NCE 30%

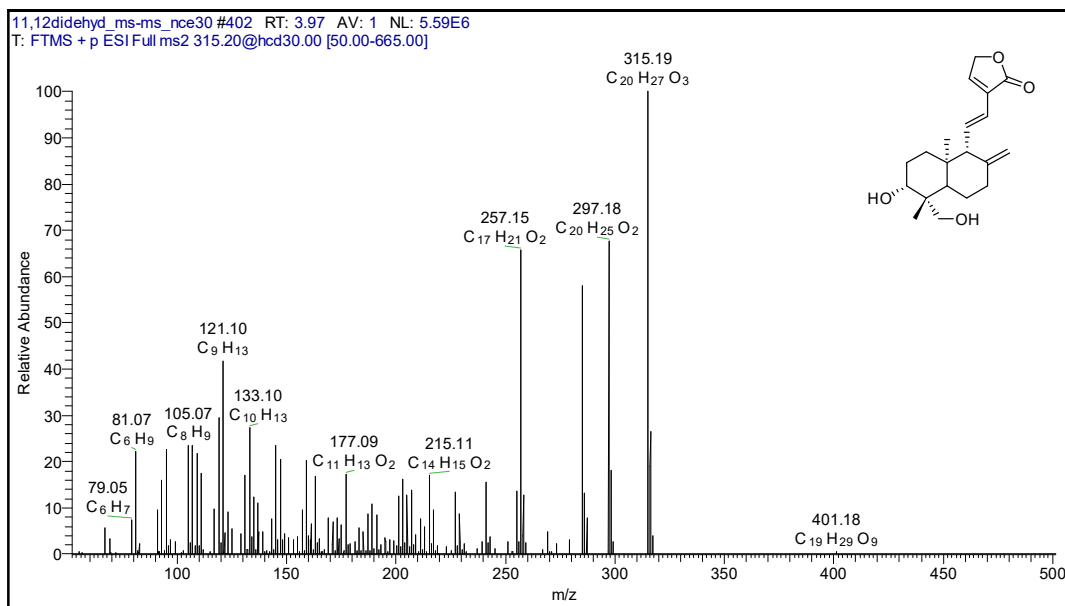


Figure 2B.10. ESI(+)-MS/MS spectrum of 11,12-didehydro-14-deoxyandrographolide in NCE 30 %

Chapter 2: Section C

**Cytotoxicity study and investigation of cellular
localization of Andrographolide by fluorescent tagging**

2C.1 Introduction

Cancer is the uncontrolled disease; approximately 18.1 million new cases have been reported in 2018 according to global cancer statistics out of 9 million were deaths from cancer worldwide.³³ Cancer is a vital problem faced by the world and is differentiated into different types according to the site in the human body. Breast cancer is a common form of cancer observed in women.^{34,35} Traditional therapy and surgical procedures are insufficient in the management and treatment of breast cancer hence there is need of the anti-cancerous natural product.³⁶ Natural products are the source of effective and selective anticancer agents in order to prevent and treat cancer.^{37,38} Andrographolide, a labdane diterpenoid major, constitute isolated from *A. paniculata* earlier reports; andrographolide has a cytotoxic effect against a broad range of cancer cell lines.^{39,40} However, the effects of Andrographolide on breast tumorgrowth and angiogenesis remain to be elucidated and not study in detailed.⁴¹ In order to enhance the understanding of the bioactive molecule, it is covalently attached to the fluorescent probe are used to unveil the cellular processes (including localisation or specific interactions) involved with their activity.⁴² Henceforth to improve the understanding of andrographolide anticancer activity, mechanism, and site of action fluorescent labelling is helpful. Fluorescent labelling of bioactive natural products reported earlier has disadvantages such as several steps of chemical synthesis, complicated purification procedure, low overall yield, bulky nature of fluorophore.^{43,44}

Henceforth there is a need of an efficient fluorescent probe to visualise the site of action andrographolide inside the cancerous cell. Also, the low availability of the natural product makes it difficult to carry all reaction steps henceforth, there is a need for the expensive, mild, and high yielding protocol for fluorescent labelling. As discussed, ready to use fluorescent tags are available commercially, but they are quite expensive and require extreme reaction conditions for labelling (e.g. NBD-F or DBD-COCl needs 60°C at basic pH) which restrict their use for tagging sensitive multifunctional andrographolide.⁴⁵

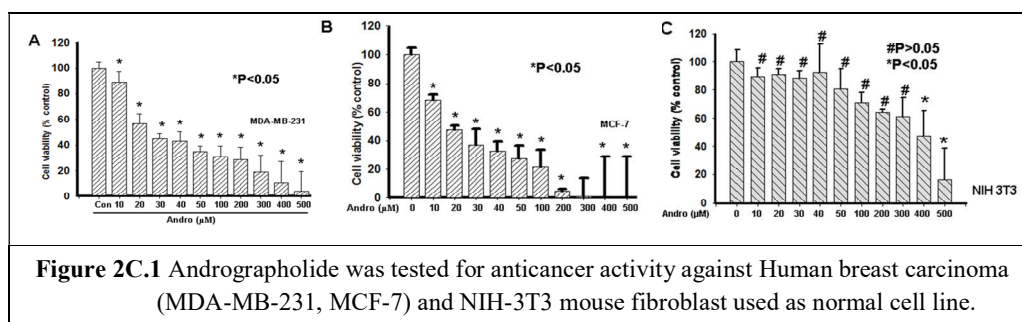
Herein we study the effect of Andrographolide on MDA-MB-231 and MCF-7 by MTT. Further, we synthesised a fluorescent tagged of andrographolide by using NBD-as a fluorescent probe (Scheme 2C.1) and study the fluorescent imaging.

2C.2. Result and Discussion

2C.2.1 Cell Viability Assay of Andrographolide

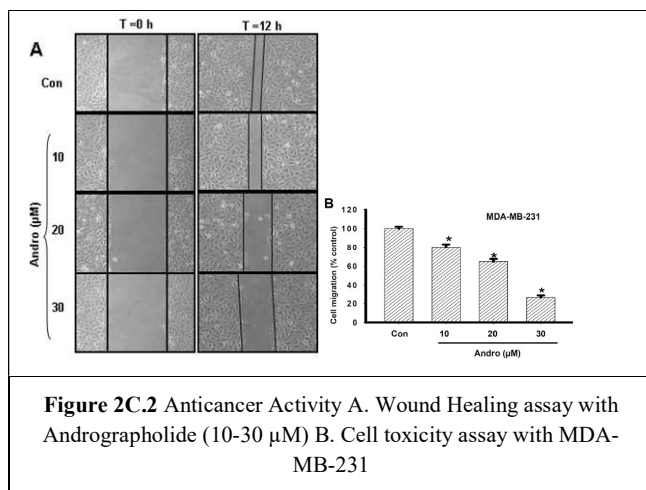
We have studied andrographolide cytotoxicity against Human breast carcinoma (MDA-MB-231, MCF-7) and controlled NIH-3T3 mouse fibroblast used as a normal cell line. (This work is performed in collaboration with Dr. Kundu (NCCS, Pune) and Dr. Santosh Kumar) Cytotoxicity was examined by MTT assay to study the effect of andrographolide on breast cancer cell viability.

Breast cancer (MCF-7 and MDA-MB-231) cells were incubated in the presence of concentration (0-500 μ M) of Andrographolide for 24 h and viability was determined by using MTT assay. The effect of Andrographolide on the viability of breast cancer cells is expressed as the percentage of viable cells compared to control. Results suggested that 20 μ M of Andrographolide displayed significant inhibition of viability on both MDA-MB-231 (Figure 2C.1A) and MCF-7 cells. To further study the toxicity of Andro on normal cells, NIH-3T3 cells were treated with Andrographolide (0-500 μ M), and MTT assay was performed. The result demonstrated that Andro is non-toxic to normal cells up to 50- 100 μ M (Figure 2C.1C).



2C.2.2 Wound Healing Assay Andrographolide

Tumorangiogenesis is a multistep process in which branching of blood vessels and its migrations towards the distant tumours occur by breaking the basement membrane. Each phenomenon such as basement membrane disruption, cell migration, cell proliferation, and tube formation can be a target for intervention to inhibit tumorgrowth. In the present study, andrographolide cytotoxicity on HUVEC wound migration was studied. The wound migration data revealed that andrographolide significantly inhibits HUVEC migration in a dose-dependent manner (Figure 2C.2). To further confirm our observation, Boyden chamber migration assay for HUVEC was performed. The



Chemotactic model of comigration and coinvasion of HUVEC and MDA-MB-231 cells using Boyden chamber is correlated with a typical tumour-endothelial interaction study. To study this interaction, the chamber was used with or without matrigel for HUVEC migration and invasion assays.

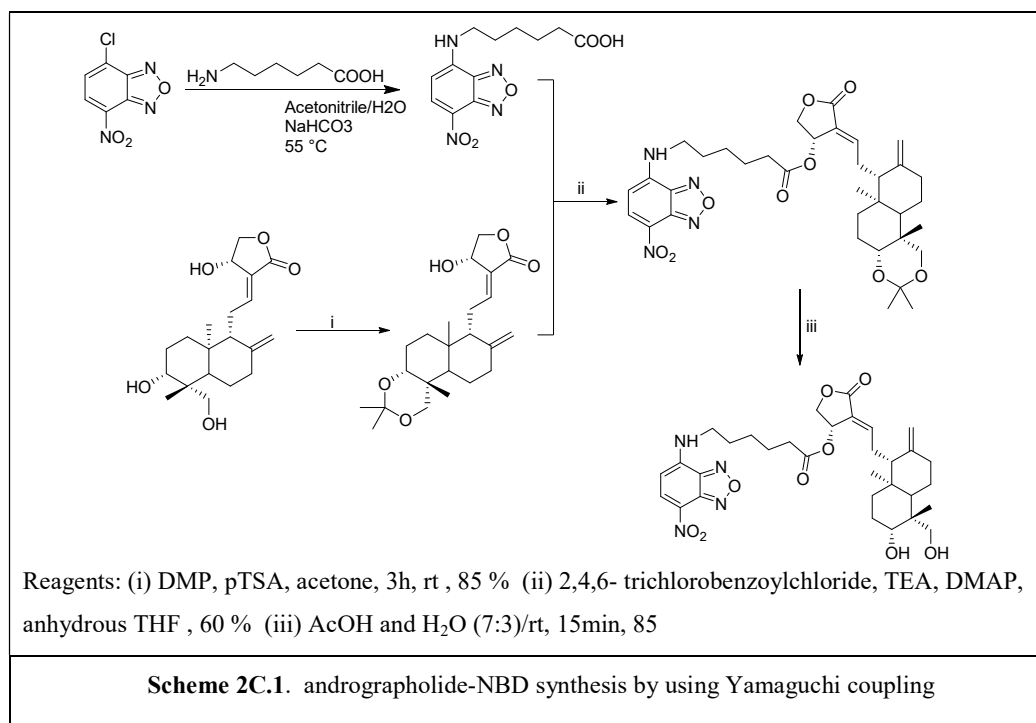
Conditioned media collected from MDA-MB-231 cells treated with Andrographolide were used in the lower chamber and HUVEC were seeded in the upper chamber. The data showed that Andrographolide significantly inhibits endothelial cell migration and invasion towards the lower side of the Boyden chamber suggesting the inhibitory effect of Andro on tumour-endothelial cell interaction.

2C.2.3 One Pot Labeling Protocol

NBD-Cl is a non-fluorescent molecule, which undergoes nucleophilic substitution by amine functionality and becomes a highly sensitive fluorescent entity. Here, our protocol involves the aromatic nucleophilic substitution on NBD-Cl by the amine functionality of amino acids in the initial step to generate fluorescent reagent followed by coupling between the free carboxylic end and the hydroxylated bioactive molecule in the same round bottom flask (Scheme 2C.1). It is always preferable to synthesise fluorescent reagent freshly in one-pot rather than using it as an individual tagging dye due to several reasons. Fluorescent reagents are photosensitive, and they require special care during preparation and storage such as dim light and low temperature. Preferably they are used immediately after preparation and purification. Therefore, it is more convenient to generate fluorescent reagent freshly in one-pot from two non-fluorescent starting materials (NBD-Cl and amino acids). Again, after the preparation of fluorescent reagent, it necessarily needs to be purified before storage. However, the reported one-pot protocol is devoid of one additional purification step making it less tedious.

2C.2.4 Characterization of NBD-Andrographolide

The presence of ester bond in NBD tagged Andrographolide was confirmed due to the presence of a newly appeared quaternary signal at δ_C 172.9 compared to andrographolide and was assigned to the ester carbonyl. The chemical shift values for andrographolide skeleton in ^{13}C NMR of NBD-andrographolide remained similar in comparison to andrographolide except for C-14, C-13, and C-15. The downfield shift of C-14 (by 3 ppm) and upfield shift of C-13 (by 5 ppm) and C-15 (by 3 ppm) indicated the esterification at 14-OH. Further, the position of attachment of NBD was confirmed based on HSQC and HMBC spectra (Figure 4B.3). The signal at δ_H 5.94 (d, $J=5.52$ Hz) was assigned to H-14 according to the correlations of H-14 with C-12 (δ_C 150.6), C-13 (δ_C 123.8) and C-16 (δ_C 169.1) in the HMBC spectrum. The signal at δ_C 172.9 was ascribed to C-16' due to the presence of its correlation with H-15' (δ_H 2.43). The esterification at 14-OH was unambiguously affirmed based on a strong correlation between H-14 (δ_H 5.94) and C-16' (δ_C 172.9).



NBD-andrographolide 17.7 mg (0.028 mmol) was isolated from 30.0 mg (0.086 mmol) of 17 with 33 % yield. Orange solid. $[\alpha]^{25} = -80.7$ (*c*, 0.95, CHCl₃). IR (CHCl₃) ν_{max} (cm⁻¹): 3409, 1738. ¹H NMR (400 MHz, CDCl₃) δ : 8.50 (d, *J*=8.53 Hz, 1H), 7.01 (m, 1H), 6.51 (m, 1H), 6.18 (d, *J*=8.53 Hz, 1H), 5.94 (d, *J*=5.52 Hz, 1H), 4.85 (s, 1H), 4.56 (m, 1H), 4.47 (s, 1H), 4.23 (m, 1H), 4.15 (d, *J*=11.04 Hz, 1H), 3.50 (m, 3H), 3.32 (d, *J*=11.04 Hz, 1H), 2.35-2.45 (m, 5H), 1.25 (s, 3H), 0.62 (s, 3H). ¹³C NMR (100 MHz, CDCl₃) δ : 172.9, 169.1, 150.6, 146.9, 144.2, 143.9, 143.8, 136.5, 123.9, 123.8, 108.7, 98.6, 80.3, 71.6, 67.8, 64.1, 55.7, 55.0, 43.6, 42.8, 38.7, 37.6, 36.9, 33.7, 29.7, 28.1, 26.3, 25.3, 24.2, 23.6, 22.7, 15.1. HRMS (ESI) *m/z*: [M+H]⁺ Calcd for C₃₂H₄₃N₄O₉, 627.3030; found, 627.3024.

2C.2.5 Cell Imaging Studies

Cancer cells (MDA-MB-231, A375) were treated with NBD-andrographolide (20 $\mu\text{g/mL}$) for 1 h and analysed for cellular internalisation and localisation under a

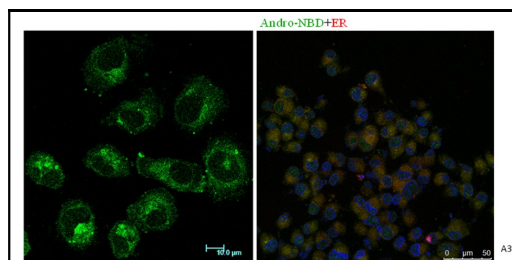


Figure 2C.3 Confocal microscopy images of HeLa cells treated with NBD-andro and colocalization

confocal microscope. Results depicted the cellular uptake of NBD labelled compounds irrespective of the cancer cell lines and no specific localisation in the nucleus. Further, these imaging probes can be used for studying the localisation in sub-cellular organelles. HeLa cells treated either with NBD- andrographolide were stained by

Mito-tracker Red and analysed through confocal microscopy which shows colocalization with mitochondria (Figure 2C.3). Similarly, the colocalization experiment was performed with ER-tracker red and labelled analogue were found to be localised in the endoplasmic reticulum (ER) based on yellow fluorescence observed in the overlaid image.

2C.3 Conclusion

Cytotoxicity studies and that on MDA-MB-231, MCF-7 showed that the andrographolide is a potent anticancer agent. Wound healing assays suggested that andrographolide inhibits cell growth. Further simple and highly efficient one-pot methodology for the NBD based fluorescent labeled andrographolide was developed, which can be applied to track their mode of action through fluorescence cell imaging. The internalization and localization of those probes were imaged successfully inside the cancer cells and found to be localized in the endoplasmic reticulum.

2C.4 Experimental Section

2C.4.1 Cell Lines, Antibodies, and Reagents

Human breast adenocarcinoma (MDA-MB-231, MCF-7) and mouse fibroblast (NIH-3T3) cell lines were obtained from American Type Culture Collection (ATCC, Manassas, VA, USA) and maintained in L-15 (MDA-MB-231) and DMEM (MCF-7, NIH-3T3) media (Sigma) supplemented with 10 % FBS, 100 units penicillin and 100 $\mu\text{g/ml}$ streptomycin. MDA-MB-231-Luc cells were purchased from Xenogen Corporation (Alameda, CA) and maintained according to the manufacturer's instructions. Human umbilical vein endothelial cells (HUVEC) were purchased from Lonza and grown in EGM 2 bullet kit. Wortmannin and SN50 were purchased from Calbiochem (San Diego, CA). The [$\mu\text{-}^{32}\text{P}$] ATP was procured from the Board of Radiation and Isotope Technology (Hyderabad, India). All other chemicals were of analytical grade.

2C.4.2 Cell Viability assay (MTT) Assay

The cell viability assay was performed as described previously.⁴⁶ Briefly, 2×10^4 cells/well were plated in a 96-well flat-bottom microplate. Cells were treated with Andro (0-500 μM) for 24 h. 200 μL of MTT (0.5 mg/mL) was added into each well and incubated at 37 C for 4h. After incubation, formazan crystals were dissolved with 200 μL of isopropanol. The optical density of formazan solution, as a measure of cell viability, was taken using a microplate reader at 570 nm (Molecular Devices). Experiments were performed in triplicates.

2C.4.3 Wound Healing Assay

The wound migration assay was performed using MDA-MB-231 and HUVEC as described earlier. Briefly, cells were grown in monolayer and synchronised for 24 h in serum-free medium. Wound with uniform size was made using a sterile tip, and the cells were treated with Andrographolide (0-30 μ M). After 12 h, wound photographs were captured using a phase contrast microscope (Nikon). Distance migrated was measured by Image-Pro plus software, analysed and represented in the form of a bar graph.

2C.4.4 Instrumentation

For chromatography, technical grade solvents were distilled prior. Compounds were purified over silica gel (230-400 mesh) flash chromatography columns using dichloromethane/methanol gradient mixture as the eluent. Reactions and purification processes were monitored by thin layer chromatography, which was carried out on pre-coated silica gel plates using UV light (254 nm) as the visualisation medium and anisaldehyde charring solution as the staining agent. Thin film IR spectra were recorded in CHCl_3 , and optical rotations were determined in the same solvent at 589 nm using 10 mm cell (*c* in g/100 mL unit). Chemical shift values in NMR (^1H , ^{13}C , DEPT-135) spectra were reported in ppm concerning the residual solvent or TMS signals as the reference. HRMS data were collected on Q Exactive Quadrupole-Orbitrap Mass Spectrometer.

2C.4.5 One-pot Labeling Protocol

A solution of NBD-Cl (1.00 equiv) in acetonitrile (18 mL/mmol) was added dropwise to a solution of an amino acid (1.00 equiv) and sodium bicarbonate (3.00 equiv) in water (6 mL/mmol) at 55°C and incubated for 1 h. Then acetonitrile was concentrated under reduced pressure and pH of the aqueous reaction mixture was adjusted to \sim 2.0 using 1N HCl. Further, it was concentrated to dryness under 20 mbar pressure and 62°C temperature. The deep orange crude solid was again dissolved in a minimum amount of acetonitrile and dried in the same condition to make sure that there is no residual moisture remaining. Further Yamaguchi coupling was carried out in the same vessel following the reported procedure with slight modifications.

2C.4.6 Synthesis of 3, 19-isopropylidene andrographolide

Andrographolide dissolved in acetone keep round bottom flask at room temperature, dimethoxy propane was added in the reaction mixture further catalytic amount of pTSA was added. The reaction was kept for 3 h at room temperature, and the product was extracted in ethyl acetate, and the organic layer was concentrated. Further 3, 19-isopropylidene andrographolide was purified using column chromatography.

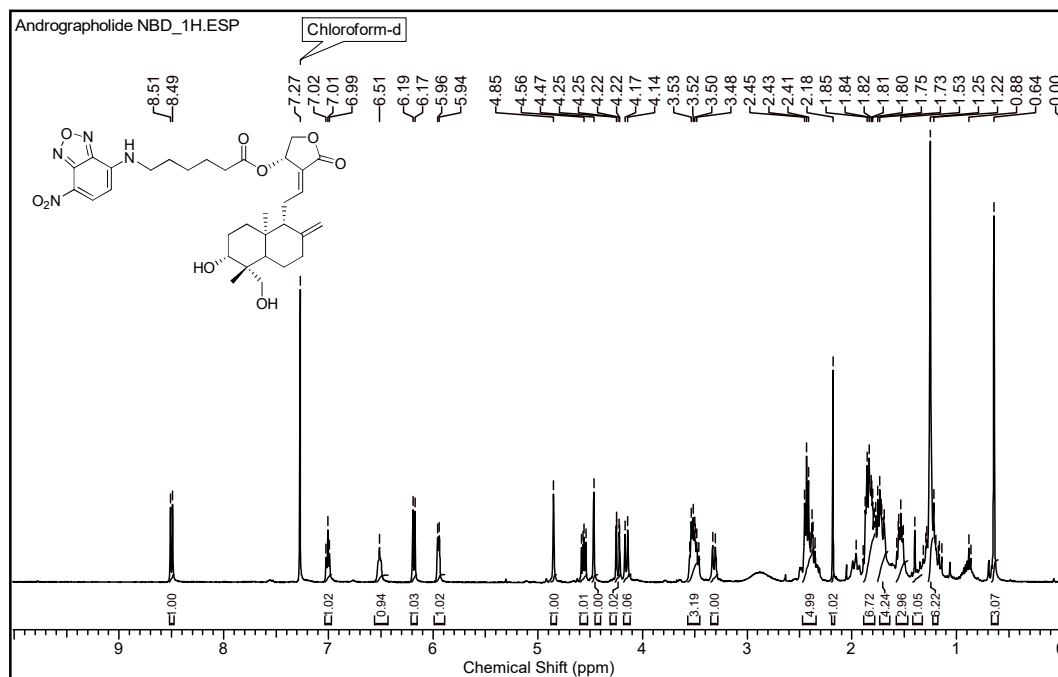
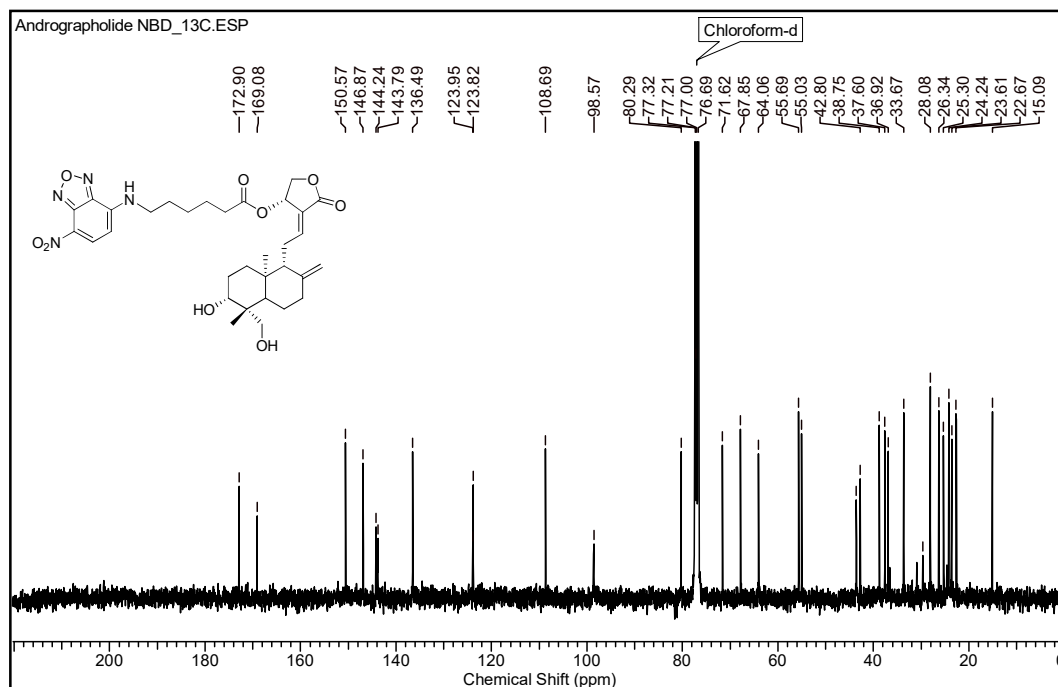
2C.4.7 Synthesis of NBD-andrographolide

Andrographolide (0.75 equiv) with hydroxyl functionality in anhydrous THF (20 mL/mmol) was added to the dried crude under an inert atmosphere with stirring. 2,4,6-trichlorobenzoyl chloride (1.00 equiv) and anhydrous TEA (1.00 equiv) were successively added dropwise to the reaction mixture. After 5 min, DMAP (1.00 equiv) was added to the reaction vessel and continued with stirring for another 30 min. The reaction was quenched by adding a few drops of water. Then it was concentrated to dryness and directly purified over a silica gel column. All the steps were performed under dim light, and labelled compounds were stored at -20°C in the dark. Further, the 3, 19-isopropylidene andrographolide was deprotected reaction conditions acetic acid in water (7:3) at room temperature for 15 min.

2C.4.8 Confocal Microscopy

MDA-MB-231 was grown on coverslips, treated with andro-NBD (20 µg/mL) for 1 h and fluorescence imaging analysis was performed. For colocalization study, cancer cells were treated with either andro-NBD for 1 h, followed by treatment with Mito-tracker (50 nM) for 20 min. Treated cells were fixed with 2 % paraformaldehyde for 10 min, washed twice with PBS and mounted onto a glass slide with mounting media. Nuclei were stained with DAPI and visualised under a confocal microscope (excitation 460 nm, emission 530 nm) with 60x magnification. Similarly, the co-localization experiment was performed with fluorescently (green) tagged derivatives of andro-NBD and red ER tracker in MDA-MB-231 cells. Cells treated either with andro-NBD (20 µg/mL for 1 h) were stained with ER-tracker (1 µM for 20 min) and analysed under the confocal microscope with 100x magnification after fixation and nuclear staining with DAPI (blue).

2C.5 Spectral Copies

Figure 2C.4a. ^1H NMR spectrum of 14-NBD-andrographolideFigure 2C.4b. ^{13}C NMR spectrum 14-NBD-andrographolide

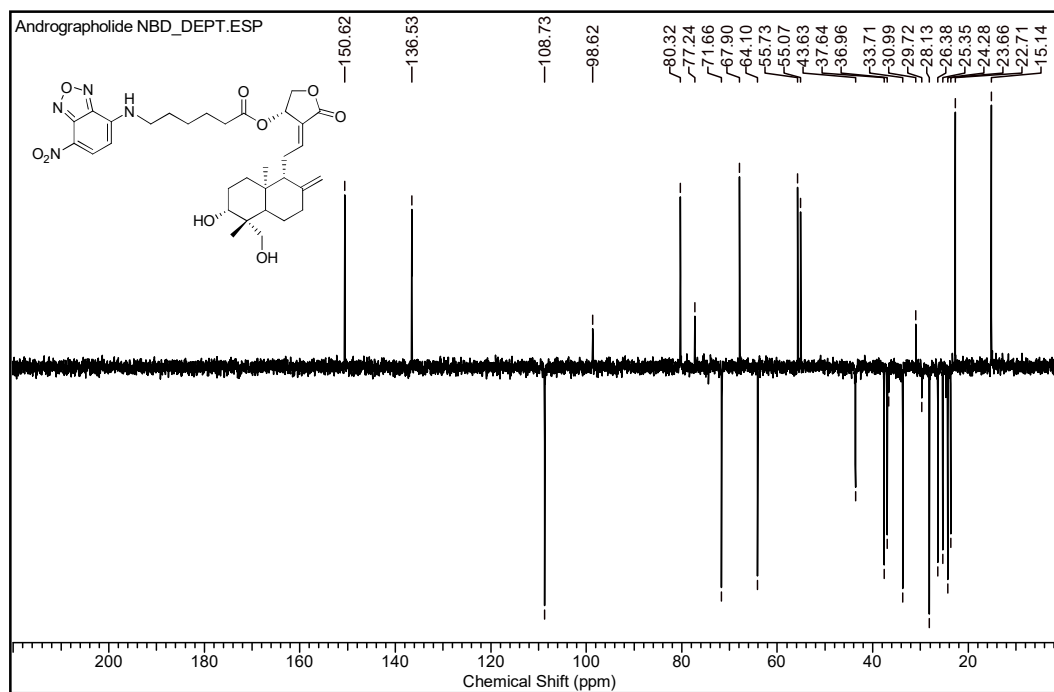


Figure 2C.4c. DEPT-135 NMR spectrum 14-NBD-andrographolide

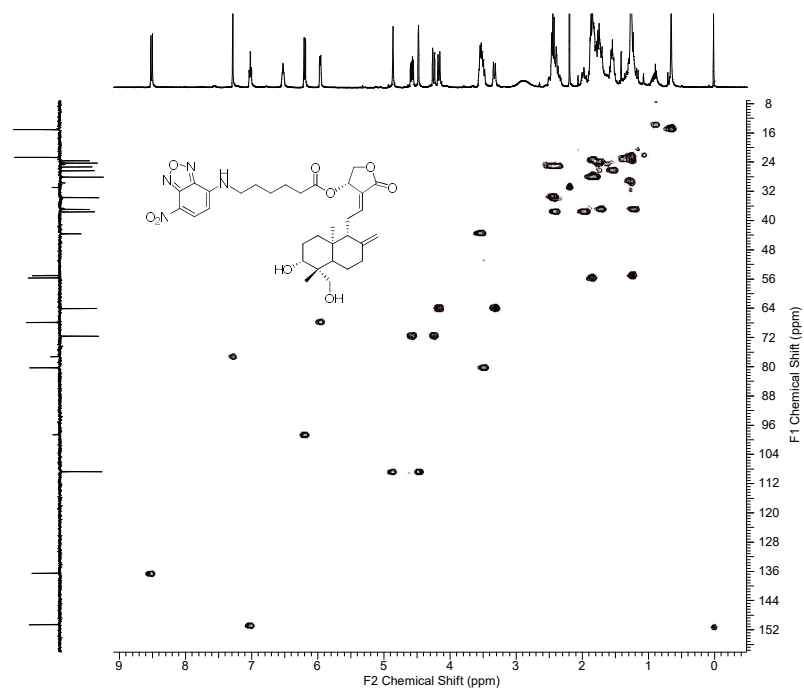


Figure 2C.4d. HSQC spectrum 14-NBD-andrographolide

2D. References

- 1 A. Garg, L. Agrawal, R. C. Misra, S. Sharma and S. Ghosh, *BMC Genomics*, 2015, **16**, 1–16.
- 2 M. Sanower Hossain, Z. Urbi, A. Sule and K. M. Hafizur Rahman, *Sci. World J.*, 2014, **2014**, 1–28.
- 3 A. Valdiani, M. A. Kadir, S. G. Tan, D. Talei, M. P. Abdullah and S. Nikzad, *Mol. Biol. Rep.*, 2012, **39**, 5409–5424.
- 4 Y. Dey, S. Kumari, S. Ota and N. Srikanth, *Int. J. Nutr. Pharmacol. Neurol. Dis.*, 2013, **3**, 3.
- 5 M. T. and J. F. Roman Paduch¹, Martyna Kandefer–Szerszeń¹, *Arch. Immunol. Ther. Exp.*, 2007, **55**, 315.
- 6 J. Bohlmann and C. I. Keeling, *Plant J.*, 2008, **3**, 656–669.
- 7 H. Yuan, Q. Ma, L. Ye and G. Piao, *Molecules*, 2016, **21**, 1–16.
- 8 W. W. Chao, Y. H. Kuo and B. I. F. Lin, *J. Agric. Food Chem.*, 2010, **58**, 2505–2512.
- 9 W. W. Chao and B. F. Lin, *Chin. Med.*, 2010, **5**, 1–15.
- 10 Y. H. Shen, R. T. Li, W. L. Xiao, Gang-Xu, Z. W. Lin, Q. S. Zhao and H. D. Sun, *J. Nat. Prod.*, 2006, **69**, 319–322.
- 11 M. A. Fernández, M. P. Tornos, M. D. García, B. de las Heras, A. M. Villar and M. T. Sáenz, *J. Pharm. Pharmacol.*, 2001, **53**, 867–72.
- 12 A. Urzúa, M. C. Rezende, C. Mascayano and L. Vásquez, *Molecules*, 2008, **13**, 882–891.
- 13 P. Prabhakar Reddy, R. Ranga Rao, J. Shashidhar, B. S. Sastry, J. Madhusudana Rao and K. Suresh Babu, *Bioorganic Med. Chem. Lett.*, 2009, **19**, 6078–6081.
- 14 H. W. Xu, G. F. Dai, G. Z. Liu, J. F. Wang and H. M. Liu, *Bioorganic Med. Chem.*, 2007, **15**, 4247–4255.
- 15 P. K. Singha, S. Roy and S. Dey, *J. Ethnopharmacol.*, 2007, **111**, 13–21.
- 16 P. K. Singha, S. Roy and S. Dey, *Fitoterapia*, 2003, **74**, 692–694.
- 17 Y.-F. Xia, B.-Q. Ye, Y.-D. Li, J.-G. Wang, X.-J. He, X. Lin, X. Yao, D. Ma, A. Slungaard, R. P. Hebbel, N. S. Key and J.-G. Geng, *J. Immunol.*, 2014, **173**, 4207–4217.
- 18 C. G. Jiang, J. Bin Li, F. R. Liu, T. Wu, M. Yu and H. M. Xu, *Anticancer Res.*, 2007, **27**, 2439–2447.
- 19 B. N. Zhou, N. J. Baj, T. E. Glass, S. Malone, M. C. M. Werkhoven, F. Van Troon, David, J. H. Wisse and D. G. I. Kingston, *J. Nat. Prod.*, 1997, **60**, 1287–1293.
- 20 L. K. Sy and G. D. Brown, *J. Nat. Prod.*, 1997, **60**, 904–908.
- 21 P. Rijo, C. Gaspar-Marques, M. F. Simões, A. Duarte, M. del C. Apreda-Rojas, F. H. Cano and B. Rodríguez, *J. Nat. Prod.*, 2002, **65**, 1387–1390.
- 22 Q. Du, G. Jerz and P. Winterhalter, *J. Chromatogr. A*, 2003, **984**, 147–151.
- 23 V. Sharma, S. Walia, J. Kumar, M. G. Nair and B. S. Parmar, *J. Agric. Food Chem.*, 2003, **51**, 3966–3972.
- 24 S. Haldar, P. B. Phapale, S. P. Kolet and H. V. Thulasiram, *Anal. Methods*, 2013, **5**, 5386–5391.
- 25 S. Haldar, F. A. Mulani, T. Aarthy, D. S. Dandekar and H. V. Thulasiram, *J. Chromatogr. A*, 2014, **1366**, 1–14.
- 26 H. G. Gika, G. A. Theodoridis, R. S. Plumb and I. D. Wilson, *J. Pharm. Biomed. Anal.*, 2014, **87**, 12–25.
- 27 J. W. Allwood and R. Goodacre, *Phytochem. Anal.*, 2010, **21**, 33–47.
- 28 X. Zhang, L. Luo and Z. Ma, *Anal. Bioanal. Chem.*, 2011, **400**, 3463–3471.
- 29 S. G. Musharraf, A. Ali, N. T. Khan, M. Yousuf, M. I. Choudhary and Atta-ur-Rahman,

- Steroids*, 2013, **78**, 171–181.
- 30 Z. Yan, G. Lin, Y. Ye, Y. Wang and R. Yan, *Anal. Chim. Acta*, 2014, **819**, 56–64.
- 31 B. Shafii, R. Vismeh, R. Beaudry, R. Warner and A. D. Jones, *Anal. Bioanal. Chem.*, 2012, **403**, 2683–90.
- 32 H. Danhelova, J. Hradecky, S. Prinosilova, T. Cajka, K. Riddellova, L. Vaclavik and J. Hajslova, *Anal. Bioanal. Chem.*, 2012, **403**, 2883–2889.
- 33 J. Ferlay, M. Colombet, I. Soerjomataram, C. Mathers, D. M. Parkin, M. Piñeros, A. Znaor and F. Bray, *Int. J. Cancer*, 2019, **144**, 1941–1953.
- 34 J. Cao, X. Wang, D. Wang, R. Ma, X. Li, H. Feng, J. Wang, S. Liu and L. Wang, *Cancer Cell Int.*, 2019, **19**, 93.
- 35 L. Chuang, G. Chen, S. Moi, F. Ou-Yang, M. Hou and C. Yang, *Biomed Res. Int.*, 2019, **2019**, 1–12.
- 36 L. Fan, K. Strasser-Weippl, J. J. Li, J. St Louis, D. M. Finkelstein, K. Da Yu, W. Q. Chen, Z. M. Shao and P. E. Goss, *Lancet Oncol.*, 2014.
- 37 E. K. Rowinsky and R. C. Donehower, *N. Engl. J. Med.*, 1995, **332**, 1004–1014.
- 38 J. D. McChesney, S. K. Venkataraman and J. T. Henri, *Phytochemistry*, 2007, **68**, 2015–2022.
- 39 N. V. L. S. Mulukuri, N. B. Mondal, M. Raghu Prasad, S. Renuka and K. Ramakrishna, *Int. J. Pharmacogn. Phytochem. Res.*, 2011, **3**, 39–42.
- 40 J. C. W. Lim, T. K. Chan, D. S. Ng, S. R. Sagineedu, J. Stanslas and W. F. Wong, *Clin. Exp. Pharmacol. Physiol.*, 2012, **39**, 300–310.
- 41 Z. Zhai, X. Qu, H. Li, Z. Ouyang, W. Yan, G. Liu, X. Liu, Q. Fan, T. Tang, K. Dai and A. Qin, *Mol. Med. Rep.*, 2015, **11**, 1139–1145.
- 42 B. J. Leslie and P. J. Hergenrother, *Chem. Soc. Rev.*, 2008, **37**, 1347–1360.
- 43 T. Toyo'oka, *Anal. Chim. Acta*, 2002, **465**, 111–130.
- 44 M. Sameiro and T. Gonçalves, *Chem. Rev.*, 2009, **1**, 190–212.
- 45 D. Wüstner, *Chem. Phys. Lipids*, 2007.
- 46 S. Kumar, H. S. Patil, P. Sharma, D. Kumar, S. Dasari, V. G. Puranik, H. V. Thulasiram and G. C. Kundu, *Curr. Mol. Med.*, 2012, **12**, 952–966.

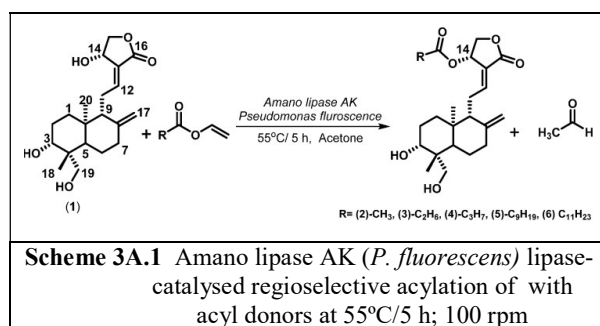
Chapter:3
**Enzymatic Modification and
Formulation of Andrographolide**

Chapter 3: Section A

Regioselective and Efficient Enzymatic Synthesis of Anti-microbial Andrographolide Derivatives

3A.1 Introduction

Andrographolide (1), is the major active constituent isolated from *A. paniculata*, It showed several pharmacological activities such as anti-cancer, anti-diabetic, anti-viral and anti-allergic.^{1,2} Owing to its promising biological activities, efforts being made to synthesize several derivatives of (1) and studied for their activity. Detailed structure-activity-relationship (SAR) studies of (1) have been carried out for finding synthetic analogues with improved biological activities.^{3,4} Several reports are available on the synthesis of andrographolide analogues using traditional chemical synthesis methods to improve bioactivities.⁵ Andrographolide monoester derivatives have been reported



to demonstrate enhanced anti-cancer, anti-HIV and antibacterial activities.^{6,7} However, the achievement of regioselective monoesterification of (1) through conventional reactions is a difficult task due to the presence

of similar reactive hydroxyl groups and α , β unsaturated lactone. Therefore, conventional synthetic methods involve multiple steps with protection-deprotection strategy, which often deliver low yield further, and solvents. On the other hand, biocatalysis offer an excellent alternative route for conventional synthesis.^{8,6} Lipases are known to efficiently catalyse a wide variety of organic reactions such as esterification, a chiral resolution with enhanced regio- and stereoselectivity in non-aqueous media.⁹ Due to their environmentally benign nature, lipase-catalyzed *trans*-esterification for the synthesis of drug intermediates, surfactants, and natural product analogues has attracted increasing attention in recent times.¹⁰ Although the biological activity of (1) is well studied, very little is known on biocatalyst mediated synthesis of monoesters of (1) and mode of action of their anti-microbial activities.^{11, 7} In order to further enhance the activity of (1),^{12, 13, 14} we have screened several lipases for the regioselective esterification of one of the hydroxyl group of andrographolide (1) in the presence of various acyl donors (Scheme 3A.1). Furthermore, (1) and its monoesters have been screened for their anti-microbial and hemolytic activities. Bacterial cell permeability assay was carried out using fluorescent staining assay and SEM imaging.

3A. 2 Results and discussion

3A.2.1 Screening of Lipases for Andrographolide Acylation

Several commercially available lipases (Table 3A.1) were screened for regioselective acylation of (1) in the presence of acyl donors with different chain length. Screening results indicated that among all the lipases studied, Amano lipase AK (*P. fluorescens*) was able to carry out the esterification of the hydroxyl group at C-14 of (1) in a very efficient manner compared to the other lipases studied.

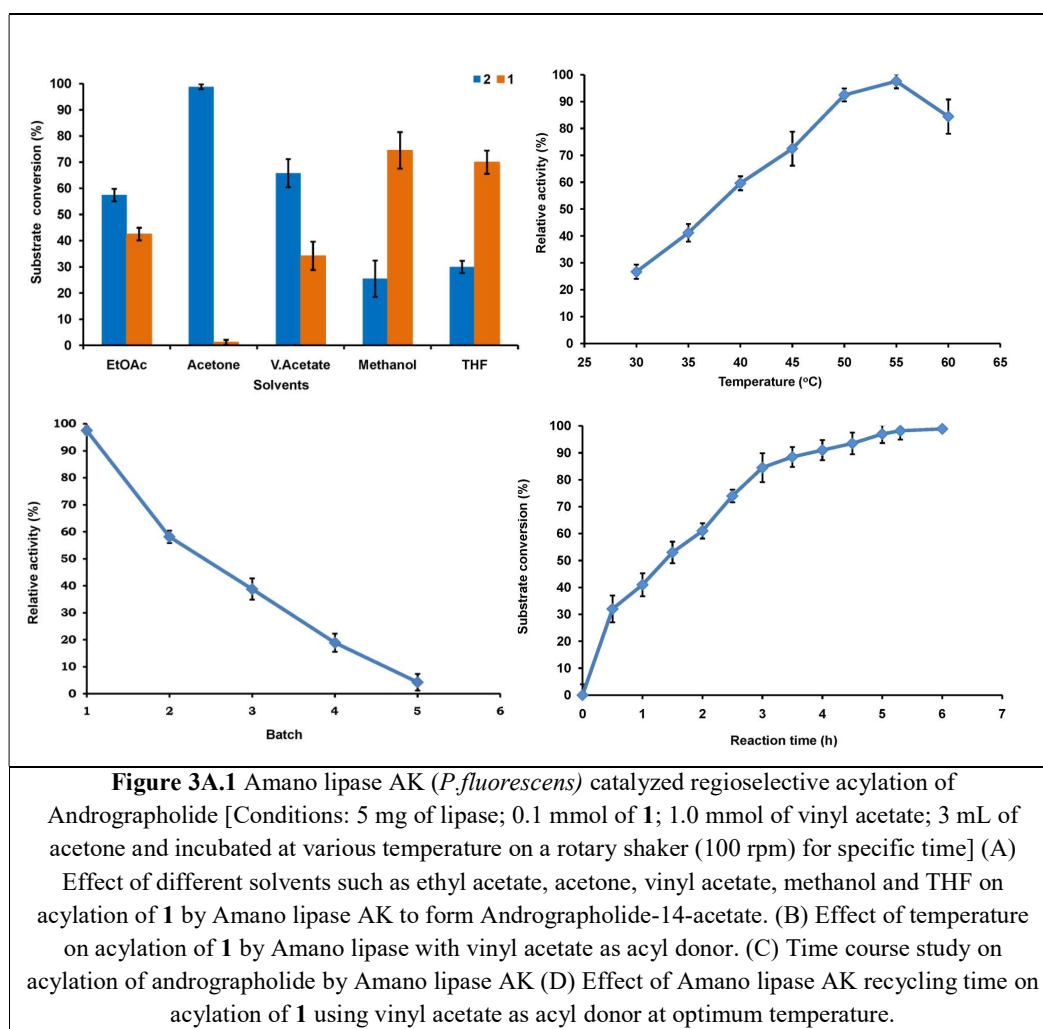
Table 3A.1 Screening of various lipases with acyl donors for acylation of andrographolide

S.No.	Enzyme	Source	Acetyl donors						
			V1	V2	V3	V4	V5	V6	V7
1.	Novozyme 435	CAL-B	r.	n.r.	r.	n.r.	r.	n.r.	n.r.
2.	Immobilized on Immobead 150	CAL-A	n.r.	r	n.r.	r.	n.r.	n.r.	n.r.
3.	Amano lipase PS	<i>B. cepacia</i>	n.r.	n.r.	n.r.	n.r.	n.r.	n.r.	n.r.
4.	Immobilized on diatomite	Amano lipase PS	r	n.r.	n.r.	n.r.	n.r.	n.r.	r
5.	Amano lipase A	<i>A.niger</i>	n.r.	n.r.	r	n.r.	n.r.	n.r.	n.r.
6.	Amano lipase AK	<i>P.fluroscence</i>	r	r	r	n.r.	r	n.r.	r
7.	CRL	<i>C.cylindracea</i>	n.r.	n.r.	n.r.	n.r.	n.r.	n.r.	n.r.
8.	Type II PPL	<i>P. pancreas</i>	n.r.	n.r.	n.r.	n.r.	n.r.	n.r.	n.r.
9.	Lipase type VII	<i>C.rugosa</i>	n.r.	n.r.	n.r.	n.r.	n.r.	n.r.	n.r.
10.	Lipase	<i>P.camemberti</i>	r.	n.r.	n.r.	n.r.	n.r.	n.r.	n.r.
11.	Lipase	<i>R. niveus</i>	r.	n.r.	n.r.	n.r.	n.r.	n.r.	n.r.

V1, Vinyl acetate; V2, Vinyl propionate; V3, Vinyl butyrate; V4., Vinyl decanoate; V5., Vinyl laurate; V6., Vinyl benzoate; V7, Vinyl Trifluoroacetate. *B.cepacia*, *Burkholderia cepacia*; *C. cylindracea*, *Candida cylindracea*; *P.pancreas* *Porcine pancreas*; *P. camemberti*, *Penicillium camemberti*; *R. niveus*, *Rhizopus niveus*.

n.r. = no reaction. r = reaction. ^aThe reaction conditions: 0.1 mmol Andrographolide; 1.0 mmol various vinyl donors; 5mg enzyme; 5 mL Acetone; 200 rpm; 6 days.^b The detailed information about the enzyme.

Among the screened lipases, Amano lipase PS (*B. cepacia*), CRL (*C.cylindracea*), Lipase Type II PPL (*P. pancreas*) and Lipase type VII (*C.rugosa*) did not show esterification with any acyl donors. Lipases from *P. camemberti* and *R. niveus* accepted vinyl acetate as an acyl donor, and Amano lipase A (*A.niger*) accepted only vinyl butyrate as acyl donor to carry out the esterification of C-14 hydroxyl moiety of (**1**). CAL-A lipase showed reaction with vinyl propionate and vinyl caproate whereas CAL-B lipase gave ester product only with acyl esters such as acetate, butyrate and laurate.



All these lipases did not show acylation activity with a range of acyl donors with the desired yield. On the other hand, Amano lipase AK (*P. fluorescens*) catalysed acylation reactions in the presence of vinyl acyl donors such as vinyl acetate, vinyl

propionate, vinyl butyrate, vinyl caproate and vinyl laurate with good to excellent regioselectivity, and hence we further optimised the reaction conditions using Amano lipase AK. In control, which is devoid of lipase, no acylated product formation was observed.

3A.2.2 Effect of Solvents on Andrographolide Acetylation

The solvent is known to play an essential role in lipase-catalysed esterification concerning the reaction time and yield.¹⁵ Amano lipase AK catalysed acetylation of (**1**) was examined in various solvents at standardised reaction conditions. These results suggested that acetone seems to be a better solvent for carrying out acetylation of (**1**) (Figure 3A.1A). The reason for good yield with acetone in 6 h, may be due to the higher solubility of (**1**) in acetone and also may be due to inactivation of the enzyme by other solvents.¹⁶

Table 3A.2 Effect of acyl donor chain length on the initial rate of Amano lipase AK (*P. fluorescens*) catalysed acylation of (**1**).

Acyl donor	V_o (mMh ⁻¹)	Yield (%) ^b	Regioselectivity (%)
Vinyl acetate	37.1 ± 1.4	98.2	100
Vinyl propionate	33.4 ± 1.5	98.5	100
Vinyl butyrate	29.5 ± 0.5	96.3	100
Vinyl decanoate	25.2 ± 1.8	95.6	100
Vinyl laurate	20.2 ± 2.5	94.5	100

^a The reaction condition: 5 mg of lipase; 0.1 mmol of **1**; 1.0 mmol of acyl donor; 3 mL of acetone and incubated at 55 °C on a rotary shaker (100 rpm) for 5 h. ^b The yield was determined by HPLC analysis.

3A.2.3 Effect of Temperature on Andrographolide Acetylation

In lipase-mediated reactions, the temperature has an essential role in the enzyme activity, stability and thermodynamic equilibrium.¹⁷ Thermal stability of Amano lipase AK (*P. fluorescens*) during acetylation of (**1**) was examined. Substrate conversion was increased with increase in temperature from 30 °C to 55 °C (Figure 3A.1C). Further increase in temperature, the rate of product formation was decreased. These results suggested that 50 °C to 55 °C was the optimal temperature for Amano

lipase AK mediated acetylation of (1). However, there was no change in the acylation position on (1) was observed with varying the temperature.

3A.2.4 Time course Study of Andrographolide Acetylation

Time-dependent progress of (1) acetylation under optimised reaction conditions was studied (Figure 3A.1 C) by monitoring the substrate and product ratios using HPLC attached UV-Visible detector at 235 nm. These results suggested that the reaction rate was high at initial incubation period and reached maximum at 5 h, at the end of 5 h incubation period, > 98.0 % of (1) was converted into andrographolide-14-acetate.

3A.2.5 Operational Stability of Amano Lipase AK (*P. fluorescens*) in Andrographolide Acetylation

Operational stability of lipase was studied by performing acylation of (1) in batch at optimised reaction conditions. Amano lipase AK was recovered after each batch of incubation by ultrafiltration (3 kDa cutoff membrane) and washed with acetone. This recovered protein was again incubated with (1) in the presence of vinyl acetate in acetone. The HPLC analysis of each batch extracts indicated that there was a reduction in lipase activity and after the fifth batch, the lipase activity was completely lost (Fig. 1D). These results indicated that Amano lipase AK can be reused for the production of andrographolide-14-acetate using (1) as a substrate.

3A.2.6 Effect of Alkyl Substituent of the Acyl Donor on Andrographolide Acylation

Initial rate of the Amano lipase AK mediated acylation of 1 was varied with the chain length of the acyl donor. In all cases, the Amano lipase efficiently carried out the hydroxy group at C-14 acylation of (1) to form respective acylated products. Initial rate of acylation increased as the chain length increased from C-2 to C-4 in the acyl donor. Further increase in the chain length of the side chain of vinyl donors (5 and 6) marginally decreased in the level of individual acylated product of (1) (Table 3A.2). These results suggested that Amano lipase AK efficiently catalyse the acylation of (1) to produce the andrographolide-14-acylated product with a different alkyl chain length from C-2 to C-12 (Table 3A.2).

3A.2.7 Anti-microbial activity of andrographolide and derivatives

Amano lipase AK catalysed acylated products of **1** (**2** to **6**) were evaluated for their anti-microbial activity against several bacteria and fungi (Table 3A.3). The inhibitory activities of (**1**) and its derivatives showed some potential anti-bacterial activity with minimum inhibitory concentration (MIC) values between 4-16 $\mu\text{g/mL}$ and moderate activity against *Candida albicans* with MIC 16-64 $\mu\text{g/mL}$ (Table 3A.3).

Table 3A.3 The anti-microbial MIC of andrographolide and its derivatives with their hemolytic activity.

Microorganism	1	2	3	4	5	6	Gentamicin sulfate	Benzamide sodium	Amphoterecicin B
<i>M. luteus</i>	>128	32	16	32	64	16	nd	1	nd
<i>S. aureus</i>	>128	16	4	8	16	16	0.5	1.8	nd
<i>P. fluorescens</i>	>128	4	32	16	64	>128	0.5	0.5	nd
<i>E. coli</i>	>128	64	8	4	32	64	1	2	nd
<i>A. fumigatus</i>	>128	>128	>128	>128	>128	>128	nd	nd	0.5
<i>R. oryzae</i>	>128	>128	>128	>128	>128	>128	nd	nd	1.0
<i>C. albicans</i>	>128	32	16	64	>128	32	nd	nd	nd
% Hemolysis HD ₁₀ , 25 $\mu\text{g/L}$	8.5	4.8	6.4	7.1	35	46	---	---	---

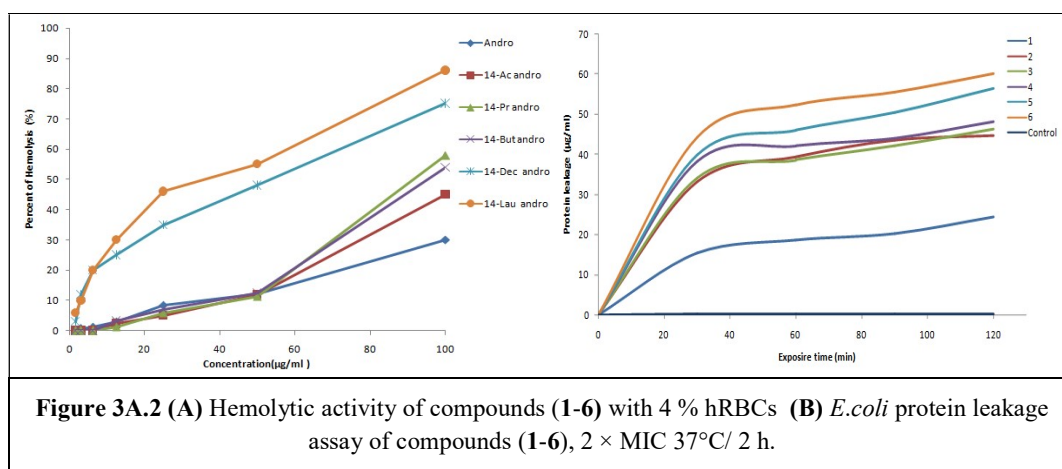
Andrographolide-14-caprylate, **6**. Andrographolide-14-laurinate. ^a The calculated average MIC values are presented. ^b MIC > 128 $\mu\text{g/mL}$ was considered as inactive. ^c nd : not determine. ^d Positive control

Andrographolide-14-acetate (**2**), andrographolide-14-propionate (**3**) and andrographolide-14-butyrate (**4**) displayed antibacterial activity at lower concentration of 4 $\mu\text{g/mL}$. Andrographolide-14-acetate was found to be effective against gram-negative *Pseudomonas fluorescens* and *Staphylococcus aureus* at 4 $\mu\text{g/mL}$ and 16 $\mu\text{g/mL}$ concentration, respectively. While (**3**) was effective against *S. aureus* (4 $\mu\text{g/mL}$), *Escherichia coli* (8 $\mu\text{g/mL}$) and *C. albicans* (16 $\mu\text{g/mL}$), (**4**) was found to be effective against Gram-negative *E. coli* (4 $\mu\text{g/mL}$) and Gram-positive *S. aureus* (8 $\mu\text{g/mL}$) bacterial strains. On the other hand, these derivatives (**2**, **3** & **4**) showed moderate activity against *C. albicans* at MIC values of 32, 16 and 64 $\mu\text{g/mL}$

respectively whereas no antifungal activity against *Aspergillus fumigatus* and *Rhizopus oryzae* was observed (Table 3A.3). Andrographolide itself showed very low anti-bacterial activities against tested cultures, which are in line with the earlier reports,^{18,19} whereas esterification of the hydroxyl group at C-14 of (1), increased its antibacterial potency.

3A.2.7 Hemolytic Assay

The encouraging anti-bacterial activities of Andrographolide monoesters prompted us to investigate their hemolytic activity against human red blood cells (hRBC). The results of hemolytic activities are shown in Figure 3A.2 A indicate that as for these compounds, hemolytic activity is lower at their respective anti-microbial MIC. (1) showed 8.5 % (at 25 $\mu\text{g/mL}$) hemolytic activity whereas (5 and 6) showed hemolytic activity 35 % and 46 % respectively at 25 $\mu\text{g/mL}$ (Figure 3A.2 B). This may be due to the highly hydrophobic nature of alkyl chain, which is responsible for cell lysis as reported elsewhere.^{20,21} However, (2), (3) and (4) (25 $\mu\text{g/mL}$) showed hemolytic activity at 4.8 %, 6.4 % and 7.1 % respectively.



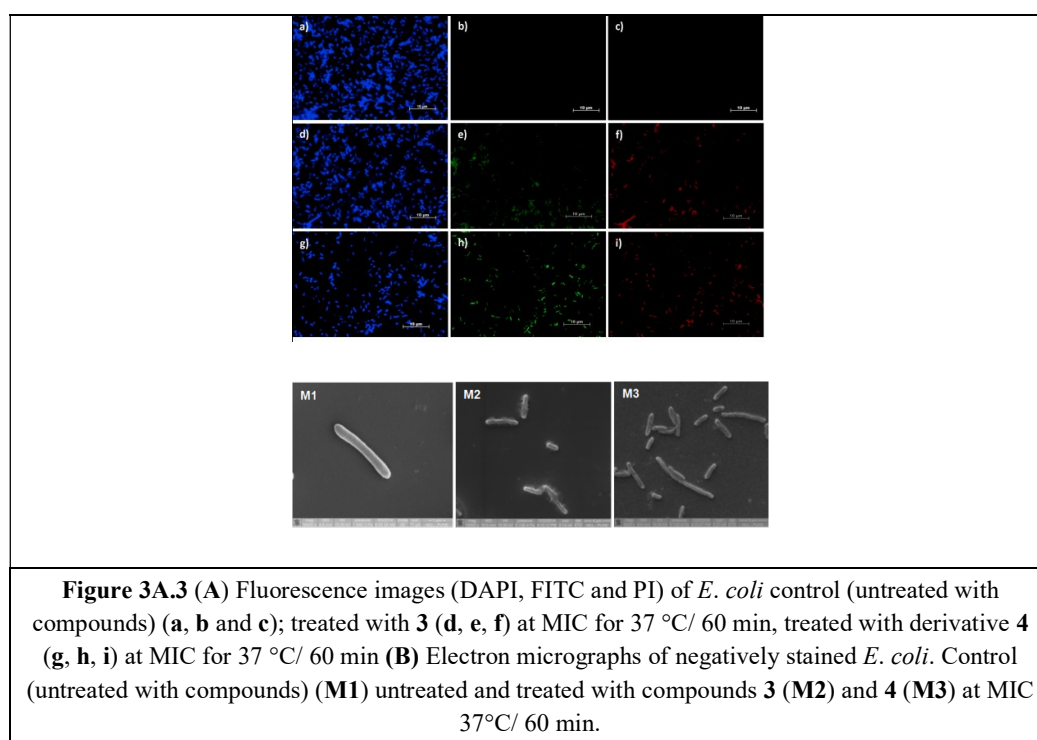
3A.2.8 Membrane Integrity Studied with Bacterial Protein Leakage Assay

The membrane of Gram-negative bacteria protects the cells from the anti-microbial activity of xenobiotics, and hence it is known to play a critical role as a barrier. To understand the effect of andrographolide and its derivatives on the cell membrane, we studied the protein leakage assay using (1) to (6) (Figure 3A. 2B). *E. coli* cells membrane disruption was confirmed by using the protein leakage quantifying. *E. coli*

cells were treated with MIC of compounds and protein released was measured in a time-dependent manner. These results suggested that highest protein release was observed when cells were treated with compounds (2, 4, 5, and 6) indicating that higher levels of cell membrane damage were induced in comparison to that of andrographolide. In control, the minimal release of protein was observed.

3A.2.9 Effect on Membrane Integrity and Cell Viability

The membrane-perturbing and microbial ability of (3) and (4) were investigated by triple fluorescent staining (DAPI, PI and FITC). *E. coli* cells treated with MIC concentrations of (3) and (4) were subsequently stained with fluorescent dyes DAPI, FITC and PI. Fluorescent microscopy images of control (Figure 3A.3 a-c) was not shown to uptake FITC and PI, whereas *E. coli* cells treated with (3) (d-f) and (4) (g-i) showed FITC and PI uptake. The observed fluorescence behaviour of the *E. coli* cells suggests that compounds (3 and 4) might be responsible for an increase in the permeability of the bacterial cell membrane.



3A.2.10 Visualization of Cell Damage by using Scanning Electron Microscopy (eSEM)

The effects on *E. coli* cells after treatment of compound (3) and (4) were visualised using SEM imaging. An exposure *E. coli* cells for 60 min to MIC concentration of compounds (3 and 4). eSEM images of *E. coli* control (Figure 3A. 3B) was seen defined, rigid, and opaque, whereas *E. coli* cells treated with compounds (3 and 4) (Fig. 2B M2, M3) appeared a blurred, deflated, and translucent. The observed SEM images of the *E. coli* cells treated with compounds (3 and 4) suggest that they may be involved in the bacterial cell membrane disruption.

3A.3 Conclusion

C-14 ester analogues of andrographolide were synthesised through Amano lipase AK (*P.fluorescens*) catalysed acylation using various acyl donors. The products were obtained in high yield and with excellent regioselectivity under mild reaction conditions. Andrographolide-14-acetate (2), andrographolide-14-propionate (3), andrographolide-14-butanolate (4), andrographolide-14-caproate (5) and andrographolide-14-laurate (6) showed promising anti-microbial activities than andrographolide. These monoesters showed anti-microbial activity, which significantly changed with a chain length of alkyl substitution. Furthermore, they exhibited low hemolytic activities and investigation revealed that monoesters might act on the bacterial cell membrane. The regioselective enzymatic synthesis approach can be further explored for improving the bioactivity of andrographolide (1).

3A.4 Experimental Section

¹ 3A.4.1 Chemical and biological materials

Andrographolide was isolated from *Andrographis paniculata* as mentioned in chapter 2. Acyl donors including Vinyl acetate, Vinyl propionate, Vinyl butyrate, Vinyl decanoate, Vinyl laurate, Vinyl trifluoroacetate, Vinyl benzoate, lipases including Amano lipase PS *Burkholderia cepacia*, Amano lipase A from *A.niger*, CRL from *Candida cylindracea*, Type II PPL from *Porcine pancreas*, Lipase type VII from *C.rugosa*, Lipase from *Penicillium camemberti*, Lipase from *Rhizopus niveus*, lipase immobilized on Immobead 150 *Candida Antarctica* lipase-A (CAL-A), Novozymes 435 from *Candida Antarctica* lipase-B (CAL-B), Amano lipase AK source *Pseudomonas fluorescens* were purchased from Sigma-Aldrich (USA). Fluorescein Isothiocyanate (FITC), 4', 6-diamidino-2-phenylindole (DAPI), Propidium iodide (PI) were purchased from Sigma-Aldrich (USA). Reaction progress was monitored by thin-layer chromatography (TLC) performed on silica gel G-coated plates (0.25 mm, Merck) with methanol: dichloromethane (1:19) as the mobile phase. Migration of the compounds on TLC was visualised by spraying it with a solution of 3.2 % anisaldehyde, 2.8 % H₂SO₄, 2 % acetic acid in ethanol, followed by heating for 1-2 mins. Andrographolide derivatives were purified over silica gel (230-400 mesh) column chromatography using acetone/ pet ether gradient. Test microorganisms were obtained from the National Collection of Industrial Microorganism (NCIM), CSIR-NCL Pune. Anti-microbial activities were assessed using Gram-positive bacteria *Staphylococcus aureus* (NCIM2100), *M. luteus* (NCIM 2170), Gram-negative bacteria *E. coli* (NCIM 2575), *Pseudomonas fluorescens* (NCIM 2638), fungus *Aspergillus fumigatus* (NCIM 902), *Rhizopus oryzae* (NCIM 1299) and yeast *Candida albicans* (NCIM 3471).

3A.4.2 General Procedure for Lipase-Catalysed Acylation of Andrographolide

In general experimental conditions, 0.1 mmol andrographolide, 1.0 mmol vinyl esters, and 5 mg enzyme were dissolved in 3 mL of acetone/ethyl acetate/vinyl acetate/methanol/ tetrahydrofuran and incubated in a shaking incubator, as reported earlier.^{22,19} After a specific time of interval, aliquots were drawn from the reaction mixture, filtered through 0.45 µm syringe filter and diluted with methanol for HPLC

analysis. The initial water activity (a_w) of the reaction (the lipase with the substrates) was controlled in a different saturated salt solution at 25 °C by gaseous equilibrium in separate closed containers as reported earlier. Reaction with the predetermined condition without enzyme served as a negative control, which did not detect the acylated product. All experiments were performed in triplicate, and the average results with standard deviation are reported. For characterization of product formed in a general experiment, 0.1 mmol Andrographolide, 1 mmol vinyl esters were dissolved in acetone, and 90 mg of Amano lipase AK from *P. fluorescens* was incubated at 55 °C in a shaking incubator set at 100rpm for 5 h. The reaction mixture was filtered to get rid of lipase and filtrate was concentrated under vacuum. The obtained residue was further purified by silica gel column chromatography with acetone-petroleum ether mixture as solvent system.

3A.4.3 Anti-bacterial Activity

The antibacterial activity of andrographolide and its derivatives was determined in a 96-well microtiter plate using broth microdilution method as reported earlier.²³ The activity was calculated in a total volume of 100 μ L containing the test compounds (final concentration range between 0.25-128 μ g/ mL) and the bacterial suspension (final concentration of 2×10^5 cfu/mL). An assay with Gentamicin sulphate and Benzamide sodium served as positive controls. The experiment was performed in triplicates independently along with growth and sterility controls in each set. Then the microtiter plate was incubated at 37 °C for 20 h. The growth inhibition was visualized, and the minimum inhibitory concentration (MIC) was determined as the lowest concentration of compound required for complete growth inhibition.

3A.4.4 Antifungal Activity

Andrographolide and its derivatives were tested for their antifungal activity against fungal/yeast strains obtained from NCIM. The activity was determined by the broth microdilution method.²⁴ An assay with Amphotericin B served as a positive control. The assay mixture containing the fungi and test compounds was incubated at 30 °C for 24 h for *A. niger* and 49–72 h for *Candida Albicans* and *R. oryzae*. The growth inhibition was visualised, and the MIC was determined as the concentration of compound required for complete growth inhibition.

3A.4.5 Hemolytic Assay

The hemolytic assay was performed according to the protocol reported earlier.²⁰ Human RBCs were collected freshly and stored with ethylene diamine tetraacetic acid (EDTA). Before performing assay the hRBCs were washed four times with Tris-buffered saline (150 mM NaCl, 10 mM Tris pH 7.2,) and diluted to a final concentration of 4 % v/v. The assay was performed at a final volume of 100 μ L as follows: an aliquot of 50 μ L of hRBCs suspension was added to 50 μ L of 2-fold serially diluted (100 μ g/mL) andrographolide and its derivatives in the minimum amount of dimethyl sulfoxide (DMSO) diluted with Tris buffer. The plate was incubated at 37 °C for 1.5 h and then centrifuged for 15 min. at 3000 rpm. The supernatant (50 μ L) from each well was transferred to a new 96-well plate containing 50 μ L of water, and the release of haemoglobin was monitored by measuring the absorbance at 540 nm.

All the experiments were performed in triplicate with hRBC suspensions in tris buffer; tris buffer served as negative control and in 1 % Triton-X comprised as a positive control, respectively. The percentage of hemolysis was defined as $(A - A_N) / (A_P - A_N) \times 100$, where A is the absorbance of the test. Well, A_N is the absorbance of the negative control, and A_P is the absorbance of the positive control.

3A.4.6 Fluorescent Staining for Assessing Cell Viability and Membrane Integrity

A triple staining procedure was followed to assess the viability as well as membrane integrity of the cells as reported earlier.³ *E. coli* cells were grown in Luria Bertani broth (LB) till an OD₆₀₀ of 0.6 units was attained. The cells were washed twice with 10 mM sodium phosphate buffer (pH 7.4) to remove media and re-suspend in the same buffer. After exposure to inhibitory concentrations of andrographolide and its derivatives at 37 °C for 60 mins, the bacterial cells were immobilised on poly (L-lysine)-coated glass slides for 50 mins. at 30 °C, followed by addition of 100 μ L of DAPI (2 μ g/mL in buffer). After 30 mins incubation at 30 °C, the DAPI solution was washed away and rinsed again with sodium phosphate buffer, followed by addition of 100 μ L of FITC (6 μ g/ mL in the buffer). It was then incubated at 30 °C for 30 mins followed by rinsing and addition of 100 μ L Propidium Iodide (PI) (2 μ g/mL in buffer), further continuing incubation at 30 °C for 30 mins. The slide was then washed as described above. The cells without the compounds served as controls. Fluorescent

images were recorded using a Zeiss Axio-observer Z1 microscope equipped with an oil-immersion objective (64x) and an AxioCam camera. Image acquisition and processing were performed using Axiovision software.

3A.4.7 Bacterial Protein Leakage Assay

To detect leakage of intercellular proteins over time, the bacterial protein leakage assay was performed as reported earlier.²⁵ The cells were washed with phosphate buffer to remove any extracellular proteins present before incubating with test compounds. The cells were then incubated with test compounds at concentrations double the MICs. at 37 °C for 2 h. At periodic time interval of 30 mins, the cell suspension was centrifuged at 7000 g and supernatant collected was used to determine the protein content. Bradford's assay determined the protein concentration in the supernatant.²⁶ All the experiments were performed independently in triplicates. The amount of protein in the supernatant was determined by extrapolating values in the Bovine Serum Albumin standard curve.

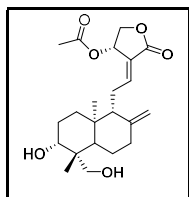
3A.4.8 Scanning Electron Microscopy

To observe the morphological changes in bacterial cells, SEM images were recorded for *E. coli* treated with the test compounds. The samples for recording SEM images were prepared as reported earlier.²⁷ The cells were grown in LB media to an OD₆₀₀ of 0.6 units. and then washed with 10 mM sodium phosphate buffer (pH 7.4) twice, to remove media. The cells were re-suspended in the same buffer and treated with MICs of andrographolide and its derivatives at 37 °C for 60 mins; The cells were washed twice with buffer and then pelleted down by centrifugation at 3000 rpm for 20 mins. The cells were fixed with 1 % glutaraldehyde in PBS for 30 mins and re-suspended again. A drop containing the bacteria was deposited onto a silicon wafer and dried overnight. It was then coated with gold and observed in a scanning electron microscope.

3A.4.9 Characterization Data of Monoester Derivatives of Andrographolide

Andrographolide-14-acetate White solid; m.p. 168.4-170.2°C; IR (CHCl₃, cm⁻¹) ν_{\max} = 1673, 1738, 1760, 3366; HRMS (ESI) m/z : [M+Na]⁺ Calcd for C₂₂H₃₂O₆ Na, 415.2091, found, 415.2084. ¹H NMR (400 MHz, CDCl₃, ppm) : δ 6.95-6.98 (td, J =

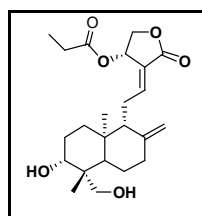
6.84, 1.72 Hz, 1H), 5.87-5.89 (d, $J = 5.81$, 1H), 4.83 (s, 1H), 4.50-4.53 (m, 1H), 4.46 (s, 1H), 4.19-4.22 (dd, $J = 1.52$, 10.99 Hz, 1H), 4.12-4.14 (d, $J = 11$, 1H), 3.61-3.63 (m, 1H), 3.40-3.44 (dd, $J = 2.65$, 10.99 Hz, 1H), 3.34-3.37 (m, 1H), 3.25-3.28 (m, 1H), 2.80 (s, 1H), 2.32-2.41 (m, 4H), 2.14-2.13 (m, 1H), 2.08 (s, 3H), 1.97-2.01 (m,



2H), 1.76-1.80 (m, 2H), 1.62-1.71 (m, 2H), 1.20-1.21 (m, 3H), 0.63 (s, 3H). ^{13}C NMR (100 MHz, CDCl_3 , ppm): δ 170.53, 169.09, 150.53, 146.67, 123.78, 108.70, 80.28, 71.58, 67.72, 64.06, 55.77, 55.11, 42.77, 38.76, 37.65, 36.93, 28.06, 25.25, 23.63, 22.68,

20.67, 15.07.

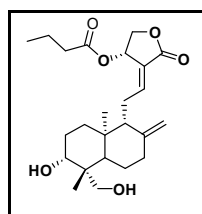
Andrographolide-14-propionate White Solid; m.p. 153.2-155.2°C; IR (CHCl_3 , cm^{-1})



$\nu_{\text{max}} = 1673, 1720, 1735, 3490$; HRMS (ESI) m/z : $[\text{M}+1]^+$ Calcd for $\text{C}_{23}\text{H}_{35}\text{O}_6$, 407.2424, found, 407.2428. ^1H NMR (400 MHz, CDCl_3 , ppm): δ 6.95-6.96 (td, $J = 6.84, 1.72$ Hz, 1H), 5.89-5.91 (d, $J = 5.81$, 1H), 4.82 (s, 1H), 4.53-4.56 (dd, $J = 6.11, 11.25$ Hz, 1H), 4.45 (s, 1H), 4.17-4.19 (dd, $J = 1.71, 11.0$ Hz, 1H), 4.11-4.14 (d, $J = 11.0$

Hz, 1H), 3.40-3.43 (m, 1H), 3.25-3.27 (m, 1H), 2.30-2.40 (m, 6H), 1.91-1.96 (m, 1H), 1.77-1.81 (m, 4H), 1.66-1.68 (m, 1H), 1.19-1.25 (m, 6H), 1.07-1.15 (m, 4H), 0.62 (s, 3H). ^{13}C NMR (100 MHz, CDCl_3 , ppm): δ 173.92, 169.15, 150.51, 146.65, 123.71, 108.64, 80.00, 71.59, 67.52, 63.93, 55.61, 55.95, 42.49, 38.62, 37.52, 36.80, 27.83, 27.28, 25.14, 23.60, 22.63, 14.98, 8.89.

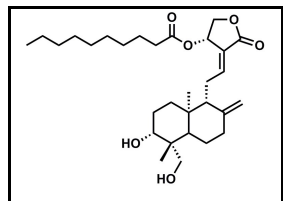
Andrographolide-14-butanoate White needles; m.p. 128.9-130.2°C; IR (CHCl_3 , cm^{-1})



$\nu_{\text{max}} = 1672, 1709, 1756, 3454$; HRMS (ESI) m/z : $[\text{M}+\text{Na}]^+$ Calcd for $\text{C}_{24}\text{H}_{36}\text{O}_6\text{Na}$, 443.2396; found, 443.2404. ^1H NMR (400 MHz, CDCl_3 , ppm): δ 6.95-6.99 (td, $J = 6.84, 1.72$ Hz, 1H), 5.89-5.91 (d, $J = 5.81$, 1H), 4.84 (s, 1H), 4.52-4.56 (dd, $J = 6.11, 11.25$ Hz, 1H), 4.46 (s, 1H), 4.16-4.21 (dd, $J = 1.71, 11.0$ Hz, 1H), 4.13-4.17 (d, $J =$

11.0 Hz, 1H), 3.41-3.45 (m, 1H), 3.27-3.29 (d, 1H), 2.38-2.45 (m, 2H), 2.30-2.34 (m, 3H), 1.94-1.98 (m, 1H), 1.78-1.82 (m, 4H), 1.62-1.70 (m, 4H), 1.17-1.28 (m, 7H), 0.92-0.96 (m, 3H), 0.63 (s, 3H). ^{13}C NMR (100 MHz, CDCl_3 , ppm): δ 173.21, 169.13, 150.47, 146.65, 123.83, 108.80, 80.24, 71.71, 67.51, 64.04, 55.72, 55.08, 42.73, 38.72, 37.62, 36.93, 35.86, 28.03, 25.23, 23.60, 22.68, 18.33, 15.04, 13.59.

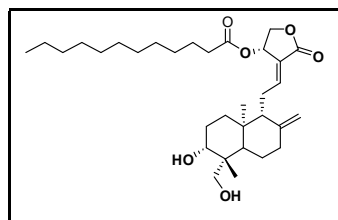
Andrographolide-14-caproate Colourless semi-solid; m.p. 105.9-108.2°C; IR (CHCl₃, cm⁻¹) ν_{\max} = 1673, 1740, 1752, 3389; HRMS (ESI) m/z : [M+1]⁺ Calcd for C₃₀H₄₉O₆, 505.3520; found, 505.3524. ¹H NMR (400 MHz, CDCl₃, ppm): δ 6.91-6.95



(td, J = 6.84, 1.72 Hz, 1H), 5.85-5.88 (d, J = 5.81, 1H), 4.82 (s, 1H), 4.44-4.55 (m, 2H), 4.09-4.18 (m, 2H), 3.38-3.46 (m, 1H), 3.24-3.46 (m, 1H), 2.26-2.39 (m, 4H), 1.72-1.81 (m, 4H), 1.51-1.65 (m, 3H), 1.16-1.28 (m, 22H), 0.75-0.87 (m, 4H), 0.60 (s, 3H).

¹³C NMR (100 MHz, CDCl₃, ppm) : δ 173.44, 169.15, 150.48, 146.61, 123.86, 108.86, 80.33, 71.73, 67.52, 64.06, 55.73, 55.08, 42.80, 38.74, 37.63, 36.92, 34.08, 31.86, 29.37, 29.29, 29.17, 29.08, 28.19, 28.08, 25.25, 24.89, 23.61, 22.65, 15.08, 14.10.

Andrographolide-14-laurate Colourless solid; m.p. 109.2-111.4 °C; IR (CHCl₃, cm⁻¹) ν_{\max} = 1671, 1726, 1743, 3346; HRMS (ESI) m/z : [M+Na]⁺ Calcd for C₃₂H₅₂O₆ Na,



555.3647; found, 555.3656. ¹H NMR (400 MHz, CDCl₃, ppm): δ 6.95-7.02 (td, J = 6.84, 1.72 Hz, 1H), 5.89-5.92 (d, J = 5.81, 1H), 4.86(s, 1H), 4.48-4.59 (m, 2H), 4.13-4.23 (m, 2H), 3.28-3.51 (m, 3H), 2.30-2.44 (m, 5H), 1.76-1.86 (m, 4H), 1.53-1.69 (m, 3H), 1.12-1.36 (m, 23

H), 0.80-0.94 (m, 4H), 0.65 (s, 3H). ¹³C NMR (100 MHz, CDCl₃, ppm) : 173.47, 169.18, 150.51, 146.64, 123.89, 108.89, 80.36, 71.76, 67.55, 64.09, 55.76, 55.11, 42.83, 38.77, 37.66, 36.95, 34.10, 31.89, 29.96, 29.58, 29.40, 29.32, 29.19, 29.11, 28.22, 28.11, 25.27, 24.92, 23.63, 22.68, 15.11, 14.13.

3A.5 Spectra copies

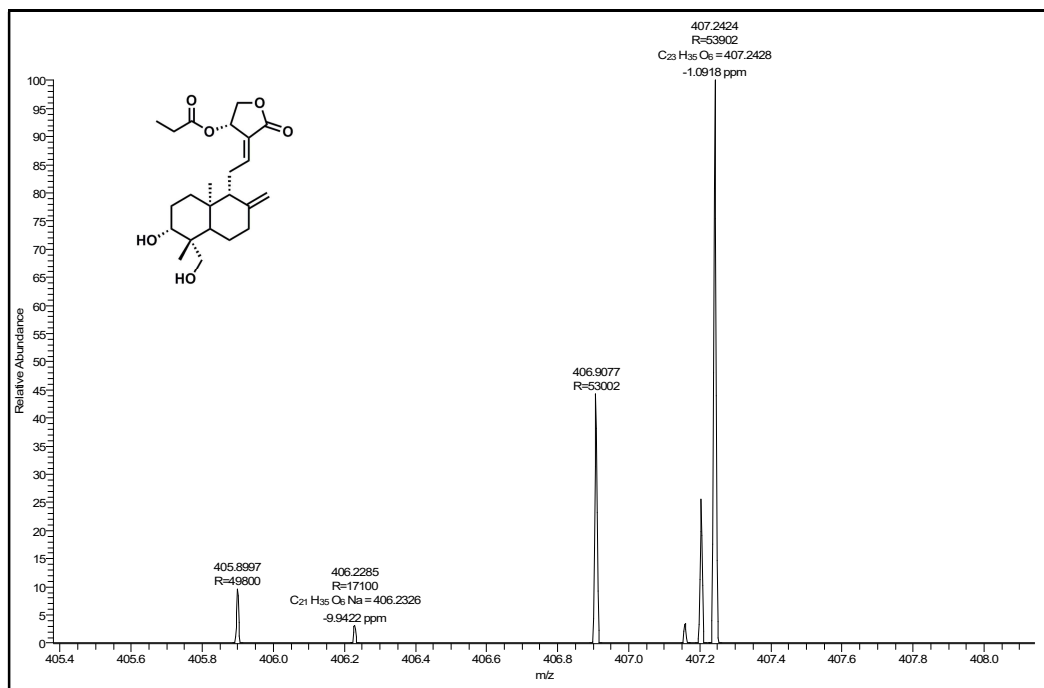
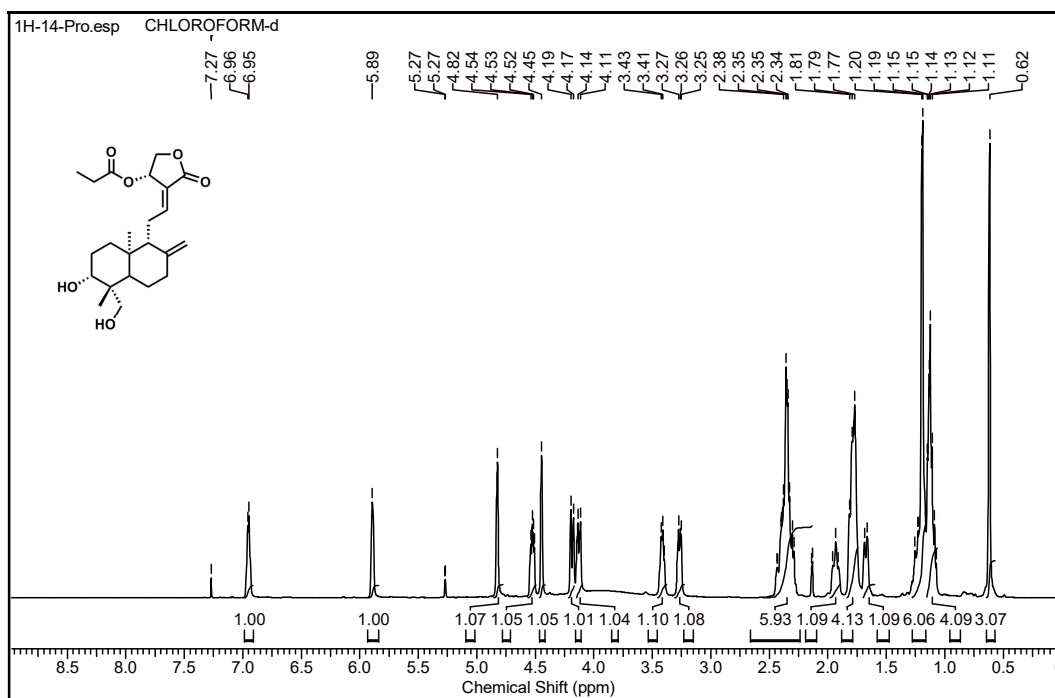


Figure 3A.4a. High-Resolution Mass spectra of andrographolide-14-propionate

Figure 3A.4b. ^1H -NMR spectrum of andrographolide-14-propionate

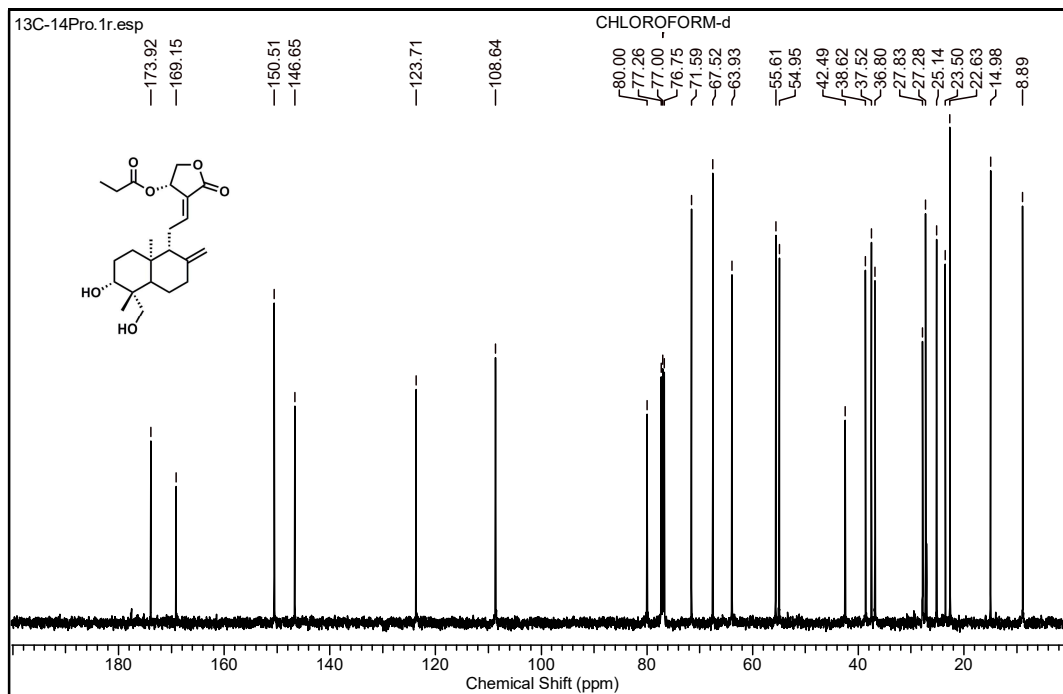


Figure 3A.4c. ^{13}C - spectra of andrographolide-14-propionate

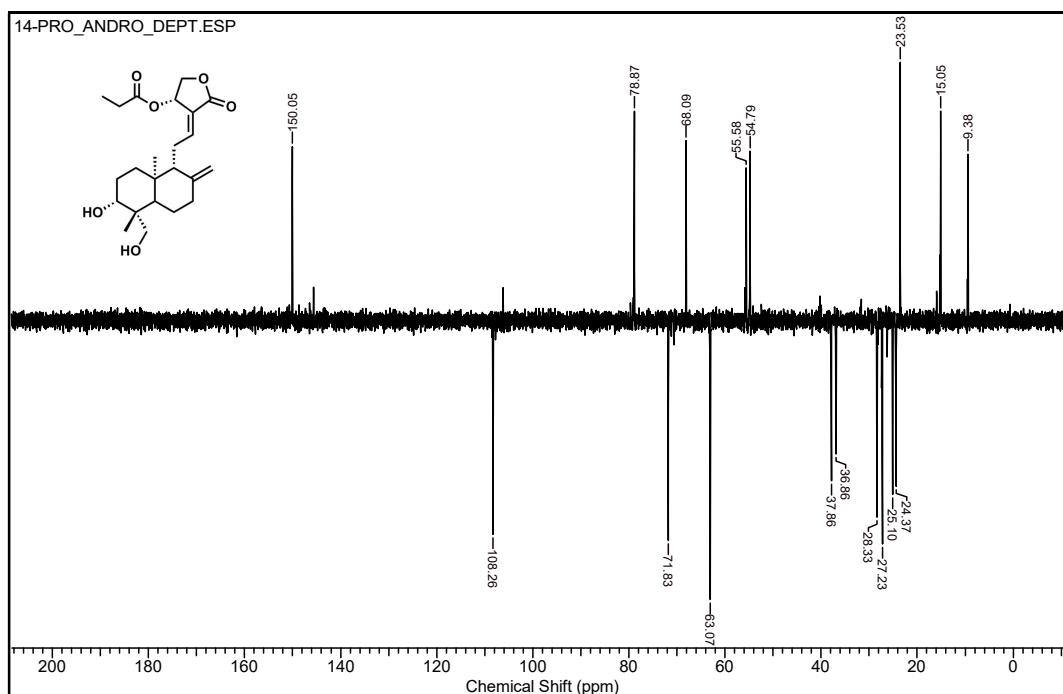


Figure 3A.4d. Distortionless enhancement by polarization transfer (DEPT) NMR spectrum of andrographolide-14-propionate

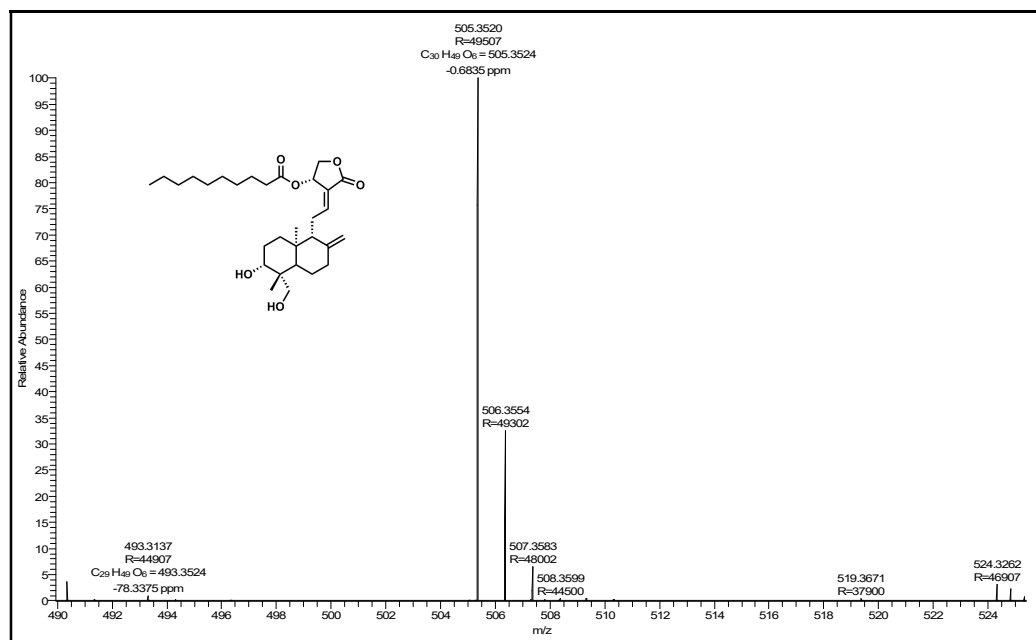


Figure 3A.5a. High-Resolution Mass spectra of andrographolide-14- caproate

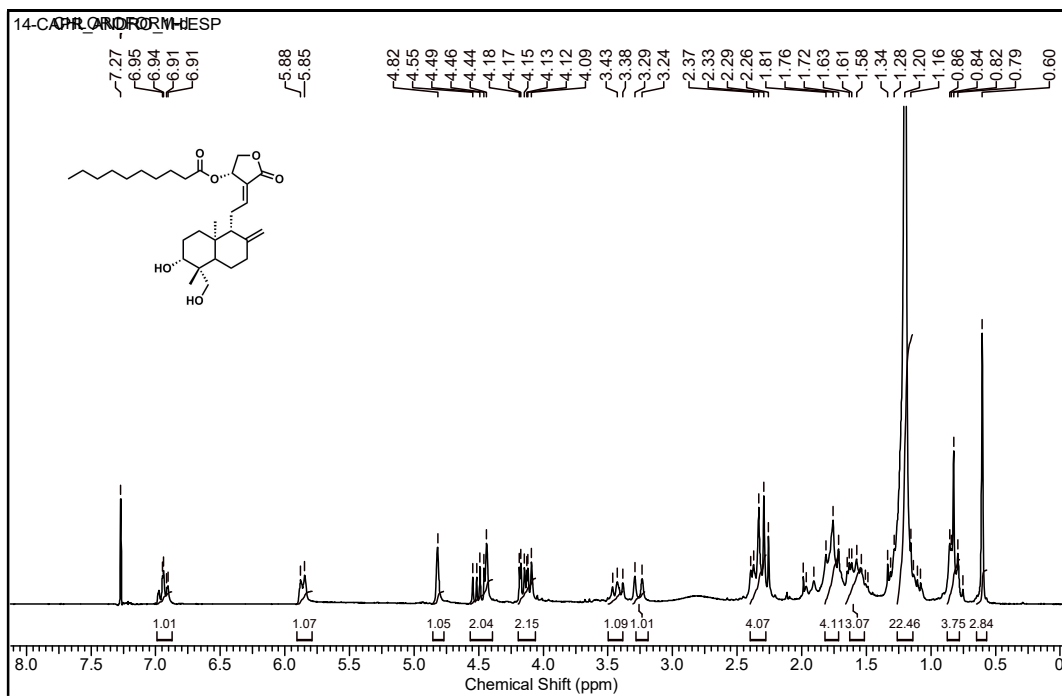


Figure 3A.5b. ^1H - NMR spectrum of andrographolide-14-caproate

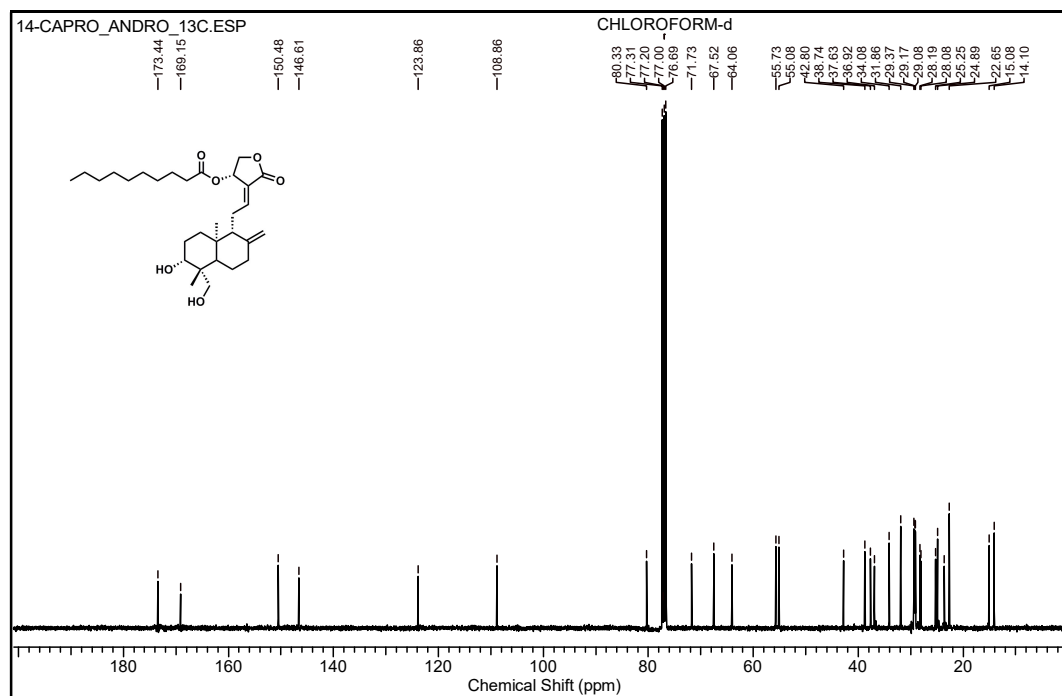


Figure 3A.5c. ^{13}C - spectra of andrographolide-14-caproate

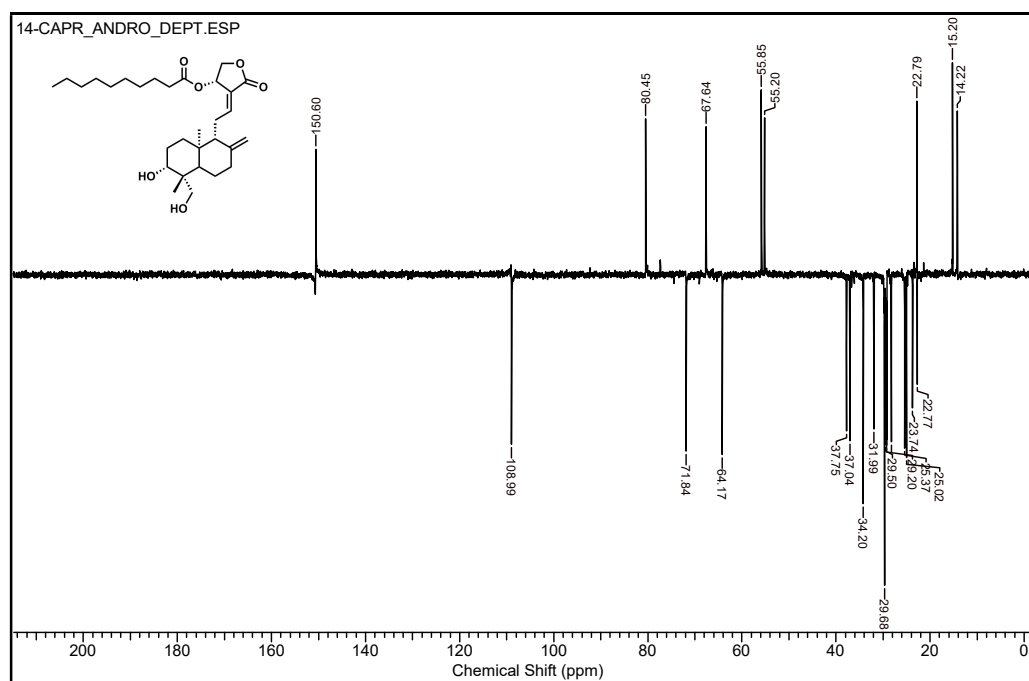


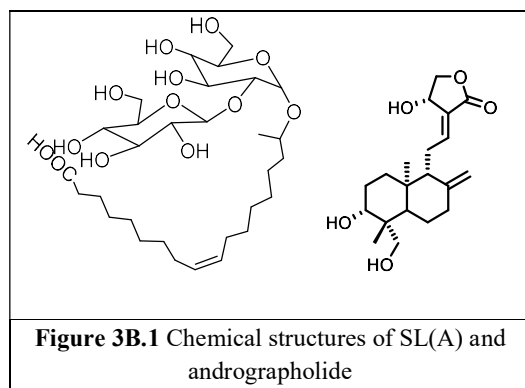
Figure 3A.5d. Distortionless enhancement by polarization transfer (DEPT) NMR spectrum of andrographolide-14-caproate

Chapter 3: Section B

Anticancerous Nanoparticles of Andrographolide by Sophorolipid Formulation

3B.1 Introduction

Andrographolide (**1**) is a diterpene isolated from herb *Andrographis paniculata*.²⁸ **1** is known to exhibit a broad range of pharmacological activities such as antioxidant, immunomodulatory, anti-inflammatory, anti-malarial, anti-cancer, anti-proliferative activity etc.^{29,30,31} Andrographolide and its derivatives are cytotoxic against sever cancer cell lines such as Leukaemia (HL-60 and NB4), breast (MCF-7 / ADR), central nervous system (U251), colon (SW620) and lung (H522) etc.^{32,28} However, bioactivities of **1** was not explored



efficiently due to inadequate water solubility and negligible bioavailability.³³ The water solubility of **1** is $3.29 \pm 0.73 \mu\text{g}/\text{mL}$ at 25°C , while the lipophilicity measured in terms of the experimental log P value is 2.632 ± 0.135 .³⁴ Till date, all available reports about the

andrographolide aqueous solubility improvement are not efficient enough to broaden its applications. Zhao *et al.* used cyclodextrin to enhanced **1** solubility, but slow rate of complexation, cyclodextrin cost and required specific P^{H} make it practically challenge.³⁵ In another process, a spray-drying technique using polyvinylpyrrolidone (PVP K-30) was applied for solid dispersions of **1**, but expensive and toxic nature of reagents, non-biodegradable, and requirement of multistep chemical synthesis limits its applications.³⁶ Henceforth, there is an urgent need of a greener, economical and efficient material to improve the aqueous solubility of andrographolide.³³ Aqueous solubility of hydrophobic drugs due to their amphiphilic behaviour, which tends to reduce drugs surface tension.³⁷ Surfactants produced by yeast, bacteria, and fungi are recognized as biosurfactants.^{38,39} They are emerging as an excellent choice for drug stabilization, as well as drug carrier materials, compare to chemical surfactants.⁴⁰ Sophorolipids (SL) is biosurfactants which are surface active glycolipid synthesized by non-pathogenic yeast *Candida bombicola*. Clinical studies have confirmed that sophorolipids are not harmful to the skin and do not cause allergic reactions. Also, their oral safety level is higher than or equal to

0.05 g/kg body-weight.⁴¹ Sophorolipids are two types of acidic SL(A) and lactonic SL(L). In acidic sophorolipid SL(A), sophorose unit is attached to an oleic acid moiety through an ether bond on the C17 carbon. This particular characteristic leaves the -COOH group available and responsive for any change causes in solution p^H ; causes a series of self-assembled structures.^{42,43} Acidic sophorolipid was used to improve aqueous solubility curcumin and enhanced cytotoxicity by formulation.⁴⁴

In order to improve the aqueous solubility and bioavailability of andrographolide, we have co-sonicated it with SL(A), which also help for stabilization the **1** nanostructures. Advanced microscopic techniques and spectroscopic characterization confirmed structure analysis of SL(A)-**1**. Nanoparticles of **1** with SL (A) enhanced anti-cancer efficacy against breast cancer cell lines, due to the size reduction and enhanced bioavailability. The effective MIC concentration of **1** in SL (A)+**1** is lower down (3 $\mu\text{g/mL}$).

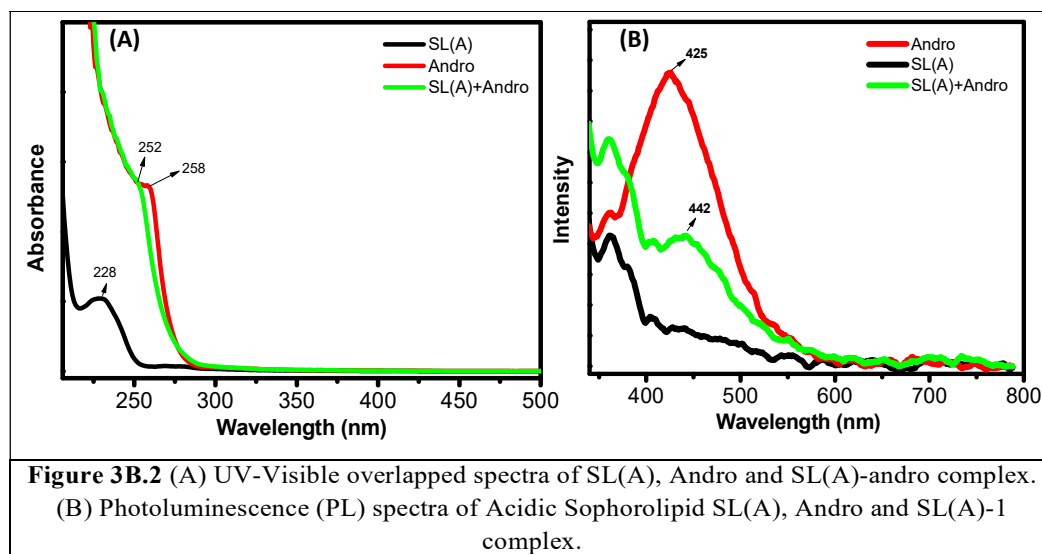
3B. 2 Results and discussion

3B.2.1 Complexation of Andrographolide with Sophorolipid

The low aqueous solubility of andrographolide was the major obstacle in the SL(A)+**1** complex formation. Therefore, we have used ethanol for dissolving **1**, further for uniform particles size and stability optimisation, we have screened various combination with SL(A) concentration. Out of various combinations applied, the solution prepared in 7:3 ratio (SL(A): **1**) was found to be a most suitable combination. The reaction mixture of water and ethanol was concentrated on rotaevaporator and further lyophilized to remove traces of the remaining water. White cotton, like fluffy material, was obtained after lyophilization. NMR of Andrographolide after two months was taken by extracting **1** from SL(A)+**1**, NMR showed that **1** is not degraded (Spectral copies 3B.5).

3B.2.2 Ultraviolet-Visible (UV) Spectrum and Photoluminescence Studies

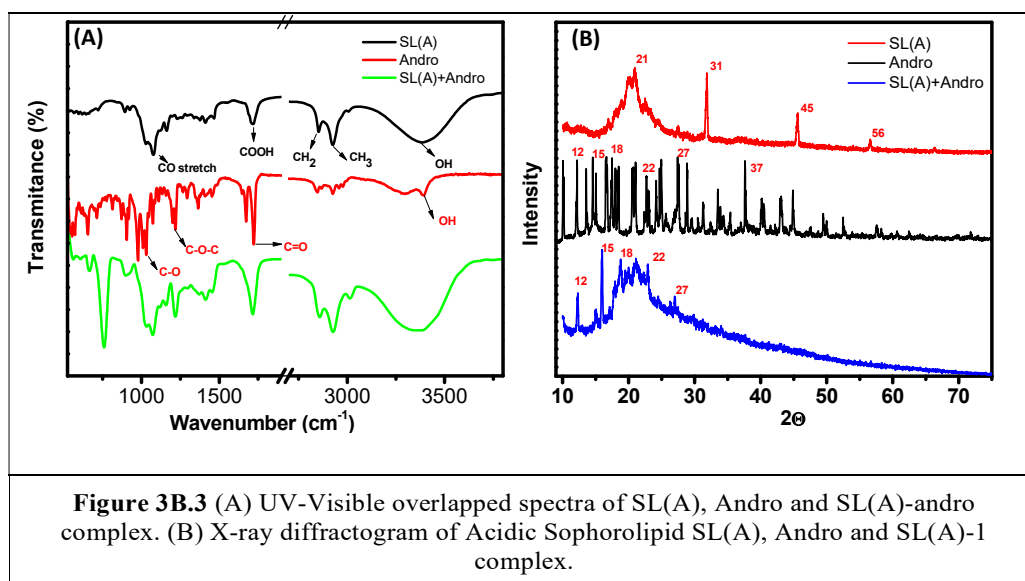
Optical properties of SL(A)+**1** were investigated by UV and PL analysis. All three samples (**1**, SL(A) and SL(A)+**1**) were dissolved in distilled water at identical concentration. Andrographolide gets crystallized in distilled water; hence it was first dissolved in 50 μ L ethanol and diluted, SL(A) solution looks transparent; whereas SL(A)+**1** complex aqueous solution appears slightly turbid. The UV-visible spectrum of SL(A), **1** and SL(A)+**1** complex shows absorption at $\lambda_{\text{max}} = 228$ nm, 258 nm, and 252 nm, respectively. The UV absorption of SL(A)+**1** exhibit a 6 nm blue shift due to the encapsulation by SL(A). Presence of conjugation in **1** skeleton gives it photoluminescence (PL) therefore, we have studied the Photoluminescence of all the samples with various exciting wavelength. **1** gives PL at $\lambda_{\text{max}} = 425$ nm, SL (A) showed no PL (because of no conjugation in structure) while SL(A)+ **1** complex rise in PL but less in comparison to that exhibited by andrographolide sample at $\lambda_{\text{max}} = 442$ nm. This reduction in PL intensity and redshifts in λ_{max} is due to the SL(A)+**1** combination, which confirmed the encapsulation. Encapsulation of **1** by SL(A) lower the incident light intensity and result in weak PL and redshift (17 nm).



3B.2.3 Fourier Transform Infrared Spectroscopy (FTIR) Analysis

FTIR spectra of SL(A), **1** and SL(A)+**1** was recorded (Figure 3B.3). SL(A) FTIR-spectrum showed a broad peak at 3350 cm^{-1} suggested the hydroxyl (O-H) stretching frequency of the glucose moiety. The asymmetrical and symmetrical stretch modes of C-H due to methylene ($-\text{CH}_2$) groups are represented by frequencies at 2928 and 2854 cm^{-1} respectively. In SL-(A) FTIR-spectrum due to C-O and C-O stretching two strong absorption bands were observed; absorption band at 1744 cm^{-1} is due to the C-O stretching of a carboxyl group from the oleic acid moiety.

Furthermore, sugar C-O- the stretch of C-O-H groups is found at 1048 cm^{-1} and the band at 1452 cm^{-1} resembles the C-O-H in-plane bending of carboxylic acid ($-\text{COOH}$) group in the structure of the product. **1** shows stretching vibrations at 3394 cm^{-1} correspondings to three OH groups. The vibration band of carboxyl functionality of lactone showed at 1719 cm^{-1} , a strong band at 1675 cm^{-1} in the spectrum indicated the symmetric stretching vibration of alkenes ($\text{C}=\text{C}$) functionality. A stretching band at 1210 cm^{-1} corresponds to the C-O-C stretching and a strong band at 1039 cm^{-1} suggested the C-O stretch of C-O-H functionality. FTIR spectrum of SL(A)+**1** shows most of the peaks related to SL(A) and **1**; some peaks are seen to have been suppressed due to encapsulation.



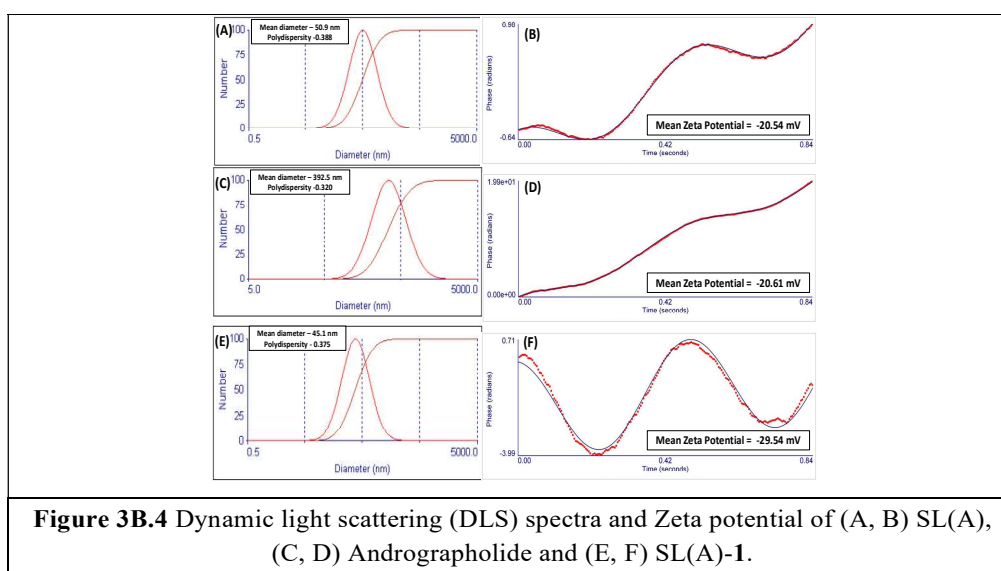
3B.2.4 X-ray Diffraction (XRD) Analysis

XRD patterns of all samples were performed over a broad angle ($2\theta = 10\text{--}80$ degrees) to analyze whether a crystalline nature of **1** in SL(A)+**1** remains or not after encapsulation. SL diffractogram (Figure 3B.4) resulted in peaks at 21, 31.45 and 56° indicating its amorphous nature, while **1** diffractogram pattern exhibited crystalline behaviour due to the presence of characteristic peaks at 12, 15, 18, 22, 27 and 37° . In SL(A)+**1**, most characteristic peaks of **1** disappeared and only a significant peak at 12, 14 and 27° were observed. A broadness is also observed in the range of $17\text{--}22^\circ$, which expressed its amorphous nature due to the SL(A) encapsulation. While it appeared to only a few peaks related to the microstructure of **1** inside SL(A) cage structures. The surface of the complex is mainly dominated by SL(A) molecules and is a correlation with the SEM images. **1** nanoparticles are dispersed on SL (A) nanofibres; hence the diffraction peak signals are decreases.

3B.2.5 Dynamic Light Scattering (DLS) and Zeta Potential Measurement

To understand the size and stability of SL(A)+**1** complex in solution, we have performed DLS and zeta potential measurement at constant shutter opening diameter. DLS measurement of SL(A), **1** and SL(A)+**1** (5 mg dissolved in 5 mL. distilled water) exhibited the hydrodynamic radii of 50.9, 392.5 and 45.1

nm respectively (Figure 3B.5 A,B; C,D; E, F). The result of DLS measurement also confirmed with the results obtained by SEM images analysis. These data clearly illustrated that the size of SL(A)+1 is \sim 30-40 nm, representing that there is a reduced agglomeration of **1** in aqueous solution. There is a slight decrease in the size of SL(A)+1 as compared to only SL(A) because of the encapsulation of **1** nanoparticle. Solution stability of SL(A)+1 was analyzed by zeta potential measurement. The zeta potential value of SL(A), **1** and SL(A)+1 were 20.54 mV, 20.61 mV, and 29.54 mV respectively (Figure 3B.4). Increase in zeta potential values of SL(A)+1 complex was observed compared to SL(A), it clearly suggests that the solution stability of **1** was increased.



3B.2.1 Microscopic Studies of SL(A)+1 Complex

Morphology of SL(A)+1 was analysed by optical light microscopy and scanning electron microscopy (Figure 5A,D; B,E C;F). SL(A) exhibit as ribbon structure (around 1-5 μ m), **1** appears as large crystal (around 10-20 μ m). **1** nanoparticle are surrounded by SL(A) sheet-like morphology. Light microscopic analysis of SL(A)+1 clearly indicated that there is a drastic reduction in the size of **1** compared to bare **1** crystals. Due to the limited resolution of the light microscopy, a further detailed examination of all the samples was evaluated by scanning electron microscopy (SEM). The particle size of **1** decrease from micron to nano and stabilized through SL(A)

encapsulation in an aqueous environment. The molecular arrangement of these SL(A)+**1** could be explained through the hydrophobic moiety of SL(A) surrounded by the hydrophobic **1** nanoparticles and increases its aqueous solubility and stability by a hydrophilic moiety of SL(A) towards solvent molecules. SEM analysis clearly indicated that SL(A) assists **1** from crystallization rods morphology to form spheres of size ranging from 20 μm to 40 nm.

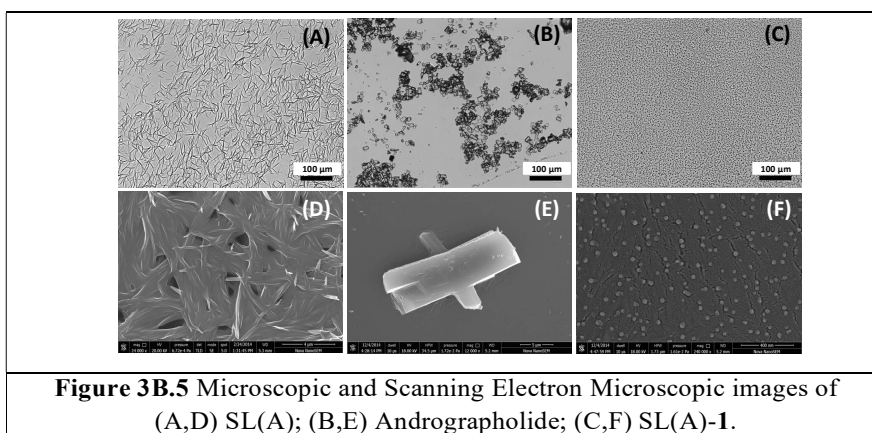
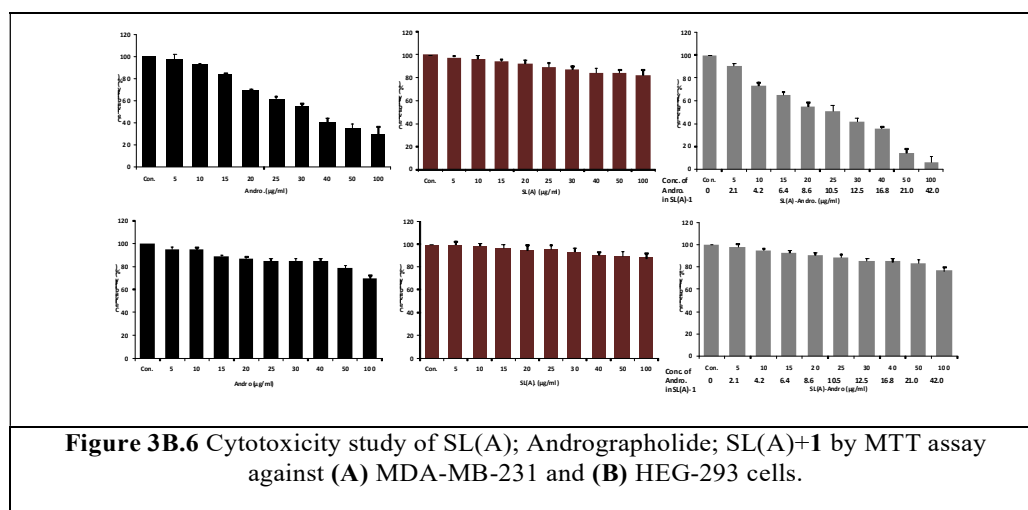


Figure 3B.5 Microscopic and Scanning Electron Microscopic images of (A,D) SL(A); (B,E) Andrographolide; (C,F) SL(A)-1.

3B.2.2 Cytotoxicity Study of SL(A)+**1** against MDA-MB-231

To study the effect of complexation of **1** and SL(A) on cytotoxicity was assessed by MTT-assay against breast cancer cell line (MDA-MB-231). Cytotoxicity of SL(A)-**1** was compared with andrographolide (**1**) used as positive control and SL(A). After SL(A) treatment against MDA-MB-231 and HEG 293 exhibit 80-100 % and 87-100 % cell viability respectively up to 100 $\mu\text{g}/\text{ml}$ showing the, it is almost non-toxic to the cells. It is observed that the SL(A)-**1** is more active compared to the sole Andrographolide (**1**). All the data are presented as mean \pm SD of independent experiments at $p < 0.0001$, indicating statistically significant differences compared to the control untreated group. In SL(A)-**1**, Andrographolide (**1**) exhibited anticancer activity (MDA-MB-231) at low dose starting from 8.6 $\mu\text{g}/\text{ml}$ compared to the 30 $\mu\text{g}/\text{ml}$ concentration of **1** (Figure 3B.6A). At IC_{50} of andrographolide in SL(A)-**1** at 10.5 $\mu\text{g}/\text{ml}$ compared to sole Andrographolide IC_{50} is $> 30 \mu\text{g}/\text{mL}$. This enhanced in cytotoxicity clearly suggested that bioavailability of **1** increased due

to SL(A) complexation. We have tested SL(A), SL(A)-1 and andrographolide against HEG 293 non-cancerous cell line. At 100 $\mu\text{g/ml}$ Andrographolide inhibit 30 % of cell viability; whereas SL(A) and SL(A)-1 inhibit 12 % and 25 % cell viability, it suggested that it's nearly non-toxic to the non-cancerous cell (Figure 3B.6B). Above results suggested that enhanced in cytotoxicity of Andrographolide in SL(A)-1 is due to an increase in aqueous solubility, the formation of nanoparticles and increase in bioavailability.



3B.3 Conclusion

Co-sonication of **1** with SL(A) enhanced its aqueous solubility and reduced particle size extremely. Herein we have used SL(A), renewable biosurfactants having a greener synthesis. DLS, Zeta-potential, microscopic, and SEM images suggested that the decrease in the size of **1** from micro to the nanoscale is due to encapsulation with SL(A). Enhanced in the anticancer activity of **1** is due to its increased bioavailability by complexation with SL(A). It is possible to use this approach for other hydrophobic bioactive natural products by nanoscale self-assembly formation. This study thus suggests green formulation technique.

3B.4 Experimental section

3B.4.1 Synthesis of Sophorolipid-andrographolide Complex

Acidic sophorolipid (3.5 g) was taken in a round bottom flask, which was dissolved in distilled water. The solution is then kept in a sonicator (20 Hz/min) at 60 °C, for 20 min. The ethanolic solution of andrographolide (500 mg) was added drop-wise into the acidic sophorolipid solution under sonicating conditions. The reaction was kept in a sonicator (24 Hz/min) at 60 °C, for 1 h. Ethanol was evaporated on rota-evaporator and water by lyophilization resulted into white solid (3.8 g), which was characterized by FTIR, UV-Visible, SEM.

3C.4.2 Cell Lines, Antibodies, and Reagents

Human breast adenocarcinoma (MDA-MB-231, MCF-7) and HEG 293 non-cancerous cell line cell lines were obtained from American Type Culture Collection (ATCC, Manassas, VA, USA) and maintained in L-15 and DMEM media (Sigma) supplemented with 10 % FBS, 100 units penicillin and 100 µg/mL streptomycin. Wortmannin and SN50 were purchased from Calbiochem (San Diego, CA). The [μ -³²P] ATP was procured from the Board of Radiation and Isotope Technology (Hyderabad, India). All other chemicals were of analytical grade.

3C.4.3 Cell Viability assay (MTT) Assay

The cell viability assay was performed as described previously.⁴⁵ Briefly, 2×10^4 cells/well were plated in a 96-well flat-bottom microplate. Cells were treated with sophorolipid, andrographolide, and SL-1 (0-100 µM) for 24 h. 200 µL of MTT (0.5 mg/mL) was added into each well and incubated at 37 °C for 4h. After incubation, formazan crystals were dissolved with 200 µL of isopropanol. The optical density of formazan solution, as a measure of cell viability, was taken using a microplate reader at 570 nm (Molecular Devices). Experiments were performed in triplicates.

Chapter 3: Section C

Nanoscale Assembly of ZnO Nanoparticles for *in vitro* Controlled Release of Andrographolide

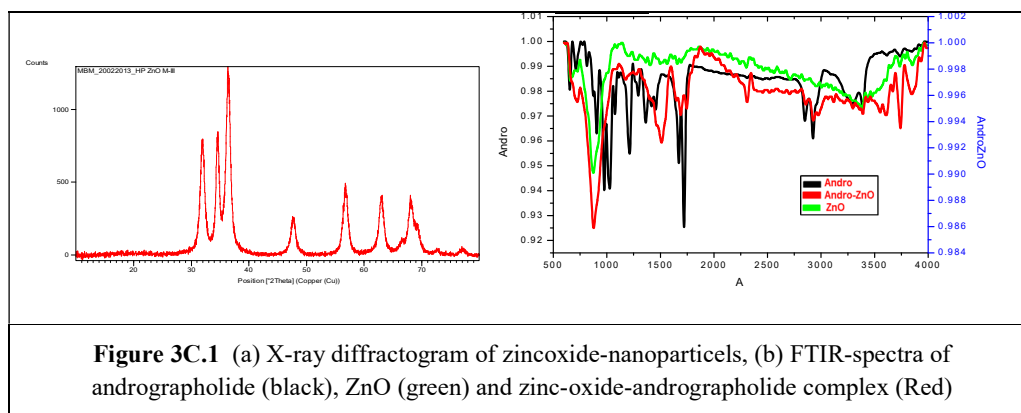
3C.1 Introduction

Andrographolide (**1**) is a bioactive labdane diterpenoid, which exhibits anticancer activities against several types of cancer like breast cancer, leukaemia, melanoma, and lung cancer etc.⁴⁶ However, the bioactivity of andrographolide was not explored efficiently due to inadequate water solubility and negligible bioavailability.³³ For control release of hydrophobic drugs or bioactive natural products, formulation with nanoparticles is one of the techniques. This can help to reduce the dose and improve the absorption potential.⁴⁷ For control drug release, three types of stimulus are required physical, chemical and biological.^{48,49} In anti-cancerous drug release pH is important stimuli, which has advantages over other two stimuli because of cancerous cells pH value is lower (4.5 - 5.5) compared to the normal tissues and blood due to the high-speed glycolysis in the cells.^{50,51} Nanoparticles are reported to have application as a drug carrier for control release due to suitable pore size and high volume interacting with bioactive molecules.⁵² However, the most important factor of inorganic nonmaterials is biodegradability *viz.* iron oxide nanoparticles, gold and silica nanoparticles.^{53,54} Zinc oxide is biocompatible material and utilized in several applications e.g. ceramic, rubber, foods, and pharmaceuticals industries.^{55,56} Zinc-oxide nanoparticles are reported as an adjuvant in breast cancer treatment for intracellular accumulation of doxorubicin with the pH-responsive release by Juan Liu *et al.*⁵⁷ Henceforth due to low toxicity, the low cost we have used of zinc-oxide nanoparticles as an andrographolide carrier.

3C.2 Result and discussion

3C.2.1 Zinc oxide Nanoparticle Synthesis

Zinc oxide nanoparticles are formed by using precipitation method, which has advantages such as simple protocol and uniformity in nanoparticles size.⁵²



By using X-ray diffractogram of zinc oxide nanoparticles (Figure 3C. 1a) showed characterized the peaks at theta value 31.2, 33.9, 36.6, 48.7, 56.7, 62.9 and 67.3 were matching with the earlier reports. FTIR-spectra of zinc-oxide nanoparticles showed peaks at 450 cm^{-1} , IR-spectrum of andrographolide showed a peak at 1456, 1671, 1720, 3289, and 3389 cm^{-1} Whereas the IR-spectra of zinc oxide-andro. complex showed characteristic the peak of zinc-oxide along with andrographolide hydroxyl peaks at 3289, 3389 cm^{-1} shifted to 3295, 3397 cm^{-1} ; results suggested that the andrographolide has non-covalently interacted with zinc-oxide nanoparticles through hydroxyl groups. Morphological analysis by using scanning electron microscopy (SEM) suggested that the zinc-oxide nanoparticles ($< 100\text{ nm}$) are spherical in nature

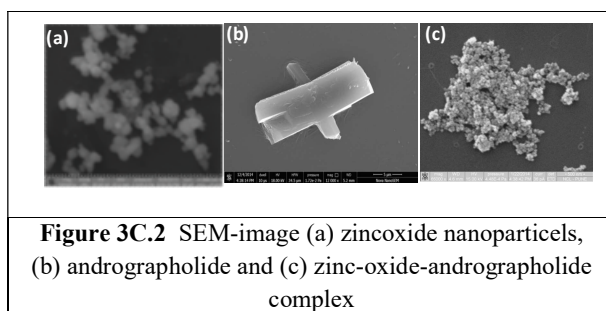
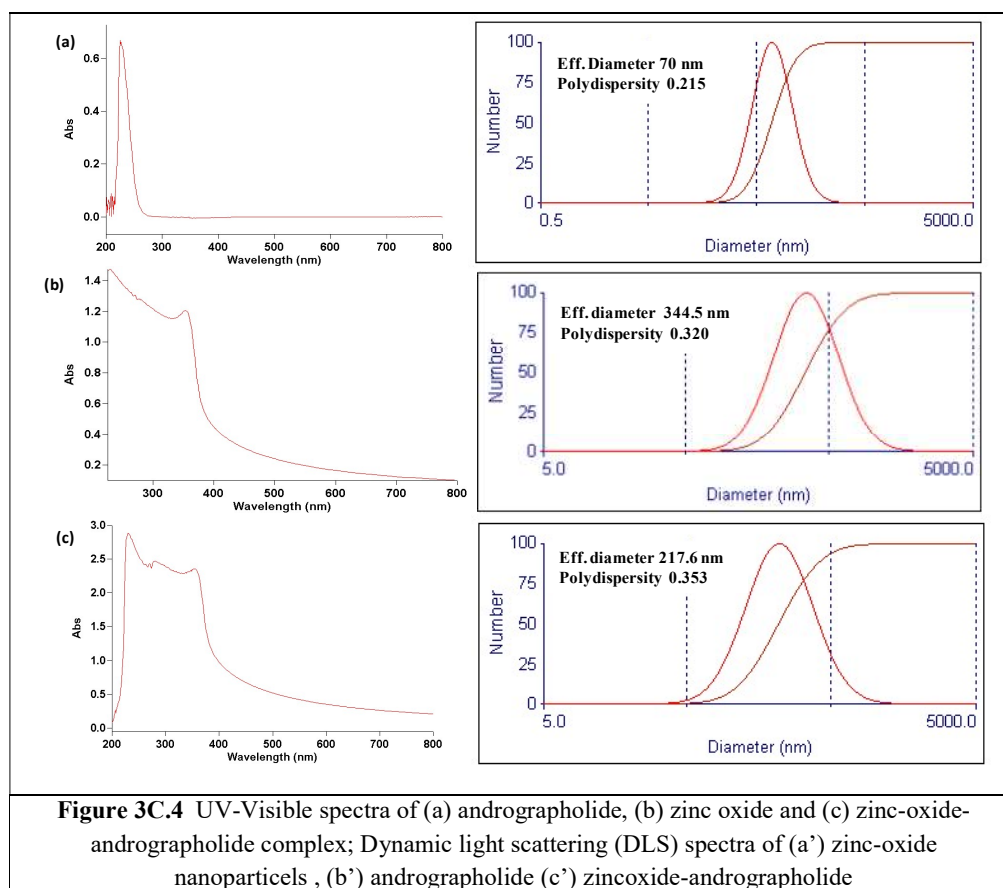


(Figure 3C. 2a), whereas SEM-image of andrographolide showed large crystal of size around $10\text{-}20\text{ }\mu\text{m}$ (Figure 3C. 2b). SEM-image of the zinc-oxide-andrographolide (Figure 3C. 2b) complex indicated the decrease in particle

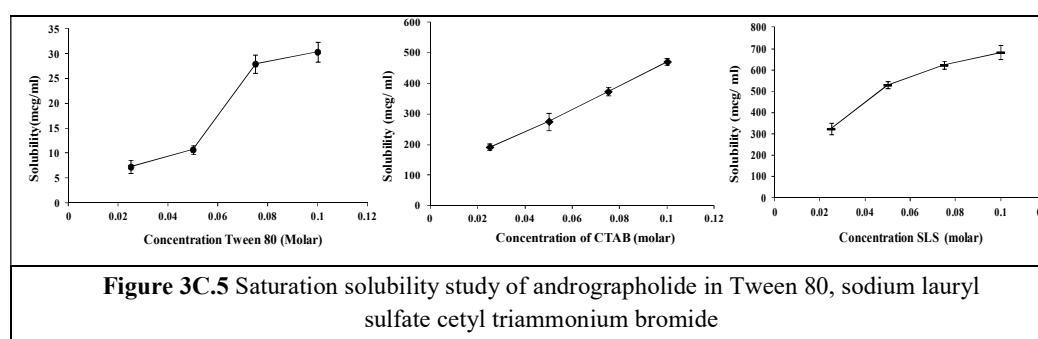
size of andrographolide and uniformity lost in zinc-oxide nanoparticles (< 200 nm). UV-Visible spectrum zinc-oxide nanoparticles and andrographolide showed



absorption at 367 nm, and at 230 nm respectively (Figure 3C. 4a, 4b, 4c). Whereas the zinc oxide-andrographolide complex. The UV-visible spectrum absorption at 230 nm, the change in absorption from 367 nm to 380 nm suggested the non-covalent interaction of zinc-oxide with andrographolide. To understand the size and stability of the zinc-oxide-andrographolide complex in solution, we have performed DLS and zeta potential measurement at constant shutter opening diameter. DLS measurement of zinc-oxide nanoparticles, andrographolide and zinc oxide-andro. complex exhibited the hydrodynamic radii of 70 nm, 217.6 nm, 344.5 nm respectively (Figure 3C.4 a',b',c'). These data clearly illustrated that there is a reduced agglomeration of andrographolide in aqueous solution by complexation with zinc-oxide nanoparticles.

3C.2.2 Saturation Solubility Study

For *in vitro* pH release study of andrographolide from zinc-oxide nanoparticles, solubility is an important factor. In order to enhanced andrographolide solubility, we have screened various surfactants (Figure 3C. 5). Saturation solubility of andrographolide is highest with anionic surfactant sodium lauryl sulfate at 0.1 M concentration its 600 mcu and lowest saturation solubility was observed with non-ionic surfactant Tween 80 at 0.1 M, 30 mcu. Saturation solubility of andrographolide with cationic surfactant cetyl triammonium bromide was 450 mcu at 0.1 M concentration.



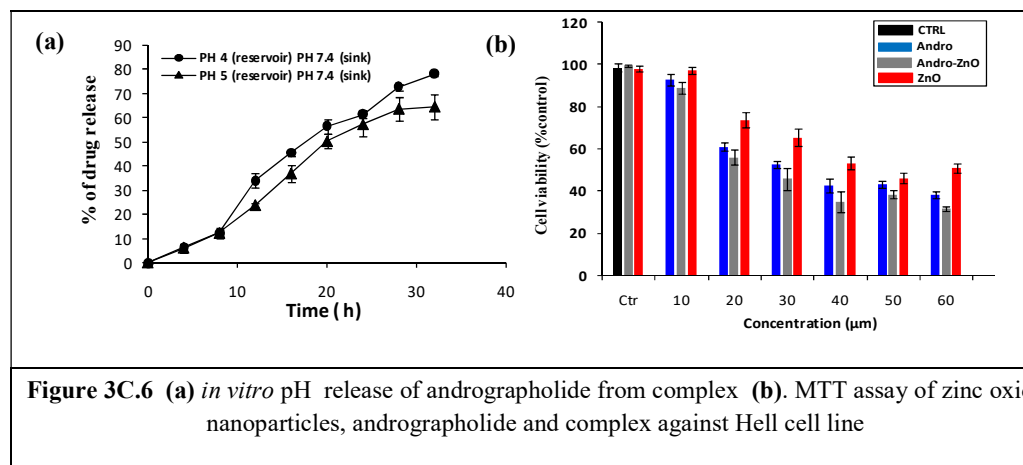
3C.2.3 *In vitro* pH Release Study of Andrographolide from ZnO Assemblies

in vitro pH release studies under reservoir-sink conditions suggested that the andrographolide release profile from zinc-oxide nanoparticles changes with change in the pH values (Figure 3C. 6a). It has been observed that andrographolide was slowly released throughout 35 h under both the pH. Andrographolide released about 80 % and 60 % was observed in acetate buffer (pH-4) and acetate buffer (pH-5) media, respectively, against PBS (pH 4) after 35 h. The andrographolide release profile is higher at lower pH (4), which was desirable for cancer treatment.

3C.2.4 Cell Viability Assay (MTT)

Cytotoxicity of zinc-oxide, andrographolide and zinc-oxide- andro. against HeLa cells were tested by incubation at various concentrations (10 μ M-60 μ M) for 24 h.^{58,45} The result suggested that the zinc-oxide nanoparticles did not showed cytotoxicity against HeLa cells, suggested the biocompatibility and used for *in vivo* study. The IC₅₀ value for pure andrographolide was found to be 40 μ M (Figure 3C. 6b). The IC₅₀ value of zinc-oxide-andro was estimated to be 50 μ M; the relatively higher IC₅₀ value

suggested the lower toxicity, might be due to the presence of zinc oxide. Results suggested that zinc-oxide nanoparticles still could be used as carries for sustained or slow release of andrographolide (> 30 h) for other bioactivities.



3C.3 Conclusion

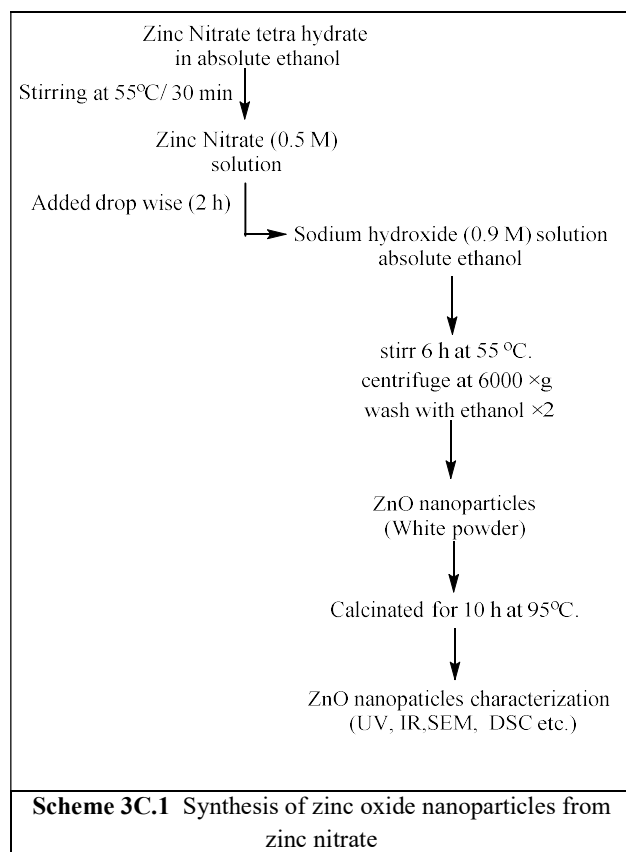
Zinc oxide nanoparticles were synthesised by using a simple, facile method. The IR, UV-spectra, and elemental analysis suggested the non-covalent interaction of andrographolide with zinc oxide nanoparticles. Andrographolide release from zinc oxide nanoparticles was studied with pH change. Andrographolide release with a change in pH is significant because the cancerous cells have lower pH compared to the normal cells.

3C.4 Experimental section

3C.4.1 Materials and Methods

Andrographolide isolation protocol was reported in chapter-2. Zinc nitrate hexahydrate ($\text{Zn}(\text{NO}_3)_2 \cdot 6\text{H}_2\text{O}$) (97 % extra pure) and potassium hydroxide were sourced from Sigma-Aldrich. All the solutions were prepared in deionised water. Thin-layer chromatography (TLC) analysis performed on silica gel G-coated plates (0.25 mm, Merk) with methanol: dichloromethane (5 %) as mobile phase. IR spectra were recorded on Perkin Elmer FT-IR spectrophotometer in CHCl_3 , and optical rotations were determined in the same solvent on JASCO (P-2000). Leica Stereo scan 440 operated at an accelerating voltage of 15 kV with pressure $5.87\text{E}-4$ Pa, current

0.14 nA and WD 9.9-10.0 mm det EDT. HPLC grade solvents were purchased from Sigma Aldrich (USA). HPLC performed on Waters HPLC system coupled with UV-Vis detector at 225 and 254 nm. Analytical XBridge C₁₈ column (4.6 × 250mm, 5µm) at a flow rate of 1 mL/min with a gradient solvent programme of Acetonitrile (ACN)



and water (H₂O). Zeiss Axiovert apotome microscope equipped with an AxioCam camera oil-immersion objective (64x) was used for capturing images and images were processed with Axiovision 4.7 software. Leica Stereoscan 440 operated at an accelerating voltage of 15 kV with pressure 5.87E-4 Pa, current 0.14 nA and WD 9.9-10.0 mm det EDT. The pre-scanned samples were sputter coated with 10 nm thick layers of gold nanoparticles by using a Polaron SC 6420 sputter coater. The neat and irradiated samples

were sputter coated without any pre-treatment or sample preparation.

3C.4.2 Synthesis Procedure of Zinc Oxide Nanoparticles from Zinc Nitrate

Zinc nitrate tetrahydrate was dissolved in absolute ethanol to make a 0.5 M solution and stirred for one hour with a magnetic stirrer.⁵² Sodium hydroxide (0.9 M) aqueous solution was prepared, this solution was added dropwise (1 drop/ 0.5 min) in the above solution with constant stirring. After complete addition aq. NaOH solution keeps reaction mixture for 8 h at room temperature with continuous stirring and after that kept for 2 h without stirring to settle down the solid part. The solvent was decanted, and the residue was centrifuged (1000 ×g for 30 min) followed by washing the residue three times with water to remove remaining sodium hydroxide. Further,

dry the zinc oxide residue and calcinated at 95°C for 10 h. zinc-oxide nanoparticles were then characterised by UV, XRD and SEM (Scheme 3C.1).

3C.4.3 Synthesis of Zinc-oxide-andrographolide Complex

Andrographolide (5 g) was taken in a round bottom flask and dissolved in absolute ethanol in a sonicator (35 Hz/min) at 70 °C, for 30 min. An aqueous solution of zinc oxide nanoparticles (2 g) was added drop-wise into the andrographolide solution through syring. The reaction was kept in a sonicator (24 Hz/min) at 60 °C, for 24 h. The solvent was removed from the reaction mixture by centrifugation (1000 × g /min) after the centrifugation supernatant was discard and nanoparticles were dry at room temperature in dust free environment. Further, the zinc-oxide-nanoparticles complex was characterised by FTIR, UV-Visible, SEM.

3C.4.5 pH-Stimulated Andrographolide Release

In order to study the andrographolide *in vitro* pH release with reservoir:⁵⁸ acetate buffer-pH 4, acetate buffer-pH 5, SLS 0.8 M. Sink: Phosphate buffered saline (PBS-pH 7.3), SLS 0.8 M; at temperature: 37 °C at 200 rpm in a shaker. pH-triggered andrographolide release was carried out under reservoir-sink conditions. zinc-oxide-nanoparticles complex (10 mg) was immersed into 5 mL of release medium (acetate buffer-pH 4, acetate buffer-pH 5) and then put into a dialysis bag. The dialysis was performed against 200 mL of phosphate buffered saline (PBS-pH 7.3) under continuous stirring at 37°C to mimic the cellular environment. 1 mL of the external medium was withdrawn and replaced with fresh PBS at fixed times to maintain sink conditions. The amount of andrographolide released was determined by measuring the intensity in HPLC against the standard plot prepared under similar conditions. Each experiment was performed in triplicate; the standard deviation is given in the plot. MTT assay was performed under similar conditions as mentioned above.

3D References

- 1 C. Aromdee, *Expert Opin. Ther. Pat.*, 2012, **22**, 169–180.
- 2 M. Sivananthan and M. Elamaram, *Int. J. Biomol. and Biomed.*, 2013, **3**, 1–12.
- 3 S. Pandeti, R. Sonkar, A. Shukla, G. Bhatia and N. Tadigoppula, *Eur. J. Med. Chem.*, 2013, **69**, 439–448.
- 4 H. Chen, Y. B. Ma, X. Y. Huang, C. A. Geng, Y. Zhao, L. J. Wang, R. H. Guo, W. J. Liang, X. M. Zhang and J. J. Chen, *Bioorganic Med. Chem. Lett.*, 2014, **24**, 2353–2359.
- 5 H. Xu, P. Jiang, W. Li, J. Wang and H. Liu, *Chinese J. Chem.*, 2011, **29**, 2114–2118.
- 6 S. Wei, Y. B. Tang, H. Hua, E. Ohkoshi, M. Goto, L. T. Wang, K. H. Lee and Z. Xiao, *Bioorganic Med. Chem. Lett.*, 2013, **23**, 4056–4060.
- 7 Z. G. Chen, Q. Zhu, M. H. Zong, Z. X. Gu and Y. Bin Han, *Process Biochem.*, 2011, **46**, 1649–1653.
- 8 C. A. Drăgan, D. Buchheit, D. Bischoff, T. Ebner and M. Bureik, *Drug Metab. Dispos.*, 2010, **38**, 509–515.
- 9 K. B. Borges, W. de S. Borges, R. Durán-Patrón, M. T. Pupo, P. S. Bonato and I. G. Collado, *Tetrahedron Asymmetry*, 2009, **20**, 385–397.
- 10 P. M. Dinh, J. A. Howarth, A. R. Hudnott, J. M. J. Williams and W. Harris, *Tetrahedron Lett.*, 1996, **37**, 7623–7626.
- 11 X. He, X. Zeng, H. Hu and Y. Wu, *J. Mol. Catal. B Enzym.*, 2010, **62**, 242–247.
- 12 P. P. Daramwar, P. L. Srivastava, S. P. Kolet and H. V. Thulasiram, *Org. Biomol. Chem.*, 2014, **12**, 1048–1051.
- 13 S. P. Kolet, S. Niloferjahan, S. Haldar, R. Gonnade and H. V. Thulasiram, *Steroids*, 2013, **78**, 1152–1158.
- 14 S. Haldar, S. P. Kolet and H. V. Thulasiram, *Green Chem.*, 2013, **15**, 1311–1317.
- 15 M. Persson, D. Costes, E. Wehtje and P. Adlercreutz, *Enzyme Microb. Technol.*, 2002, **30**, 916–923.
- 16 S. Park and R. J. Kazlauskas, *J. Org. Chem.*, 2001, **66**, 8395–8401.
- 17 T. Sakai, I. Kawabata, T. Kishimoto, T. Ema and M. Utaka, *J. Org. Chem.*, 2002, **15**, 4906–4907.
- 18 Y. Qiao, Y. Huang, F. Feng and Z. G. Chen, *Process Biochem.*, 2016, **51**, 675–680.
- 19 Z. G. Chen, R. X. Tan and M. Huang, *Process Biochem.*, 2010, **45**, 415–418.
- 20 S. S. Shankar, S. N. Benke, N. Nagendra, P. L. Srivastava, H. V. Thulasiram and H. N. Gopi, *J. Med. Chem.*, 2013, **56**, 8468–8474.
- 21 K. Kuroda, G. A. Caputo and W. F. DeGrado, *Chem. - A Eur. J.*, 2009, **15**, 1123–1133.
- 22 Z. G. Chen, R. X. Tan and L. Cao, *Green Chem.*, 2009, **11**, 1743–1745.
- 23 S. Nanduri, V. K. Nyavanandi, S. Sanjeeva Rao Thunuguntla, S. Kasu, M. K. Pallerla,

- P. Sai Ram, S. Rajagopal, R. Ajaya Kumar, R. Ramanujam, J. Moses Babu, K. Vyas, A. Sivalakshmi Devi, G. Om Reddy and V. Akella, *Bioorganic Med. Chem. Lett.*, 2004, **14**, 4711–4717.
- 24 V. Tullio, A. Nostro, N. Mandras, P. Dugo, G. Banche, M. A. Cannatelli, A. M. Cuffini, V. Alonzo and N. A. Carlone, *J. Appl. Microbiol.*, 2007, **102**, 1544–1550.
- 25 R. A. Dixon and I. Chopra, *Antimicrob. Agents Chemother.*, 1986, **29**, 781–788.
- 26 T. Zor and Z. Selinger, *Anal. Biochem.*, 1996, **236**, 302–308.
- 27 U. M.M., D. T., P. R.S., B. B., M. V., Nutan, G. S.K. and B. S.V., *Eur. J. Med. Chem.*, 2012, **56**, 368–374.
- 28 M. L. Tan, M. Kuroyanagi, S. F. Sulaiman, N. Najimudin and T. S. Tengku Muhammad, *Pharm. Biol.*, 2005, **43**, 501–508.
- 29 A. Valdiani, M. A. Kadir, S. G. Tan, D. Talei, M. P. Abdullah and S. Nikzad, *Mol. Biol. Rep.*, 2012, **39**, 5409–5424.
- 30 Shirisha K and Mastan M, *Pharmacophore*, 2013, **4**, 212.
- 31 D. Talei, A. Valdiani, M. Maziah, S. R. Sagineedu and M. S. Saad, *Biomed Res. Int.*, 2013, **2013**, 1–11.
- 32 S. R. Jada, G. S. Subur, C. Matthews, A. S. Hamzah, N. H. Lajis, M. S. Saad, M. F. G. Stevens and J. Stanslas, *Phytochemistry*, 2007, **68**, 904–912.
- 33 A. Pawar, S. Rajalakshmi, P. Mehta, K. Shaikh and C. Bothiraja, *RSC Adv.*, 2016, **6**, 69282–69300.
- 34 B. Chellampillai and A. P. Pawar, *Eur. J. Drug Metab. Pharmacokinet.*, 2011, **35**, 123–129.
- 35 D. Zhao, K. Liao, X. Ma and X. Yan, *J. Incl. Phenom.*, 2002, **43**, 259–264.
- 36 C. Bothiraja, M. B. Shinde, S. Rajalakshmi and A. P. Pawar, *J. Pharm. Pharmacol.*, 2009, **61**, 1465–1472.
- 37 S. Shafiq, F. Shakeel, S. Talegaonkar, F. J. Ahmad, R. K. Khar and M. Ali, *Eur. J. Pharm. Biopharm.*, 2007, **66**, 227–243.
- 38 I. M. Banat, R. S. Makkar and S. S. Cameotra, *Appl. Microbiol. Biotechnol.*, 2000, **53**, 495–508.
- 39 I. M. Banat, A. Franzetti, I. Gandolfi, G. Bestetti, M. G. Martinotti, L. Fracchia, T. J. Smyth and R. Marchant, *Appl. Microbiol. Biotechnol.*, 2010, **87**, 427–444.
- 40 L. Rodrigues, I. M. Banat, J. Teixeira and R. Oliveira, *J. Antimicrob. Chemother.*, 2006, **57**, 609–618.
- 41 C. U. Anyanwu, S. K. C. Obi and B. N. Okolo, *Our Nat.*, 2011, **8**, 1–11.
- 42 H. J. Asmer, S. Lang, F. Wagner and V. Wray, *J. Am. Oil Chem. Soc.*, 1988, **65**, 1460–1466.
- 43 N. Baccile, F. Babonneau, J. Jestin, G. Pehau-Arnaudet and I. Van Bogaert, *ACS Nano*, 2012, **6**, 4763–4776.

- 44 P. K. Singh, K. Wani, R. Kaul-Ghanekar, A. Prabhune and S. Ogale, *RSC Adv.*, 2014, **4**, 60334–60341.
- 45 S. Kumar, H. S. Patil, P. Sharma, D. Kumar, S. Dasari, V. G. Puranik, H. V. Thulasiram and G. C. Kundu, *Curr. Mol. Med.*, 2012, **12**, 952–966.
- 46 M. Banerjee, S. Chattopadhyay, T. Choudhuri, R. Bera, S. Kumar, B. Chakraborty and S. K. Mukherjee, *J. Biomed. Sci.*, 2016, **23**, 40.
- 47 R. Diab, C. Jaafar-Maalej, H. Fessi and P. Maincent, *AAPS J.*, 2012, **14**, 688–702.
- 48 C.-Y. Lai, B. G. Trewyn, D. M. Jeftinija, K. Jeftinija, S. Xu, S. Jeftinija and V. S.-Y. Lin, *J. Am. Chem. Soc.*, 2003, **125**, 4451–4459.
- 49 S. Ganta, H. Devalapally, A. Shahiwala and M. Amiji, *J. Control. Release*, 2008, **126**, 187–204.
- 50 M. Das, S. Mardyani, W. C. W. Chan and E. Kumacheva, *Adv. Mater.*, 2006, **18**, 80–83.
- 51 Y. Bae, W. D. Jang, N. Nishiyama, S. Fukushima and K. Kataoka, *Mol. Biosyst.*, 2005, **1**, 242–250.
- 52 A. S. Lanje, S. J. Sharma, R. S. Ningthoujam, J.-S. Ahn and R. B. Pode, *Adv. Powder Technol.*, 2013, **24**, 331–335.
- 53 B. Fadeel and A. E. Garcia-Bennett, *Adv. Drug Deliv. Rev.*, 2010, **62**, 362–374.
- 54 Z. P. Xu, Q. H. Zeng, G. Q. Lu and A. B. Yu, *Chem. Eng. Sci.*, 2006, **61**, 1027–1040.
- 55 A. Kołodziejczak-Radzimska and T. Jesionowski, *Materials (Basel)*, 2014, **7**, 2833–2881.
- 56 Y. K. Mishra and R. Adelung, *Mater. Today*, 2018, **21**, 631–651.
- 57 J. Liu, X. Ma, S. Jin, X. Xue, C. Zhang, T. Wei, W. Guo and X. J. Liang, *Mol. Pharm.*, 2016, **13**, 1723–1730.
- 58 K. C. Barick, S. Nigam and D. Bahadur, *J. Mater. Chem.*, 2010, **20**, 6446–6452.

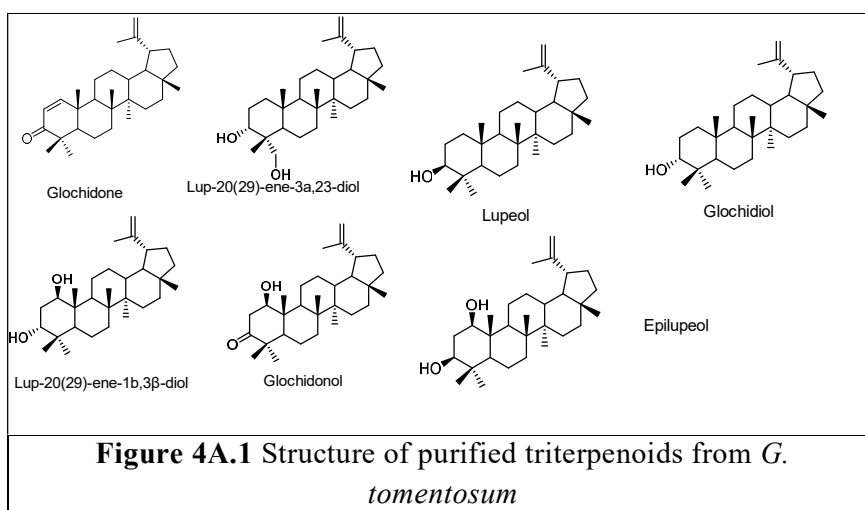
Chapter 4
**Isolation, Purification and
Characterization of Terpenoids from
Glochidion tomentosum, *Wedelia paludosa***

Chapter 4: Section A

MPLC Based Isolation of Lupane Triterpenoids from *Glochidion tomentosum*

4A.1 Introduction

Glochidion tomentosum Nutt. ex. Seem belongs to genus *Glochidion* comprises approximately 300 species distributed mainly in tropical Asia, and across Madagascar, to the Pacific Islands.¹ *G. tomentosum* is a medium size evergreen tree endemic to Western Ghats region of Southern India. It is used by Indian tribal communities in traditional medicines for treatment, e.g. grounded pate of leaves used for the treatment of wounds.^{1,2,3} Several species of this genus are described to have medicinal values^{4,5,6} and used in folk medicine for the treatment of dyspesoa, dysentery,⁷ stomach ache, rheumatoid arthritis, wounds, diabetes.^{8,9} Till now no literature was available on *G. tomentosum* phytochemical investigation, but reports on the phytochemical investigation of plants from this genus have revealed the presence of alkaloids, terpenoids, flavonoids, lignin's, steroids, triterpenoid glycosides, butenolides and saponins. Bioactive terpenoids purification is associated with several obstacles such as skeletal similarities, complex structure with several stereocenters, and sensitive functionality; these factors make it troublesome.^{10,11,12,13} Hence, there is a need to develop a useful, rapid and reproducible technique for terpenoids purification, which facilitates the efficient method for preparative scale availability for detailed bioactivity study.



Medium pressure liquid chromatography is a robust, automated technique for developing an effective, rapid and reproducible protocol for preparative scale isolation of natural products.¹⁴ In this study, we have developed MPLC based purification

protocol for the isolation of seven terpenoids from the bark powder of *G. tomentosum* with the high (>95 %) purity. Characterization and confirmation of compounds were

done by GC-MS and NMR analysis.

4A.2 Results and Discussion

4A.2.1 Extraction of Bark Powder

Five hundred gram bark of *Glochidion tomentosum* was crushed using a grinder and extracted with petroleum ether (2 L × 4) for 3. After the concentration of extracts yellow solid (4.5 g, 0.9 % weight of powder), which contains a mixture of terpenoids indicated by GC-MS analysis. Compounds in the crude extract did not show absorption under UV lamp on TLC. Then fractionation followed by purification was performed by using medium pressure liquid chromatography fitted with PDA detector.

4A.2.2 MPLC Based Fractionation and Purification of *G. tomentosum* Crude Extract

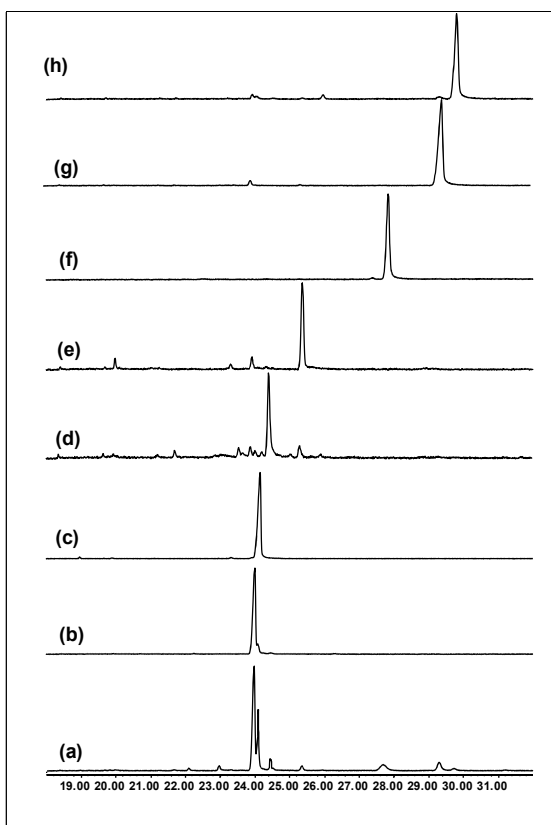


Figure 4A.2 A. MPLC based separation protocol monitoring by GC chromatogram of (a) crude diterpenoid extract, (b) purified Glochidonol, (c) purified Glochidone, (f) purified Glochidiol, (g) purified Lup-20(29)-ene-1 β , 3 β -diol, (h) purified Lup-20(29)-ene-3 α , 2 β -diol, (h) purified Lupeol, (h) purified Epilupeol.

Purification was performed using normal phase silica gel RediSep Rf cartridges of varying particle sizes (40-60 μm) were used as the stationary phase. One gram of yellow crude extract (1 g) adsorbed on celite was subjected for MPLC purification of pure compounds using 24 g cartridge with the at 200-400 nm and the flow rate of 20 mL/ min. Ethyl acetate in hexane was used as a solvent system and a gradient solvent program of 140 min with the increased in ethyl acetate concentration. TLC of all the fractions was obtained taken, and fraction showed a similar spot on TLC were combined. Seven fractions were obtained (Scheme 4A.4), fraction-F1 (46 mg), weight of fraction-F2 (80.2 mg), fraction-F3 (44.1 mg), fraction-F4 (200 mg),

fraction-F5 (52.7 mg), fraction F6 (34.2 mg) and fraction-F7 (26.7 mg). Fractions-F1 showed three spots on TLC, further fraction-F1 purification on reverse phase cartridge separated into 97.4 % pure compound. From fraction- F2, 74 mg compound was purified with 96 % GC-purity. Similarly, all other fractions were purified over MPLC normal phase cartridge. Purification protocol was monitored by TLC and purity of compounds checked by using gas chromatography.

4A.2.3 Characterization of Terpenoids

Purified compounds were characterized by the analyses of NMR spectrometric and GC-MS data, which were in full agreement with the previous reports.¹⁵ Compound-1 was obtained after purification of fraction-1 as a white amorphous solid. GC-MS-EI-QToF spectra showed a mass of m/z 422.3518 and the earlier report suggested molecular formula $C_{30}H_{46}O$, from molecular formula calculated degree of unsaturation is eight. The molecular formula suggested it was triterpenoid. IR spectrum showed a stretching frequency at 1725 cm^{-1} indicating the presence of α,β -unsaturated lactone, stretching frequency at $1663, 1654\text{ cm}^{-1}$ suggested alkyl double bond. IR-peak at 3400 cm^{-1} showed the presence of hydroxyl group. ^{13}C , DEPT NMR spectrums peak at δ 125.14, 150.76, 159.89 and 109.48 showed the presence of four alkenes carbon out of which one are quaternary carbon, two is secondary and one is primary. DEPT showed nine - CH_2 groups, seven - CH_3 methyl group, and six quaternary carbon. 1D NMR results were in combination with correlated ^{13}C with ^1H in HMBC spectroscopic data. HSQC and HMBC correlations observed between H-19 (δ 1.98 and 2.32) with C-20 at δ 89.36 and H-20 (δ 1.98 and 2.32) with C-11 at δ 89.36 confirmed the stereochemistry. HMBC Correlation observed of H-5 (δ 1.98) and H-6 (δ 1.98) with C-18 δ 89.36 confirmed position. Lactones H-14 was confirmed on the basis of HSQC and HMBC spectra. The signal at δH 5.94 (d, $J=5.52\text{ Hz}$) was assigned to H- 14 according to the correlations of H-14 with C-12 (δC 150.6), C-13 (δC 123.8) and C- 16 (δC 169.1) in the HMBC spectrum. The characterization data analysis and comparing with the earlier reports compound-1 was characterised as glochidone. Similarly, the structural analyses of all the other compounds were performed and compounds were characterised.⁶

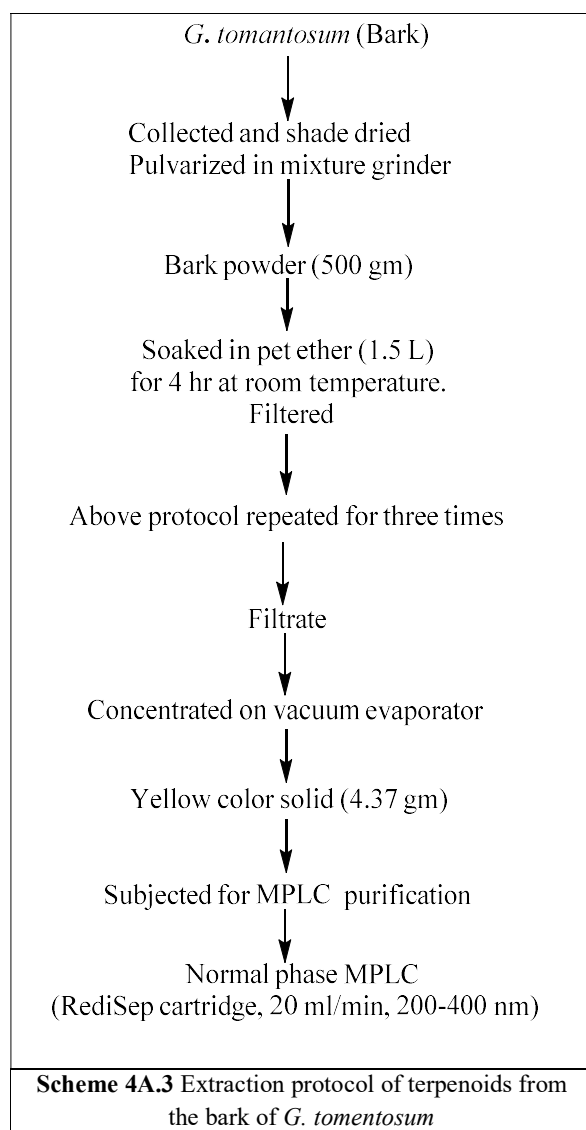
4A.3 Conclusion

Lupane triterpenoids from the bark of *Glochidion tomentosum* were isolated first time by automated Medium pressure chromatographic (MPLC) technique. Compounds were isolated on a preparative scale further characterized by spectroscopic techniques like NMR's and mass. Glochidone, Epilupeol, Lupeol, Glochidonol, Lup-20(29)-ene-3 α ,23-diol, Glochidiol and Lup-20(29)-ene-1 β ,3 β -diol. The present result evokes further investigation of phytochemicals and provides new prospect about this endangered medicinal tree.

4A.4 Experimental Section

4A.4.1 General Experimental Procedures

Glochidion tomentosum, the bark was collected from the Charmadi Ghat region of Chickmagalur district, Karnataka, India during the month of June-2012 and deposited as herbarium of the Department of Bioscience, Post Graduate Centre, University of Mysore, Hemagangothri, Hassan, Karnataka, India identified by Dr. P. Sharanappa (Sp. No. THV-3). Extraction solvents for plant material were a technical grade (Spectrochem) and distilled prior to use. MPLC and HPLC solvents were purchased from Sigma (St. Louis, MO, USA). Thin-layer chromatography (TLC) analysis, reaction progress was monitored by Thin-layer chromatography



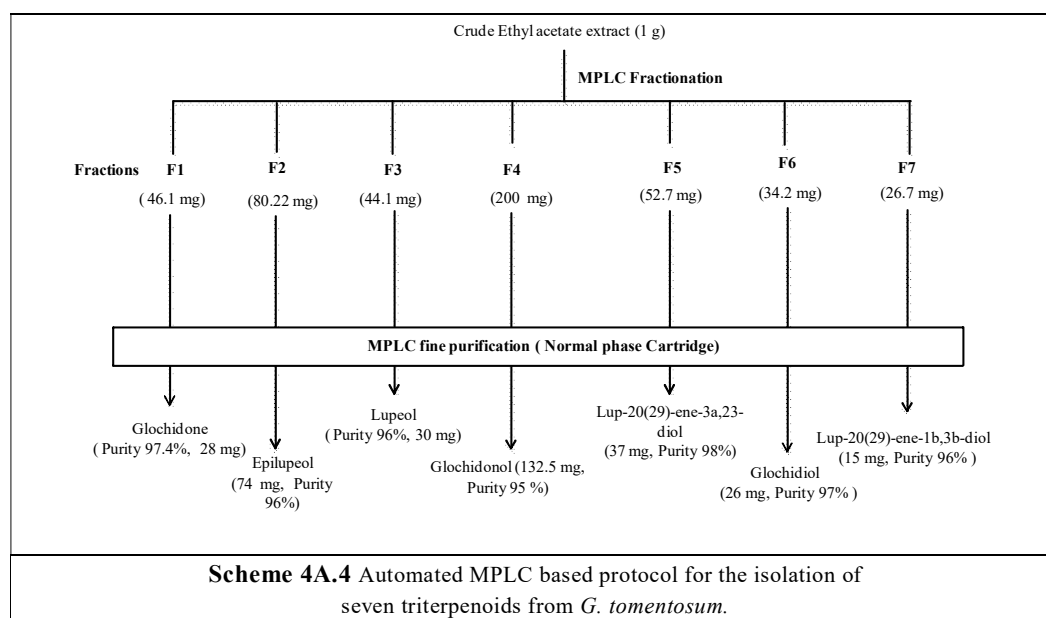
(TLC) performed on silica gel G-coated plates (0.25 mm, Merk). Migration of the compounds on TLC was visualized by spraying it with a solution of 3.2 % anisaldehyde, 2.8 % H₂SO₄, 2 % acetic acid in ethanol followed by heating for 1-2 min. Teledyne, Isco-(Combi-flash Rf 200) MPLC system with PDA detector was used for the normal and reverse phase purification. GC analyses were carried out on an Agilent 7890 instrument equipped with flame ionization detector and HP-5 capillary column (30 m X 0.32 mm X 0.25 μm, J & W Scientific). Nitrogen was used as carrier gas at a flow rate of 1 mL/min. GC-MS was performed on an Agilent 5975 mass selective detector interfaced with an Agilent 7890 gas chromatograph. GC-MS analyses were performed

under similar conditions.

NMR (^1H , ^{13}C , DEPT) spectra were recorded on Varian INOVA spectrometer (400, 500 MHz) and chemical shift values were reported in ppm with respect to the residual solvent or Tetramethylsilane (TMS) signals as the reference. HRMS data were collected on Thermo Scientific Q Exactive Quadrupole-Orbitrap Mass Spectrometer. IR spectra were recorded on Perkin Elmer FT-IR spectrophotometer in CHCl_3 and optical rotations were determined in the same solvent on JASCO (P-2000), polarimeter using 10 mm cell (c in gm/100 ml unit).

4A.4.2 Extraction and Purification of Terpenoids from *G. tomentosum* Bark Extract

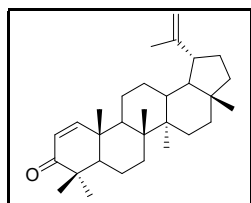
Freshly collected *G. tomentosum* bark was shade dried and powdered in the grinder. Powder (1 Kg) was soaked in pet ether (4 L), extracted in soxhlet apparatus for 3 h; further solvent was filtered and concentrated on rotaevaporator. For maximum extraction yield, the same procedure was repeated for four times. Yellow solid (9 g, 0.9 % weight of powder) obtained after extraction. Pet ether extract was purified over silica gel (230- 400 mesh) column chromatography using ethyl acetate/pet ether gradient and the compound obtained was characterised using GC, GCMS, NMR, FT-IR. GC analysis



4A.4.3 MPLC Purification

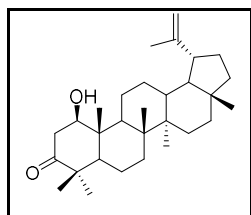
Yellow extract (1 g) obtained was adsorbed on celite (1:3 w/w) filled in cartridge, which was subjected to normal phase separation on MPLC using 24 g normal phase RediSep cartridge with a 20 mL/min flow rate with ethyl acetate/ pet ether as solvent system, monitoring at 200-400 nm. MPLC Solvent program : 0-15 min 0 % EtOH, 5 min hold, 20 min 5 % EtOH, 5 min hold, 40 min 10 % EtOH, 5 min hold, 60 min 15 % EtOH, 5 min hold, 80 min, 20 % EtOH, 5 min hold, 100 min 25 % EtOH, 5 min hold, 120-135 min, 30 % EtOH, 5 min hold).

Glochidone White solid; m.p. 163-164 °C; IR (CHCl₃) ν_{\max} = 1108, 1453, 1663, 1654, 1725, 2359, 2897, 3425, cm⁻¹; GC-MS (ESI) *m/z*: Calcd for C₃₀H₄₆O, 422.35; found, 422.3518. ¹H NMR (CDCl₃, 400 MHz) : δ ppm 0.82 (s, 3 H), 0.93 - 0.99 (m, 4 H), 1.13



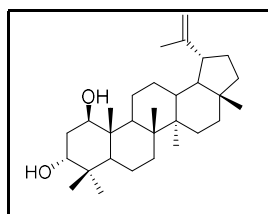
(d, *J*=8.85 Hz, 6 H), 1.22 - 1.28 (m, 9 H), 1.38 - 1.45 (m, 5 H), 1.49 - 1.56 (m, 5 H), 1.57 - 1.64 (m, 5 H), 1.66 - 1.74 (m, 6 H), 4.60 (s, 1 H), 4.67 - 4.74 (m, 1 H), 5.80 (d, *J*=10.07 Hz, 1 H), 7.11 (d, *J*=10.07 Hz, 1 H). ¹³C NMR (CDCl₃, 100 MHz): δ ppm 14.41 , 16.45 , 18.03 , 19.01 , 19.19 , 19.31 , 21.24 , 21.41 , 25.08 , 27.36 , 27.79 , 29.69 , 29.79 , 33.75 , 35.48 , 38.22 , 39.55 , 39.96 , 41.75 , 43.01 , 43.10 , 44.42 , 47.89 , 48.15 , 53.42 , 109.48 , 125.14 , 150.76 , 159.89 , 205.58.

Glochidonol White solid; m.p. 228 °C; IR (CHCl₃) ν_{\max} = 1108, 1453, 1710, 1654, 1652, 2359, 2933, 3425 cm⁻¹. GC-MS (ESI) *m/z*: Calcd for C₃₀H₄₈O₂, 440.2; found, [M-H₂O], 422.3477; ¹H NMR (CDCl₃, 400) : δ ppm 0.80 (s, 4 H), 0.84 (s, 4 H), 0.98 (s, 4 H), 1.04 (s, 5 H), 1.06 (s, 9 H), 1.31 (d, *J*=5.50 Hz, 3 H), 1.37 - 1.45 (m, 8 H), 1.47 - 1.57 (m, 7 H), 1.67 - 1.74 (m, 8 H), 2.23 (dd, *J*=14.20, 3.21



Hz, 1 H), 2.39 (d, *J*=5.50 Hz, 2 H), 3.01 (dd, *J*=13.97, 8.47 Hz, 1 H), 3.90 (dd, *J*=8.01, 3.43 Hz, 1 H), 4.53 - 4.60 (m, 1 H), 4.65 - 4.72 (m, 1 H). ¹³C NMR (CDCl₃, 100 MHz): δ ppm 11.81 , 14.40 , 15.88 , 17.99 , 19.23 , 19.56 , 19.78 , 22.93 , 25.08 , 27.43 , 27.93 , 29.65 , 29.72 , 32.85 , 35.46 , 37.91 , 39.91 , 41.06 , 42.84 , 42.89 , 45.06 , 47.08 , 47.87 , 48.18 , 50.63 , 51.25 , 79.54 , 109.45 , 150.68 , 216.06.

Glochidiol Solid; m.p. 258 °C; IR (CHCl₃) ν_{\max} = 904, 1663, 2900, 3325, 3400 cm⁻¹,

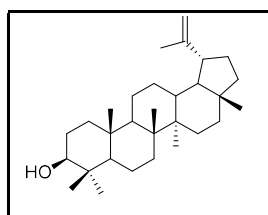


GC-MS (ESI) m/z : Calcd for C₃₀H₅₀O₂, 442.38; found, [M-2H₂O], 406.3541; ¹H NMR (CDCl₃, 400 MHz): δ ppm 0.80 (s, 3 H) 0.84 (s, 3 H) 0.92 (s, 6 H) 0.98 (s, 3 H) 1.06 (s, 3 H) 1.68 (s, 3 H) 2.13 (d, J =13.28 Hz, 1 H) 2.36 (s, 1 H) 3.50 (s, 1 H) 3.79 (dd, J =10.87, 4.92 Hz, 1 H) 4.56 (s, 1 H) 4.68 (s, 1 H). ¹³C

NMR (CDCl₃, 100 MHz): δ ppm 11.70, 14.53, 16.22, 18.03, 18.45, 19.20, 19.78, 21.92, 23.84, 25.08, 27.45, 27.66, 29.77, 34.04, 35.61, 36.33, 37.42, 37.61, 40.00, 41.59, 42.90, 42.97, 43.58, 47.76, 48.01, 48.33, 51.19, 75.88, 109.41, 150.86.

[M-2 H₂O]⁺

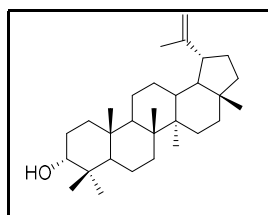
Lupeol White solid; m.p. 115-116 °C; IR (CHCl₃) ν_{\max} = 904, 1663, 1734, 2900, 3325, 3400 cm⁻¹; GC-MS (ESI) m/z : Calcd for C₃₀H₅₀O, 426.39; found, [M-H₂O], 408.3700;



¹H NMR (CDCl₃, 400 MHz): δ ppm 0.77 (s, 3 H) 0.80 (s, 4 H) 0.84 (s, 3 H) 0.96 (d, J =9.29 Hz, 7 H) 1.04 (s, 4 H) 1.26 (s, 7 H) 1.40 (br. s., 6 H) 1.54 (br. s., 6 H) 1.69 (s, 6 H) 2.05 (s, 2 H) 2.35 - 2.42 (m, 1 H) 3.20 (d, J =16.14 Hz, 1 H) 4.12 (s, 1 H) 4.57 (s, 1 H) 4.70 (s, 1 H). ¹³C NMR (CDCl₃, 100 MHz): δ ppm

14.18, 14.54, 15.36, 15.97, 16.11, 17.99, 18.31, 19.29, 20.92, 21.04, 25.14, 27.41, 27.44, 27.98, 29.69, 29.84, 34.28, 35.58, 37.16, 38.05, 38.70, 38.86, 40.00, 40.83, 42.82, 43.00, 47.98, 48.30, 50.44, 55.29, 76.68, 79.01, 109.31, 150.98.

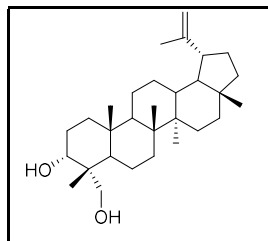
Epilupeol White solid; m.p. 113-114 °C; IR (CHCl₃) ν_{\max} = 904, 1663, 1734, 2900,



3325, 3400 cm⁻¹; GC-MS (ESI) m/z : Calcd for C₃₀H₅₀O, 426.39; found, [M-H₂O], 408.3707; ¹H NMR (CDCl₃, 400 MHz): δ ppm 0.80, 0.84 (d, J =8.85 Hz), 0.97, 0.94, 1.00 - 1.07 (m), 1.09 (br. s.), 1.15 - 1.29 (m), 1.29 - 1.43 (m), 1.44 - 1.58 (m), 1.60 - 1.75 (m), 1.88 - 1.99 (m), 2.39 (d, J =5.80 Hz), 3.36 - 3.42 (m), 4.58,

4.70 (d, J =1.83 Hz); ¹³C NMR (CDCl₃, 100 MHz): δ ppm 14.63, 15.92, 15.98, 18.01, 18.28, 19.29, 20.79, 22.14, 25.14, 25.41, 27.40, 28.25, 29.86, 33.26, 34.15, 35.59, 37.30, 37.54, 38.03, 40.02, 41.04, 42.91, 43.02, 48.03, 48.30, 49.03, 50.22, 76.75, 109.30, 151.02

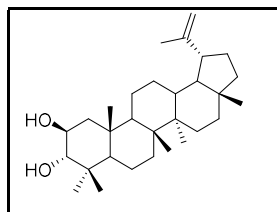
Lup-20(29)-ene-3 α ,23-diol White solid; m.p. 209 °C; IR (CHCl₃) ν_{\max} = 904, 1663,



1734, 2900, 3325, 3400 cm⁻¹; GC-MS (ESI) m/z : Calcd for C₃₀H₅₀O, 426.39; found, [M-H₂O], 408.3707; ¹H NMR (CDCl₃ 400 MHz): δ ppm 0.70 (s, 3 H), 0.80 (s, 3 H), 0.88 (s, 3 H), 0.99 (s, 3 H), 1.05 (s, 3 H), 1.09 - 1.34 (m, 7 H), 1.36 - 1.52 (m, 11 H), 1.57 - 1.80 (m, 8 H), 1.81 - 2.02 (m, 2 H), 2.37 (dd, J =11.05, 5.62 Hz, 1 H), 3.34 - 3.60 (m, 2 H), 3.62 - 3.73 (m, 1 H), 4.53 -

4.62 (m, 1 H), 4.70 (d, J =2.40 Hz, 1 H); ¹³C NMR (CDCl₃, 100 MHz): δ 14.65, 15.94, 16.18, 17.73, 17.98, 18.01, 19.27, 20.83, 25.08, 26.43, 27.36, 29.81, 32.94, 33.76, 35.54, 37.03, 37.99, 39.98, 40.39, 40.94, 42.86, 42.90, 42.99, 48.01, 48.24, 50.22, 71.34, 76.69, 109.27, 151.04

Lup-20(29)-ene-1 α ,3 β -diol White solid; m.p. 212 °C; IR (CHCl₃, cm⁻¹) ν_{\max} = 1653,



1764, 3400 cm⁻¹; GC-MS (ESI) m/z : Calcd for C₃₀H₅₀O₂, 426.39; found, [M-2H₂O], 406.3554; ¹H NMR (CDCl₃ 400 MHz): δ 0.70 (6 H, s), 0.80 (6 H, s), 0.88 (6 H, s), 0.99 (6 H, s), 1.05 (6 H, s), 1.69 (9 H, s), 2.39 (2 H, d, J =5.56 Hz), 3.34 - 3.60 (4 H, m), 3.67 (2 H, s), 4.57 (2 H, s), 4.69 (2 H, s); ¹³C

NMR (CDCl₃, 100 MHz): δ ppm 14.65, 15.94, 16.18, 17.73, 17.98, 18.01, 19.27, 20.83, 25.08, 26.43, 27.36, 29.81, 32.94, 33.76, 35.54, 37.03, 37.99, 39.98, 40.39, 40.94, 42.86, 42.90, 42.99, 48.01, 48.24, 50.22, 71.34, 76.69, 109.27, 151.04.

4A. 5 Spectral Copies

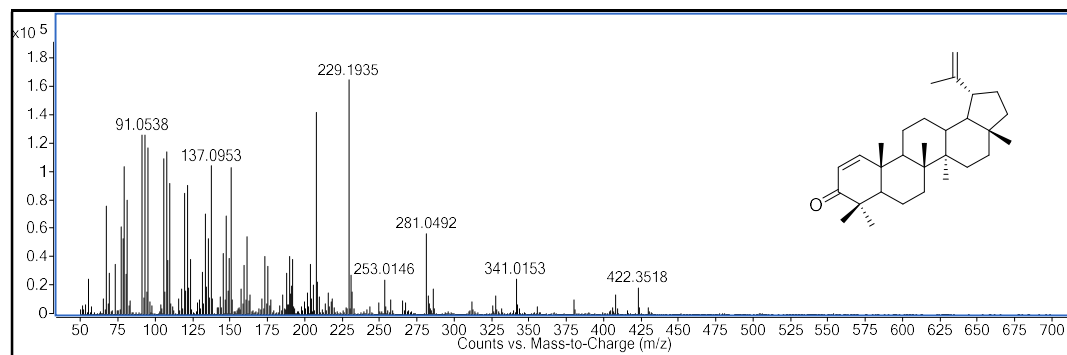
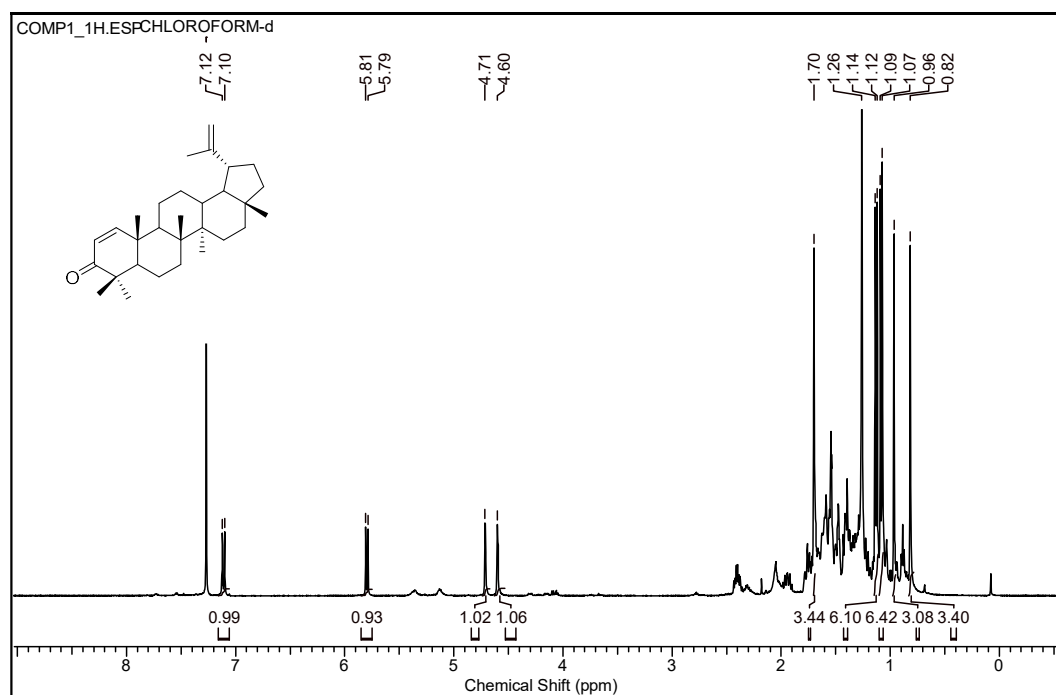


Figure 4A.3a. GC-EI-QToF-MS spectrum of glochidion [M]

Figure 4A.3b. ¹H-NMR spectrum of Glochidion (CDCl₃)

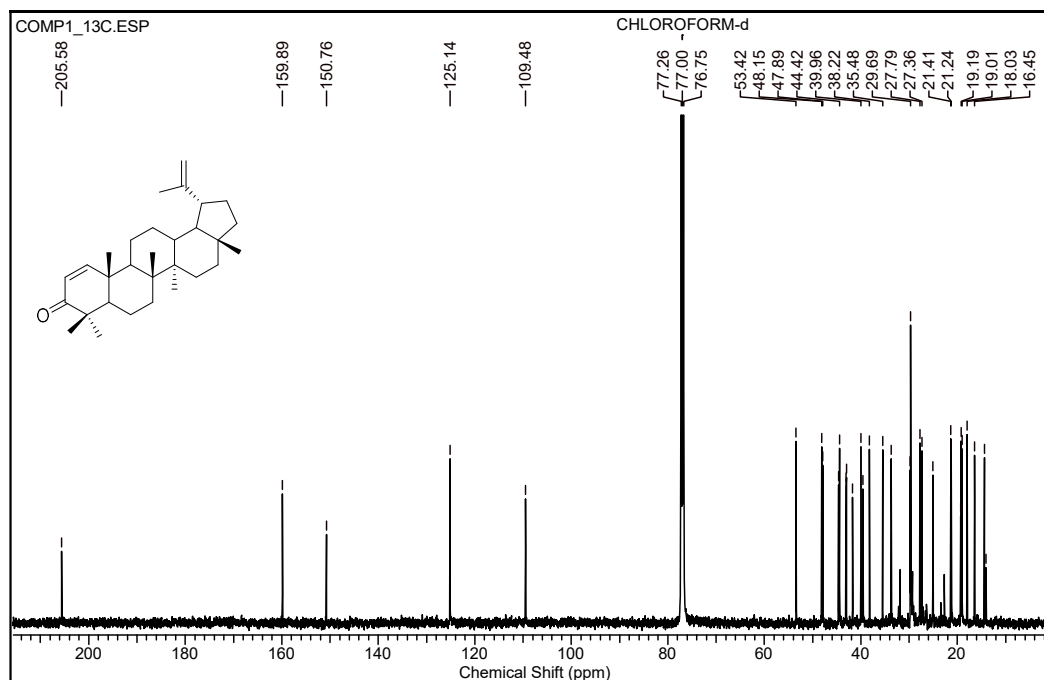
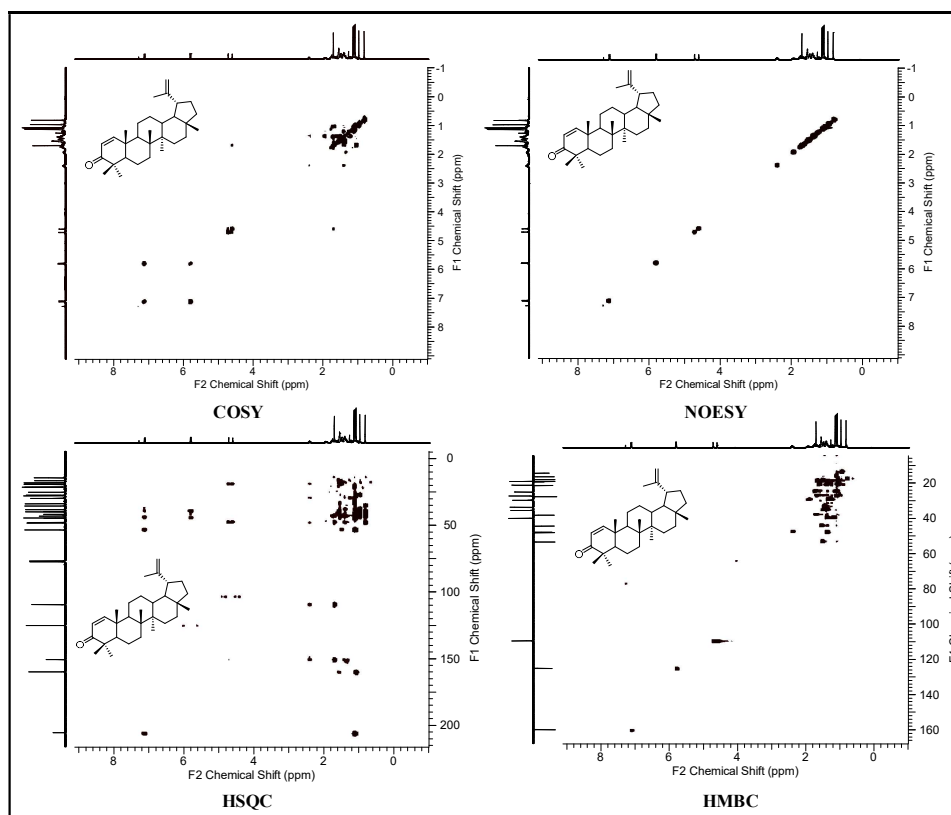
Figure 4A.3c. ^{13}C -NMR spectrum of Glochidion (CDCl_3)

Figure 4A.3d. COSY, NOESY, HMBC and HSQC spectrum of glochidion.

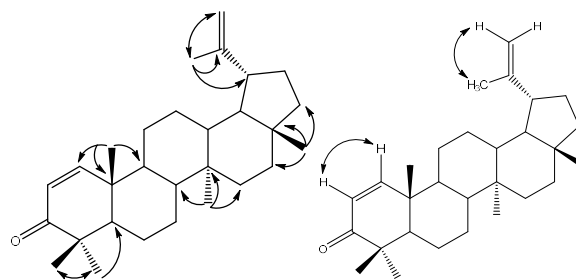
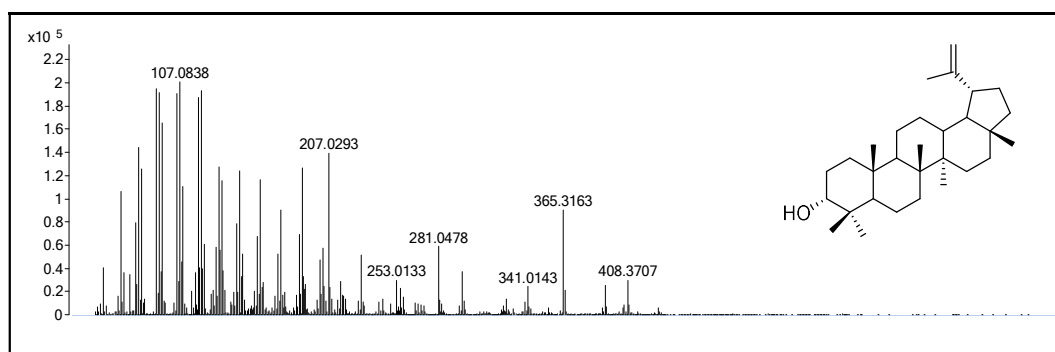
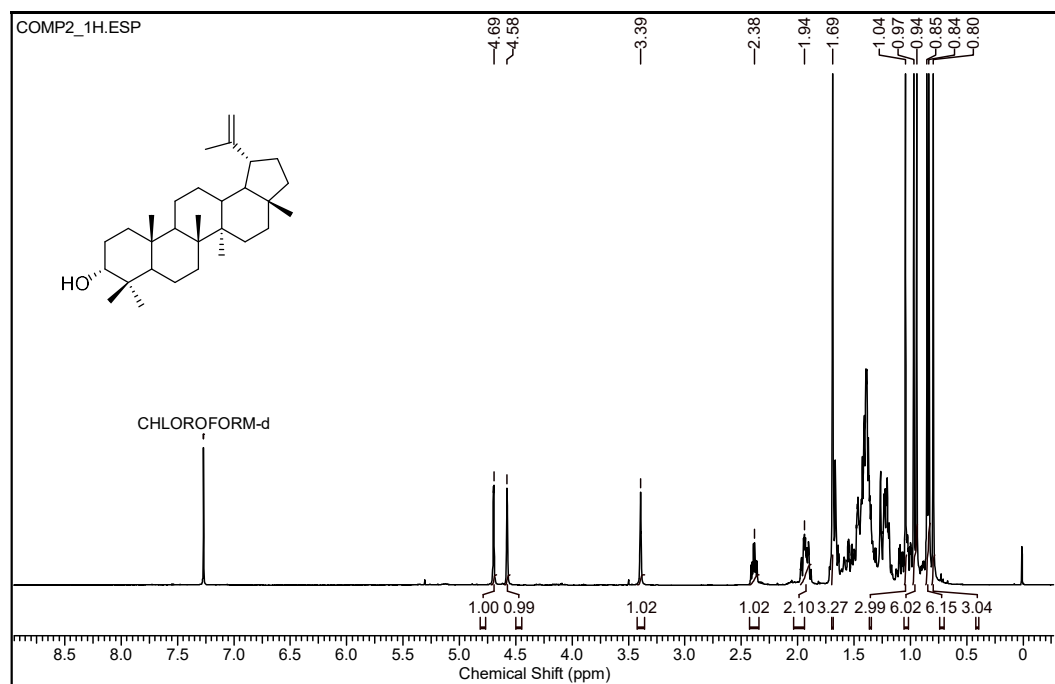
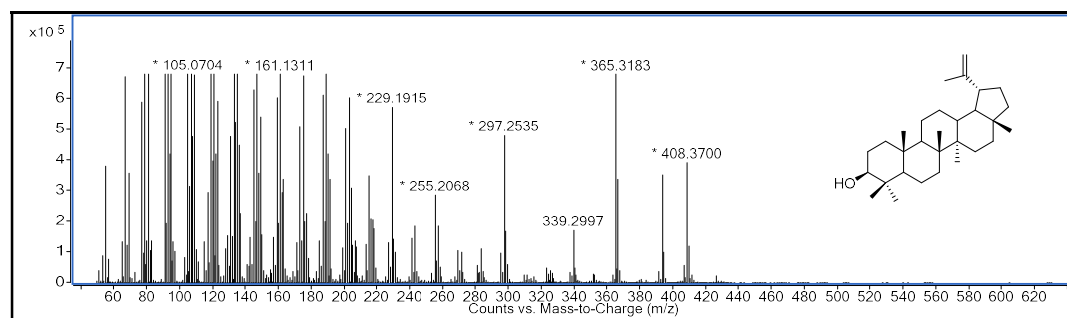
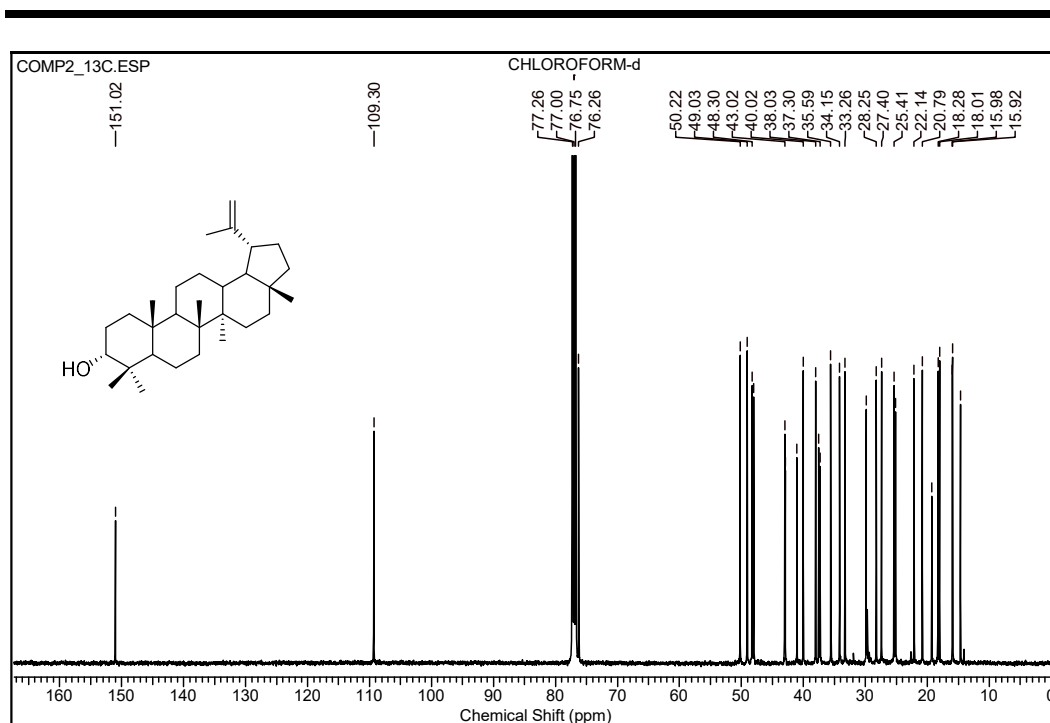
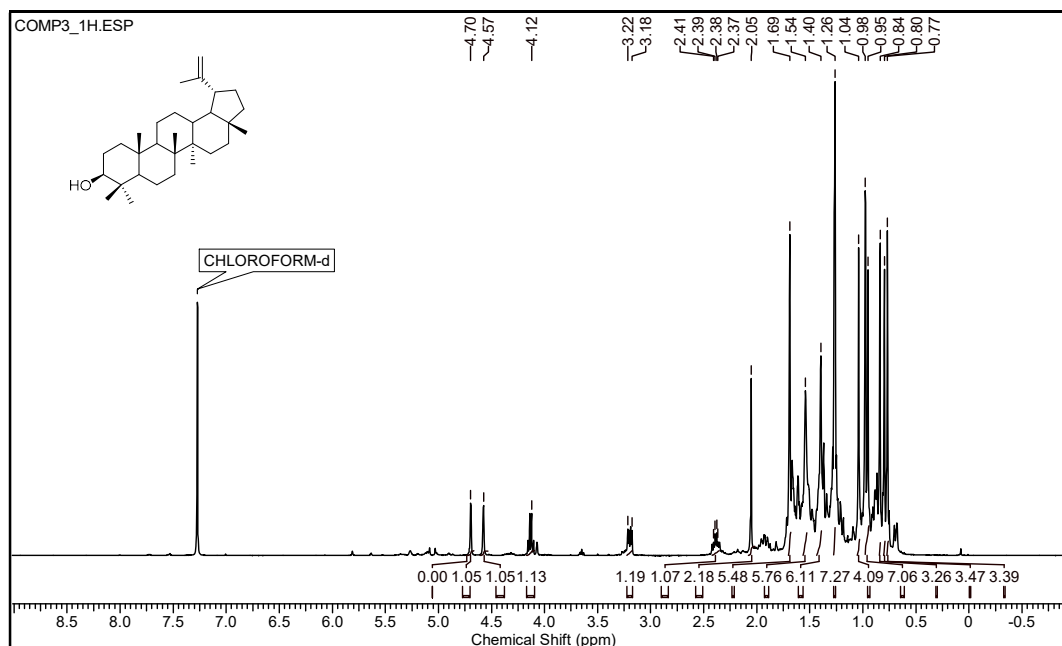
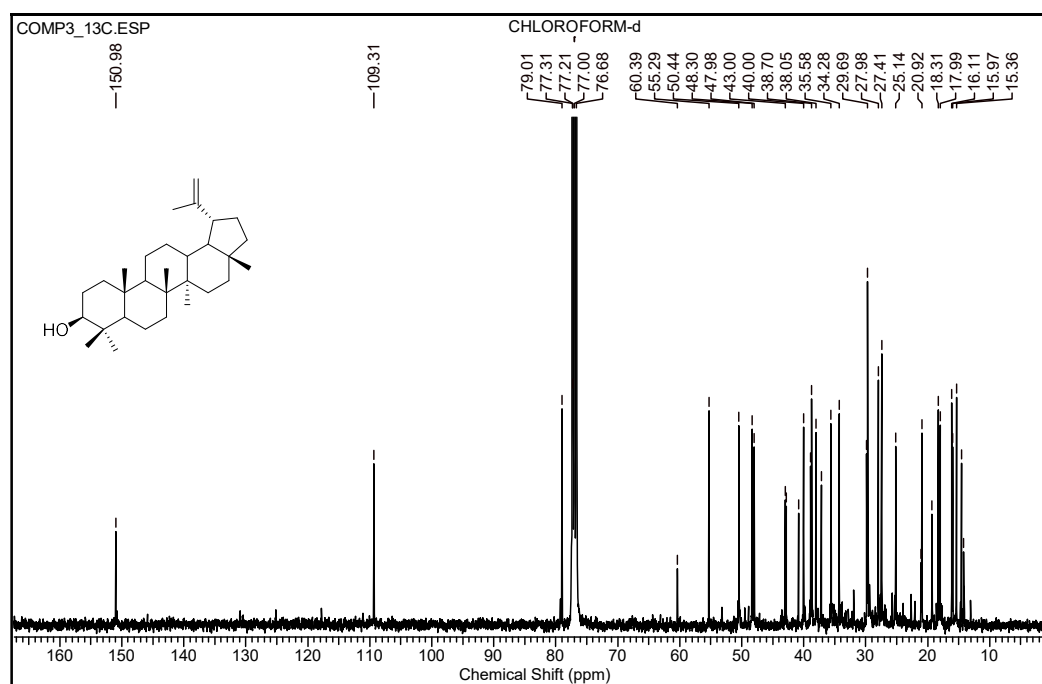


Figure 4A.3f. HMBC and COSY correlation of glochidion

Figure 4A.4a. GC-EI-QToF-MS spectrum of epilupeol [M-H₂O]Figure 4A.4b. ¹H-NMR spectrum of epilupeol (CDCl₃)



Figure 4A.5b. ^1H -NMR spectrum of lupeol (CDCl_3)Figure 4A.5c. ^{13}C -NMR spectrum of lupeol (CDCl_3)

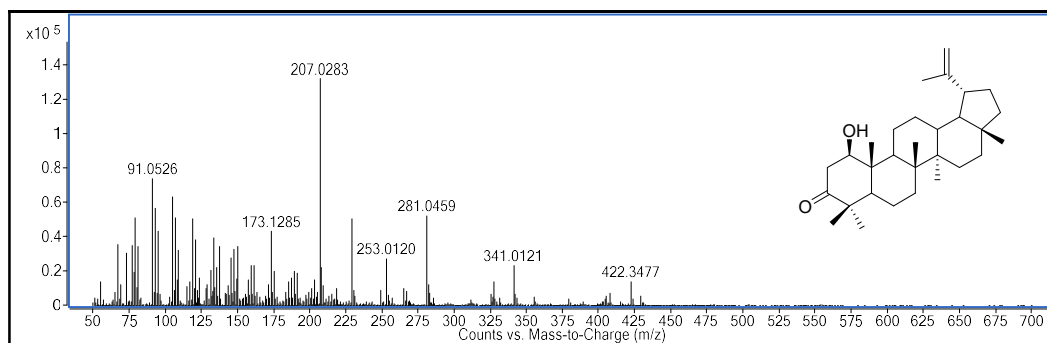


Figure 4A.6a. GC-EI-QToF-MS spectrum of glochidonol [M-H₂O]

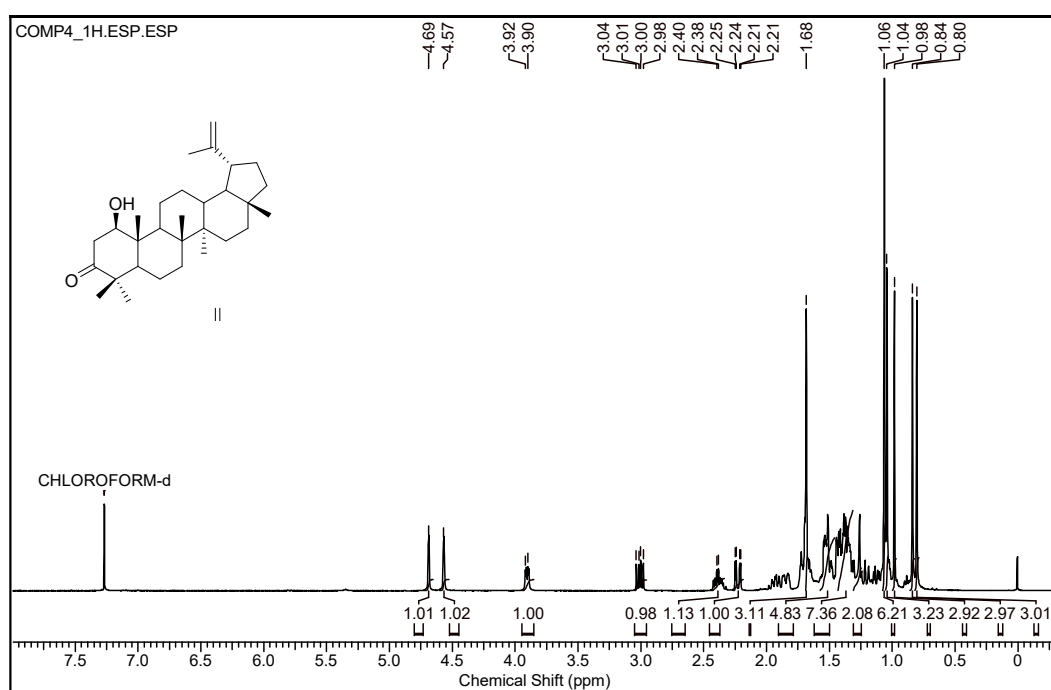


Figure 4A.6b. ¹H-NMR spectrum of Glochidonol (CDCl₃)

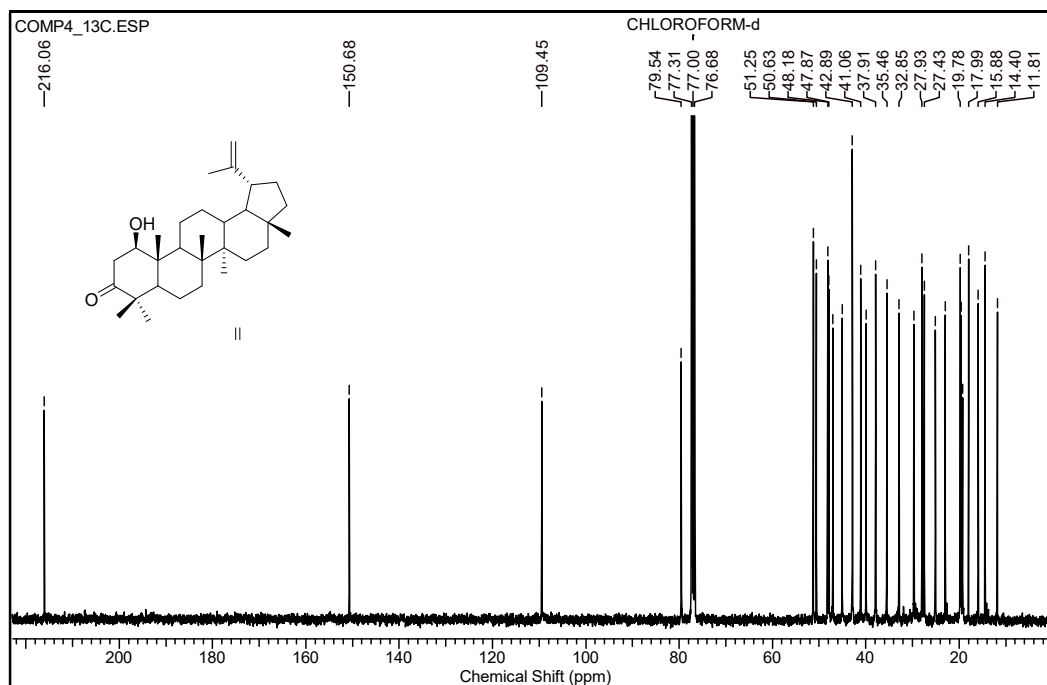


Figure 4A.6c. ^{13}C -NMR spectrum of Glochidonol (CDCl_3)

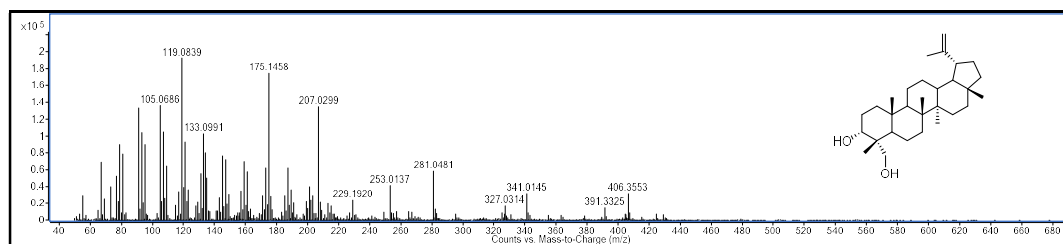


Figure 4A.7a. GC-EI-QToF-MS spectrum of Lup-20(29)-ene-3 β ,23-diol [$\text{M}-2 \text{H}_2\text{O}$]

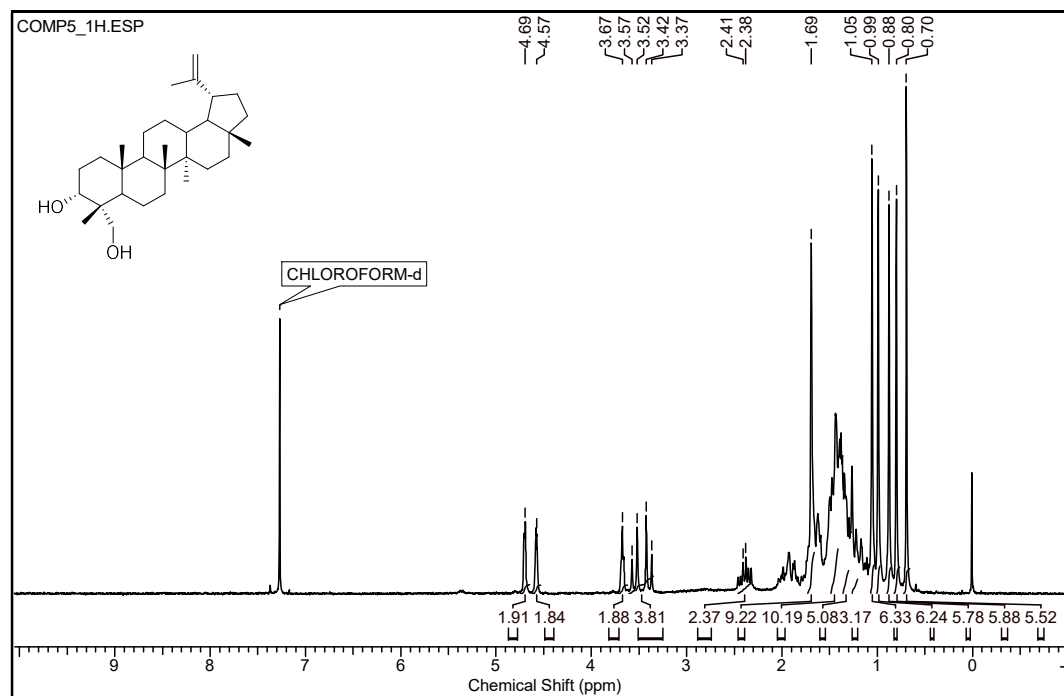


Figure 4A.7b. ^1H -NMR spectrum of Lup-20(29)-ene-3 α ,23-diol (CDCl_3)

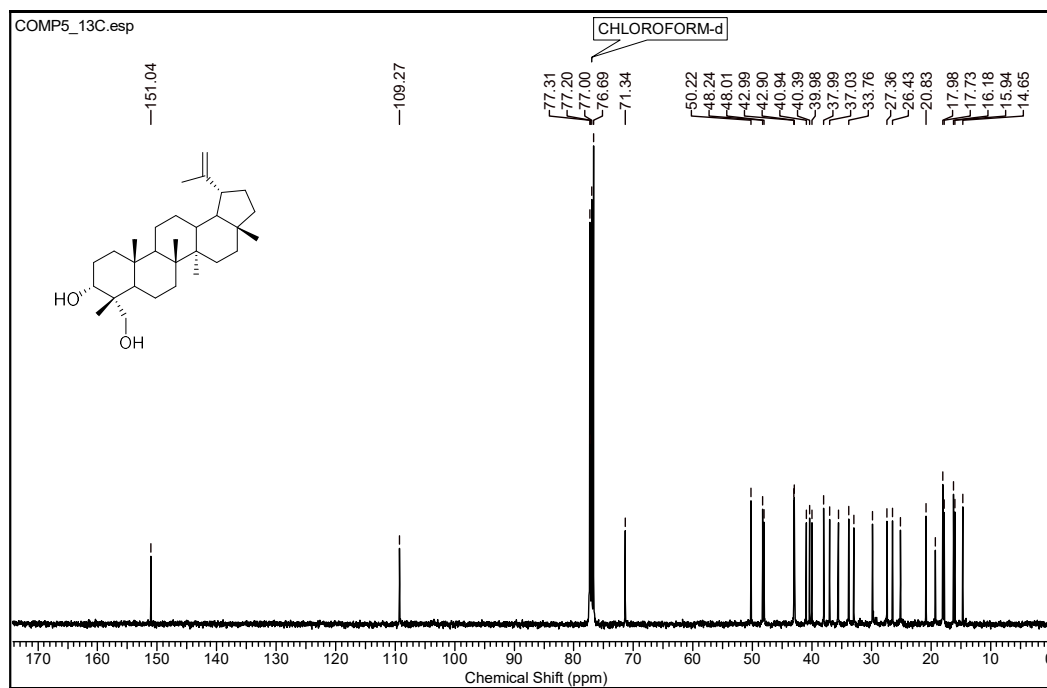


Figure 4A.7c. ^{13}C -NMR spectrum of Lup-20(29)-ene-3 α ,23-diol (CDCl_3)

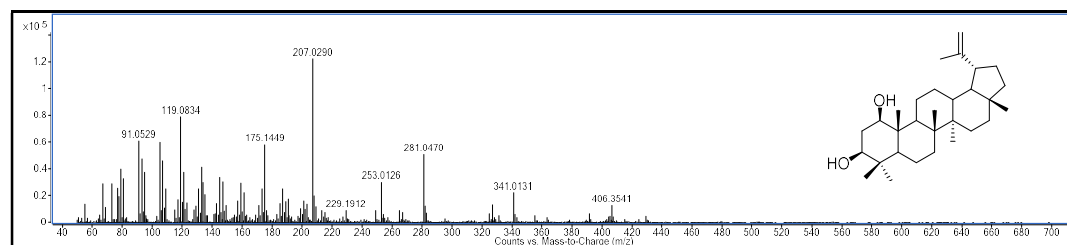


Figure 4A.8a. GC-ESI-QToF-MS spectrum of Glochidiol [M-2 H₂O]

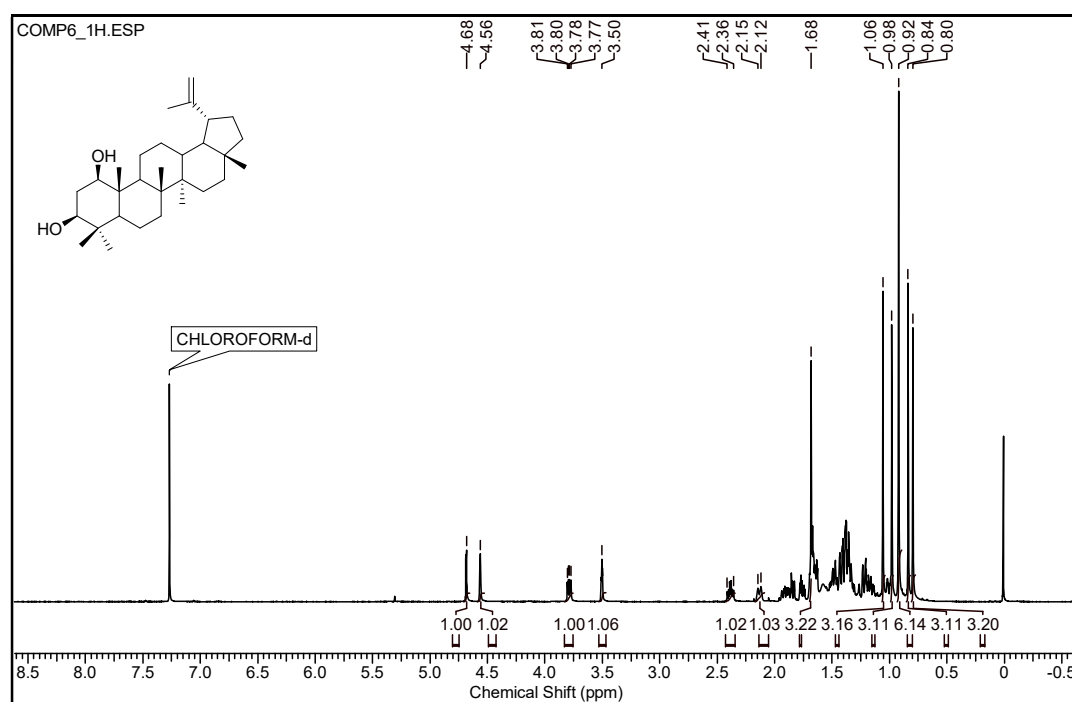


Figure 4A.8b. ¹H-NMR spectrum of Glochidiol (CDCl₃)

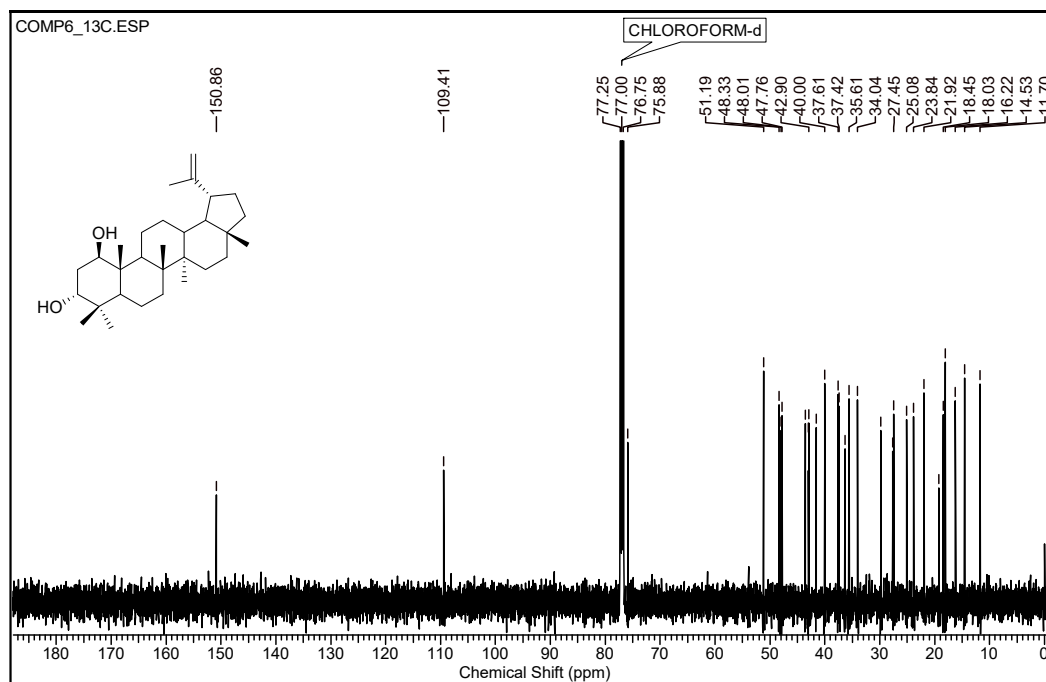


Figure 4A.8c. ^{13}C -NMR spectrum of Glochidiol (CDCl_3)

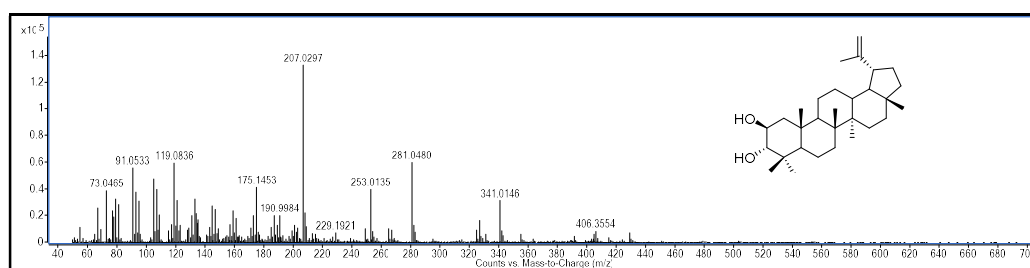


Figure 4A.9a. GC-EI-QToF-MS spectrum of Lup-20(29)-ene- $[\text{M}-2\text{H}_2\text{O}]$

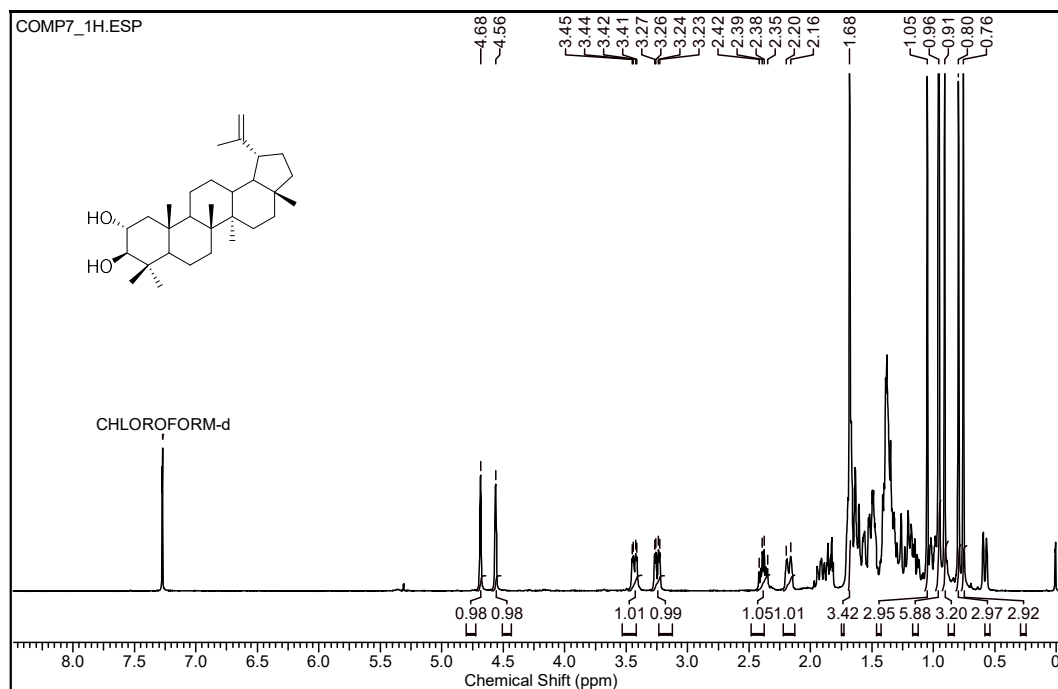


Figure 4A.9b. $^1\text{H-NMR}$ spectrum of Lup-20(29)-ene-11 β ,3 α -diol (CDCl_3)

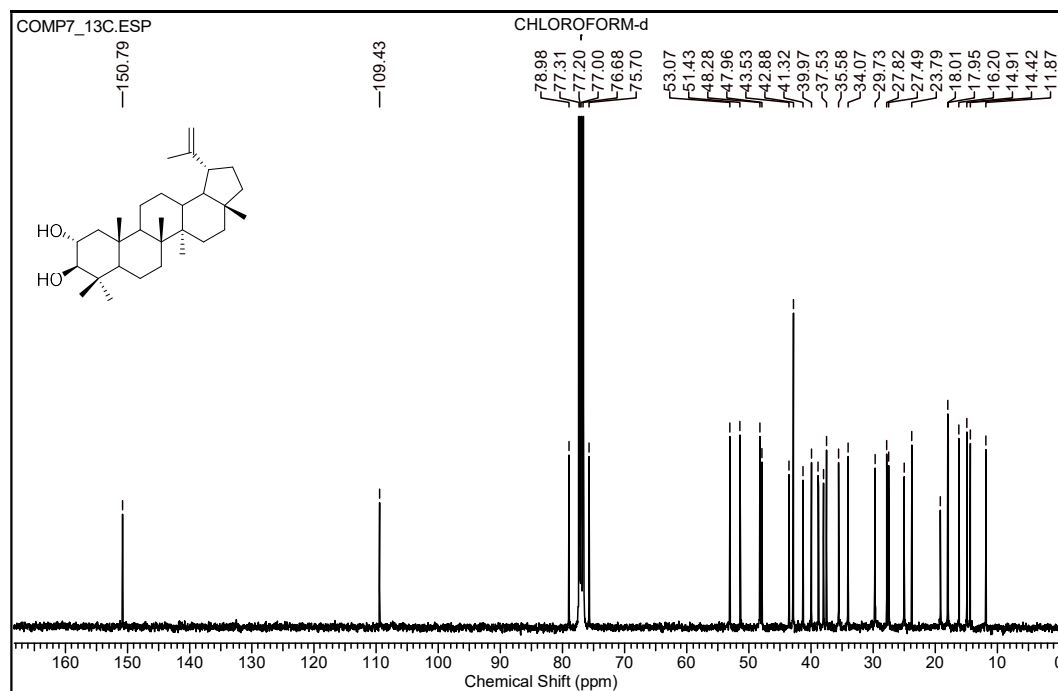


Figure 4A.9c. $^{13}\text{C-NMR}$ spectrum of of Lup-20(29)-ene-11 β ,3 α -diol (CDCl_3)

Chapter 4: Section B

**Self-Assembly Study of a Renewable Triterpenoid
Glochidonol Isolated from *Glochidion tomentosum***

4B.1 .Introduction

Self-assembly of low molecular weight gelators (LMWGs) in organic solvents has become an interesting research area in recent years.^{16,17,18,19} LMWGs form a supramolecular structure by self-assembly, which yields porous microstructure, e.g. spherical, flower-like, vesicles, fibrillar network.^{20,21,22,23} Which are reported to have significant applications such as, to capture pollutant,²⁴ as drug delivery vehicle in tissue engineering, and as a template for nanomaterials.

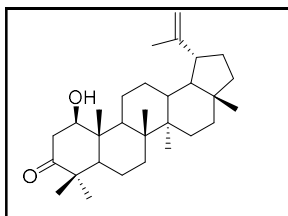


Figure 4B.1 Chemical Structure of Glochidonol

^{25,26} Literature survey on self-assembly of LMWGs resulted in studies on varying classes of molecules such as sophorolipid, fatty acids, peptides, steroids, with very few reports on terpenoids self-assembly.^{27,28,29,30} Terpenoids are desirable candidates as LMWGs because of their easy accessibility, rigid structure with several chiral centres on the skeleton, various functional groups, availability with renewable supply and no need of multistep chemical synthesis but

very few reports were available on terpenoid gelation.³¹

This study involves Glochidonol (1), a lupane pentacyclic (6-6-6-6-5) triterpenoid isolated from *G. tomentosum*, possesses gelation properties in various solvents. This is the first report on glochidonol gelation in a various solvent with systematic self-assembly study. Further, to gain insight in glochidonol self-assembled structures, its physical properties were studied by using optical, scanning electron and atomic force microscopy, Fourier-transform infrared spectroscopy. Glochidonol form self-assembled fibrillar network (SAFIN) and morphology of gel changed as the gelation solvent change. The further gel has been utilized in order to entrap the fluorescein isothiocyanate as a model drug.

4B.2 Result and discussion

4B.2.1 Glochidonol Gelation Test in Various Solvent

The gelation ability of glochidonol was tested in a various solvent by dissolving compound in solvents by sonication and allowed the solution to cool at room temperature. As the materials did not flow by turning the vials upside down, we called it as a gel.

Table 4B.1 Self-assembly studies of Glochidonol gels in various solvents

Entry	Solvent	State	Gel	Conc. % (w/v)
1.	Benzene	G	Transparent	2.5
2.	o-xylene	G	Transparent	2.5
3.	m-xylene	G	Transparent	2.5
4.	Toluene	G	Transparent	2.4
5.	Bromobenzene	G	Transparent	4
6.	Chlorobenzene	PG	opaque	5
7.	Dichlorobenzene	PG	opaque	5
8	Nitrobenzene	PG	opaque	5
9.	Methanol	G	opaque	2.7
10.	Ethanol	G	opaque	2.7
11.	Acetone	G	opaque	2.7
12.	n-butanol	G	opaque	2.7
13.	Pet ether	G	opaque	25
14.	Carbon tetrachloride	G	opaque	3
15.	Ethanol: water (1:1)	G	opaque	3.5
16.	DMSO :water (1:1)	CS	opaque	5

G. = gel, PG= partial gel, CS= colloidal suspension, sonication at 40 °C.

Among the sixteen solvent tested glochidonol formed a gel in twelve solvents, partial gel in three solvents and formed colloidal solution in dimethyl sulfoxide: water (1:1) (Table 4B.1). Gel

formed in benzene (2.5 w/v), o-xylene (2.5 w/v), m-xylene (2.5 w/v), toluene (2.4 w/v) and bromobenzene (4 w/v) was tough and appeared transparent in nature but in case of butanol, pet ether and chloroform gel was opaque in nature. In chlorobenzene, dichlorobenzene and nitrobenzene partial gelation observed. In petrol, Glochidonol formed a gel with at 4 % w/v.

4B.2.3 Optical Microscopic Images of Glochidonol Self-assembly

Solvents effect on the morphology of self-assembly was investigated by optical microscopy. Optical microscopic images of self-assembled glochidonol gel in carbon tetrachloride showed needle-like morphology, in butanol resulted in fibrillar morphology in which fibres were interwind. Whereas in toluene it appeared like folded sheets (Figure. 4B a, b, c).

4B.2.4 Scanning Electron Microscopy Images of SAFIN Self-assemblies

To gain better insight into the gel structures formed, SEM images of gels formed in butanol, toluene and carbon tetrachloride were taken. Scanning electron microscopy studies carried out with glochidonol xerogel.

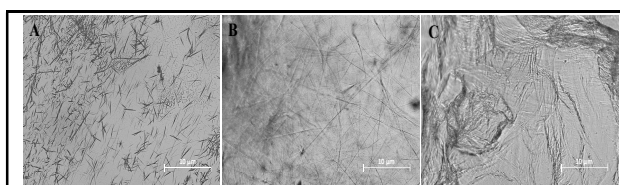


Figure 4B.2 Optical microscopy image of glochidonol self-assembly in, (a) carbon tetrachloride (3 % w/v), (b) butanol (2.5 % w/v), (c) toluene (2.4 % w/v).

It was prepared by evaporating of solvent slowly from a glochidonol solution at gelation concentration in dust free environment at room temperature. SEM images showed that gel is a densely packed fibrillar network of a microstructure having intertwined fibres ranging from nm to μm in size, which varies with the solvent system used. Xerogel formed in butanol is loosely packed fibres of diameter (70-200 nm) (Figure 4B.2 a, d), whereas the densely packed fibrillar network formed in toluene xerogel (Figure 4B.2 b, 4e), and tiny crystal-like structure observed in carbon tetrachloride (Figure 4B.2 c, f). Scanning electron microscopic images are in agreement with optical microscopic images.

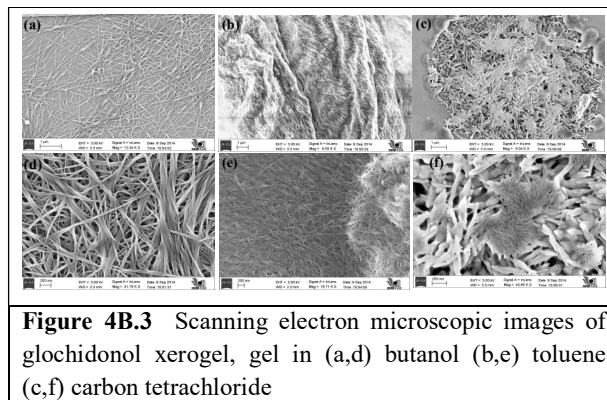


Figure 4B.3 Scanning electron microscopic images of glochidonol xerogel, gel in (a,d) butanol (b,e) toluene (c,f) carbon tetrachloride

4B.2.5 Atomic Force Microscopy (AFM) Studies

Gel surface nature was examined by using AFM analysis. The AFM image of an air-dried sample of glochidonol in butanol (2.7 % w/v) and toluene (2.4 % w/v) (Figure 4.5A) suggested the inter wind fibrillar nature of self-assembly. The AFM images are in also agree with that of SEM and optical microscopic images

4B.2.5 Atomic Force Microscopy (AFM) Studies

Gel surface nature was examined by using AFM analysis. The AFM image of an air-dried sample of glochidonol in butanol (2.7 % w/v) and toluene (2.4 % w/v) (Figure 4.5A) suggested the inter wind fibrillar nature of self-assembly. The AFM images are in also agree with that of SEM and optical microscopic images

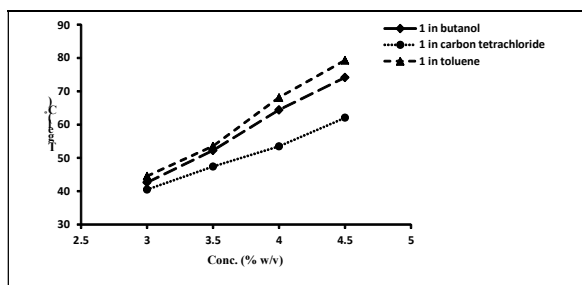


Figure 4B.4 Plot of T_{gel} Vs concentration of glochidonol in butanol, carbon tetrachloride and toluene

4B.2.6 Gelation Temperature

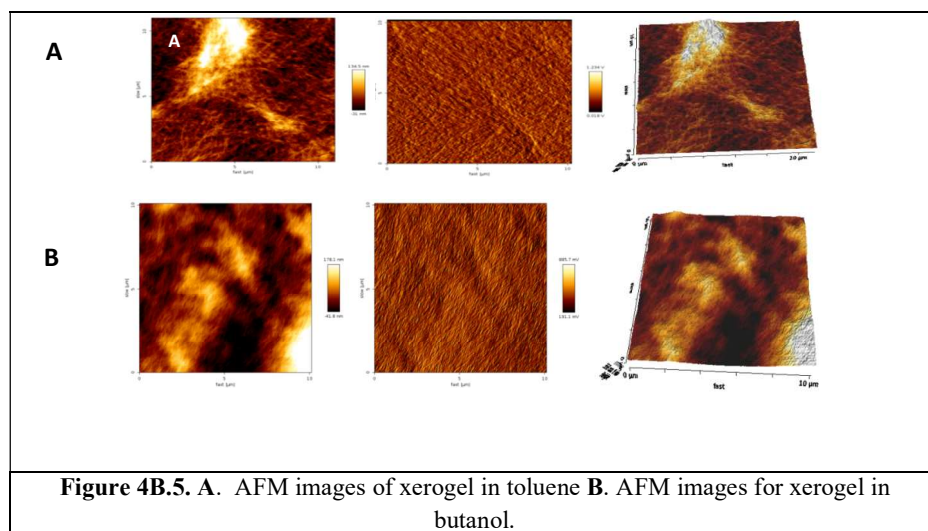
Thermal stability of gel in various solvent was determined by plotting gel-to-sol melting temperature, T_{gel} versus glochidonol concentration (% w/v). T_{gel} increased with the gel concentration which indicated that self-assembly formed due to intermolecular interactions. The gel in butanol and toluene has higher T_{gel} value

compared to the gel in carbon tetrachloride (Figure 4B.3). A steeper increase in T_{gel} values with concentration was observed.

4B.2.7 Structural Analysis FTIR Studies

Formation of molecular self-assembly is believed because of the availability of free hydroxyl moiety in the molecule, which forms the non-covalent interactions H-bonding, the dispersive interactions in backbones. The stretching frequency of the “-OH” group in FTIR-spectra of neat powder appeared at 3413.6 cm^{-1} , whereas the “-O-H” stretching frequencies of xerogel in toluene, butanol and carbon tetrachloride appeared at 3425.7 cm^{-1} , 3395.5 cm^{-1} , 3426.3 cm^{-1}

respectively. Results suggested that the hydroxyl and carbonyl stretching frequency shift indicated that the self-assembly is due to the H-bonding.



4B.2.8 Rheological Study of Self-assembly

In order to study the structural integrity of the molecular gel, dynamic rheological experiments were performed, when subjected to shear deformation (γ) and corresponding shear stress (τ). The storage modulus (G') and loss modulus (G'') are measures of the recoverable elastic response and dissipative viscous behaviour, respectively.^{32,18} The storage (G') and loss (G'') moduli of the gel samples are distinct from one another. Storage moduli are higher the order of $G' \approx 106$ Pa was observed in case of bromo-, chlorobenzene and toluene. The loss moduli lower the order of $G'' \approx 104$ - 106 Pa was observed in case of bromobenzene, chlorobenzene and toluene (Figure 4B a, b, c). The loss tangent ($\tan \delta = G'/G''$) versus frequency plot shows characteristic peaks appearing in case of bromo-, chlorobenzene and toluene corresponding to phase changes gradually from 0.0 -100 rad/sec. Strain sweep rheological properties for glochidonol gel (a') bromobenzene, (b') chlorobenzene, (c'), toluene as a function of strain, $\omega = 0.001$ -00 %, at 25 °C storage moduli G' , loss moduli G'' , and loss tangent ($\tan \delta = G'/G''$) (Figure 4B a', b', c')

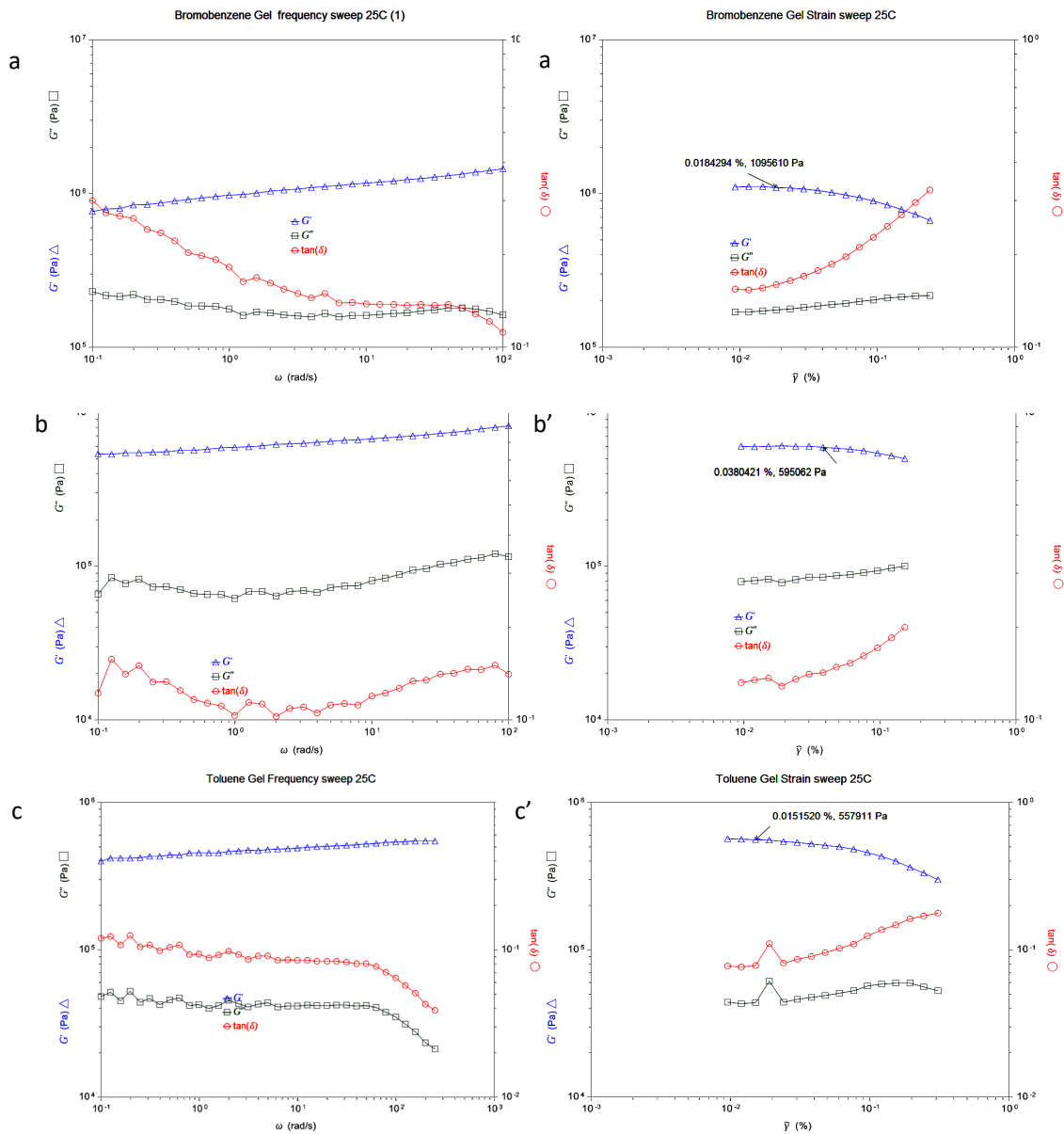


Figure 4B.6. Frequency sweep rheological properties under shear deformation for glochidonol gel (a) bromobenzene, (b) chlorobenzene, (c) Toulene as a function of oscillatory angular frequency, $\omega = 0.1$ – 100 Hz: strain = 1% , at 25°C storage moduli G' , loss moduli G'' , and loss tangent ($\tan \delta = G''/G'$). Strain sweep rheological properties for glochidonol gel (a') bromobenzene, (b') chlorobenzene, (c') Toulene as a function of strain, $\omega = 0.001$ – 00% , at 25°C storage moduli G' , loss moduli G'' , and loss tangent ($\tan \delta = G''/G'$).

4B.2.9 Adsorption of 5(6)carboxyfluorescein (CF) in Glochidonol Fibrillar Microstructure

Biocompatible nanocarrier development for efficient drug delivery has been an emerging area of

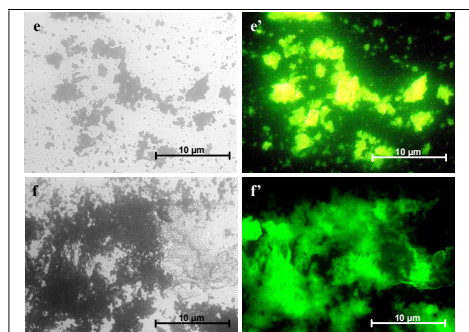


Figure 4B.7 Optical and epifluorescence microscopic images of (e, e') glochidonol gel in 1,4-dioxane containing CF entrap; Release of CF (f, f'), from 1 gel

research. In order to examine the adsorption capability of glochidonol fibrillar self-assembly to the small molecules, we have studied the adsorption of 5(6)carboxyfluorescein fluorophore as a model compound. Epifluorescence images suggested that the fluorescence was adsorbed in the self-assembly, (Figure 4B.6 e, e') and dispersed after triton-X treatment (Figure 4B.6 f, f'). The result suggested that the glochidonol self-assembly entrap the fluorophore.

4B.3 Conclusions

Self-assembly of glochidonol was investigated in a different solvent. It is formed a fibrillar network, which made up of individual fibres with nanometer diameter to micrometre width. Rheological studied showed that the material is viscoelastic dispersion. The fibrillar microstructures of glochidonol have been utilised for the entrapping small molecule as shown by the epifluorescence experiment. Future investigating will explore the application of fibrillar dispersion as target drug delivery agents and other nanobiotechnological applications.

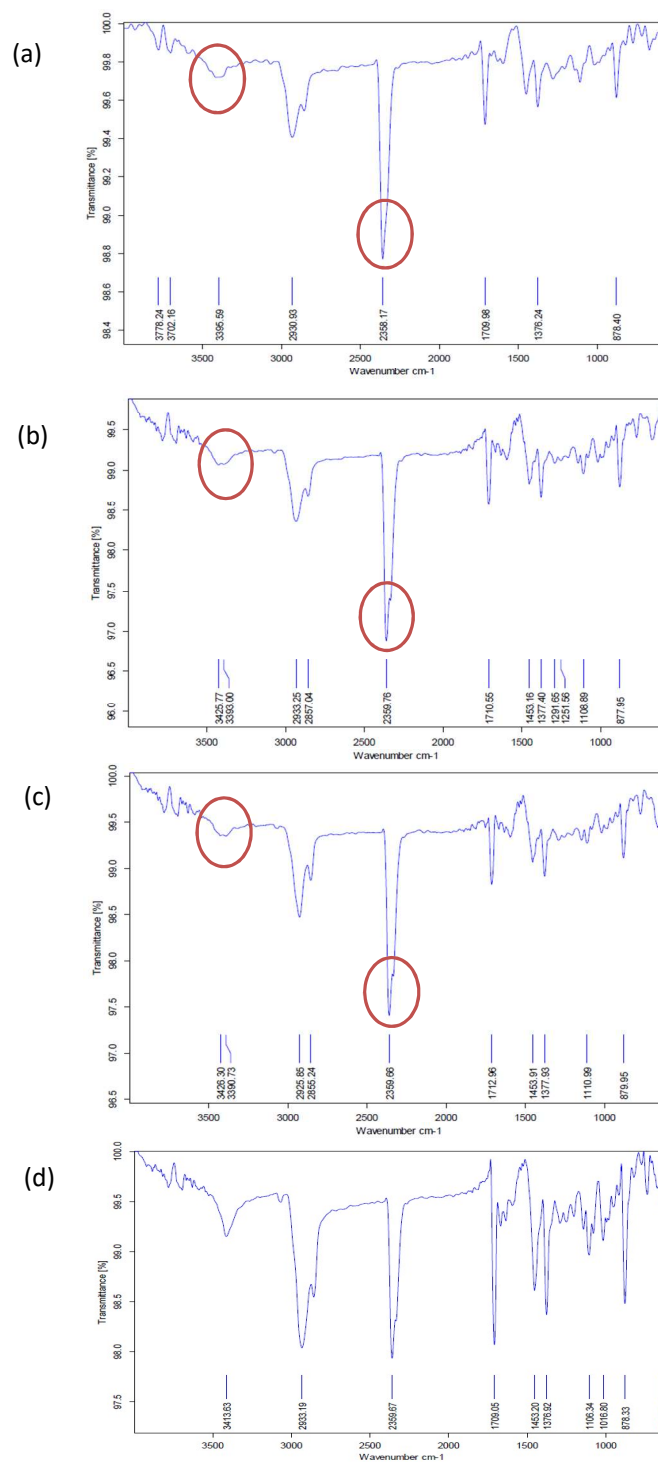


Figure 4B.8 IR-spectra of glochidonol in (a) neat powder glochidonol. (b) Glochidonol gel in toluene, (c) glochidonol gel in butanol, (d) glochidonol gel in bromobenzene.

4B.4 Experimental section

4B.4.1 Screening of Triterpenoid Gelation

Concentration was expressed in as % w/v toluene was used as the solvent for gelation screening and 5 % w/v of triterpenoid concentration. Glochidonol gelation was performed in 16 different organic solvents, the selection of which was based on nature of the solvent, e.g. aromatic, aliphatic as well as an aqueous solvent mixture (Table 4B.1, 4B.2). Compounds were weighed in the closed vial and toluene was added in it. The mixture was sonicated at 40 °C until it formed a clear solution and kept it at room temperature (typically ~ 1h). Gel formation is confirmed by the appearance and inverted vial method. For a detailed investigation of glochidonol self-assembly, we have screened various solvents. For similar gelation procedure was repeated as mentioned above.

Table 4B.2. Glochidion gelation test in aqueous and mixture of solvents

Entry	Solvent	State	Solubility of compound
1	Water	CS	Insoluble
2	Phosphate buffer (pH – 7.2)	CS	Insoluble
3	Ethanol: Water	G	Partially Insoluble
4	DCM: Water	CS	Partially soluble

G-gel, CS= colloidal suspension, glochidonol Concentration = 5 % (w/v), Sonication, 40 °C.

4B.4.2 Glochidinol Self assembly Studies

Glochidonol (1 to 6 % w/v) was dissolved in 1 mL of different solvent in 5 mL glass vial and sonicated at 40 °C until it gets dissolved. The solution was allowed to cool at room temperature; in the case of mixed solvents, Glochidonol was initially solubilised in the organic solvent under hot conditions then water was added gradually until cloudiness appeared. Further, the mixture was re-dissolved by sonication the clear solution thus obtained was allowed to cool at room temperature. The gelation was confirmed by an inverted vial method. Sonicator from BandelinSonorex 230 V ~ 50 /60 Hz, 1.0 A, 80/ 320 w, 35 KHz was used. Gel formation was confirmed by inverting the vial and observing for gelation. The gel obtained was resonicated at 40 °C to their sol phase add quickly transferred into capillary for further analysis of gelation temperature. The gel to sol transition temperatures T_{gel} was recorded by gradual heating of a gel sample contained in a capillary until the material started melting. Microscopy studies on the gel formed were performed taking sample spread on a glass slide, and self-assemblies were observed by optical microscopy. Zeiss Axiovertapotome microscope equipped with an AxioCam camera and oil-immersion objective (64x) was employed to record the images and processed with Axiovision 4.7 software. Scanning electron microscope (SEM) samples were

prepared by placing a thin film of a gel on a carbon grid and drying it at room temperature in the dust free environment and kept for 1-2 days in dust free environment. The gels were sputter coated with gold before SEM analysed in a Joel emission scanning electron microscope. Leica stereo scan 440 operated at an accelerating voltage of 15 kV with pressure $5.87E-4$ Pa, current 0.14 and WD 9.9-10.0 mm det EDT. The pre-scanned samples were sputter coated with 10 nm thick layers of gold nanoparticles by using a polaron SC 6420 sputter coater.

Table 4B.3 Gelation test at various concentrations in petrol and diesel

Entry	Glochidonol Conc. % (w/v)	Petrol
1	1	S
2	2	S
3	3	S
4	4	G

G= gel, S = solution.

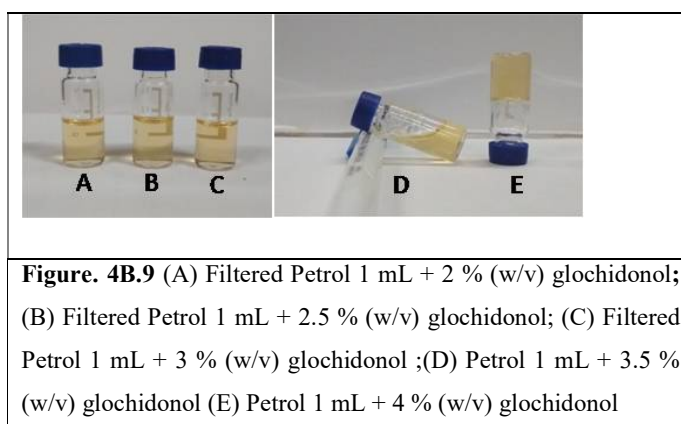


Figure. 4B.9 (A) Filtered Petrol 1 mL + 2 % (w/v) glochidonol; (B) Filtered Petrol 1 mL + 2.5 % (w/v) glochidonol; (C) Filtered Petrol 1 mL + 3 % (w/v) glochidonol ;(D) Petrol 1 mL + 3.5 % (w/v) glochidonol (E) Petrol 1 mL + 4 % (w/v) glochidonol

4B.4.3 Atomic Force Microscopy (AFM)

Drop casting the dilute dispersion of glochidonol in various solvents on a silicon wafer followed by drying under vacuum for 4 h. The Further AFM analysis was performed by using the Keysight atomic force microscope (model: AFM 5500) with tapping mode technique EHT = 3.00 kV, InLens.

4B.4.4 Rheological Study.

Rheology was performed using a TAARES rheometer equipped with a force rebalance transducer. Frequency sweep rheological properties under shear deformation for glochidonol gel in bromobenzene, chlorobenzene, toluene as a function of oscillatory angular frequency, $\omega = 0.1-100$ Hz: strain = 1%, at 25 °C storage moduli G' , loss moduli G'' , and loss tangent ($\tan \delta = G''/G'$).

4B.4.6 Small Molecule Adsorption Study

5(6)carboxyfluorescein was used as a model drug for glochidonol gel entrapment studies.^{33,34} For entrapment of fluorophores in glochidonol fibrillar self-assembly, added a hot solution of glochidonol(42.0mM) in 1,4-dioxane containing 5(6)carboxyfluorescein (0.06 mM) kept at room temperature for 15 min and observed under a fluorescent microscope. Further, entrap vesicular self-assembly of glochidonol was treated with of Triton X-100. The vesicles became larger within 20 min and appeared as green colour fluorescent background. The disappearance of the fibrillar self-assembly was observed within a couple of 30 min in the fluorescent microscopic images (Figure 4B.7).

Chapter 4: Section C

Terpenoids Isolation from *Wedelia paludosa* and Chemical Modification for Its Function as Glucosidase Inhibitors

4C.1 Introduction

Wedelia paludosa D. C. spread in warm temperate and tropical regions such as India, China, Burma, and Japan.³⁵ Several species of the genus *Wedelia* are employed in the traditional medicinal system e.g. Ayurvedic medicine and Chinese system of medicine for the treatment of respiratory tract infections, digestive problems, and fever.^{36,37,38} *W. paludosa* have significant

Order	<i>Asterales</i>
Family	<i>Asteraceae</i>
Subfamily	<i>Asteroideae</i>
Tribe	<i>Heliantheae</i>
Subtribe	<i>Ecliptinae</i>
Genus	<i>Wedelia</i>
Species	<i>W. paludosa</i>

medicinal properties such as antipyretic, antimicrobial, anti-diabetic, hepatoprotective.³⁹ *W. paludosa* plant extract was tested for analgesic, anti-inflammatory, anti-rheumatic, antipyretic and anti-anaemic activities. The effect of *W. paludosa* against various disorders, including cough and painful conditions reported by Roque *et al.*⁴⁰ Leaves extracts from *W. paludosa* were exhibits antifungal activity reported by Sartori *et al.*⁴¹

Bioactive natural product with their derivatives is the remain a strategy for the discovery of new lead compounds for new therapeutic agents developments.⁴² Kaurenoic acid (KA) is the principal constituent present in *W. paludosa* which exhibits bioactivities such as antibacterial, antifungal, muscle relaxant effects, anti-diabetic.^{43,44,45} Chemical derivatization of kaurenoic acid exhibits various bioactivities with the improve in potency.^{46,47} Matos *et al.* tested semisynthetic derivatives of kaurenoic acid and copalic acid for anti-tuberculosis activity. (4 β)-10 α -hydroxy-4 β ,8,8-trimethyldodecahydrophenanthren-2(1H)-one is the derivative showed enhanced in the anti-tuberculosis activity compared to the parent kaurenoic acid.⁴⁸

Herein we have isolated kaurane terpenoids along with alanatalactone and steroids from *Wedelia paludosa*. We have synthesised semi-synthetic derivatives of kaurenoic acid and grandiflorenic acid. Further kaurenoic acid and derivatives tested as α -glucosidase inhibitors.

4C.2 Results and Discussion

4C.2.1 Isolation of Terpenoids from *Wedelia paludosa* Powder

Extraction and purification of *Wedelia paludosa* aerial part powder resulted in the isolation of five terpenoids. Out of which three are kaurane diterpenoid, steroids, sesquiterpenoid which are characterised as kaurenoic acid, grandiflorenic acid, isokaurenoic acid, stigmasterol, alanatalactone.

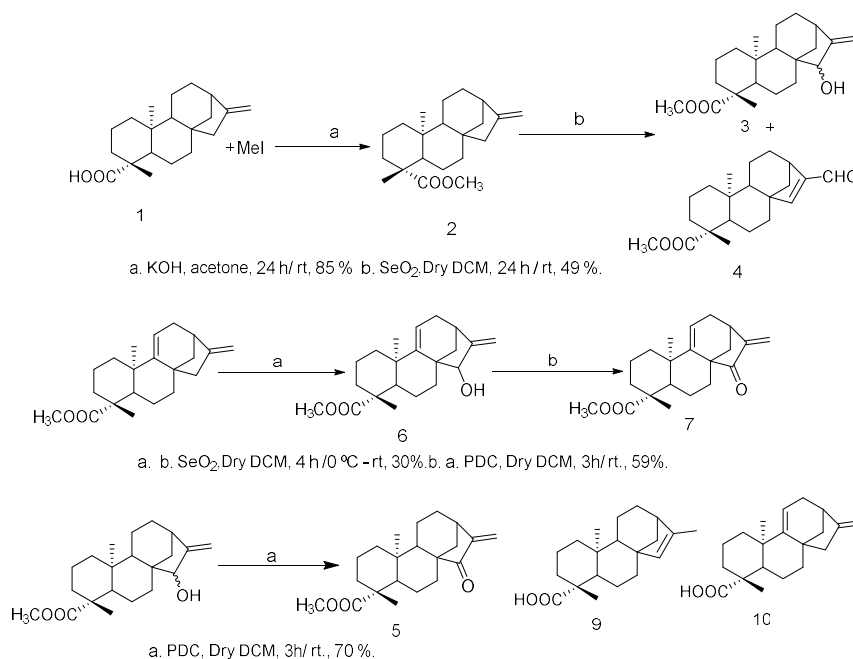
The green extract obtained after aerial part powdered extracted in acetone. The extract was then fractionated by using flash column chromatographic techniques with ethyl acetate in pet ether as eluent. Fractionated obtained was further purified by repeated flash chromatography with fine silica gel. Few fractions were unable to separate on normal silica gel chromatography hence purified over silver nitrate coated silica gel. Isolation of terpenoids on a preparative scale followed similar parameters as mentioned in chapter 2 with high purity. The purity as determined by GC of kaurenoic acid, grandiflorenic acid, isokaurenoic acid, stigmasterol, alanatalactone was 99.2 %, 97 %, 97.1 %, 99.1 %, and 98% respectively.

4C.2.2. Characterization of Terpenoid

Purified terpenoids were characterised by using NMR spectrometric and GC-MS data, which were in agreement with the earlier reported. Compound 1 was obtained as a solid GC-EI-QToF-MS spectrum of the compound showed at m/z 302. 2187 with molecular formula $C_{20}H_{30}O_2$ as reported earlier, it was diterpenoid with six degrees of unsaturation. IR spectrum showed a stretching frequency at 1735 cm^{-1} indicating the presence of acid, stretching frequency at 1645 cm^{-1} suggested alkene double bond. UV-peak at 280 nm showed the presence of acidic functionality in the compound. ^{13}C -NMR spectrums of the compound showed a peak at δ 155.93, and 103.01 showed the presences of two alkenes carbon out of which one are primary, one is quaternary. DEPT showed seven methylene groups, three methyl groups, two quaternary carbons and seven methines. ^1H -NMR spectrums showed a peak for two hydrogens at 4.80 and 4.74 of alkenes group. The characterization data analysis and comparing with the earlier reports compound-1 was characterised as kaurenoic acid. Similarly, the structural analyses of all the other compounds were performed and compounds were characterised.⁴⁹

4C.2.3 Synthesis of Kaurenoic Acid Derivatives

An earlier report suggested that it showed antidiabetic activity,⁵⁰ in order to explore active skeleton of kaurenoic acid for more potent derivatives we have synthesized various kaurenoic acid derivatives (Scheme 4C.1).



Scheme 4C.1 Synthesis of kaurenoic acid derivatives

4C.2.4 Glucosidase assay

Kaurenoic acid and its derivatives were screened for α -glucosidase inhibitory activity at 10 mM concentration (Table 4C.1). The result suggested that maximum derivatives were exhibited α -glucosidase inhibition compared to the parent molecule. Kaurenoic acid showed IC₅₀ of 42.33 μ M; whereas the Methyl *ent*-kaur-16-*en*-19-*oate* exhibits IC₅₀ of 38.19 μ M indicated that carboxyl hydroxyl might be involved in the inhibition. Methyl *ent*-kaur-15-*hydroxy*-19-*oate* derivative was most potent with an IC₅₀ of 79.35 μ M compared to the other kaurenoic acid derivatives.

Table 4C.1 Glucosidase Inhibitory Activity of Kaurenoic acid and derivatives

Compound	α -Glucosidase
Kaurenoic acid (1)	42.33
Methyl <i>ent-kaur-16-en-19-oate</i> (2)	38.19
Methyl <i>ent-kaur-15-hydroxy-19-oate</i> (3)	79.35
Methyl <i>ent-kaur-15-en-17-ald-19-oate</i> (4)	68.24
Methyl grandiflorenic-15- <i>keto-19-oate</i> (5)	48.32
Methyl grandiflorenic-15- <i>hydroxy-19-oate</i> (6)	38.17
Methyl <i>ent-kaur-17-ald-19-oate</i> (7)	72.62
Isokaurenoic acid (8)	33.52
Grandiflorenic acid (9)	48.94

^aInhibition (%) determined at 10 mM concentration of compound; ^bIC₅₀ (μ M); ^c No inhibition at 10 mM;

^dNot determined Acarbose served as a positive control. The percentage of inhibition of 1 mM acarbose was 56.5 %.

4C.3 Conclusion

Kaurens diterpenoids from *Wedelia paludosa* were isolated by silica gel normal phase column chromatography technique. Compounds were characterised as kaurenoic acid, gandiflorenic acid, isokaurenoic acid, alantacton and stigmasterol. Kaurenoic acid, grandiflorenic acid was isolated on a preparative scale and chemical derivatise; furthermore the evaluated for α -glucosidase inhibitors activity.

4C.3 Experimental section

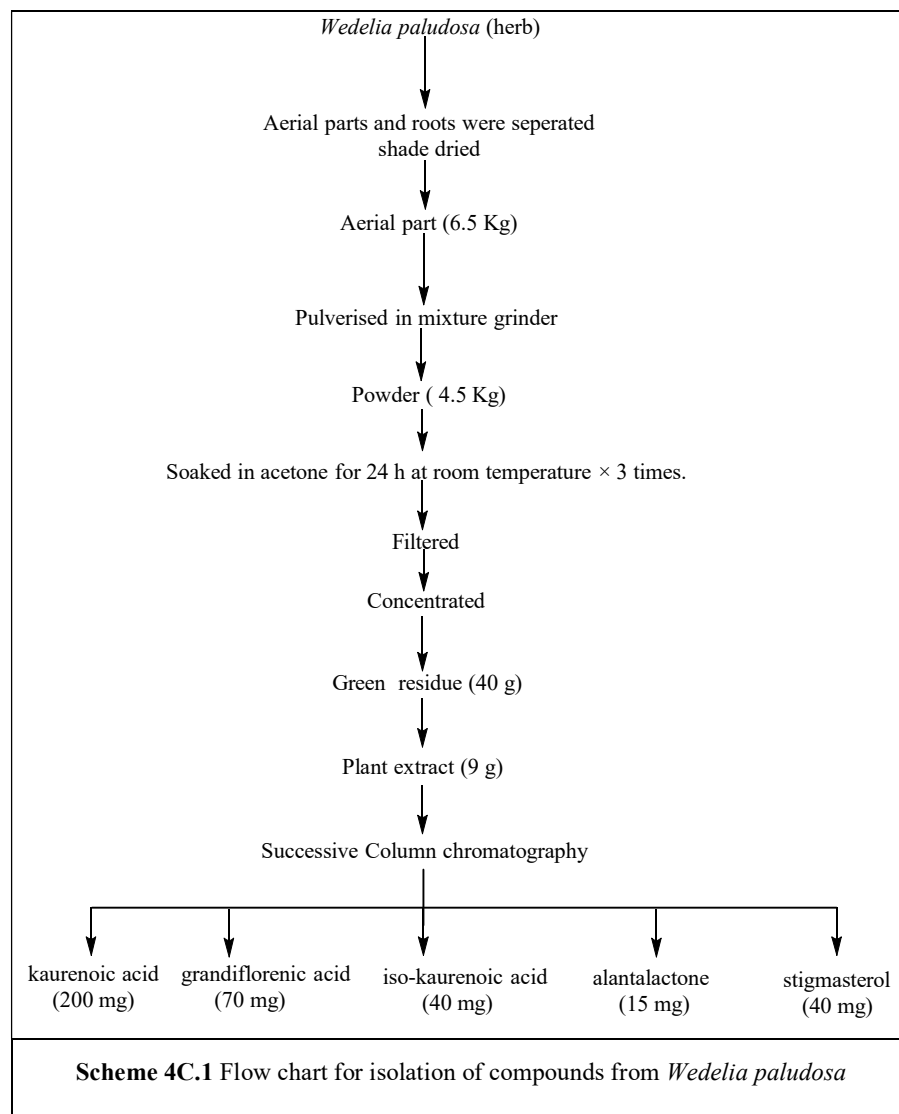
4C.3.1 Collection and Extraction and Isolation

Whole plants, in the flowering stage, were collected from campus NCL, Pune, Maharashtra during winter (September 2011). Herbarium deposited in Research Institute (ARI Sp. No. THV-2), Pune, India identified and authenticated as *Wedelia paludosa*. The collected plant material was shade dried and cleaned off to remove unwanted plant material and the adhering dust. Roots were separated from aerial part and pulverised in mixture grinder powder, obtained has been stored in a dry place. Aerial part powder (4.5 Kg) was soaked in acetone (5 L), stirred using homogeniser at room temperature. After 24 h extract had filtrated using filter paper, obtained residue again soaked in an equal volume of acetone and the same protocol had repeated for three times. Extracts (221 g) was soaked in methanol (1 L) and macerated in homogenizer at room temperature. After 24 h the soaked material was filtered and concentrated, similar procedure

was repeated for three times for maximum extraction. Filtrates were combined and concentrated at 50 °C under reduced pressure yield a dark green extract (120 g, 2.4 % based on dry plant weight). The acetone extract was separated and purified by flash column chromatography by using ethyl acetate in pet ether gradient. 9 g of the acetone extract of enriching with terpenoids mixture was fractionated on to a silica gel column. Silica gel was first equilibrated with pet ether and further eluted with gradient solvent mixture provided 5 fractions (WP-1 to WP-5). Fraction WP4 (4 g) was major from the first column eluted in gradient solvent system 8 to 12 % (ethyl acetate: pet ether) yellow solid obtained after concentrating the solvent. Fraction WP4 showed single spot on normal TLC but on silver nitrate coated TLC appeared three separated spot after charring. Hence fraction was purified over silver nitrate coated silica gel column chromatography, which yielded three pure compounds. Fractions WP1 (120 mg) purified over normal silica gel chromatography and fractions having a similar spot on TLC were pulled together and concentrated, which was gave pure solid. Similarly, fraction WP2 (26 mg) was purified on silica gel 240-400 mesh gave which crystalline solid.

4C.3.2 General Experimental Procedures

Extraction solvents for plant material were a technical grade (Spectrochem) and distilled before use. HPLC solvents were purchased from Sigma (St. Louis, MO, USA). For LC-ESI (+)-MS experiments, solvents were procured from JT Baker (PA, USA). Thin layer chromatogram (TLC) was developed on silica gel G pre-coated plates (Merck, 0.25 mm) with 10 % methanol in chloroform (twice) as the mobile phase. Spots were visualised in a solution of 3.0 % anisaldehyde, 2.8 % H₂SO₄, 2 % acetic acid in ethanol. Melting points were taken with a BUCHI- 560 apparatus, and uncorrected. FTIR spectra were recorded on Perkin Elmer FTIR spectrophotometer in CHCl₃, and optical rotations were determined in the same solvent on JASCO (P-2000), polarimeter using 10 mm cell (*c* in g/100 mL unit). NMR's data were recorded on Bruker spectrophotometer (¹H on 200, 400, 500 MHz; ¹³C on 100 MHz) in methanol-d₄ and CDCl₃ or TMS as the reference. GC analyses were carried out using Agilent 7890 GC system equipped with a hydrogen flame ionization detector (FID) and HP-5 capillary column (30 m × 0.32 mm × 0.25 μm, J & W Scientific). Nitrogen was used as carrier gas at a flow rate of 1 mL/min. FTIR spectra were recorded on Perkin Elmer FT-IR spectrophotometer in CHCl₃, and optical rotations were determined in the same solvent on JASCO (P-2000), polarimeter using 10 mm cell (*c* in g/100 mL unit).



4C.3.3 Synthesis of Kaurenoic Acid Derivatives

a. Preparation of Methyl *ent*-kaur-16-en-19-oate (2)

Potassium hydroxide 100 mg (4 mmol) stirred in acetone 10 mL at room temperature for 20 min.⁵¹ Kaurenoic acid 150 mg (0.970 mmol) added into the reaction mixture; followed by addition of methyl iodide 1.2 equivalent 40 μ L. The reaction was monitored by TLC until the starting material get disappear of (24 h). After completion of reaction, it was concentrated and obtained residue was dissolved in ethyl acetate and it which was washed with brine further passed over sodium sulphate. The reaction mixture was purified over column chromatography and compound characterised showed identical spectroscopic data to those of Methyl *ent*-kaur-16-en-19-oate (130 mg) reported earlier.

b. Preparation of Methyl *ent-kaur-15-hydroxy-19-oate* (3) and Methyl *ent-kaur-15-en-17-ald-19-oate* (4)

Methyl *ent-kaur-16-en-19-oate* 100 mg (1 mmol) was dissolved in 10 mL of dry DCM under inert atmosphere kept for 10 min. Selenium dioxide 40.6 mg (1.2 mmol)⁴⁷ was added portion wise into the reaction after complete addition, reaction kept at room temperature until the starting material was disappeared (24 h). The solvent was evaporated and the residue was dissolved in ethyl acetate further it washed with brine. Organic layer was then dried over sodium sulphate, filtered and concentrated. The crude was purified over silica gel chromatography yielded compounds 3 (50 mg) and compound 4 (27 mg) showed identical spectroscopic data with the reported.⁴⁷

c. Preparation of Methyl *ent-kaur-15-keto-19-oate* (5)

Methyl *ent-kaur-15-hydroxy-19-oate* 30 mg (0.2 mmol) weighed in the round bottom flask was dissolved in 1 mL of dry DCM under inert conditions and kept it at 0 °C for 10 min. 60 mg PDC (1.9 equiv) in dry DCM was added into the reaction mixture and kept the reaction mixture at room temperature for 24 h.⁴⁷ After completion of reaction it was filtered through florisil. Crude was purified afford compound-5 (18.3 mg) and showed spectroscopic data identical to those reported.⁴⁷

d. Preparation of Methyl *grandiflorenic-15-hydroxy-19-oate* (6)

Similar reaction conditions were used as mentioned earlier⁴⁷ for Methyl *ent-kaur-15-hydroxy-19-oate* (3) synthesis except the reaction temperature kept 0 C to rt for 4 h.

e. Preparation of the Methyl *grandiflorenic-15-keto-19-oate* (7)

Similar reaction conditions were used as mentioned earlier for Methyl *ent-kaur-15-hydroxy-19-oate* (5) synthesis.

e. Preparation of the Methyl *ent-kaur-16-ene -19-ald* (8)

Methyl *ent-kaur-16-en-19-oate* 10 mg (0.2 mmol) was dissolved in 1 mL of dry THF under inert conditions and kept for 10 min at -50 °C. DIBAL-H (1 mL, 25 % in toluene) was added into the reaction mixture and kept reaction for 1h. Excess DIBAL-H was quench with methanol and water and filtered over solid aluminium salts further organic solvent was evaporated and the aqueous phase was extracted DCM. The crude obtained was purified over silica gel and characterised by spectroscopic techniques.

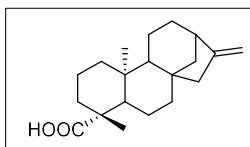
4C.3.3 General protocol of α -glucosidase inhibition assay

α -glucosidase (0.04 U/mL) from Baker's yeast, inhibition studied in phosphate buffer 0.067 M at pH 6.8 and rate was determined at 37 °C. The reaction volume was 100 μ L mixture contained

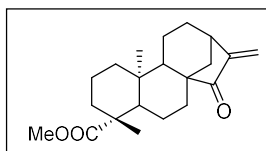
in which 20 μL *p*-Nitrophenyl- α -D-glucopyranoside, 40 μL of kaurenoic acid and its derivatives, and 40 μL α -glucosidase solutions. Acarbose (1 mM) used as a positive control. First *p*-nitrophenyl- α -D-glucopyranoside along with kaurenoic acid and its derivatives were dissolved in DMSO further diluted with phosphate buffer in order to make 10 % DMSO as a final concentration. α -glucosidase incubated with 30 min with kaurenoic acid and derivatives (100 mM) along with the *p*-Nitrophenyl- α -D-glucopyranoside (0.5 mM). Reaction mixture kept for 5 min at 37 $^{\circ}\text{C}$ and quenched by 0.1 M sodium carbonate (pH 9.8). At 405 nm absorption was measured and taken as the relative hydrolysis rate; all the experiment was performed in triplicate.

4C.3.4 Characterization Data of Compounds

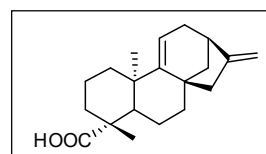
Kaurenoic acid yellow solid; GC-MS (ESI) *m/z*: Calcd for $\text{C}_{20}\text{H}_{30}\text{O}_2$, 302.2147; found, 302.2187. ^1H NMR (CDCl_3 , 400 MHz): δ ppm 0.95 (3H, s), 1.03-1.08 (3H, s), 1.24-1.26 (6H, m, $J=7.4$ Hz), 1.40-1.59 (4H, m), 1.77 (1H, s), 2.05-2.10 (4H, m, $J=8.0$ Hz), 4.74 (1H, br s), 4.80 (1H, br s); ^{13}C NMR (CDCl_3 , 100 MHz): δ ppm 184.5, 155.9, 103.0, 57.1, 55.1, 49.0, 44.2, 43.9, 43.8, 41.3, 40.7, 39.7, 37.8, 33.1, 29.7, 29.0, 21.8, 19.1, 18.4, 15.6.



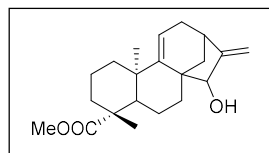
Preparation of Methyl *ent*-kaur-15-keto-19-oate pale yellow solid GC-MS (ESI) *m/z*: Calcd for $\text{C}_{21}\text{H}_{30}\text{O}_3$, 330; found, 330 ^1H NMR (CDCl_3 , 200 MHz): δ ppm 0.89 (3 H, s), 1.02 (1 H, br. s.), 1.12 (1 H, br. s.), 1.19 (4 H, s), 1.24 (2 H, s), 1.33 - 1.40 (2 H, m), 1.47 (2 H, d, $J=8.84$ Hz), 1.62 (2 H, d, $J=5.56$ Hz), 1.70 (2 H, d, $J=6.82$ Hz), 1.79 (2 H, br. s.), 1.83 - 1.88 (2 H, m), 2.37 (1 H, d, $J=11.87$ Hz), 3.62 - 3.65 (3 H, m), 5.20 - 5.26 (1 H, m), 5.93 (1 H, s); ^{13}C NMR (CDCl_3 , 100 MHz): δ ppm 14.68, 17.69, 18.20, 19.43, 28.03, 31.53, 32.97, 35.84, 37.22, 37.41, 39.25, 39.41, 43.09, 50.52, 50.90, 51.80, 55.43, 113.75, 148.84, 177.20, 210.05.



Grandiflorenic acid yellow solid; GC-MS (ESI) *m/z*: Calcd for $\text{C}_{20}\text{H}_{28}\text{O}_2$, 300.14; found, 300.12. ^1H NMR (CDCl_3 , 400 MHz): δ ppm 0.96 (3H, s), 1.03 (4 H, s), 1.25 (4H, s), 1.47 (2H, br. s.), 1.52 (3H, d, $J=2.91$ Hz), 1.60 (3H, br. s.), 1.92 (2H, br. s.), 2.06 (2H, br. s.), 2.13 - 2.21 (2H, m), 4.80 (1H, s), 5.25 (1H, t, $J=3.22$ Hz); ^{13}C NMR (CDCl_3 , 100 MHz): δ ppm 18.58, 20.20, 22.60, 25.72, 28.22, 36.15, 36.27, 37.65, 39.46, 40.09, 41.41, 44.37, 47.11, 49.46, 51.16, 115.87, 120.64, 149.58, 151.31, 178.13, 203.07.



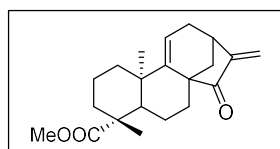
Preparation of Methyl grandiflorenic-15-hydroxy-19-oate solid; GC-MS (ESI) m/z : Calcd for



$C_{21}H_{30}O_3$, 330; found, 330. 1H NMR ($CDCl_3-d$): δ ppm 0.77 - 0.87 (3 H, m), 0.92 - 0.99 (3 H, m), 1.01 (1 H, d, $J=2.53$ Hz), 1.18 (4 H, d, $J=2.27$ Hz), 1.25 (1 H, s), 1.34 (1 H, br. s.), 1.39 - 1.46 (2 H, m), 1.54 - 1.63 (2 H, m), 1.68 - 1.76 (2 H, m), 1.80 (2 H, d, $J=6.57$ Hz),

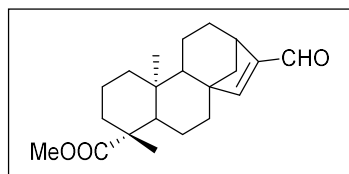
2.05 (1 H, d, $J=5.94$ Hz), 2.28 - 2.48 (2 H, m), 3.64 (4 H, d, $J=2.53$ Hz), 5.20 (2 H, s), 5.25 - 5.43 (1 H, m); ^{13}C NMR ($CDCl_3$, 100 MHz): δ ppm 178.13, 151.31, 149.58, 120.64, 115.87, 82.16, 51.16, 49.46, 47.11, 44.37, 41.41, 40.09, 39.46, 37.65, 36.27, 36.15, 28.22, 25.72, 22.60, 20.20, 18.58

Methyl grandiflorenic-15-keto-19-oate solid; GC-MS (ESI) m/z : Calcd for $C_{21}H_{28}O_3$, 328; found, 328. 1H NMR ($CDCl_3$): δ ppm 0.95 (3H, s), 1.02 (1H, d, $J=4.04$ Hz), 1.14 - 1.22 (2H,



m), 1.24 (4 H, s), 1.36 (1H, dd, $J=6.44$, 3.28 Hz), 1.47 (1H, dd, $J=6.57$, 3.16 Hz), 1.68 (3H, d, $J=2.65$ Hz), 1.76 - 1.84 (2H, m), 2.00 - 2.09 (2H, m), 2.11 - 2.22 (2H, m), 3.64 (3H, s), 5.43 (1H, s), 5.48 - 5.54 (1H, m), 5.91 (1H, s); ^{13}C NMR ($CDCl_3$, 100 MHz): δ ppm 18.58, 20.20, 22.60, 25.72, 28.22, 36.15, 36.27, 37.65, 39.46, 40.09, 41.41, 44.37, 47.11, 49.46, 51.16, 76.37, 77.64, 115.87, 120.64, 149.58, 151.31, 178.13, 203.07.

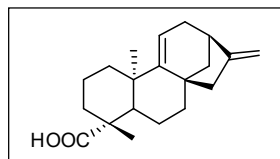
Methyl ent-kaur-15-en-17-ald-19-oate solid; GC-MS (ESI) m/z : Calcd for $C_{21}H_{30}O_3$, 330; found, 330. 1H NMR ($CDCl_3$): δ ppm 0.88 (3 H, s), 1.05 - 1.10 (2 H, m), 1.19 (4 H, s), 1.48 (2 H,



d, $J=3.03$ Hz), 1.50 - 1.53 (2 H, m), 1.54 (2 H, br. s.), 1.61 - 1.65 (1 H, m), 1.66 - 1.73 (3 H, m), 1.83 (2 H, d, $J=3.79$ Hz), 1.88 (2 H, d, $J=6.44$ Hz), 2.10 (1 H, s), 2.13 (2 H, br. s.), 3.65 (3 H, s), 6.59 (1 H, s), 9.73 (1 H, s); ^{13}C NMR ($CDCl_3$, 100

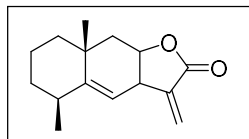
MHz): δ ppm 15.29, 18.65, 19.02, 20.30, 25.07, 28.69, 37.79, 37.98, 38.15, 39.83, 40.67, 42.97, 43.79, 45.84, 50.90, 51.19, 56.57, 148.62, 161.62, 177.77, 189.48.

Grandiflorenic acid yellow solid; GC-MS (ESI) m/z : Calcd for $C_{20}H_{30}O_2$, 302.2147; found, 302.2187. 1H NMR ($CDCl_3$): δ ppm 0.95 (3H, s), 1.03-1.08 (3H, s), 1.24-1.26 (6H, m, $J=7.4$ Hz), 1.40-1.59 (4H, m), 1.77 (1H, s), 2.05-2.10 (4H, m, $J=8.0$ Hz), 4.74 (1H, br s), 4.80 (1H, br



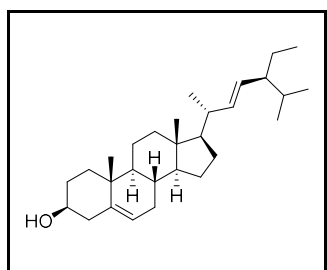
s); ^{13}C NMR ($CDCl_3$, 100 MHz): δ ppm 184.5, 155.9, 103.0, 57.1, 55.1, 49.0, 44.2, 43.9, 43.8, 41.3, 40.7, 39.7, 37.8, 33.1, 29.7, 29.0, 21.8, 19.1, 18.4, 15.6

Alantalactone solid; ^1H NMR (CDCl_3): δ ppm 1.11 (3 H, d, $J=7.58$ Hz), 1.21 (3 H, s), 1.42 - 1.58 (4 H, m), 1.58 - 1.67 (2 H, m), 2.12 (1 H, dd, $J=14.91, 2.78$ Hz), 3.46 - 3.69 (1 H, m), 4.75 - 4.91 (1 H, m), 5.16 (1 H, d, $J=4.04$ Hz), 5.62 (1 H, d, $J=1.64$ Hz), 6.21



(1 H, d, $J=1.89$ Hz). ^{13}C NMR (CDCl_3 , 100 MHz): δ ppm 16.76, 22.56, 28.58, 32.67, 32.73, 37.61, 39.51, 41.74, 42.66, 76.45, 76.68, 77.31, 118.76, 121.69, 139.83, 149.11.

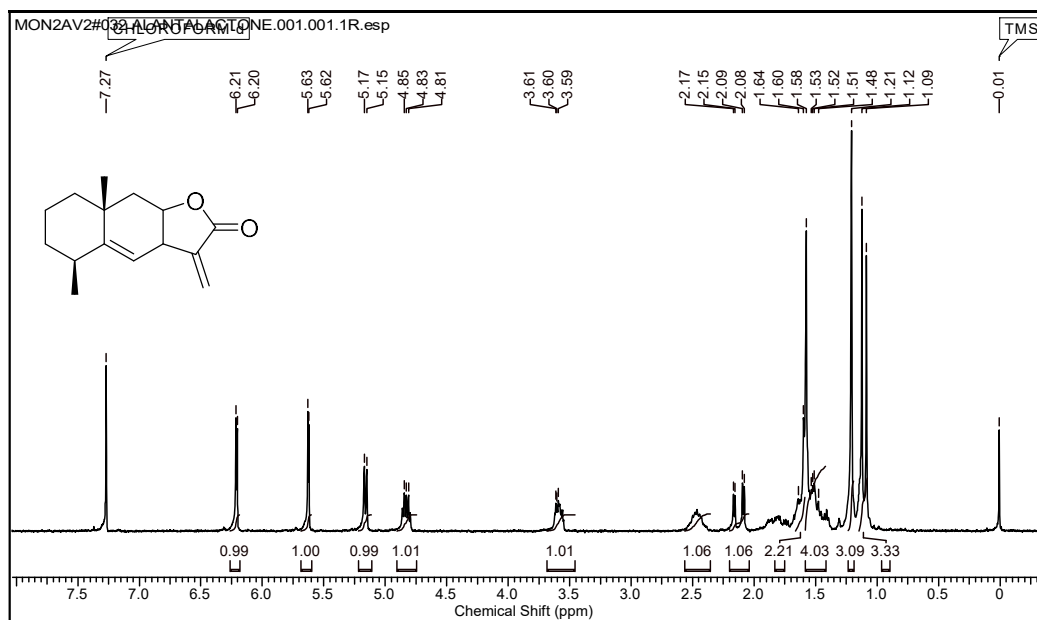
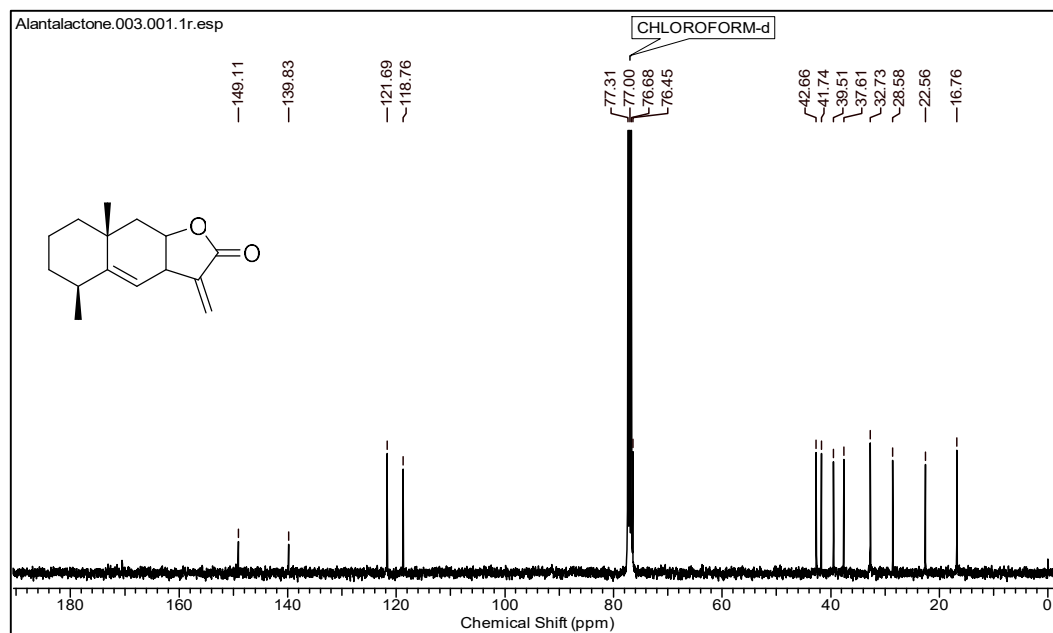
Stigmasterol ^1H NMR (CDCl_3): δ ppm 0.69 (3 H, s), 0.75 - 0.88 (10 H, m), 0.98 - 1.06 (8 H, m), 1.11 - 1.26 (4 H, m), 1.37 - 1.62 (11 H, m), 1.82



(3 H, br. s.), 1.99 (3 H, d, $J=12.25$ Hz), 2.28 (2 H, br. s.), 3.43 - 3.61 (1 H, m), 4.93 - 5.23 (2 H, m), 5.35 (1 H, d, $J=5.05$ Hz); ^{13}C NMR (CDCl_3 , 100 MHz): δ ppm 11.84, 11.97, 18.77, 19.03, 19.38, 19.80, 21.07, 23.07, 24.29, 26.10, 28.23, 29.16, 31.63, 31.90, 33.95, 36.13, 36.50,

37.25, 39.77, 42.28, 45.83, 50.14, 56.07, 56.76, 71.77, 121.68, 129.27, 138.30, 140.75.

4C.5 Spectral copies

Figure 4C.1a. ^1H -NMR spectrum of alantactone (CDCl_3)Figure 4C.1b. ^{13}C -NMR spectrum of alantactone (CDCl_3)

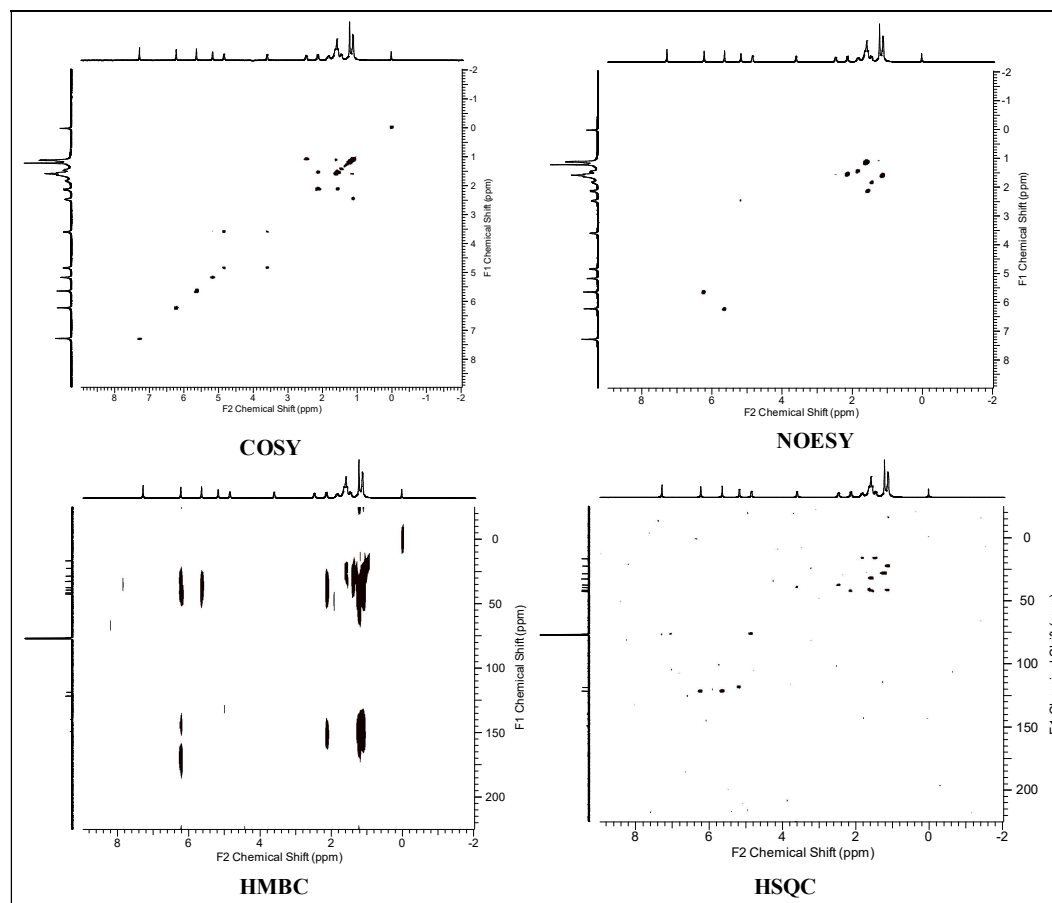


Figure 4C.1c. COSY, NOESY, HMBC and HSQC spectrum of alanatalactone

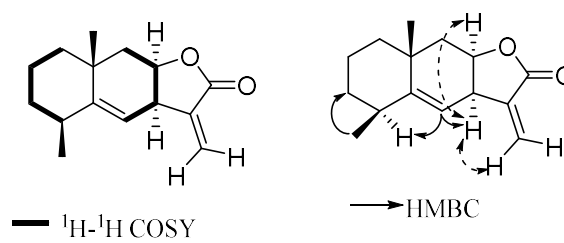


Figure 4C.1d. ^1H - ^1H COSY correlations and key HMBC of alanatalactone

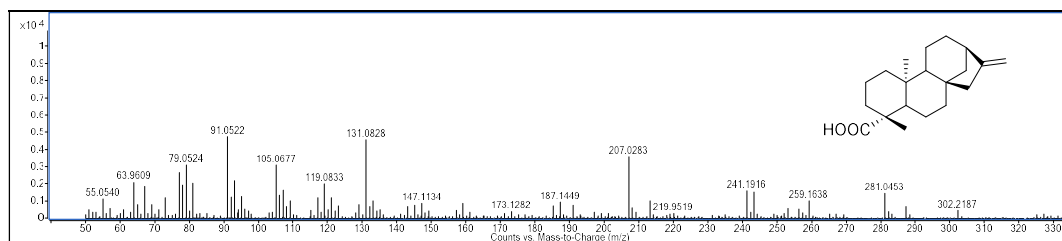
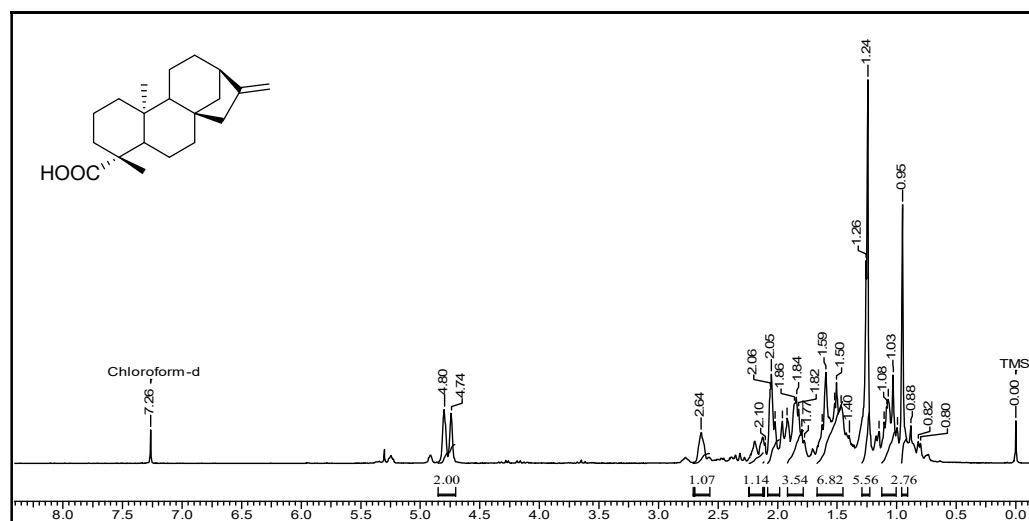
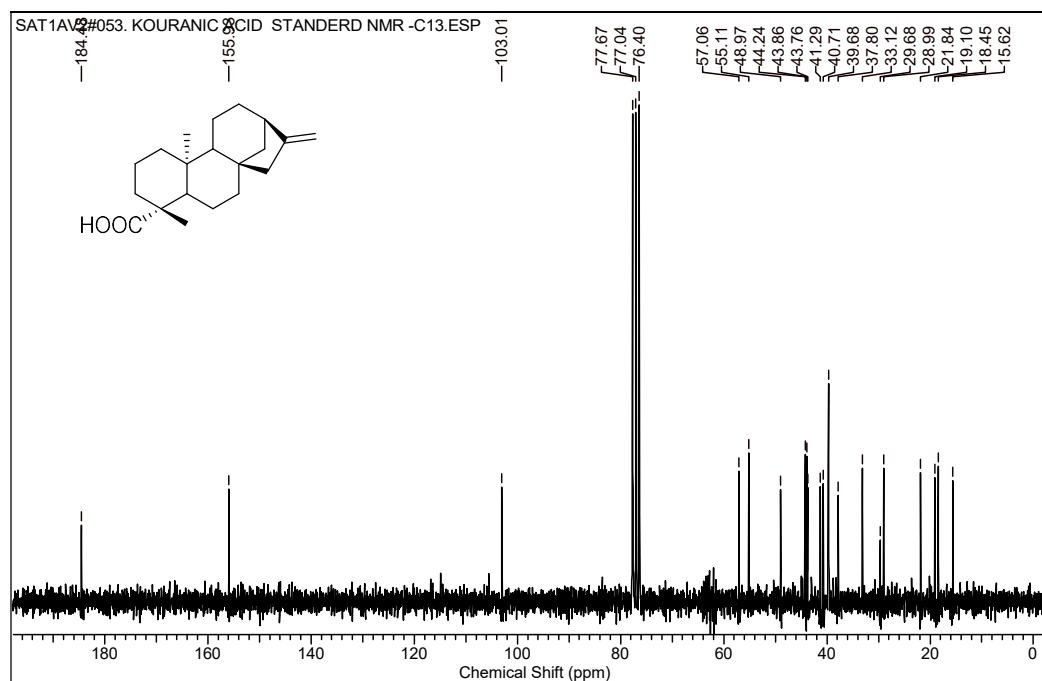


Figure 4C.2a. GC-EI-QToF-MS spectrum of kaurenoic acid

Figure 4C.2b. ^1H -NMR spectrum of kaurenoic acid (CDCl_3)Figure 4C.2c. ^{13}C -NMR spectrum of kaurenoic acid (CDCl_3)

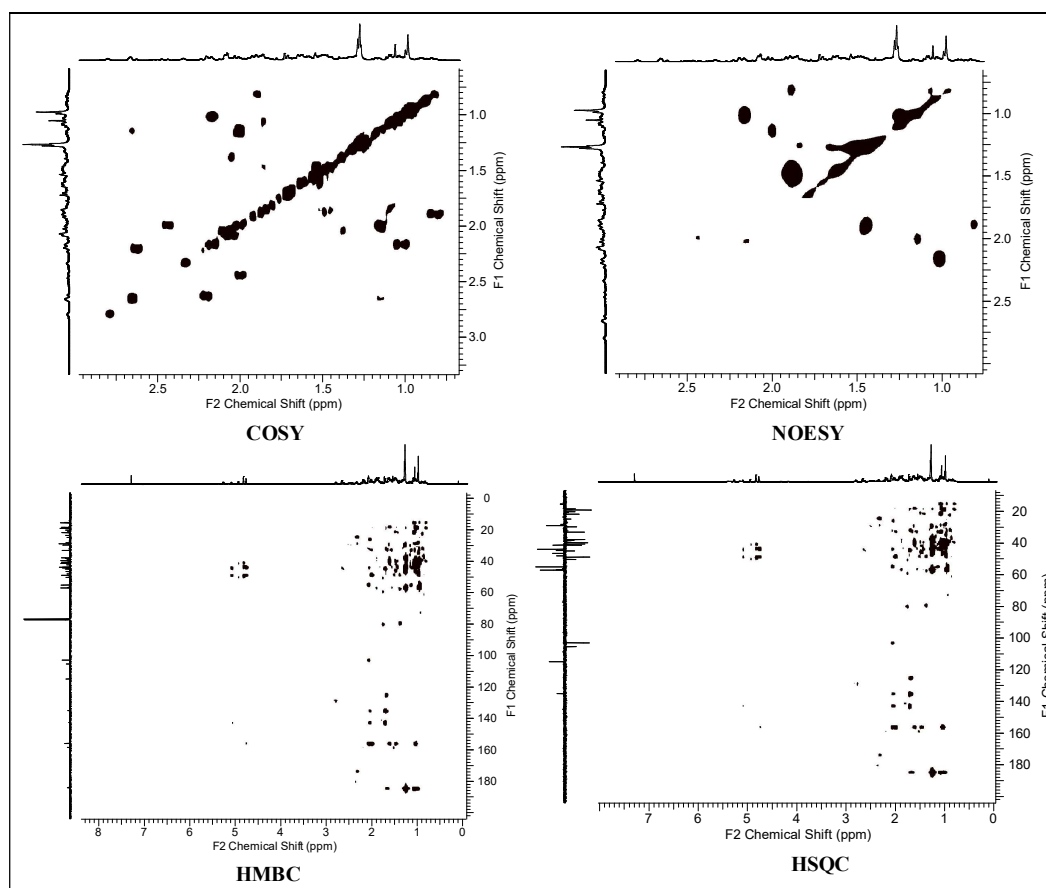


Figure 4C.2d. COSY, NOESY, HMBC and HSQC spectrum of kaurenoic acid.

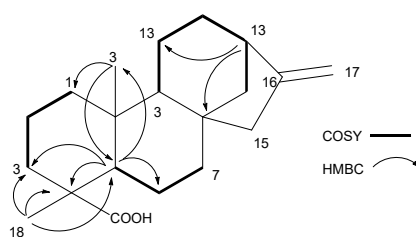


Figure 4C.2e. ^1H - ^1H COSY correlations and key HMBC of kaurenoic acid

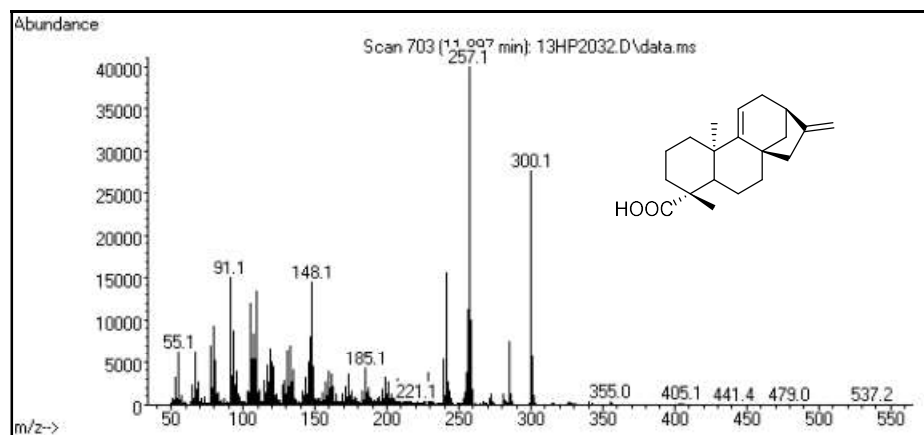


Figure 4C.3a. ESI-MS spectrum of grandiflorenic acid

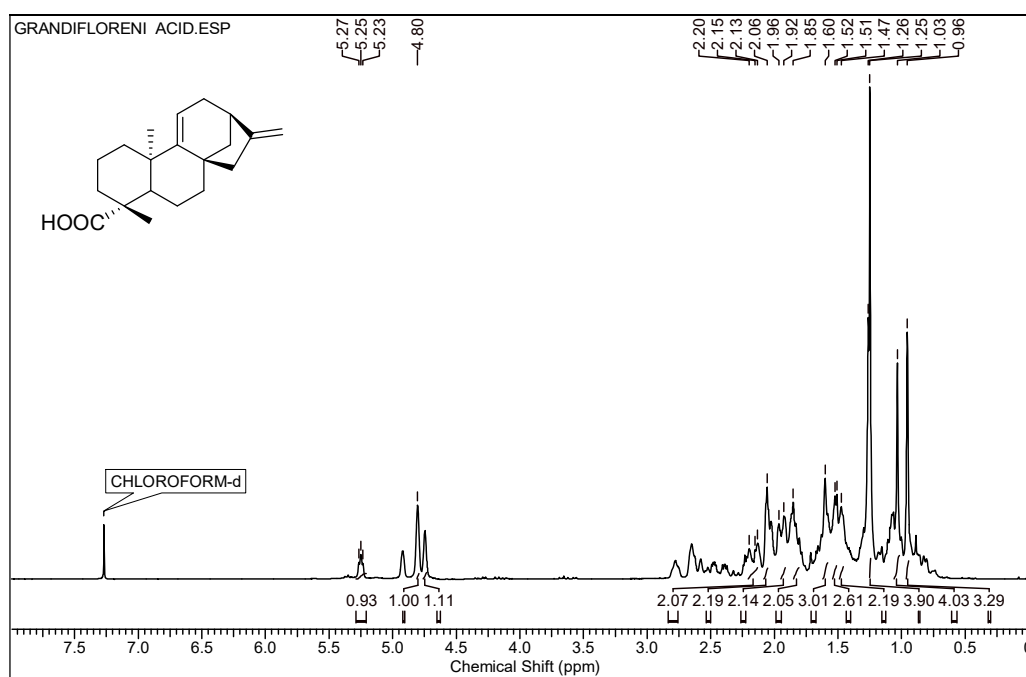


Figure 4C.3b. $^1\text{H-NMR}$ spectrum of grandiflorenic acid (CDCl_3)

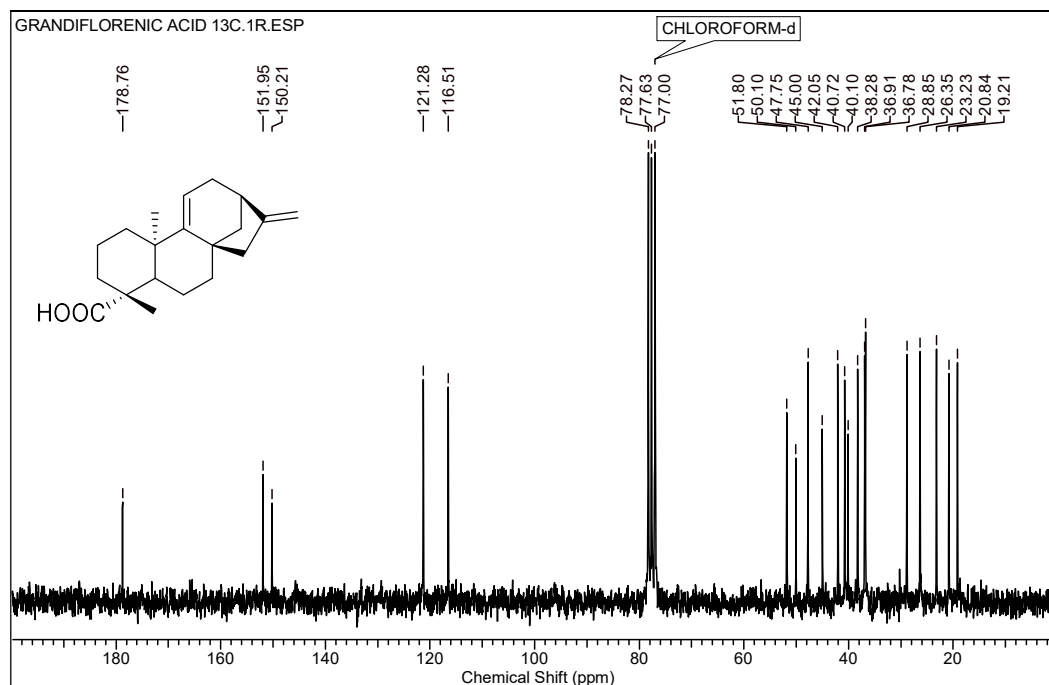


Figure 4C.3c. ^{13}C -NMR spectrum of grandiflorenic acid (CDCl_3)

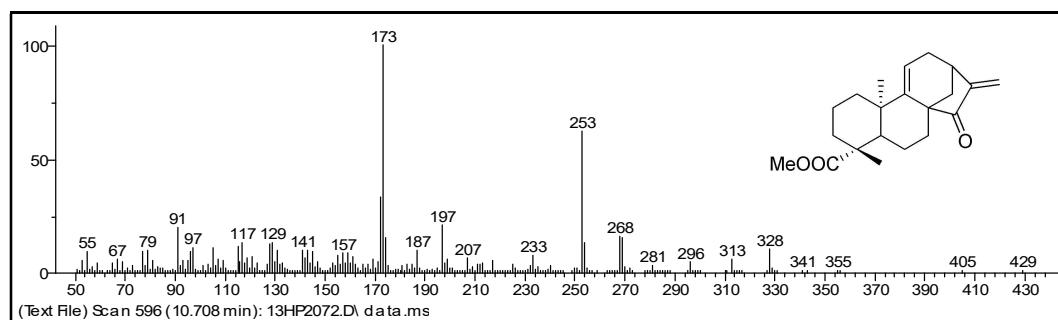


Figure 4C.4a. ESI-MS spectrum of Methyl *ent*-kaur-17-ald-19-oate

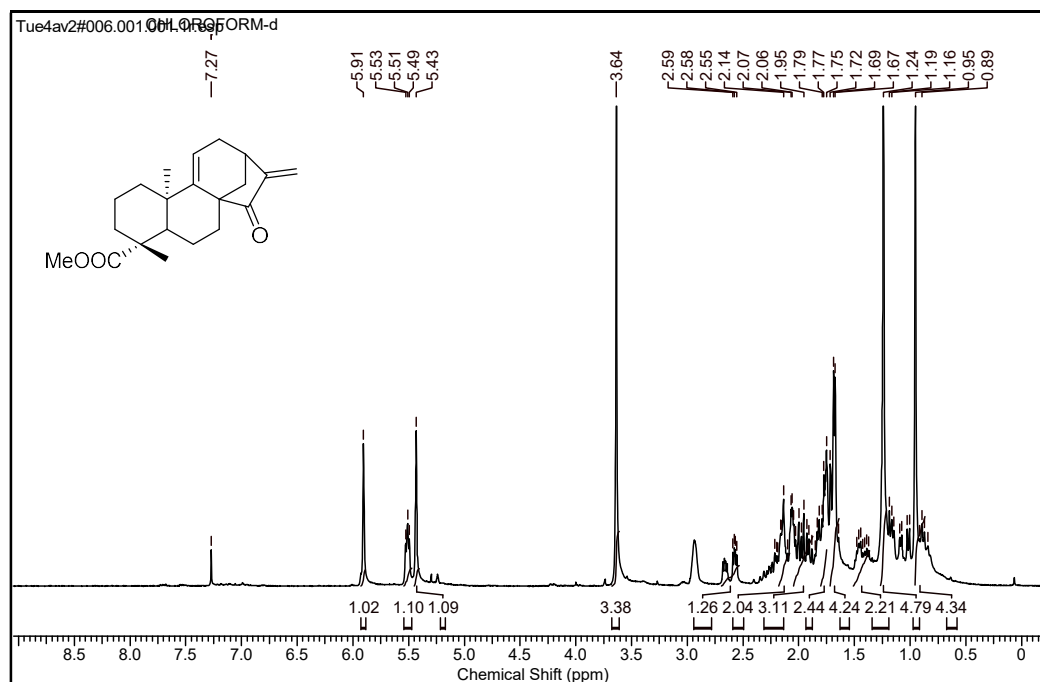


Figure 4C.4b. $^1\text{H-NMR}$ spectrum of Methyl *ent*-kaur-17-ald-19-oate (CDCl_3)

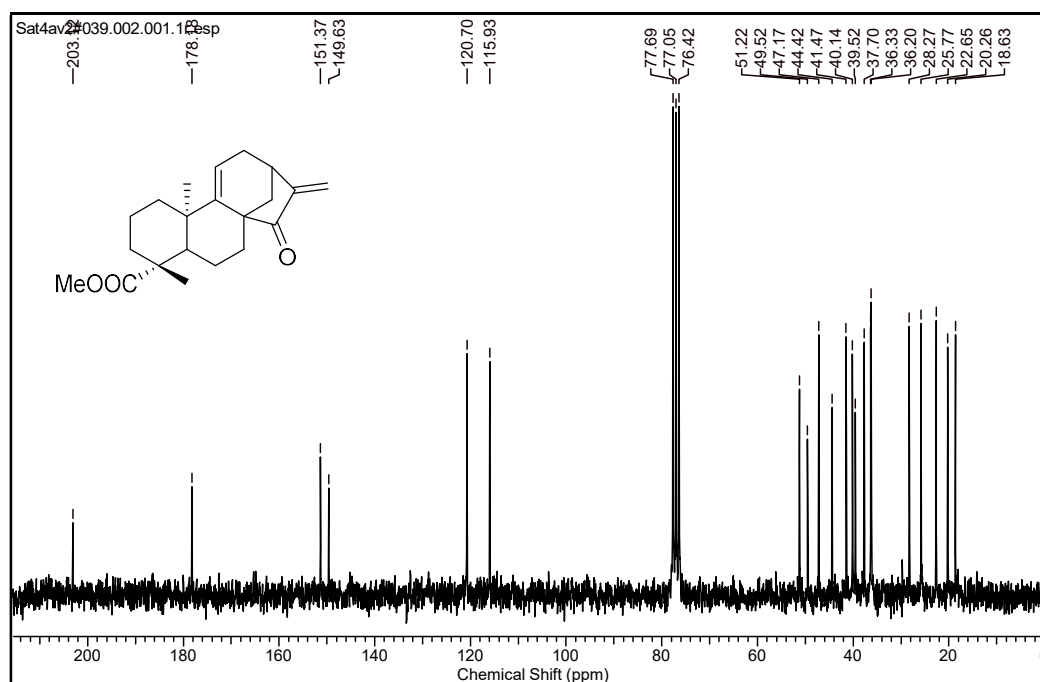


Figure 4C.4c. $^{13}\text{C-NMR}$ spectrum of Methyl *ent*-kaur-17-ald-19-oate (CDCl_3)

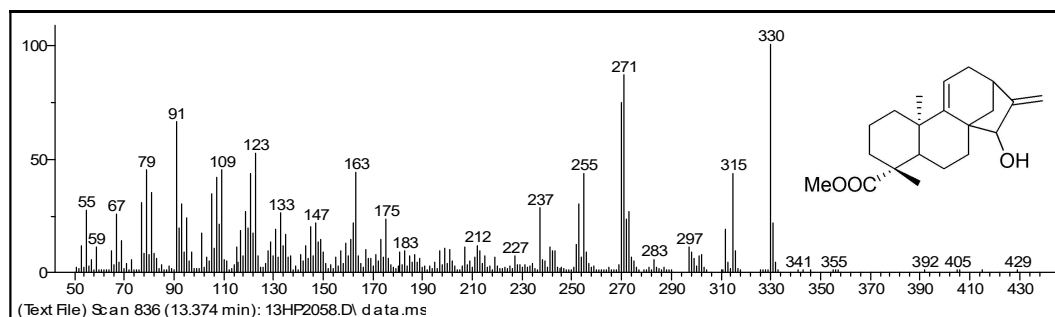


Figure 4C.5a. ESI-MS spectrum of Methyl grandiflorenic-15-hydroxy-19-oate (CDCl_3)

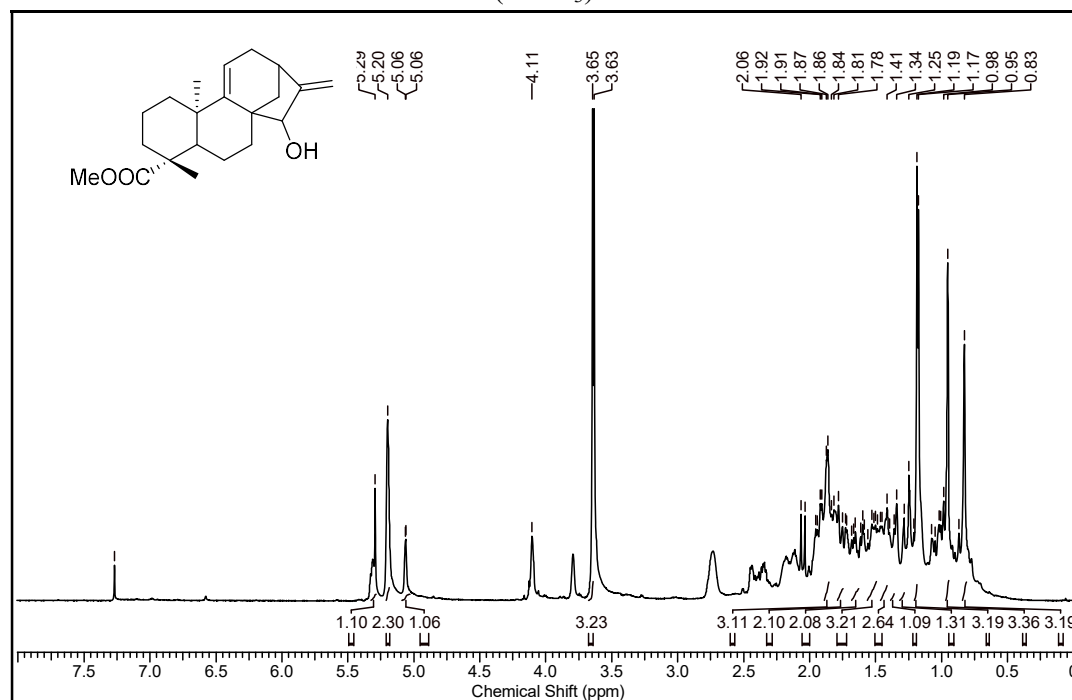


Figure 4C.5b. ^1H -NMR spectrum of Methyl grandiflorenic-15-hydroxy-19-oate (CDCl_3)

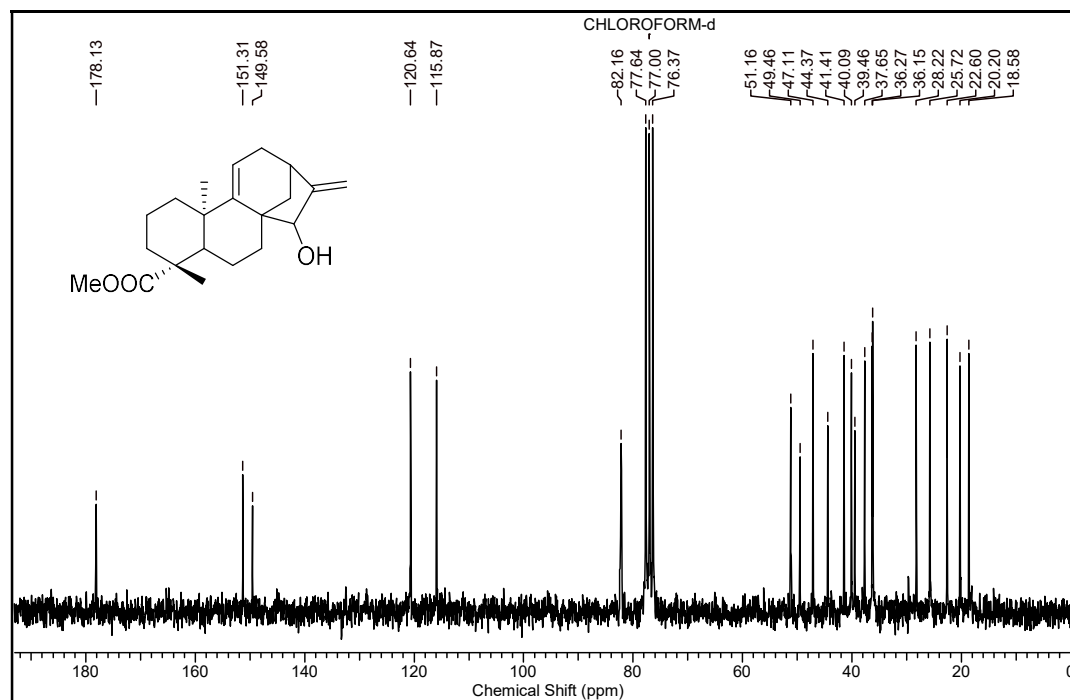


Figure 4C.5c. ^{13}C -NMR spectrum of grandiflorenic hydroxy ester (CDCl_3)

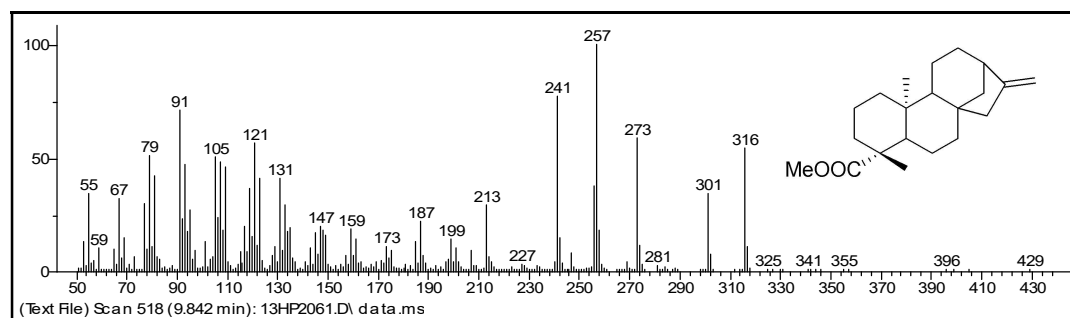


Figure 4C.6a. ESI-MS spectrum of kaurenoic methyl ester

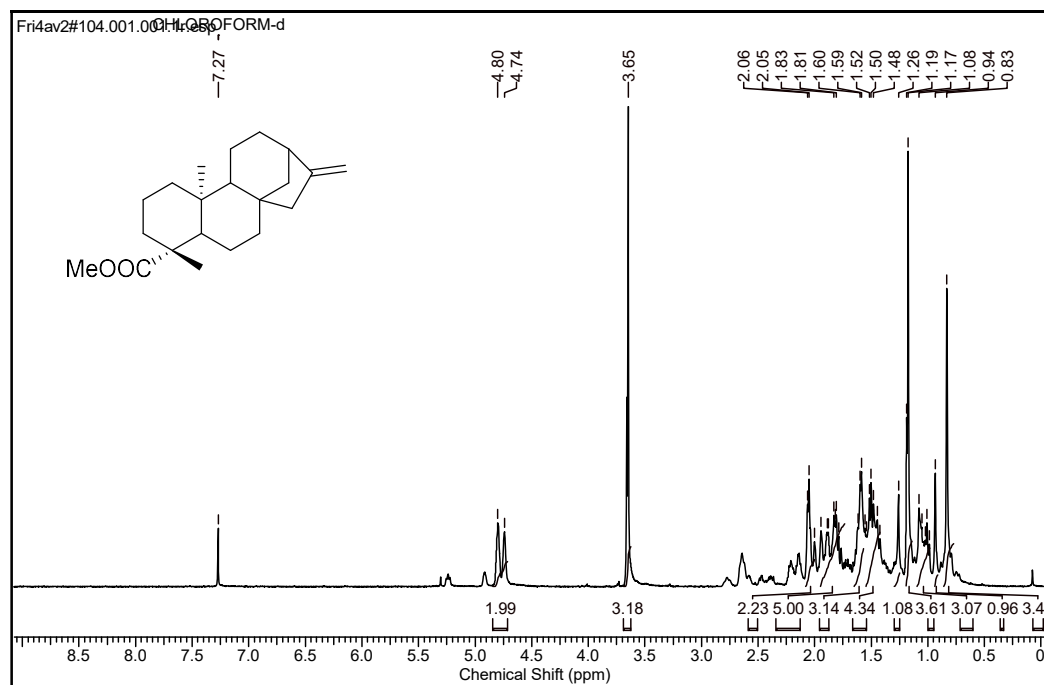


Figure 4C.6b. $^1\text{H-NMR}$ spectrum of Methyl *ent*-kaur-16-en-19-oate (CDCl_3)

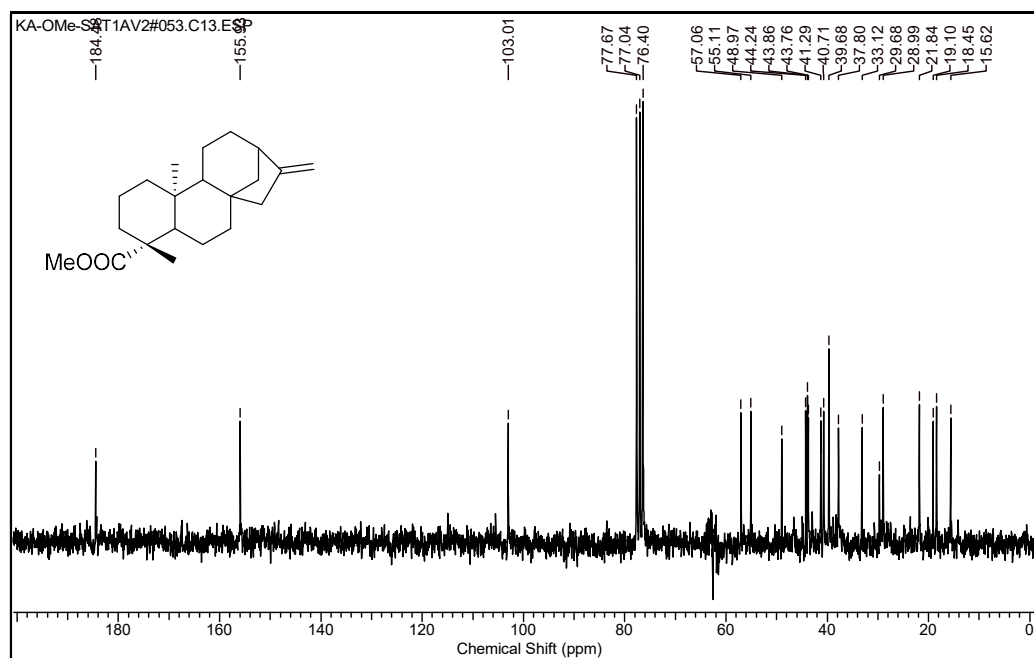


Figure 4C.6c. $^{13}\text{C-NMR}$ spectrum of Methyl *ent*-kaur-16-en-19-oate (CDCl_3)

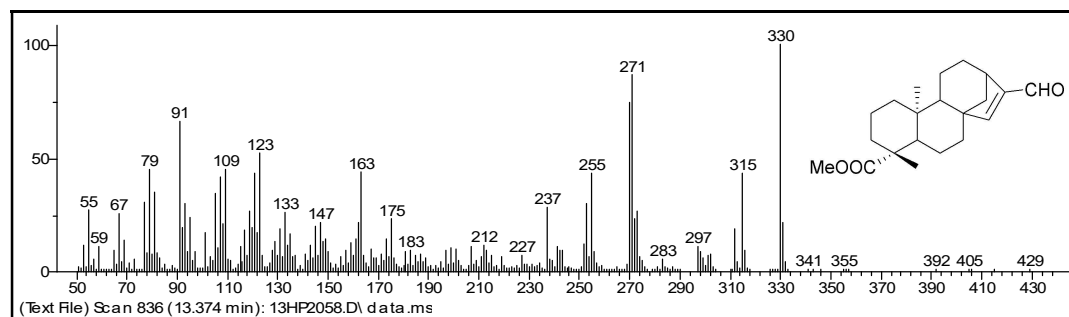


Figure 4C.7a. ESI-MS spectrum of Methyl *ent*-kaur-15-en-17-ald-19-oate

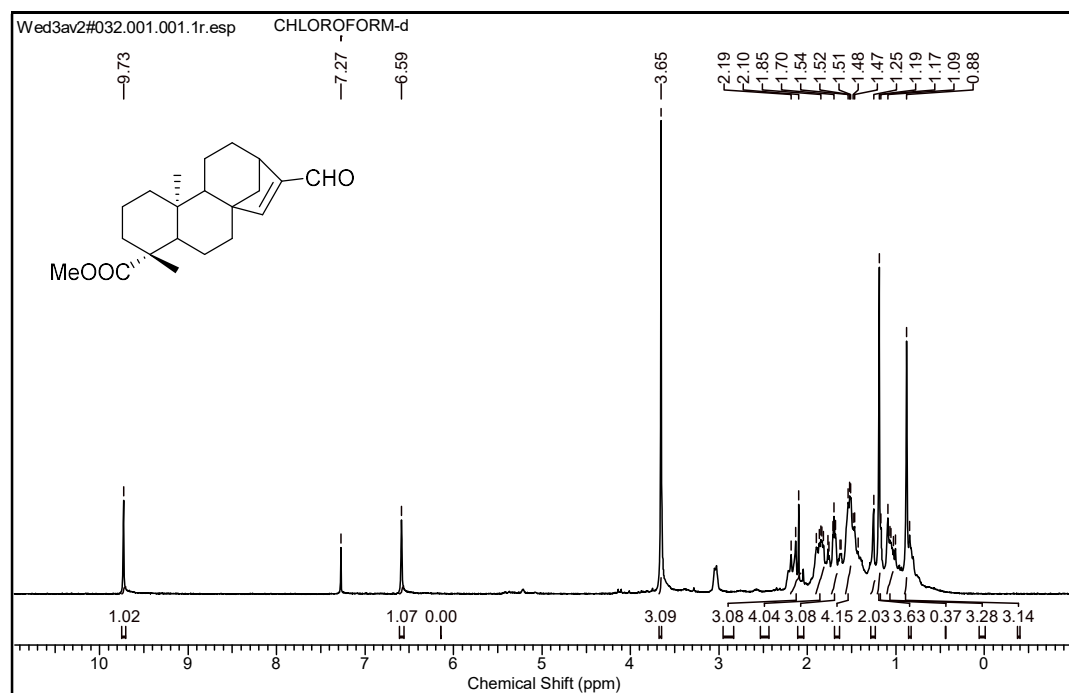


Figure 4C.7b. $^1\text{H-NMR}$ spectrum of Methyl *ent*-kaur-15-en-17-ald-19-oate (CDCl_3)

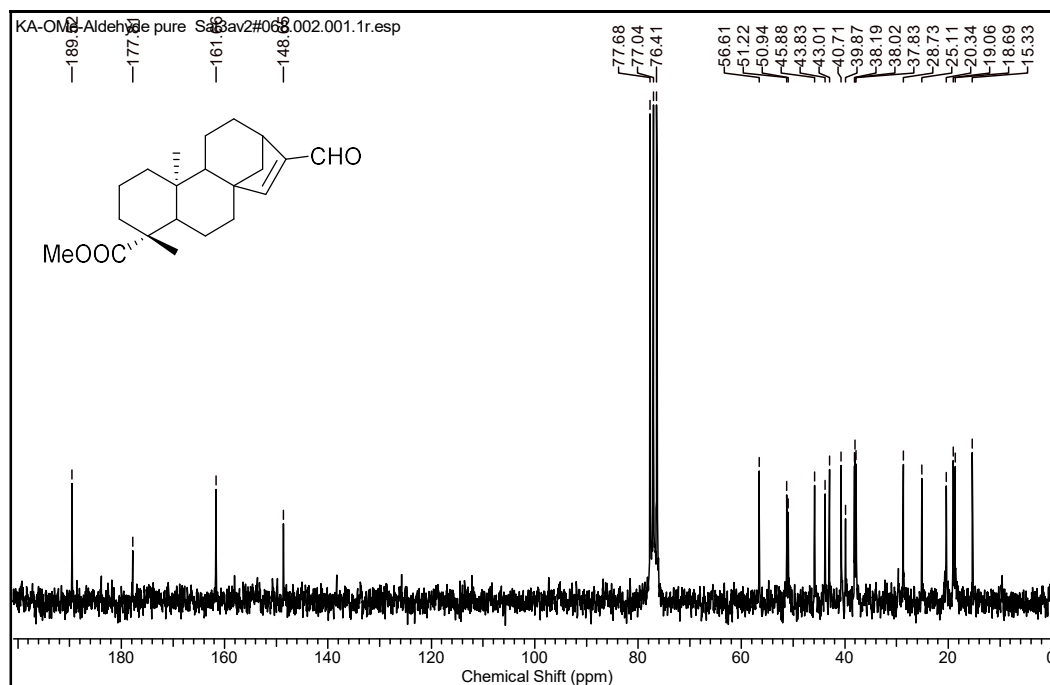


Figure 4C.7c. ^{13}C -NMR spectrum of kaurenoic ester aldehyde (CDCl_3)

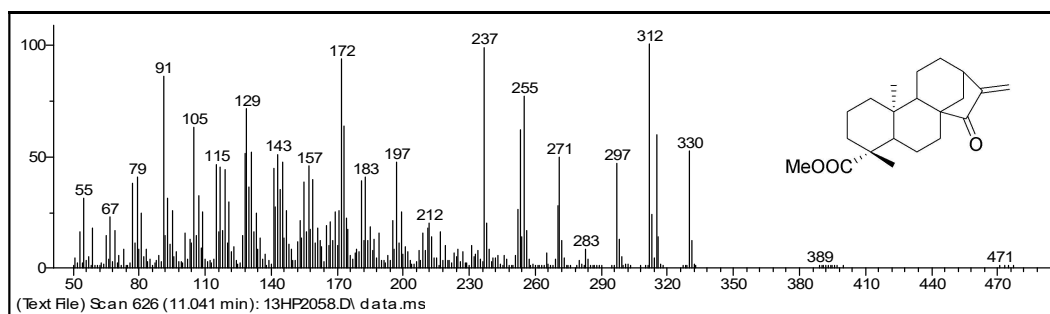


Figure 4C.8a. ESI-MS spectrum of Methyl grandiflorenic-15-keto-19-oate

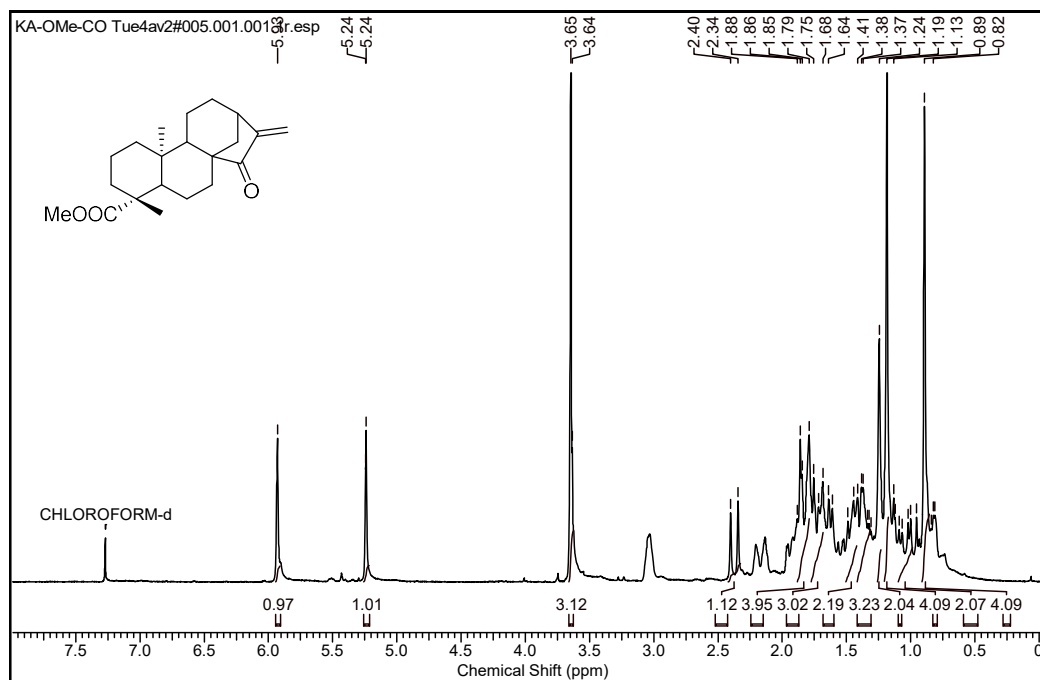


Figure 4C.8b. $^1\text{H-NMR}$ spectrum of Methyl grandiflorenic-15-keto-19-oate (CDCl_3)

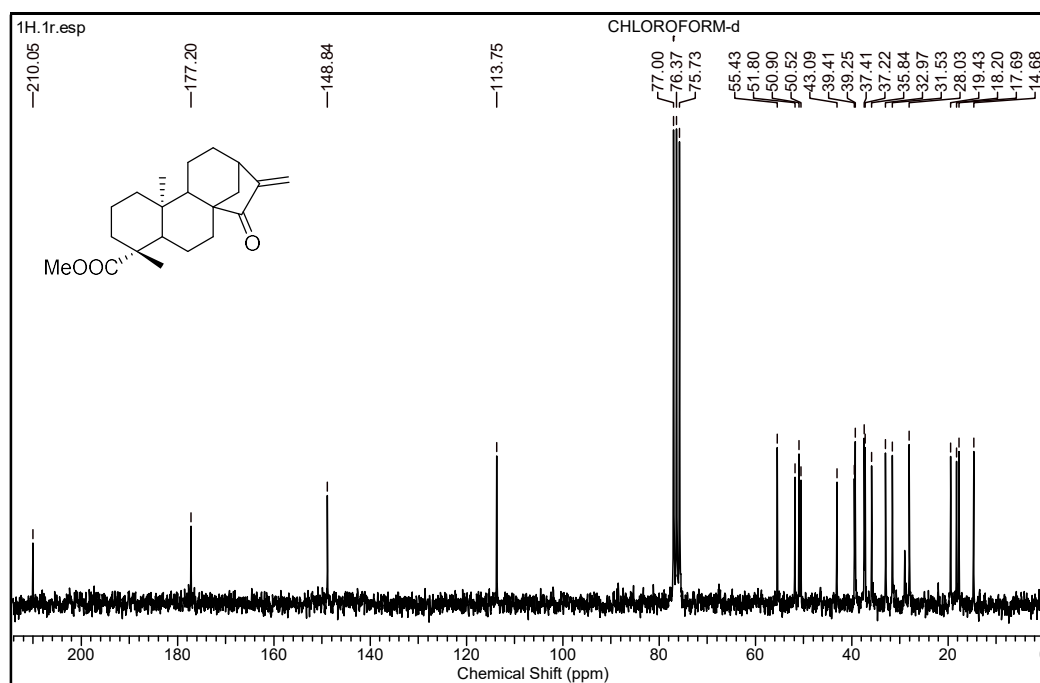
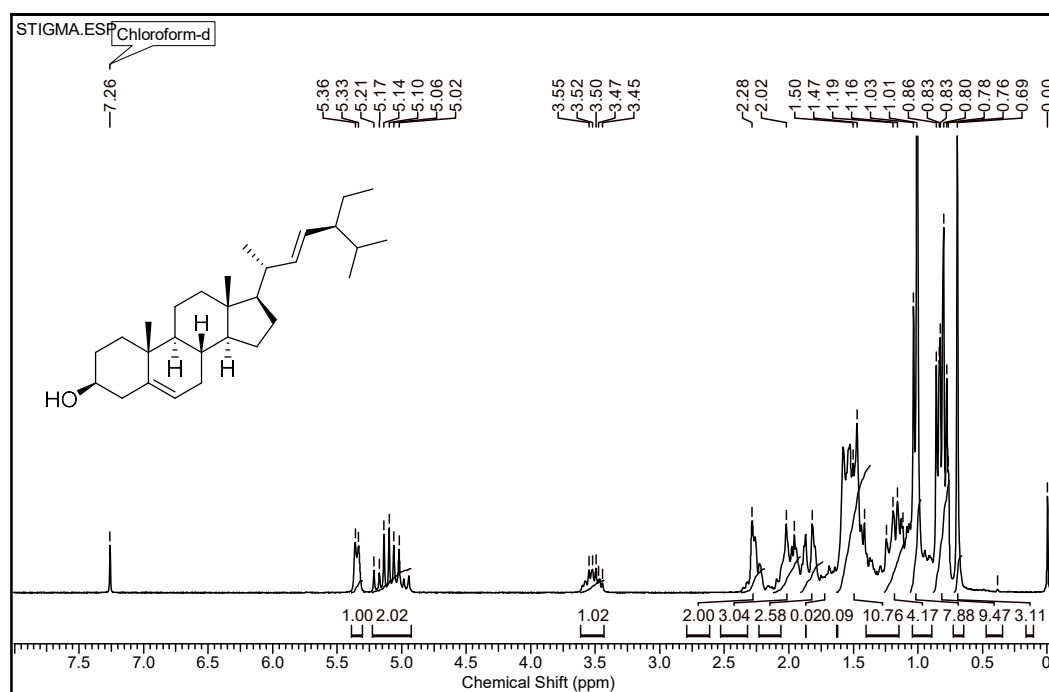
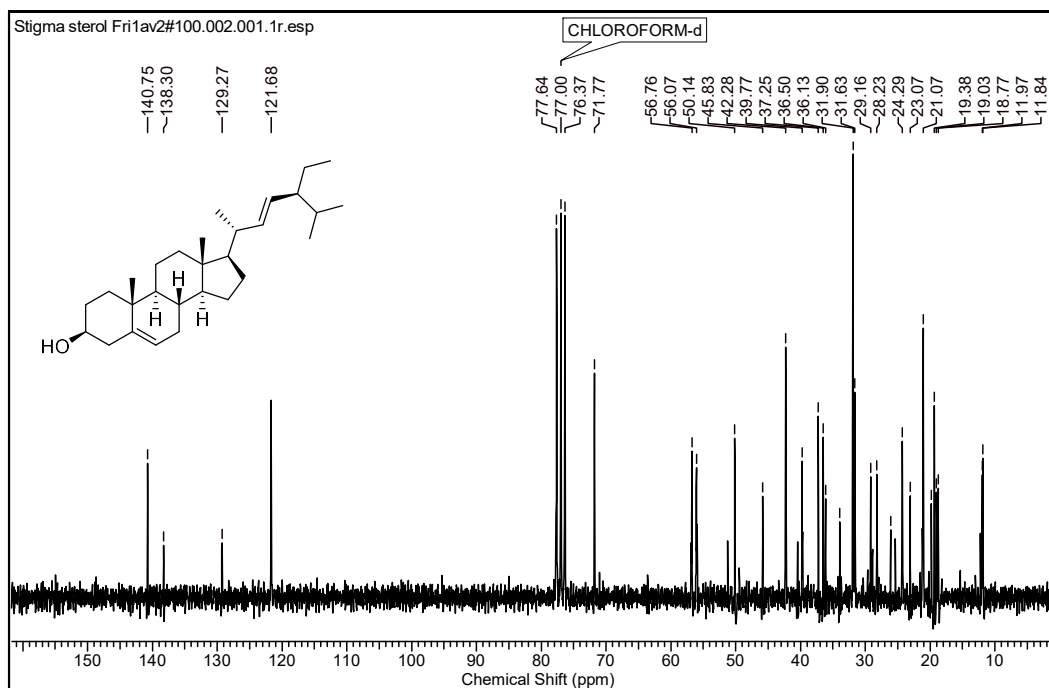


Figure 4C.8c. $^{13}\text{C-NMR}$ spectrum of Methyl grandiflorenic-15-keto-19-oate (CDCl_3)

Figure 4C.9a. $^1\text{H-NMR}$ spectrum of stigmasterol (CDCl_3)Figure 4C.9b. $^{13}\text{C-NMR}$ spectrum of stigmasterol (CDCl_3)

4D References

- 1 Y. Ratna Raju, P. Yugandhar and N. Savithramma, *Int. J. Pharm. Pharm. Sci.*, 2014, **6**, 369–374.
- 2 G. Yao and D. X. Zhang, *Nord. J. Bot.*, 2015, **33**, 25–31.
- 3 C. Pattanaik, C. S. Reddy and K. N. Reddy, *Our Nat.*, 2010, **7**, 122–128.
- 4 S. Yin, M. L. Sykes, R. A. Davis, T. Shelper, V. M. Avery, D. Camp and R. J. Quinn, *Planta Med.*, 2010, **76**, 1877–1881.
- 5 J. M. Tian, X. Y. Fu, Q. Zhang, H. P. He, J. M. Gao and X. J. Hao, *Biochem. Syst. Ecol.*, 2013, **48**, 288–292.
- 6 P. Van Kiem, V. K. Thu, P. H. Yen, N. X. Nhiem, N. H. Tung, N. X. Cuong, C. Van Minh, H. T. Huong, J.-H. Hyun, H.-K. Kang and Y. H. Kim, *Chem. Pharm. Bull. (Tokyo)*, 2009, **57**, 102–105.
- 7 S. Kabir, R. Zahan, A. M. S. Chowdhury, M. R. Haque and M. A. Rashid, *Bangladesh Pharm. J.*, 2015, **18**, 142–148.
- 8 F. Lieutier, K. Bermudez-Torres, J. Cook, M. O. Harris, L. Legal, A. Sallé, B. Schatz and D. Giron, *Adv. Bot. Res.*, 2017, **81**, 55–109.
- 9 J. V. C. Sharma, G. Pitchaiah, D. Satyavati, J. V. Rao and H. Sanjay, *Int. J. Res. Pharm. Biomed. Sci.*, 2011, **51**, 286–190.
- 10 A. P.K., T. K., C. S., M. O., P. T.H. and S. G., *Mol. Pharm.*, 2008, **5**, 167–190.
- 11 J. Bohlmann and C. I. Keeling, *Plant J.*, 2008, **3**, 656–669.
- 12 A. Ludwiczuk, K. Skalicka-Woźniak and M. I. Georgiev, *Terpenoids*, 2016.
- 13 R. J. Peters, *Nat. Prod. Rep.*, 2010, **27**, 1521–1530.
- 14 S. Haldar, F. A. Mulani, T. Aarthy, D. S. Dandekar and H. V. Thulasiram, *J. Chromatogr. A*, 2014, **1366**, 1–14.
- 15 P. Puapairoj, W. Naengchomnong, A. Kijjoa, M. M. Pinto, M. Pedro, M. S. J. Nascimento, A. M. S. Silva and W. Herz, *Planta Med.*, 2005, **71**, 208–213.
- 16 B. O. Okesola and D. K. Smith, *Chem. Soc. Rev.*, 2016, **45**, 4226–4251.
- 17 E. R. Draper and D. J. Adams, *Chem*, 2017, **3**, 390–410.
- 18 Y. Ohseido, M. Oono, K. Saruhashi, H. Watanabe and N. Miyamoto, *R. Soc. Open Sci.*, 2017, **4**, 45–49.
- 19 P. McNeice, Y. Zhao, J. Wang, G. F. Donnelly and P. C. Marr, *Green Chem.*, 2017, **19**, 4690–4697.
- 20 F. Ono, S. Shinkai and H. Watanabe, *New J. Chem.*, 2018, **42**, 6601–6603.
- 21 B. G. Bag and S. S. Dash, *Langmuir*, 2015, **31**, 13664–13672.
- 22 X. J. Kuang, A. Wajahat, W. T. Gong, M. K. Dhinakaran, X. H. Li and G. L. Ning, *Soft Matter*, 2017, **13**, 4074–4079.
- 23 B. G. Bag and K. Paul, *Asian J. Org. Chem.*, 2012, **1**, 150–154.
- 24 S. R. Jadhav, B. Sen Chiou, D. F. Wood, G. Degrande-Hoffman, G. M. Glenn and G. John, *Soft Matter*, 2011, **7**, 864–867.
- 25 A. Barnard, P. Posocco, S. Pricl, M. Calderon, R. Haag, M. E. Hwang, V. W. T. Shum, D. W. Pack and D. K. Smith, *J. Am. Chem. Soc.*, 2011, **133**, 20288–20300.
- 26 J. Teßmar, F. Brandl and A. Göpferich, *Fundam. Tissue Eng. Regen. Med.*, 2009, **101**, 495–517.
- 27 J. Peyre, A. Hamraoui, M. Faustini, V. Humblot and N. Baccile, *Phys. Chem. Chem. Phys.*, 2017, **19**, 15227–15238.
- 28 S. Sarkar, S. Chakraborty and S. Roy, *J. Mol. Liq.*, 2018, **254**, 198–207.

-
- 29 K. Dutta, D. Hu, B. Zhao, A. E. Ribbe, J. Zhuang and S. Thayumanavan, *J. Am. Chem. Soc.*, 2017, **139**, 5676–5679.
- 30 G. Wei, Z. Su, N. P. Reynolds, P. Arosio, I. W. Hamley, E. Gazit and R. Mezzenga, *Chem. Soc. Rev.*, 2017, **46**, 4661–4708.
- 31 A. Saneja, D. Arora, R. Kumar, R. D. Dubey, A. K. Panda and P. N. Gupta, *Ann. N. Y. Acad. Sci.*, 2018, **14**, 5–18.
- 32 A. K. Chaudhari, I. Han and J. C. Tan, *Adv. Mater.*, 2015, **27**, 4438–4446.
- 33 B. G. Bag and R. Majumdar, *RSC Adv.*, 2014, **4**, 53327–53334.
- 34 B. G. Bag, R. Majumdar, S. K. Dinda, P. P. Dey, G. C. Maity, V. A. Mallia and R. G. Weiss, *Langmuir*, 2013, **29**, 1766–1778.
- 35 J. K. A. Mattos and M. D. G. R. Rodrigues, *Fitopatol. Bras.*, 1980, **5**, 159–162.
- 36 N. Balekar, N. G. Katkam, T. Nakpheng, K. Jehtae and T. Srichana, *J. Ethnopharmacol.*, 2012, **141**, 817–824.
- 37 J. M. Rosa, P. S. Brocardo, D. Balz, A. L. S. Rodrigues, A. P. Waltrick, A. Bagio, E. C. Goulart, F. C. Meotti, A. L. Dafre and A. R. S. Santos, *J. Pharm. Pharmacol.*, 2005, **58**, 137–142.
- 38 V. D. Tambe, S. A. Nirmal and R. S. Jadhav, *Dhaka Univ. J. Pharm. Sci.*, 2007, **6**, 59–60.
- 39 C. Bürger, D. R. Fischer, D. A. Cordenunzi, A. P. de Borba Batschauer, V. C. Filho and A. R. dos Santos Soares, *J. Pharm. Pharm. Sci.*, 2005, **8**, 370–373.
- 40 N. F. Roque, T. L. Giannella, A. M. Giesbrecht and R. C. S. B. C. Barbosa, *Rev. Latinoam. Quim.*
- 41 M. R. K. Sartori, J. B. Pretto, A. B. Cruz, L. F. V. Bresciani, R. A. Yunes, M. Sortino, S. A. Zacchino and V. C. Filho, *Pharmazie*, 2003, **58**, 567–569.
- 42 J. D. McChesney, S. K. Venkataraman and J. T. Henri, *Phytochemistry*, 2007, **68**, 2015–2022.
- 43 V. C. Filho, L. C. Block, R. A. Yunes and F. delle Monache, *Nat. Prod. Res.*, 2004, **18**, 447–451.
- 44 T. Okoye, *European J. Med. Plants*, 2014, **4**, 579–589.
- 45 S.-I. Jeong, B.-S. Kim, K.-S. Keum, K.-H. Lee, S.-Y. Kang, B.-I. Park, Y.-R. Lee and Y.-O. You, *Evidence-Based Complement. Altern. Med.*, 2013, **2013**, 1–9.
- 46 R. Batista, J. L. Humberto, E. Chiari and A. B. de Oliveira, *Bioorganic Med. Chem.*, 2007, **15**, 381–391.
- 47 I. Hueso-Falcón, N. Girón, P. Velasco, J. M. Amaro-Luis, A. G. Ravelo, B. de las Heras, S. Hortelano and A. Estevez-Braun, *Bioorganic Med. Chem.*, 2010, **18**, 1724–1735.
- 48 P. M. Matos, B. Mahoney, Y. Chan, D. P. Day, M. M. W. Cabral, C. H. G. Martins, R. A. Santos, J. K. Bastos, P. C. B. Page and V. C. G. Heleno, *Molecules*, 2015, **20**, 18264–18278.
- 49 U. Federal and D. M. Gerais, *Ann. Brazilian Acad. Sci.*, 2010, **82**, 823–831.
- 50 L. F. V. Bresciani, R. A. Yunes, C. Bürger, L. E. De Oliveira, K. L. Bóf and V. Cechinel-Filho, *Zeitschrift fur Naturforsch. - Sect. C J. Biosci.*, 2004, **59**, 229–232.
- 51 R. G. Pereira, A. Cala, M. Fernández-Aparicio, J. M. G. Molinillo, M. A. D. Boaventura and F. A. Macías, *Pest Manag. Sci.*, 2017, **73**, 2529–2537.

Chapter 5
**Biocatalyst Mediated Functionalization
of Terpenoids**

Chapter 5: Section A

Biotransformation of Menthol using *Mucor piriformis*

5A.1 Introduction

Menthol is a cyclic monoterpenoid and major aroma constituent of *Mentha piperita*. Menthol is mostly used in pharmaceutical, medicinal applications, fragrance and flavour industries.^{1,2,3} Menthol exhibits various pharmacological activities such as anti-inflammatory, anaesthetic, antimicrobial, disinfectant and gastroprotective effects.^{4,5,6} Structural modification of bioactive natural products from the currently available arsenal for the development of analogues with improved efficiency is on a rising trend.^{7,8} Several synthetic methodologies were reported for modification of active natural products basic skeleton, but it has some disadvantages like required several steps,⁹ use of hazardous solvents,¹⁰ chemicals and is comparatively expensive.¹¹ Considering the deleterious effects of these reagents, there is a strong need to endorse mild and environmentally benign approaches for this purpose. Alternatively, biocatalysts deliver a modest and simpler solution to the current problem. Methodologies involving biocatalysts, whole cells or enzymes in their native or modified forms follow green procedures.^{12,13} Microbial biotransformation is the economic, green process for several reactions e.g. regio-, stereoselective oxidation and reduction of bioactive molecules.^{14,15} Henceforth we have used *M. piriformis*, a versatile soil isolated fungal strain for menthol biotransformation.

Herein, menthol biotransformation by using *M. piriformis* resulted in 6-hydroxymenthol, 1-hydroxymenthol as a major and 8-hydroxymenthol as minor metabolites. Metabolite exhibits antimicrobial activity at lower concentration compared to menthol against bacteria and yeast with MIC as low as 8 µg/ml. Hemolytic activity of Menthol and its metabolites was low at their respective MIC. These metabolites might be responsible to increase the permeability of the bacterial cell membrane, which was demonstrated by FITC, PI uptake studies.

5A.2 Results and Discussion

5A.2.1 Screening and Time Course Experiment

In order to find the efficient fungal strain for menthol biotransformation on the analytical scale, we have screened thirteen fungal cultures belonging to genera *Fusarium*, *Aspergillus*, *Mucor*, *Penicillium*, *Cephalophora*, *Gibberella*, *Rhizopus* and *Neurospora*. Analyses of the crude extract obtained after five days of menthol incubation in standardised biotransformation conditions were analysed by TLC, GC and GC-MS. The result indicated that *M. piriformis* efficiently transformed menthol to metabolites compared to the other fungal strain; hence *M. piriformis* was selected for preparative scale biotransformation.

Table 5A.1 Screening results of the biotransformation of menthol and metabolites distribution

Fungal culture	Menthol (%)	6-hydroxy menthol (%)	8-hydroxy menthol (%)	1-hydroxy menthol (%)	Other metabolites (%)
<i>F.proliferatum</i>	77.57	1.39	-	2.04	19
<i>A.niger-589</i>	61.74	6.9	2.36	-	29
<i>A.gigantous</i>	68.63	-	5.23	3.14	23
<i>A.chraceous</i>	67.2	-	-	-	33
<i>A.foetidus</i>	52.06	2.61	11.33	-	34
<i>N.crassa</i>	47.92	-	9.75	1.33	41
<i>R.oryzae</i>	59.35	2.88	12.86	2.91	22
<i>A.niger-582</i>	73.26	-	-	2.74	24
<i>G.fugikoroii</i>	28.96	2.75	31.29	-	37
<i>A.niger-612</i>	99.17	-	-	0.82	42
<i>M.piriformis</i>	12.62	28.16	37.02	21.7	-
<i>M.plumbiosus</i>	39.5	7.5	-	-	53
<i>C.irregularis</i>	50.6	-	14.4	-	35

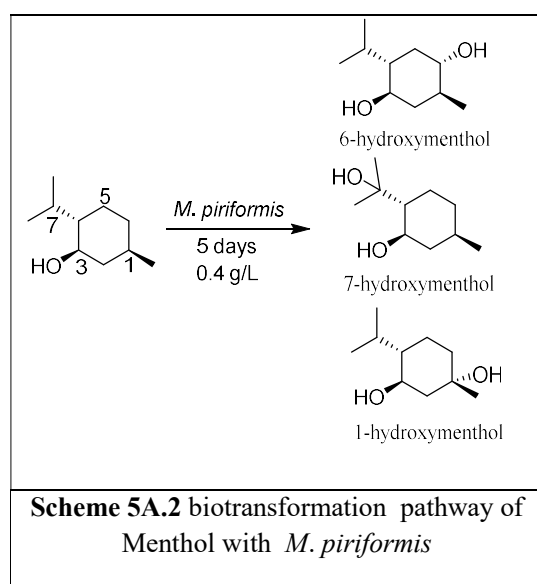
Substrate control experiment suggested that menthol was not degraded in reaction conditions without fungal strain. GC-MS of fungal control experiment suggested that no menthol peak observed, which confirmed that menthol, was metabolised by fungal

culture. Resting cell experiment confirmed the involvement of fungal system involved in menthol biotransformation.

Substrate concentration studies with menthol (0.1 g/L to 0.8 g/L) suggested that *M. piriformis* transformed menthol quantitatively at 0.4 g/L, the rate of bioconversion decreases after this, which might be due to the toxic effect on fungus. Time course study at the standardised biotransformation conditions and same menthol concentration suggested that the *M. piriformis* quantitatively convert menthol (> 85 %) to metabolites in five days (Figure 5C. 1). The major metabolites formed were 6-hydroxy menthol with the minor metabolites 1-hydroxy menthol and 8-hydroxy menthol.

5A.2.2 Purification and Characterization of Metabolites

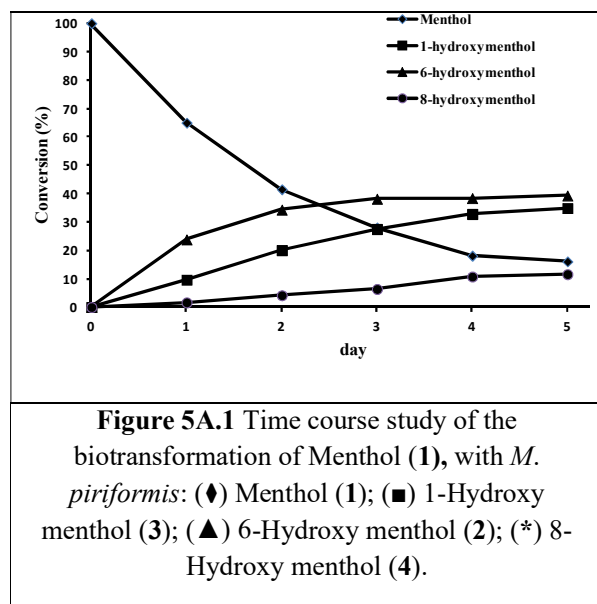
Preparative scale fermentation of menthol was carried out for metabolites isolation and characterization. Menthol large scale biotransformation was performed with a concentration of 0.4 g/L suggested by substrate concentration experiment with 1 g quantity. The crude after extraction was analysed by TLC, GC and GC-MS, which



suggested that crude contained a mixture of metabolites, with three major and some minor metabolites. The primary analysis of the crude mixture by GC revealed > 90 % conversion of menthol to three metabolites in the percentage of 60 %, 15 % and 25 % respectively. The crude obtained after preparative fermentation purified over silica gel column chromatography furnished three pure metabolites. Further EI-MS analysis, showed mass at m/z 172.1 for all the three

metabolites, indicating an increase of 16 amu in menthol molecular weight and thus an insertion of a hydroxy group on the skeleton was predicted. ^{13}C -NMR spectrum showed conversion of a methylene carbon at δ 32.2 ppm of menthol to a methine carbon in the metabolite, resonating at δ 76.0 and in DEPT decrease in one secondary carbon, this confirmed hydroxylation at C-6 and ^1H -NMR spectrum of 6-hydroxymenthol was

showed a proton resonating at δ 3.17-3.3.20 (1H, m, 6-CH), the metabolite was characterized as 6-hydroxymenthol. The solid was recrystallized in pet ether-ethyl acetate to obtained colourless needles. Single crystal X-



ray diffraction data was recorded which further supported the identification of the stereochemistry of the hydroxyl group. Optical rotation showed that the hydroxylation at stereoselective manner. GC-MS analysis and an Optical rotation showed that the hydroxylation at stereoselective manner. ^{13}C -NMR spectrum showed conversion of a tertiary carbon δ 31.2 at of substrate to a quaternary

carbon in the metabolite, resonating at δ 75.02 and in DEPT one tertiary carbon was diminished, this confirmed hydroxylation at C-8; ^1H -NMR spectrum showed a proton resonating at δ 1.99-2.18 (1H, m, 1-CH), the metabolite was characterized as 8-hydroxymenthol. Similarly, the third metabolite was identified and characterised as 1-hydroxymenthol (Scheme 5C.2).

5A.2.3 Antimicrobial Activity

Menthol and its metabolites were showed antibacterial and anti-yeast activity. Among the derivatives, 6-hydroxymenthol and 1-hydroxymenthol showed antibacterial activity at a lower concentration. 6-hydroxymenthol was found effective against *S.aureus* (8 $\mu\text{g}/\text{mL}$), *E.coli* (32 $\mu\text{g}/\text{mL}$), *C.albicans* (16 $\mu\text{g}/\text{mL}$). While 8-hydroxymenthol was found to be more effective against *E. coli* (8 $\mu\text{g}/\text{mL}$) and Gram-negative *S. aureus* (16 $\mu\text{g}/\text{mL}$), this enhancement of the activity of the metabolites may be due to an increase in bioavailability due to the insertion of the polar functionality on the hydrophobic carbon skeleton. However, menthol did not show any measurable antimicrobial activity at a lower concentration. Obtained results probe further into the hemolytic activity with the effect of metabolites on bacterial cells by fluorescence assay.

Table 5A.2 Antimicrobial Activity of Menthol and Metabolites

Microorganism	menthol	6-hydroxy menthol (%)	8-hydroxy menthol (%)	1-hydroxy menthol (%)	Gent. Sulf. ^d	Ben. Sod. ^d
<i>M.luteus</i> (G ⁺)	>128	64	64	32	nd	1
<i>S.aureus</i> (G ⁺)	64	8	16	8	0.5	2
<i>P. fluorescens</i> (G)	>128	100	90	90	0.5	nd
<i>E.coli</i> (G ⁻)	>128	32	8	16	1	4
<i>C.albicans</i>	128	16	64	16	nd	nd
%Hemolysis	46	67	63	59	---	---

Gent.sulf. Gentamicin sulfate; Ben.sod., Benzamide sodium; Amp.B. Amphotericin B ^a The calculated average MIC values are presented, ^b MIC > 128 µg/mL was considered as inactive, ^c nd: not determine, ^d Positive control.

5A.2.4 Hemolytic activity

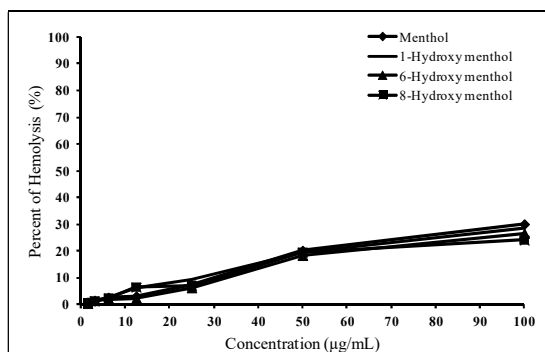


Figure 5A.2. Hemolytic activity of menthol and its metabolites with 4 % hRBCs

As the metabolites showed significant antimicrobial activity, we studied the hemolytic activity of the menthol and metabolites. Hemolytic activities of the metabolite are less than 20 % at their respected MIC concentration. Metabolites are showed antimicrobial activity at lower MIC value close to MIC value of standard used, along with low hemolytic activity, these quality make them like lead

compounds in the development of antimicrobial agents.

5A.2.5 Effect on Membrane Permeability and Cell Viability

The membrane-perturbing and microbicidal ability of the menthol derivatives were investigated by a fluorescent staining assay, where *E. coli* cells incubated with MIC concentrations of 6-hydroxymenthol and stained with fluorescent dyes FITC and PI. *E. coli* cells without menthol or metabolites treated as control. FITC stain only those cells whose cell membrane are partially or completely damaged whereas PI is known to stain

only those cells whose cell membrane is sufficiently damaged that the cell can be described as non-viable. Fluorescent images showed FITC and PI intake by *E.coli* cells suggested that 6-hydroxymenthol may increase the permeability of the bacterial cell membranes. Moreover staining of the cellular DNA with PI indicates that the concentration of the compound used might be lethal enough to cause permanent damage

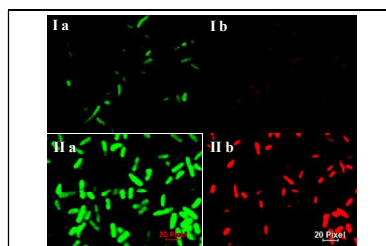


Figure 5A.3. Fluorescence images of *E. coli* control (I a and b), after the treatment with 6-hydroxymenthol (II a and b)

to cell membrane leading to cell death. These results suggest that an increase in the bacteria cell membrane of permeability after metabolites treatment.

5A.3 Conclusion

Mucor piriformis biotransformed menthol to its three oxidised metabolites as shown in studies. Metabolites were purified and characterised as 6-hydroxy menthol, 6-hydroxy menthol, 8-hydroxy menthol, 1-hydroxy menthol, and antimicrobial activity study suggested that menthol exhibited antimicrobial activity at higher concentration (MIC) compare to its metabolites. All the metabolites showed low hemolytic activities. Moreover, further investigation indicated that might be these derivatives act on bacterial cells wall. Here provide a basis for the investigation to access their potential as applicable antimicrobial agents. Furthermore, there is a need to systematically study the mode of action of metabolites on the molecular level.

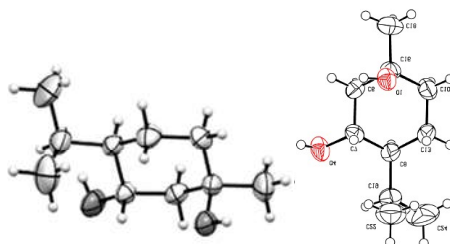


Figure 5A.4 ORTEP diagram of 1-hydroxy menthol (ellipsoids are drawn at 50 % probability)

Table 5A. 3 Crystal Data of 1-hydroxy menthol

- Bond precision: C-C = 0.0080 Å Wavelength=0.71073
- Cell: a= 7.9958(5) b=6.8903(4) c = 9.7067(5)
alpha = 90 beta = 94.897(6) gamma = 90
-
- Temperature:293K
- Correction method = MULTI-SCAN
- Data completeness = 0.73/0.36 Theta(max)= 27.860
- R(reflections) = 0.0588(1600) wR2(reflections)= 0.1747(1835)
- S = 1.142 Npar = Npar = 227
- The following ALERTS were generated. Each ALERT has the format

	Calculated	Reported
Volume	532.82(5)	532.82(5)
Space group	P 1	P 1
Hall group	P 1	-
Moiety formula	C10 H20 O2	-
Sum formula	C10 H20 O2	C10 H20 O2
Mr	172.26	172.26
Mu (mm-1)	0.072	0.072
F000	192.0	192.0
F000'	192.09	
h,k,lmax	10,9,12	10,9,12
Nref	5048[2524]	1835
Tmin,Tmax	0.974,0.986	0.974,0.986
Dx,g cm-3	1.074	1.074
Z	2	2
Tmin'	0.965	

5A.4 Experimental Section.

5A.4.1 Material and Methods

(1R, 2S, 5R)-(-) Menthol was purchased from Sigma-Aldrich. Media ingredients were purchased from HiMedia Laboratories, Mumbai, India. Fluorescein Isothiocyanate (FITC), propidium iodide (PI) purchased from Sigma-Aldrich (USA). These test microorganisms were obtained from collected from the National Collection of Industrial Microorganism (NCIM) Pune. Antimicrobial activities were assessed using Gram-positive bacteria *M. piriformis* (soil isolated), *A. niger* (NCIM 582), *F. proliferatum* (1105), *N. crassa* (910), *M. luteus* (NCIM 2170), *M. amphibiorum* (NCIM 881), *Staphylococcus aureus* (NCIM 2100), Gram-negative bacteria *E.coli* (NCIM 2575), *Pseudomonas fluorescense* and yeast *Candida albicans* (NCIM 3471). Column chromatography performed on silica gel (230-400 mesh). Migration of the compounds on TLC was visualised by spraying it with a solution of 3.2% anisaldehyde, 2.8% H₂SO₄, 2% acetic acid in ethanol followed by heating for 1-2 min. GC analyses were carried out using Agilent 7890 GC system equipped with a hydrogen flame ionization detector (FID) and HP-5 capillary column (30 m × 0.32 mm × 0.25 μm, J & W Scientific). Nitrogen was used as carrier gas at a flow rate of 1 mL/min. GC analyses were carried similar to mentioned above. The column temperature was programmed as 60 °C for 2 min, then increase to 120 °C at a rate of 3 °C/ min and then to 240 °C at a rate of 10 °C /min. The injector and detector temperatures were maintained at 230 °C and operated in split mode (1:8). Mass spectra were recorded using EI-technique on Agilent 5975C mass selective detector interfaced with a 7890A gas chromatograph and HP-5 (30 m × 0.32 mm × 0.25 μm) column with a flow of helium at the rate of 1 mL/min. NMR (¹H, ¹³C, DEPT) spectra were recorded on Varian INOVA spectrometer (400, 500 MHz) and chemical shift values were reported in ppm concerning the residual solvent or Tetramethylsilane (TMS) signals as the reference. HRMS data were collected on Thermo Scientific Q-Exactive Quadrupole-Orbitrap Mass Spectrometer. FTIR spectra were recorded on Perkin Elmer FTIR spectrophotometer in CHCl₃, and optical rotations were determined in the same solvent on JASCO (P-2000), polarimeter using 10 mm cell (*c* in g/100 mL unit). A single crystal of compound 6-hydroxy menthol was obtained during purification and grown from a mixture of Ethyl acetate: Pet ether as a colourless needle suitable for structural analysis. X-ray intensity data were collected on a Bruker SMART APEX CCD diffractometer at room temperature. All the data were corrected for Lorentzian, polarisation and absorption effects using Bruker's SAINT and SADABS programs. SHELX-9722 was used for structure solution and full matrix least-squares refinement on F2. Hydrogen atoms were included in the refinement as per the riding model. Zeiss Axiovert apotome microscope equipped with an AxioCam camera oil-immersion objective (64x) and images were processed with Axiovision 4.7 software.

5A.5.2 General Biotransformation Procedure

(a) Screening of Fungal Cultures

The sporulated fungal cultures were grown on PDA slant was transfer to Erlenmeyer flasks containing 50 mL of sterile modified *Czapek-Dox* media and incubate it at 30 °C at 220 rpm in incubator shaker for 36 h. To the well grown fungal culture flasks, a menthol was added at a concentration of 30 mg in 0.2 mL acetone/ 50 mL media and incubation was continued. After 5 days incubation period broth was extracted separately with ethyl acetate (three times) and organic layers were separated and combined together further dried over anhydrous Na₂SO₄, concentrated and analyzed by TLC, GC and GC-MS. All the screening experiments were analyzed by comparing with corresponding substrate control and organism control.

(b) Time Course Experiment

Menthol (0.4 g/L) was added to well-grown cultures in 50 mL × 5 Erlenmeyer flasks and incubated on a rotary shaker as mentioned above. Each flask was extracted with dichloromethane (CH₂Cl₂) after every 24 h and analyzed by GC and GC-MS for monitoring the level of formation of the formation of each metabolite.

(c) Substrate Concentration Experiment

Once the duration of biotransformation was known, various concentrations (0.1 g/L to 0.5 g/L) the menthol added in the 50 mL well-grown culture in standardised biotransformation conditions to check the maximum concentration that can be completely biotransformed.

(c) Resting Cell Experiment

Well-grown culture of *M. piriformis* (36 h) was filtered and the mycelia obtained were washed with distilled water and phosphate buffer (pH 7.2). The mycelia were dried by pressing between the filter papers. 2 g of mycelia (wet weight) was weighed and added into 50 mL of phosphate buffer of pH 7.2 with 100 mg dextrose. 10 mg of menthol in 0.3 mL acetone was added to the reaction mixture and incubated at 30 °C on a rotary shaker (180 rpm) for 36 h. After this incubation period, filtered mycelia and broth extracted with ethyl acetate (10 mL × 2) and analysed by TLC, GC, and GC-MS.

(d) Preparative Scale Fermentation

Large scale fermentation was carried out in a modified *Czapek-Dox* medium. The pH of the medium was adjusted to 5.8 with 1M K₂HPO₄. Erlenmeyer flasks (1000 mL × 20) containing 100 mL of sterile medium were inoculated with 2 mL of spore suspension from a well-grown culture on potato dextrose agar slants and incubated at 29-30 °C on a rotary shaker at 180 rpm for 24 h. 40 mg of menthol in acetone (0.2 mL)/ 100 mL media and the incubation was continued for an additional period of 8 days. Control experiments were also run with the menthol but without *M. piriformis* and with *M. piriformis* but without menthol. After this incubation period, the contents of the flasks were pooled and filtered through a muslin cloth to separate mycelia and broth. The broth was then saturated with sodium chloride and extracted with ethyl acetate (four times, 1:1 v/v). The dried mycelia were washed with ethyl acetate. The two extracts found to be the same by GC and TLC analyses and therefore pooled. The crude extract (1.34 g) obtained was subjected to silica gel (230-400 mesh) column chromatography. Pure metabolites were obtained after successive silica gel column chromatographic purification.

(e) Characterization of Metabolites

NMR (¹H-NMR, ¹³C-NMR, DEPT) spectra were recorded and chemical shift values were reported in ppm with respect to the residual solvent or TMS signals as the reference. HRMS data were collected on GC-HR-ESI-MS Thermo Scientific Q Exactive Quadrupole-Orbitrap Mass Spectrometer. FTIR spectra were recorded on Perkin Elmer FT-IR spectrophotometer in CHCl₃ and optical rotations were determined in the same solvent on JASCO (P-2000), polarimeter using 10 mm cell (*c* in g/100 mL unit).

5A.4.4 Fluorescent staining for assessing cell viability and membrane integrity

A double staining procedure was followed to assess the viability as well as the membrane integrity of the cell.¹⁶ *E. coli* cells were grown in LB until an optical density at 600 nm (OD₆₀₀) of 0.6 was reached. The cells were washed twice with 10 mM sodium phosphate buffer (pH 7.4) to remove media and were resuspended in the same buffer. After exposure to inhibitory concentrations of menthol and its derivatives at 37 °C for 60 min, the bacterial cells were immobilised on poly(L-lysine)-coated glass slides

for 50 min at 30 °C, followed by addition of FITC (6 µg/mL suspended in buffer). After 30 min at 30°C, the FITC solution was washed, the slides were rinsed and 100 µL of PI (2 µg/mL) was added to the slides. After incubation at 30°C for 30 min, slides were washed as described above, controls were run in the absence of compound. Fluorescent images were recorded using a Zeiss Axio-observer Z1 microscope equipped with an oil-immersion objective (64x) and an Axio Cam camera. Image acquisition and processing were performed using Axiovision software.

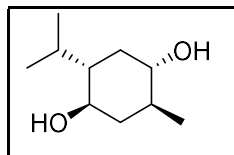
5C.5 Hemolytic assay

The hemolytic assay was performed according to the protocol reported earlier.¹⁷ This assay was performed as mentioned earlier.¹⁶ Fresh human red blood cells (hRBCs) were collected with ethylene diamine tetraacetic acid (EDTA).¹⁷ Before performing assay the hRBCs were washed four times with Tris-buffered saline (150 mM NaCl, 10 mM Tris pH 7.2,) and diluted to a final concentration of 4 % v/v. The assay was performed at a final volume of 100 µL as follows: an aliquot of 50 µL of hRBCs suspension was added to 50 µL of 2-fold serially diluted (100 µg/mL) menthol and its metabolites in the minimum amount of dimethyl sulfoxide (DMSO) diluted with Tris buffer. The plate was incubated at 37 °C for 1.5 h and then centrifuged for 15 min. at 3000 rpm. The supernatant (50 µL) from each well was transferred to a new 96-well plate containing 50 µL of water, and the release of haemoglobin was monitored by measuring the absorbance at 540 nm.

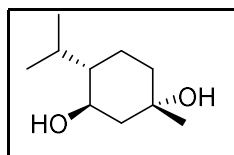
All the experiments were performed in triplicate with hRBC suspensions in tris buffer; tris buffer served as negative control and in 1 % Triton-X comprised as a positive control, respectively. The percentage of hemolysis was defined as $(A - A_N) / (A_P - A_N) \times 100$, where A is the absorbance of the test. Well, A_N is the absorbance of the negative control, and A_P is the absorbance of the positive control.

5C.6 Analytical Data

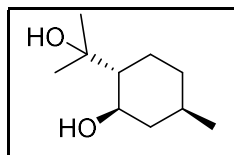
6-Hydroxy menthol Colourless needle crystals; IR (CHCl₃) λ_{\max} 3440,1463, 1348, 1051 cm⁻¹; ¹H-NMR (CDCl₃, 400 MHz): δ ppm 3.44 -3.49 (dd, J=4.28,4.58,10.68, 1H), 3.17-3.22 (dd, J= 3.66,4.27,10.68, 1H), 2.13-2.16 (ddd, J = 2.75,4.27,7.02, 1H), 1.94-1.98 (td, J = 3.96,4.27,8.55, 1H), 1.82-1.86 (td, J=3.67,3.96,12.52, 1H), 1.30-1.33 (m, J = 7.02,2.75, 1H), 1.52 (s, 1H), 1.05-1.15 (m, 2H), 1.03 (d, J = 6.41, 3H), 0.93 (d, J=7.02, 3H), 0.82 (d, J = 7.02, 3H); ¹³C-NMR (CDCl₃, 100 MHz): δ ppm 15.86, 18.18, 21.00, 25.76, 29.71, 32.34, 38.35, 42.47, 48.54, 70.70; EI-MS: m/z 172.1.



1-Hydroxy menthol Colourless needle crystals, IR (CHCl₃) λ_{\max} 3440,1463, 1348, 1051 cm⁻¹; ¹H-NMR (CDCl₃, 400 MHz): δ ppm 3.7 (ddd, J = 3.66,3.96,3.92,7.93 Hz, 1H), 2.17 (d, J = 7.02,2.75, 1H), 1.98 (dddd, J=3.05, 4.58, 7.33, 4.28, 1H), 1.63-1.59 (m, 2H), 1.49-1.43 (m, 1H), 1.29-1.38 (m, 3H), 1.24(s, 3H), 1.14-1.09(m, 1H), 1.04 (s, 1H), 0.93(d, J=7.02 Hz, 3H), 0.83(d, J=7.02 Hz, 3H); ¹³C-NMR (CDCl₃, 100 MHz): δ ppm 16.2, 19.0, 21.0, 25.8, 31.6, 38.4, 48.2, 50.0, 68.5, 71.5; EI-MS: m/z 172.1 (M⁺).



8-Hydroxy menthol Colourless needle crystal, IR (CHCl₃) λ_{\max} 3440,1463, 1348, 1051 cm⁻¹. ¹H-NMR (CDCl₃, 400 MHz): δ ppm 3.8 (s, H), 3.70 (t, J = 7.02, 2.75, 1H), 1.92 (m, 1H), 1.62-1.45 (m, 2H), 1.21 (s, 6H), 0.99-1.07 (m, 1H), 0.90 (m, 5H). ¹³C-NMR (CDCl₃, 100 MHz): δ ppm 21.95, 23.66, 27.06, 30.04, 31.33, 34.51, 44.57, 53.88, 72.89, 75.05; EI-MS: m/z 172.1 (M⁺).



5C.5 Spectral Copies

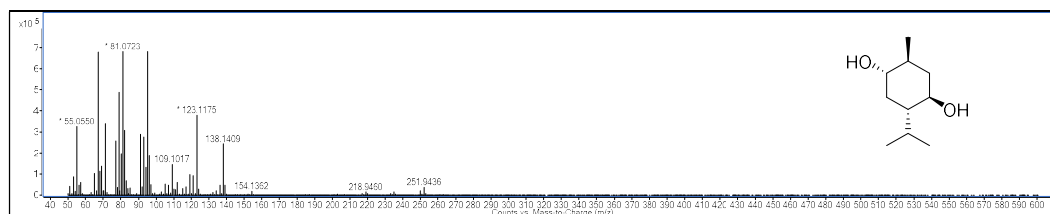
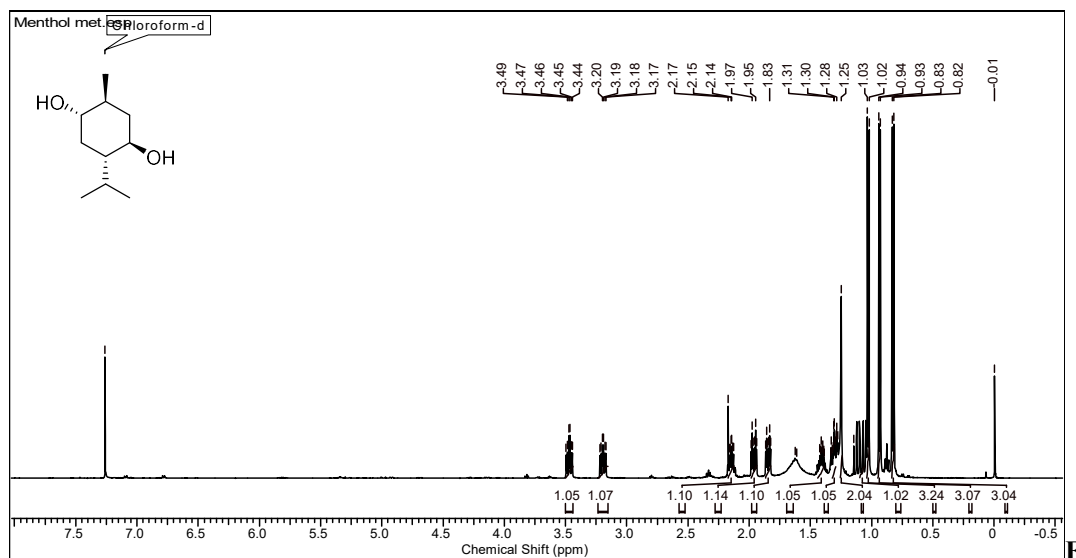
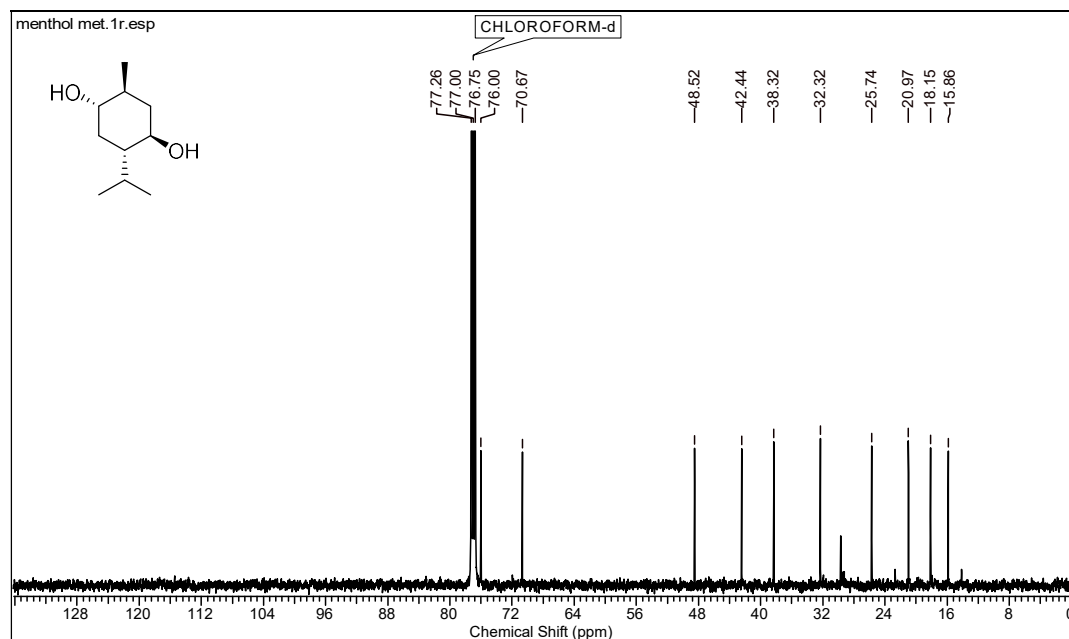


Figure 5A.5a. GC-EI-QToF-MS spectrum of 6-hydroxy menthol

Figure 5A.5b. ^1H NMR spectrum of 6-hydroxy menthol in CDCl_3 Figure 5A.5c. ^{13}C NMR spectrum of 6-hydroxy menthol in CDCl_3

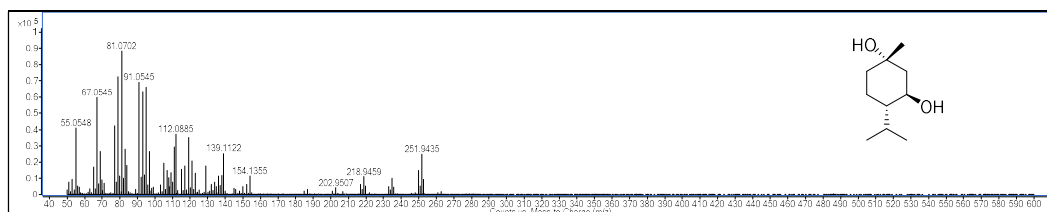
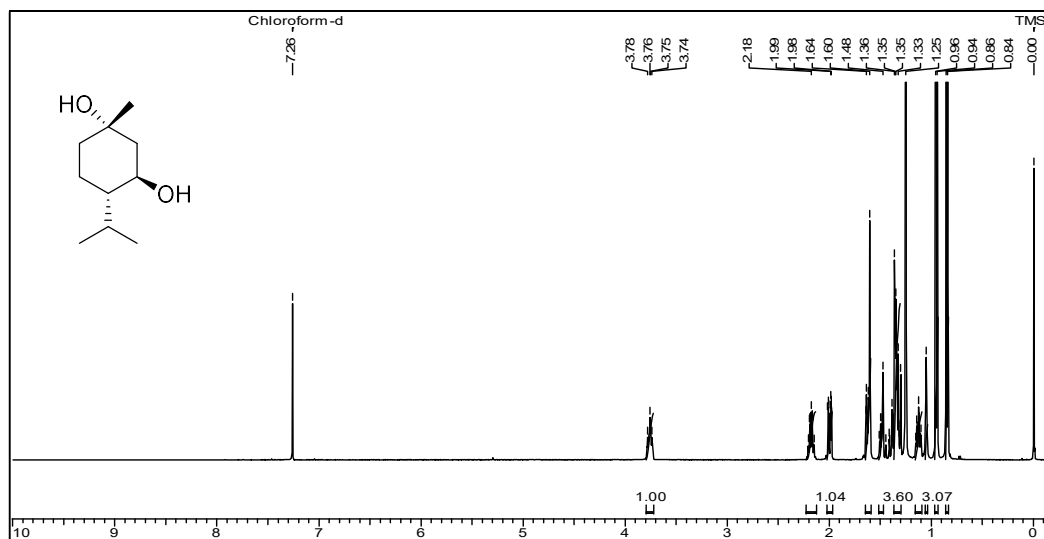
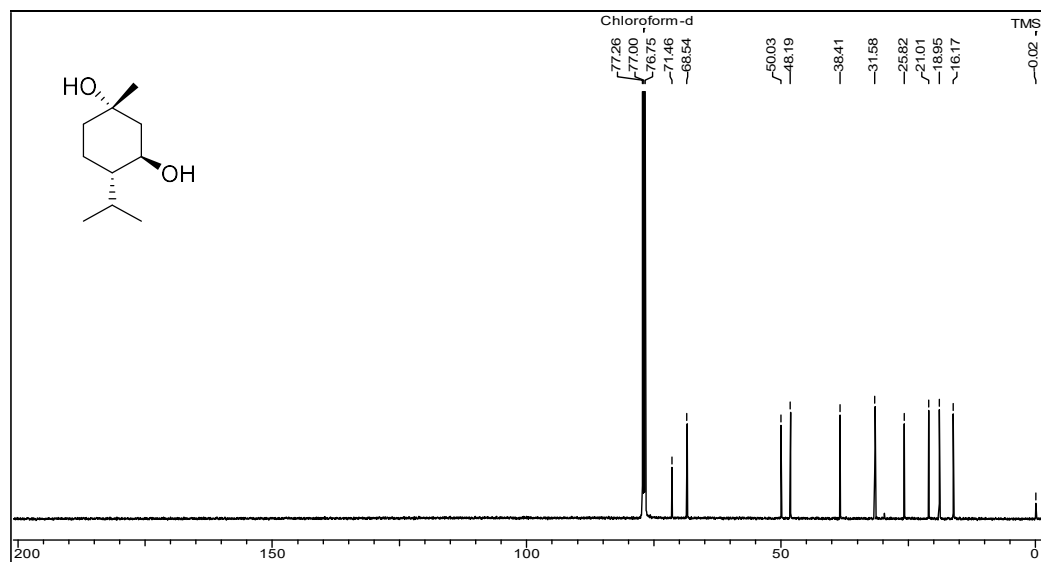


Figure 5A.6a. GC-EI-QToF-MS spectrum of 1-hydroxy menthol

Figure 5A.6b. ^1H NMR spectrum of 1-hydroxy menthol in CDCl_3 Figure 5A.6c. ^{13}C NMR spectrum of 1-hydroxy menthol in CDCl_3

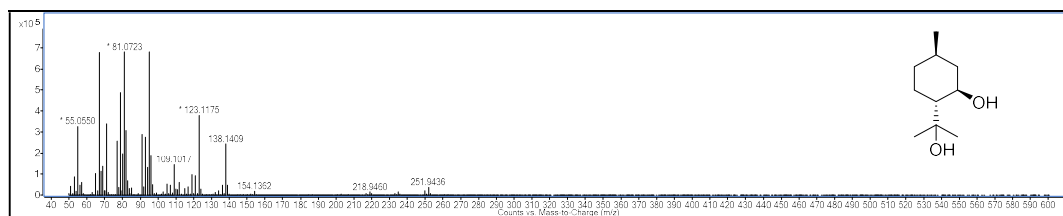
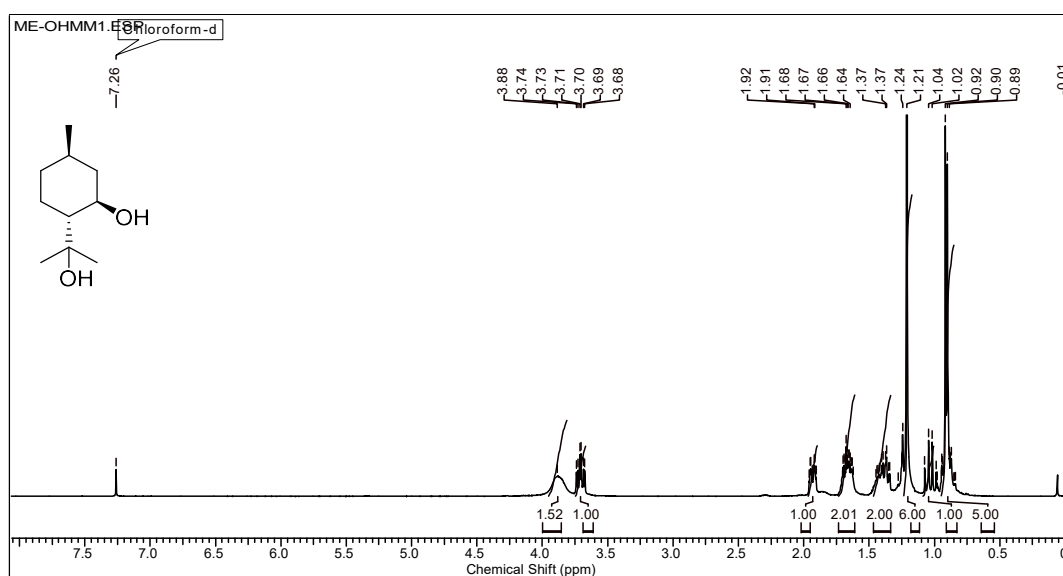
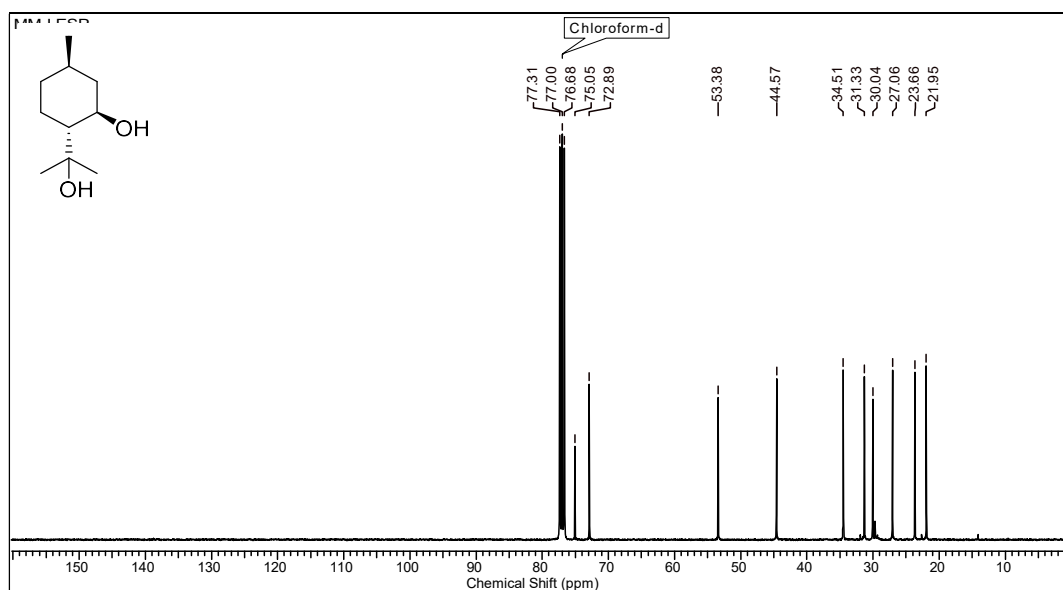


Figure 5A.7a. GC-EI-QToF-MS spectrum of 8-hydroxy menthol

Figure 5A.7b. ^1H NMR spectrum of 8-hydroxy menthol in CDCl_3 Figure 5A.7c. ^{13}C NMR spectrum of 8-hydroxy menthol in CDCl_3

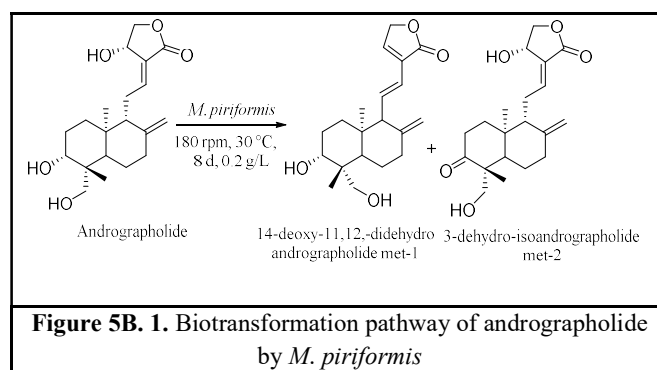
Chapter 5: Section B

**Biotransformation of Andrographolide using
*Mucor piriformis***

5B. 1 Introduction

Andrographolide is a principal constituent of an *Andrographis paniculata* medicinal herb.¹⁸ It has a broad range of pharmacological activities such as antimicrobial,¹⁹ anti-inflammatory,²⁰ hepatoprotective,²¹ anti-HIV and anti-cancer activity.²² Bioactive natural products skeletal modifications is the effective strategy for development more bioactive analogue of it.^{7,8} Literature review suggested on andrographolide derivatisation indicated that bioactivity of it can be increased with the skeletal modification by using chemical synthesis or microbial biotransformation.²³ For desired functional modification of bioactive natural products conventional synthetic methodologies was less economical, time-consuming and give a low yield.²⁴ It is due to involved protecting deprotection strategies, functional groups sensitivity,²⁵ steric hindrance,²⁶ inactive carbon, and overall low yield.²⁷ Biocatalysis is the economic and green approach for regio-²⁸ and stereo-selective²⁹ modification of the bioactive molecules.³⁰

Here we have study whole cell biotransformation of andrographolide by using *Mucor piriformis*, resulted in two metabolites. *M. piriformis* could quantitatively transform andrographolide with high region-selectivity. Metabolites have been characterised using spectral techniques as 3-dehydroandrographolide and 14-deoxy-11,12-didehydroandrographolide



5B.2 Results and Discussion

5B.2.1 Screening of Experiment for Andrographolide Biotransformation

In order to find the efficient fungal strain for andrographolide biotransformation on the analytical scale, fungal cultures belong to genera, e.g. *Mucor*, *Penicillium*, *Aspergillus*, *Rhizopus*, *Cephalophora*, *Gibberella* and *Neurospora* were screened. Andrographolide incubated with fungal cultures under standardised biotransformation conditions and extracted after 5 days, and crude extracts obtained were analysed by TLC, HPLC and LCMS. The result indicated that *M. piriformis* efficiently transformed andrographolide to metabolites compared to the other fungal strain; hence *M. piriformis* was selected for preparative scale biotransformation. Substrate control experiment suggested that andrographolide was not degraded in reaction conditions without fungal strain. HPLC chromatogram of fungal control experiment suggested that no andrographolide consumption, which confirmed that it, was metabolised by fungal culture. Resting cell experiment confirmed the involvement of fungal system involved in andrographolide biotransformation. Substrate concentration studies with andrographolide (0.1 g/L to 0.5 g/L) suggested that *M. piriformis* transformed it quantitatively at 0.2 g/L, the rate of bioconversion decreases after this, which might be due to the toxic effect on fungus. Time course study at the standardised biotransformation conditions and same andrographolide concentration suggested that the *M. piriformis* quantitatively convert menthol (> 70 %) to metabolites in eight days (Figure 5C.1). The major metabolites formed were 14-deoxy-11,12-didehydroandrographolide and 3-dehydro isoandrographolide as a minor metabolite.

5B.2.3 Preparative Scale Biotransformation, Purification and Characterization of Metabolites

Preparative scale fermentation of andrographolide was carried out for metabolites isolation and characterization. Andrographolide large scale biotransformation was performed with a concentration of 0.2 g/L suggested by substrate concentration experiment with 1 g quantity. The crude after extraction was analysed by TLC, GC and LC-MS, which suggested that crude contained a mixture of metabolites, with only two metabolites. The primary analysis of the crude mixture by GC revealed > 70 % conversion of andrographolide to two metabolites in the percentage of 48.2 % and 26.4 % respectively.

Table 5B.1 screening of fungal culture for andrographolide biotransformation

Strain	14-deoxy-11,12-didehydro.%	3-dehydro isoandro. %	Other metabolites
<i>M. amphibiorum</i>	12.4	8.1	20.5
<i>M. piriformis</i>	48.2	28.4	-
<i>A.niger</i>	15.4	-	14.7
<i>R.oryzae</i>	-	-	30.1
<i>A.chraceous</i>	8.0	-	32.0
<i>C. irregularis</i>	-	10.2	12.1

The crude was purified over silica gel column chromatography by using methanol in dichloromethane solvent system resulted in two pure metabolites. The HRMS analysis of metabolite one showed an ion peak at m/z 355.1874 ($C_{20}H_{28}O_4Na$), indicating the removal of the hydroxyl group from andrographolide ($C_{20}H_{30}O_5$). In ^{13}C -NMR, and DEPT analysis suggested the increase in methylene carbon at δ 136.5 ppm by loss of one methine carbon at δ 64.58 ppm from andrographolide which suggested that hydroxyl loss occurred on a methine carbon. Metabolite and andrographolide were similar 1H NMR spectra except for the absence of a peak at δ 4.17 ppm from carbon 14-C which appeared at δ 7.24 ppm in metabolite. Proton and carbon downfield shift in NMR suggested that the double bond formation of due to the loss of hydroxyl at C-14. The metabolite was identified as a 14-hydroxy-11,12-didehydroandrographolide which matched with the earlier report.³¹ HRMS spectrum of the second metabolite showed the mass ion peak at m/z 371.19 ($C_{20}H_{28}O_4Na$) showed the decrease in molecular weight by 2 amu compared to the andrographolide ($C_{20}H_{30}O_5$) suggested two hydrogen losses. In ^{13}C -NMR, DEPT spectrum of metabolite showed loss of peak at δ 78.5 ppm compared to andrographolide and appeared a new peak at δ 215.9 ppm suggested the introduction of the carbonyl. Metabolite and andrographolide were similar 1H NMR spectra except for the absence of a peak at δ 3.33 ppm from carbon (C-3) suggested the oxidation of hydroxyl to the ketone. The metabolite was identified as a 3-dehydroisoandrographolide which matched with the earlier report.³¹

5B.3 Conclusion

Whole-cell biocatalysis approach for andrographolide systematic biotransformation was developed. *M. piriformis* biotransformed andrographolide exclusively into two metabolites with quantitative yields. Whole cell biotransformation is the economic green approach for getting new derivatives from bioactive molecules. There is scope for biotransformation of other labdane diterpenoids. The obtained metabolites were also occurring in the plant; it concluded that the fungal enzymatic system mimics the plant system.

5B. 4 Experimental Section

5B.4.1 Chemical, reagents, and biological materials

Andrographolide was isolated from *A. paniculata*. Media ingredients were purchased from HiMedia Laboratories, Mumbai, India. Fluorescein Isothiocyanate (FITC), propidium iodide (PI) purchased from Sigma-Aldrich (USA). These test microorganisms were obtained from collected from the National Collection of Industrial Microorganism (NCIM) Pune. Antimicrobial activities were assessed using Gram-positive bacteria *M. piriformis* (soil isolated), *A. niger* (NCIM 582), *F. proliferatum* (1105), *N. crassa* (910), *M. luteus* (NCIM 2170), *M. amphibiorum* (NCIM 881), *Staphylococcus aureus* (NCIM 2100), Gram-negative bacteria *E.coli* (NCIM 2575), *Pseudomonas fluorescense* and yeast *Candida albicans* (NCIM 3471). Column chromatography performed on silica gel (230-400 mesh). Migration of the compounds on TLC was visualised by spraying it with a solution of 3.2% anisaldehyde, 2.8 % H₂SO₄, 2 % acetic acid in ethanol followed by heating for 1-2 min. HPLC runs were performed on analytical XBridge C18 column (4.6 × 250 mm, 5 µm), UV detection at 225 and 254 nm. Gradient solvent programme of Acetonitrile in water 30 min (0-5 min, 30 % ACN/ water, 5-6 min, 30-40 % ACN/ water, 6-10 min, 60 % ACN/ water, 10-11 min, 50 % ACN/ water, 11-15 min, 50 % ACN/ water, 15-16 min, 40 % ACN/ water, 16-20 min, 40 % ACN/ water, 20-21 min, 30 % ACN/ water, 21-25 min, 30 % ACN/ water, 25-30 min, 70 % ACN/ water) with a flow rate of 1 mL/min and 15 µL samples was injected. NMR (¹H, ¹³C, DEPT) spectra were recorded on Varian INOVA spectrometer (400, 500 MHz) and chemical shift values were reported in ppm concerning the residual solvent or Tetramethylsilane (TMS) signals as the reference. HRMS data were collected on Thermo Scientific Q-Exactive Quadrupole-Orbitrap Mass Spectrometer. FTIR spectra were recorded on Perkin Elmer FT-IR spectrophotometer in CHCl₃, and optical rotations were determined in the same solvent on JASCO (P-2000), polarimeter using 10 mm cell (*c* in g/100 mL unit). A single crystal of compound 6-hydroxy menthol was obtained during purification and grown from a mixture of Ethyl acetate: Pet ether

as a colourless needle suitable for structural analysis. X-ray intensity data were collected on a Bruker SMART APEX CCD diffractometer at room temperature. All the data were corrected for Lorentzian, polarisation and absorption effects using Bruker's SAINT and SADABS programs. SHELX-9722 was used for structure solution and full matrix least-squares refinement on F2. Hydrogen atoms were included in the refinement as per the riding model. Zeiss Axiovert apotome microscope equipped with an AxioCam camera oil-immersion objective (64x) and images were processed with Axiovision 4.7 software.

5A.5.2 General Biotransformation Procedure

(a) Screening of Fungal Cultures

The sporulated fungal cultures were grown on PDA slant was transfer to Erlenmeyer flasks containing 50 mL of sterile modified *Czapek-Dox* media and incubate it at 30 °C at 220 rpm in incubator shaker for 36 h. To the well grown fungal culture flasks, an andrographolide was added at a concentration of 10 mg in 0.2 mL acetone/ 50 mL media and incubation was continued. After 5 days incubation period broth was extracted separately with DCM (three times) and organic layers were separated and combined together further dried over anhydrous Na₂SO₄, concentrated and analyzed by TLC, HPLC and LC-MS. All the screening experiments were analyzed by comparing with corresponding substrate control and organism control.

(b) Time Course Experiment

Andrographolide (0.2 g/L) was added to well-grown cultures in 50 mL × 5 Erlenmeyer flasks and incubated on a rotary shaker as mentioned above. Each flask was extracted with dichloromethane (CH₂Cl₂) after every 24 h and monitoring the level the formation of each metabolite was analyzed by HPLC, LC-MS for.

(c) Substrate Concentration Experiment

Once the duration of biotransformation was known, various concentrations (0.1 g/L to 0.5 g/L) the menthol added in the 50 mL well-grown culture in standardised biotransformation conditions to check the maximum concentration that can be completely biotransformed.

(c) Resting Cell Experiment

Well-grown culture of *M. piriformis* (36 h) was filtered and the mycelia obtained were washed with distilled water and phosphate buffer (pH 7.2). The mycelia were dried by pressing between the filter papers. 2 g of mycelia (wet weight) was weighed and added into 50 mL of phosphate buffer of pH 7.2 with 100 mg dextrose. 10 mg of andrographolide in 0.1 mL acetone was added to the reaction mixture and incubated at 30 °C on a rotary shaker (180 rpm) for 36 h. After this incubation period, filtered mycelia and broth extracted with ethyl acetate (10 mL × 2) and analysed by TLC, and HPLC.

(d) Preparative Scale Fermentation

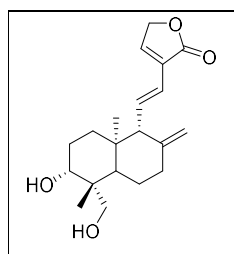
Large scale fermentation was carried out in a modified *Czapek-Dox* medium. The pH of the medium was adjusted to 5.8 with 1M K₂HPO₄. Erlenmeyer flasks (1000 mL × 20) containing 100 mL of sterile medium were inoculated with 2 mL of spore suspension from well culture grown on potato dextrose agar slants and incubated at 29-30 °C on a rotary shaker at 180 rpm for 24 h. Andrographolide (0.2 g /L) added to media and the incubation was continued for an additional period of 8 days. Control experiments were also run with the menthol but without *M. piriformis* and with *M. piriformis* but without menthol. After this incubation period, the contents of the flasks were pooled and filtered through a muslin cloth to separate mycelia and broth. The broth was then saturated with sodium chloride and extracted with ethyl acetate (four times, 1:1 v/v). The dried mycelia were washed with ethyl acetate. The two extracts found to be the same by GC and TLC analyses and therefore pooled. The crude extract (842 mg) obtained was subjected to silica gel (230-400 mesh) column chromatography.

(e) Purification and Characterization of Andrographolide metabolites

Metabolites were purified over silica gel (230-400 mesh) column chromatography using Methanol: DCM gradient mixture (0.2 % to 8 %). As the eluent, and compounds were visualised on thin-layer chromatography sheets pre-coated with silica gel 60-F254 by spraying with a solution of anisaldehyde. The purity of the metabolite was checked in HPLC; ¹H and ¹³C NMR spectra were recorded in CDCl₃. NMR (¹H-NMR, ¹³C-NMR, DEPT) spectra were recorded and chemical shift values were reported in ppm with

respect to the residual solvent or TMS signals as the reference. HRMS data were collected on GC-HR-ESI-MS Thermo Scientific Q Exactive Quadrupole-Orbitrap Mass Spectrometer. FTIR spectra were recorded on Perkin Elmer FT-IR spectrophotometer in CHCl_3 and optical rotations were determined in the same solvent on JASCO (P-2000), polarimeter using 10 mm cell (c in g/100 mL unit).

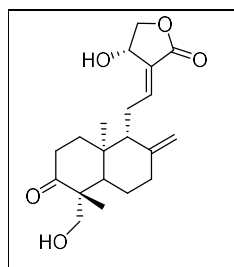
11, 12-Didehydro-14-deoxyandrographolide White crystal; m.p. 204-206 °C; IR (CHCl_3 , cm^{-1}) ν_{max} = 904, 1663, 1734, 2900, 3325, 3400 cm^{-1} ; HRMS (ESI) m/z : $[\text{M}+\text{Na}]^+$



Calcd for $\text{C}_{20}\text{H}_{28}\text{O}_4\text{Na}$, 355.1885; found, 373.1874. ^1H NMR (CDCl_3 , , 400 MHz) : δ ppm 7.33-7.34 (td, J = 1.83, 3.66 Hz, 1H), 6.17-6.13 (d, J = 16.03 Hz, 1H), 5.59-5.65 (d, dd, J = 10.07, 5.50 Hz, 1H), 4.99 (m, 1H), 4.81 (m, 2H), 4.65 (m, 1H), 3.30-3.39 (m, 3H), 2.36-2.43 (m, 2H), 1.93-2.13 (m, 2H), 1.75-1.83 (m, 4H), 1.25-1.33 (m, 2H), 1.20-1.22 (m, 4H), 0.84 (s, 1H), 0.68 (s, 3H). ^{13}C NMR (CDCl_3 , , 100 MHz): δ ppm 172.15, 147.82, 139.55, 136.59, 134.84, 122.60, 107.81, 81.14, 72.22, 65.12, 62.94, 47.21, 43.81, 40.29, 38.17, 34.82, 29.20, 25.54, 23.26, 15.84.

3-dehydro isoandrographolide

White powder; m.p. 206-208 °C; IR (CHCl_3 , cm^{-1}) ν_{max} = 1646, 1740, 2900, 3378, 3400



cm^{-1} ; HRMS (ESI) m/z : $[\text{M}+\text{Na}]^+$ Calcd for $\text{C}_{20}\text{H}_{28}\text{O}_5\text{Na}$, 371.19; found, 371.24. ^1H NMR (CDCl_3 , 400 MHz) δ ppm 0.65 (3 H, s), 1.08 (3H, s), 1.16- 1.39 (3 H, m), 1.60 – 1.72 (4 H, m), 1.87-1.98 (2 H, d, J =11.80 Hz), 2.28 - 2.35 (1 H, m), 3.24- 3.26 (1 H, d, J =2.65, 8.21 Hz), 3.80- 3.87 (1 H, dd, J =2.65, 8.21 Hz), 4.00- 4.06 (1 H, dd, J =1.89, 7.94 Hz), 4.12-4.18 (1 H, m, J =4.80, 7.45 Hz), 4.35- 4.43 (1 H, m, J =10.29, 6.27 Hz), 4.62 (1H, s, br), 4.81 (1H, s, br), 4.88- 4.91 (1 H, m), 5.07-5.10 (1 H, d, J = 4.08 Hz), 5.72- 576 (1 H, d, J = 6.06 Hz), 6.58- 6.62 (1 H, t, J =6.78 Hz); ^{13}C NMR (DMSO-d_6 , 100 MHz): δ ppm 14.81, 23.12, 24.03, 27.93, 36.55, 37.55, 38.64, 42.32, 54.41, 55.53, 62.71, 64.57 74.41, 78.50, 108.33, 129.01, 146.43, 147.65, 170.06, 215.12.

5B.5 Spectral

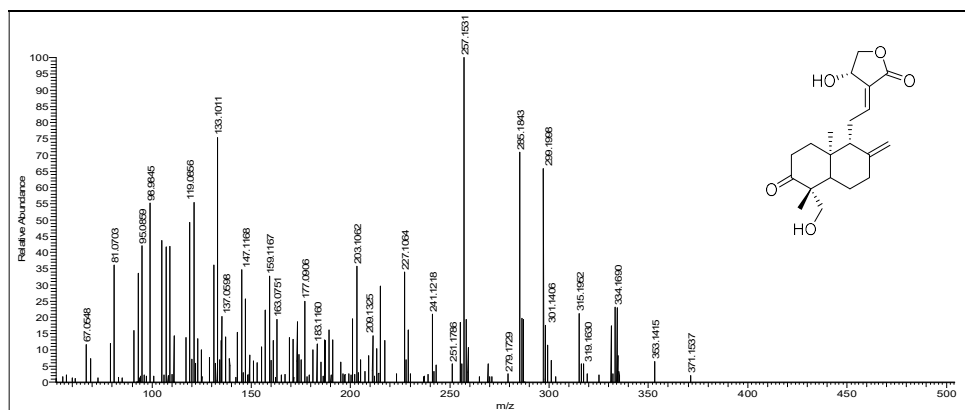
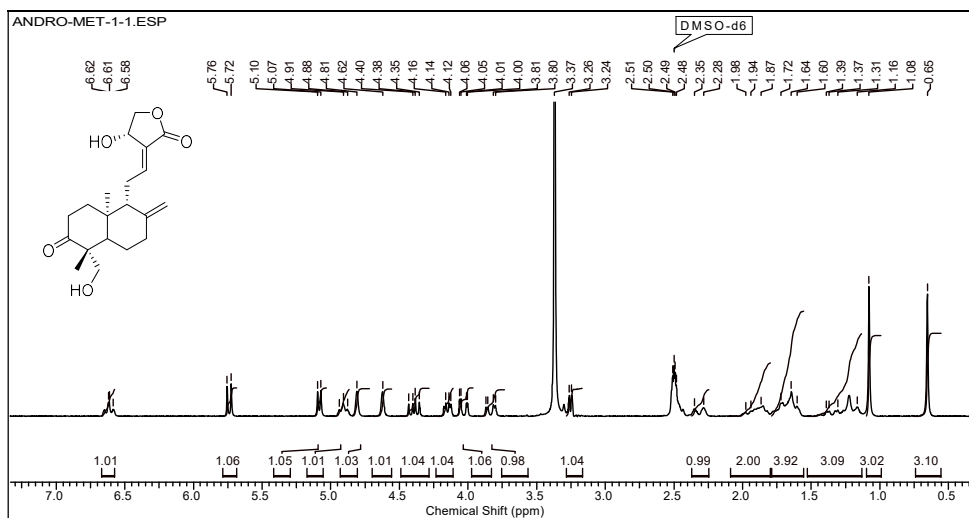
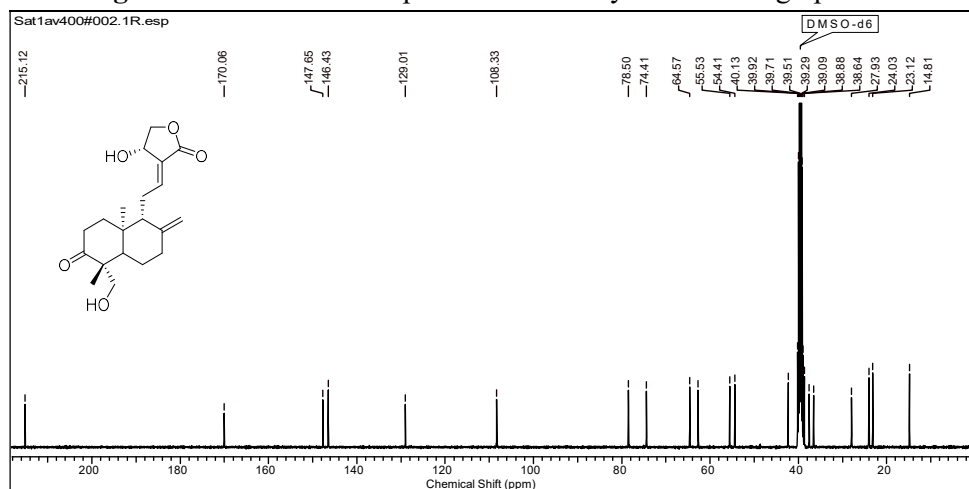


Figure 5B.2a. LC-ESI (+)-HRMS of 3-dehydro isoandrographolide

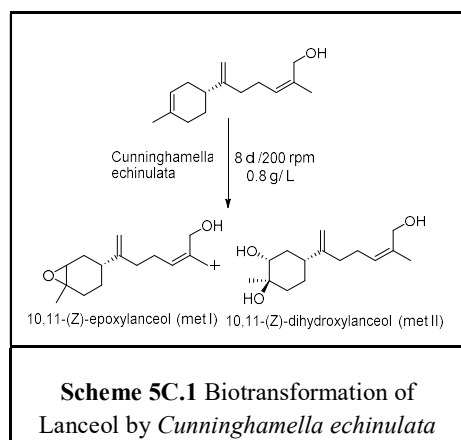
Figure 5B.2b. ¹H-NMR spectrum of 3-dehydro isoandrographolideFigure 5B.2c. ¹³C NMR spectrum of 3-dehydro isoandrographolide

Chapter 5: Section C

**Biotransformation of Lanceol by *Cunninghamella
echinulata***

5C.1 Introduction

Lanceol is monocyclic sesquiterpenoid alcohol isolated first time from the essential oil of *Santalum lanceolatum* wood.³² Lanceol was found in various Sandalwood oil (*Santalum album* L.) however it is a major component present in East African sandalwood oil *Osyris tenuifolia* along with other terpenoids.³³ *Osyris tenuifolia* is used traditionally for several health issues treatment such as adjusting of cracked bones and gynaecological disorder.^{34,35} Massai community used *Osyris tenuifolia* shoot extract is



used as an antipyretic agent for cattle. Lanceol purification from oil is critical due to the mixture of other compounds having similar physical properties, hence it has not explored more for bioactive.^{36,37} In our research group we have developed the purification of complex sandalwood oil mixture purification by using silver nitrate coated medium pressure liquid chromatography (MPLC) method.³⁷ Lanceol has

exhibited potent antimicrobial activity against the antibiotic-resistant strain of *Helicobacter pylori*.³⁵ An earlier report suggested that functional group introduction or modification on bioactive natural product skeleton enhanced the activity.^{24,38,39} Regio- and stereo-selective of bioactive molecules modification by chemical synthesis is difficult due to the several reaction steps, costlier reagent, hazardous chemicals, severe reaction conditions and most important yields of reaction.^{40,41} Biocatalysts are proven importance alternatives in the asymmetric catalysis; additionally, it has economically and green process at the mild condition.^{42,43,30} The remarkable antibacterial activity of lanceol inspired us to forms more potent bioactive analogue by using fungal biotransformation. Herein we describe the biotransformation of Lanceol using *Cunninghamella echinulata* produces two novel metabolites 10,11-(Z)-epoxylanceol and 10,11-(Z)-dihydroxylanceol. Antibacterial activities of lanceol along with these metabolites were studied.

5C. 2 Results and discussion

5C. 2.1 Screening and Time Course Experiment

Over five different species of filamentous fungal belong to genera *Pleurotus*, *Aspergillus*, *Mucor*, *Penicillium*, *Rhizopous* and *Cunninghamella* were screened to check their ability to carry out the useful transformation of lanceol. After five days of incubation fungal media was extracted in an organic solvent, then the crude extract obtained was concentrated and analysed by TLC, GC and GC-MS. Analysis results suggested that compared to all other fungal culture *Cunninghamella echinulata*

Table 5C.1 Screening of fungal culture for Lanceol biotransformation

Strain	Lanceol (%)	10,11-(Z)-epoxyl.	10,11-(Z)-dihydroxy.	Other met. (%)
<i>A. niger-589</i>	95.35	0	0	4.65
<i>C. echinulata</i>	6.62	25.16	70.02	6
<i>M. piriformis</i>	52.06	2.61	11.33	34
<i>R. oryzae</i>	59.35	2.88	12.86	22
<i>A.niger-582</i>	73.26	-	-	24
<i>G. fugikoroii</i>	28.96	2.75	31.29	37
<i>A.niger-612</i>	99.17	-	-	42
<i>P. Chrysogenum</i>	68.63	-	5.23	23
<i>M. plumbiosus</i>	39.5	7.5	-	53
<i>C. irregularis</i>	50.6	-	14.4	35

Substrate: Lanceol, *Incubation period:* 5 days,
Substrate concentration: 0.2 g /L

converted lanceol into its metabolites efficiently and quantitatively.

Biotransformation was confirmed by organism and substrate control experiment. GC-chromatogram of crude metabolite extract was overlapped on chromatogram of organism control extract observed that the metabolites were absent in organism control extract. In substrate control experiment no substrate degradation observed which concluded that the lanceol metabolites are biotransformed by the fungal system. Resting cell experiments confirm the fungal hydroxylase system might be involved in lanceol

oxidation; henceforth *C. echinulata* was selected for preparative scale. Time course experiment was performed in order to standardise the incubation period for optimum conversion of lanceol into its metabolites. Results suggested that *Cunninghamella*

echinulata quantitatively converted lanceol into two metabolites in eight days at concentration 0.8 g/L. In time course study it was observed that as the formation of the first metabolite concentration decrease after the second metabolite started forming suggesting that the metabolite-1 was being converted into the second metabolite.

5C.2.2 Preparative Scale Fermentation, Purification and Characterization

Lanceol large-scale fermentation was performed to get an ample amount of lanceol metabolites for characterization and antimicrobial activity studies. Substrate concentration experiment (0.1 g/L to 0.5 g/L) suggested that *C. echinulata* transformed lanceol quantitatively at 0.8 g/L, the rate of bioconversion decreases after this concentration may be due higher concentration is toxic to the fungus. Further 0.8 g/L of substrate concentration for 8 days were used for the preparative scale fermentation with

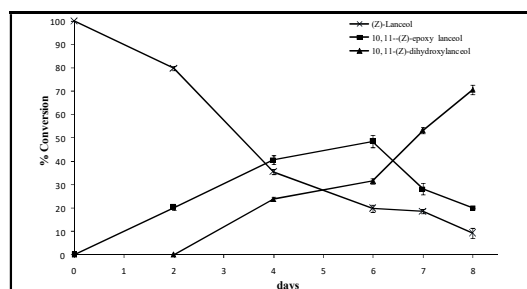


Figure 5C.1 Time course study of the biotransformation of (◆) (Z)-Lanceol (1) with *Cunninghamella echinulata*: (■) (Z)-10,11-(Z)-epoxylanceol (2); (▲) 10,11-(Z)-dihydroxylanceol (3).

1 g of lanceol. The primary analysis of the crude mixture by GC revealed >65 % conversion of lanceol into two metabolites (Figure 5A.1). The crude was purified over a silica gel column chromatography using ethyl acetate in pet ether gradient solvent system two pure metabolites. GC-MS analysis, for metabolites-1, showed mass $[M-H_2O]^+$ peak obtained in EI-MS at m/z

218.20 ($C_{15}H_{22}O$, calcd m/z 218.20), 16 amu higher than that of lanceol molecular weight, thus an insertion of an oxygen group on the skeleton was predicted. FTIR spectrum of metabolite-1 showed the presence of a new peak at 1036 cm^{-1} (C–O–C) indicated the presence of an ethereal linkage. The ^{13}C -NMR spectrum showed the conversion of two carbons of lanceol at δ 133.8 ppm and 120.7 ppm to a new peak in the metabolite NMR, resonating at δ 77.00 and 74.22 ppm, indicated carbon connected to oxygen. The 1H -NMR spectrum showed a proton at carbon (C-2) resonating at δ 5.25 (t, $J = 7.15\text{ Hz}$), shifted to δ 3.14 (t). All metabolites data analysis confirmed lanceol epoxidation at double bond on the ring at C-10 and C-11 position and metabolite were characterised as 10, 11-(Z)-epoxylanceol. Further column elution in a gradient of ethyl acetate/ pet ether (53 %) eluted fractions (289-330) contained second polar metabolite. The GC-MS analysis of the metabolite-2 showed mass $[M+3H_2O]$ at EI-MS m/z 200.20,

indicating a mass increase by 32 amu in lanceol predict the insertion of two oxygen molecule in the skeleton. FTIR spectrum of 10,11-(*Z*)-epoxylanceol showed the absence of a peak at 1036 cm^{-1} (C–O–C) suggested the epoxide ring cleavage. The ^{13}C -NMR spectrum showed the conversion of same two carbons at δ 133.8 ppm and 120.7 ppm of 10, 11-(*Z*)-epoxylanceol to a carbon in the metabolite, resonating at δ 77.00 and 74.22

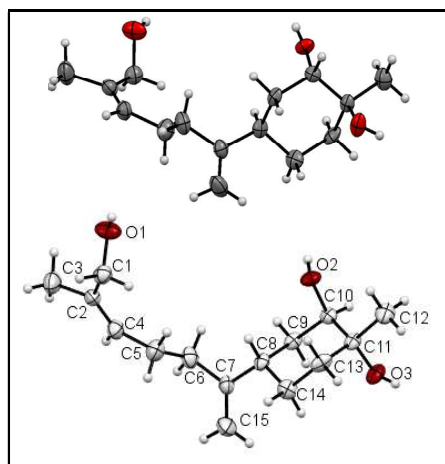


Figure 5C.2 Crystal structure ORTEP diagram of 10, 11-(*Z*)-dihydroxylanceol (ellipsoids are drawn at 50 %probability)

ppm these values suggested that both carbons attached to a hydroxyl group. The ^1H -NMR spectrum showed a proton of C-2 resonating at δ 5.25 (t, $J=7.15\text{ Hz}$), shifted to δ 3.14 (t, $J=3.12\text{ Hz}$), suggested the proton on such carbon, which was connected to the hydroxyl group. The analysis confirmed that the epoxide opens and formed diol, which was characterized as 10, 11-(*Z*)-dihydroxylanceol. The second solid metabolite was recrystallized by ethyl acetate in pet ether to obtained colourless needles. Single crystal X-ray diffraction data (Table 5A.3) was

recorded which further supported the stereochemistry of hydroxyl groups.

5C.2.3 Antimicrobial Activity

In order to study the effect of skeletal functionalization on antimicrobial activity of lanceol, we have screened them for the antimicrobial activity against gram positive, gram negative bacteria and yeast. Results suggested that the lanceol did not show any significant antimicrobial activity at a lower concentration, 10, 11-(*Z*)-epoxylanceol and 10, 11-(*Z*)-dihydroxylanceol displayed significant antimicrobial activity. 10,11-(*Z*)-dihydroxylanceol found more effective against *E.coli* ($16\text{ }\mu\text{g/mL}$) and *M. luteus* ($32\text{ }\mu\text{g/mL}$). However, 10,11-(*Z*)-epoxylanceol showed activity only against *C. albicans* ($32\text{ }\mu\text{g/mL}$). Enhancement of the antimicrobial activity of the lanceol metabolites might be due to the increase in bioavailability of the metabolites with the increase in polarity.

Table 5A.2 Antimicrobial MICs of the Lanceol and metabolites

Microorganism	Lanceol	10,11-(Z)- epoxy lanceol	10,11-(Z)- dihydroxy lanceol	G. sulphate ^d	B. sodium ^d
<i>M. luteus</i> (G ⁺)	>128	64	32	nd ^c	1
<i>S. aureus</i> (G ⁺)	>128	>128	64	0.5	2
<i>E. coli</i> (G ⁻)	64	>128	16	1	4
<i>C. albicans</i>	>128	32	64	0.5	nd ^c

^a The calculated average MIC values are presented. ^b MIC > 128 µg/ml was considered as inactive. ^cnd : not determine. ^dPositive control.

5C.4 Conclusion

(Z)-lanceol was oxidized regio- and stereo-selectively into two novel metabolites. Metabolites were identified and characterized as 10, 11-(Z)-epoxy lanceol, 10, 11-dihydroxy lanceol. Both the metabolites are more potent antimicrobial agent compared to (Z)-lanceol. This fungal culture seems to be useful for stereo-selective epoxidation and hydroxylation of similar skeleton compounds and metabolites will test for various bioactivities.

5C.5 Experimental Section

5C.5.1 Material and Methods

Lanceol was isolated from African sandalwood oil (*Osyris tenuifolia*). Media ingredients were purchased from HiMedia Laboratories, Mumbai, India. These test microorganisms were obtained from collected from National Collection of Industrial Microorganism (NCIM) Pune. Antimicrobial activities were assessed using Gram-positive bacteria *Cunninghamella echinulata* (NCIM 691), *Staphylococcus aureus* (NCIM 2100), *M. luteus* (NCIM 2170), Gram-negative bacteria *E.coli* (NCIM 2575), *Pseudomonas fluorescens* and yeast *Candida albicans* (NCIM 3471). Column chromatography performed on silica gel (230-400 mesh). Migration of the compounds on TLC was visualised by spraying it with a solution of 3.2 % anisaldehyde, 2.8 % H₂SO₄, 2 % acetic acid in ethanol followed by heating for 1-2 min. GC analyses were carried out using Agilent 7890 GC system equipped with a hydrogen flame ionization

detector (FID) and HP-5 capillary column (30 m × 0.32 mm × 0.25 μm, J & W Scientific). Nitrogen was used as carrier gas at a flow rate of 1 mL/min. The column temperature was increased from 70 °C to 140 °C at 2 °C min⁻¹ and held constant for 10 min at 140 °C, then raised to a temperature of 160 °C at 2 °C min⁻¹ and finally to a temperature of 200 °C with a 10 °C min⁻¹ rise and maintained for 10 min at 200 °C. The injector and detector temperatures were maintained at 230 °C and operated in split mode (1:8). Mass spectra were recorded using EI-technique on Agilent 5975C mass selective detector interfaced with a 7890A gas chromatograph and HP-5 (30 m × 0.32 mm × 0.25 μm) column with a flow of helium at the rate of 1 mL/min. NMR (¹H, ¹³C, DEPT) spectra were recorded on Varian INOVA spectrometer (400, 500 MHz) and chemical shift values were reported in ppm concerning the residual solvent or Tetramethylsilane (TMS) signals as the reference. HRMS data were collected on Thermo Scientific Q-Exactive Quadrupole-Orbitrap Mass Spectrometer. IR spectra were recorded on Perkin Elmer FT-IR spectrophotometer in CHCl₃ and optical rotations were determined in the same solvent on JASCO (P-2000), polarimeter using 10 mm cell (*c* in g/100 mL unit). Confirmation of hydroxyl position by compared with the chemical shifts of lanceol and stereochemistry confirmed by the crystal structure. A single crystal of compound dihydroxy metabolites was obtained during purification and metabolite 3 was grown from a mixture of ethyl acetate: pet ether as a colourless needle suitable for structural analysis. X-ray intensity data were collected on a Bruker SMART APEX CCD diffractometer at room temperature. All the data were corrected for Lorentzian, polarisation and absorption effects using Bruker's SAINT and SADABS programs. SHELX-9722 was used for structure solution and full matrix least-squares refinement on F2. Hydrogen atoms were included in the refinement as per the riding model.

5C.5.2 General Biotransformation Procedure

(a) Screening of Fungal Cultures

The sporulated fungal cultures were grown on PDA slant was transfer to Erlenmeyer flasks containing 50 mL of sterile modified *Czapek-Dox* media and incubate it at 30 °C at 220 rpm in incubator shaker for 36 h. To the well grown fungal culture flasks, a (*Z*)-lanceol was added at a concentration of 10 mg in 0.2 mL acetone/ 50 mL media and incubation was continued. After 5 days incubation period broth was extracted separately

with ethyl acetate (three times) and organic layers were separated and combined together further dried over anhydrous Na₂SO₄, concentrated and analyzed by TLC, GC and GC-MS. All the screening experiments were analyzed by comparing with corresponding substrate control and organism control.

(b) Time Course Experiment

(Z)-Lanceol (0.8 g/L) was added to well-grown cultures in 50 mL × 5 Erlenmeyer flasks and incubated on a rotary shaker as mentioned above. Each flask was extracted with dichloromethane (CH₂Cl₂) after every 24 h and analyzed by GC and GC-MS for monitoring the level of formation of each metabolites.

(c) Substrate Concentration Experiment

Once the duration of biotransformation was known, various concentrations (0.1 g/L to 0.5 g/L) the individual substrates were added in the 50 mL well-grown culture in standardised biotransformation conditions to check the maximum concentration that can be completely biotransformed.

(d) Resting Cell Experiment

Well-grown culture of *Cunninghamella echinulata* (36 h) was filtered and the mycelia obtained were washed with distilled water and phosphate buffer (pH 7.2). The mycelia were dried by pressing between the filter papers. 2 g of mycelia (wet weight) was weighed and added into 50 mL of phosphate buffer of pH 7.2 with 100 mg dextrose. 10 mg of lanceol in 0.2 mL acetone was added to the reaction mixture and incubated at 30 °C on a rotary shaker (180 rpm) for 36 h. After this incubation period, filtered mycelia and broth extracted with ethyl acetate (10 mL × 2) and analysed by TLC, GC, and GC-MS.

(e) Preparative Scale Fermentation

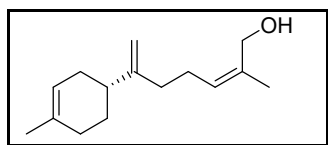
Large scale fermentation was carried out in a modified *Czapek-Dox* medium. The pH of the medium was adjusted to 5.8 with 1M K₂HPO₄. Erlenmeyer flasks (1000 mL × 20) containing 100 mL of sterile medium were inoculated with 2 mL of spore suspension from well culture grown on potato dextrose agar slants and incubated at 29-30 °C on a rotary shaker at 180 rpm for 24 h. 80 mg in acetone 0.2 mL/ 100 mL media was added to each flask and the incubation was continued for an additional period of 8 days.

Control experiments were also run with the substrate but without microorganism and with microorganism but without substrate. After this incubation period, the contents of the flasks were pooled and filtered through a muslin cloth to separate mycelia and broth. The broth was then saturated with sodium chloride and extracted with ethyl acetate (four times, 1:1 v/v). The dried mycelia were washed with ethyl acetate. The two extracts found to be the same by GC and TLC analyses and therefore pooled. The crude extract (1.4 g) obtained was subjected to silica gel (230-400 mesh) column chromatography and the metabolites were eluted using a gradient of ethyl acetate in petroleum ether (95:5 to 50:50). Pure metabolites were obtained after successive silica gel column chromatographic purification.

(f) Characterization of Metabolites

NMR ($^1\text{H-NMR}$, $^{13}\text{C-NMR}$, DEPT) spectra were recorded and chemical shift values were reported in ppm with respect to the residual solvent or TMS signals as the reference. HRMS data were collected on GC-HR-ESI-MS Thermo Scientific Q Exactive Quadrupole-Orbitrap Mass Spectrometer. FTIR spectra were recorded on Perkin Elmer FT-IR spectrophotometer in CHCl_3 and optical rotations were determined in the same solvent on JASCO (P-2000), polarimeter using 10 mm cell (c in g/100 ml unit).

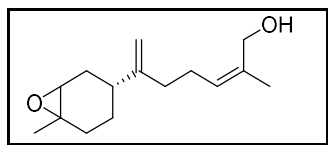
Lanceol: Colourless liquid; m.p. 31.5- 32.7 °C; IR (CHCl_3) ν_{max} = 904, 1640, 1675,



2920, 3435 cm^{-1} ; $^1\text{H NMR}$ (CHCl_3 , 400 MHz): δ ppm 1.53 (2 H, br. s.), 1.66 (3 H, s), 1.80 (4 H, s), 1.98 (2 H, br. s.), 2.05 - 2.08 (2 H, m), 2.10 (2 H, br. s.), 2.17 - 2.25 (2 H, m),

4.13 (2 H, s), 4.73 (1 H, s), 4.79 (1 H, s), 5.31 (1 H, s), 5.41 (1 H, br. s.); $^{13}\text{C NMR}$ (CDCl_3 , 100 MHz): δ ppm 21.2, 23.4, 26.3, 28.2, 30.7, 31.3, 35.0, 39.7, 61.5, 107.5, 120.6, 128.1, 133.7, 134.5, 153.9.02

Lanceol-10,11-epoxide



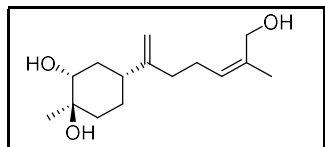
Colourless liquid; m.p. 37.1- 38.2 °C; IR (CHCl_3 , cm^{-1}) ν_{max} = 1140, 1640, 1675, 2920, 3400 cm^{-1} ; $^1\text{H NMR}$ (CHCl_3 , 400 MHz): δ ppm 1.45-1.48

(2 H, s), 1.61 (4 H, m), 1.75-1.79 (5 H, m), 1.82-1.89 (2 H, m), 2.01-2.05 (4 H, m), 2.13 - 2.18 (2 H, m), 4.08 (2 H, s), 4.68 (1 H, s), 4.74 (1 H, s), 5.36 (1 H, br. s.) ;

^{13}C NMR (CDCl_3 , 100 MHz): ppm 14.1, 21.0, 21.2, 26.2, 26.7, 33.8, 34.2, 35.4, 60.4, 61.5, 74.0, 108.3, 128.1, 134.3, 152.9.

Lanceol-10,11-diol

White crystalline solid; m.p. 55.4-56.1°C; $[\alpha]_{\text{D}}^{20}$: +13.23 (2.34, CHCl_3); IR (CHCl_3 , cm^{-1}) ν_{max} = 1622, 1667, 2960, 3375, 3450 cm^{-1} ; ^1H NMR (CHCl_3 , 400 MHz): δ ppm 1.26-



1.34 (5H, m), 1.46 - 1.52 (2H, m), 1.77 - 1.79 (4H, m), 2.05-2.10 (5H, m), 2.12 - 2.17 (2H, m), 2.22 - 2.29 (2H, m), 3.52 - 3.63 (1H, m), 4.1 (1H, br. s.), 4.7 (1H, s), 4.8 (1H, s), 5.27 - 5.30 (1H, m), 7.26 (1H, s); ^{13}C NMR (CHCl_3 , 100 MHz): δ ppm 19.8, 25.4, 25.7, 25.9, 32.6, 33.5, 34.2, 35.2, 59.6, 69.8, 72.5, 106.5, 126.7, 133.6, 153.0.

5A.5.3 Anti-bacterial Activity

Anti-bacterial activity of lanceol and metabolites were tested against gram positive and gram negative bacteria and yeast. The anti-bacterial activity carried out in a 96-well microtitre plate using the broth microdilution method.^{44,16} The activity was carried out in a total volume of 100 μL as follows: ten serial 2-fold dilutions of MHB media containing lanceol, 10,11-(*Z*)-epoxylanceol and 10,11-(*Z*)-dihydroxylanceol (prepared from a stock solution of 2.56 mg/mL of metabolite in MHB) was carried out to obtain a concentration range of 10-128 $\mu\text{g}/\text{mL}$, in a sterile 96-well plate to a volume of 50 μL in each. The final volume was adjusted to 100 μL by adding an aliquot of 50 μL bacterial suspensions (4×10^5 cfu/ mL) to obtain a final concentration of compounds range 128-0.25 $\mu\text{g}/\text{mL}$ and final bacterial concentration of 2×10^5 cfu/mL. Growth controls and sterility controls were maintained alongside. The plate was incubated at 37 °C for 20 h. The experiment was conducted in triplicates. Bacterial growth was determined by visualization. Anti-bacterial activities expressed as the MIC, the concentration at which no growth observed after 20 h of incubation.

Table. 5A.3 Crystal structure data of 10, 11-(Z)-dihydroxylanceol.

- Bond precision: C-C = 0.0047 Å Wavelength = 0.71073
- Cell: a = 6.4871 (5) b = 10.3035 (6) c = 21.9742 (17)
- Alpha = 90 beta = 94.897(6) gamma = 90
- Temperature: 296 K

	Calculated	Reported
Volume	1468.75(18)	1468.75(18)
Space group	P 21 21 21	P2(1)2(1)2(
Hall group	P 2ac 2ab	-
Moiety formula	C ₁₅ H ₂₆ O ₃	C ₁₅ H ₂₆ O ₃
Sum formula	C ₁₅ H ₂₆ O ₃	C ₁₅ H ₂₆ O ₃
Mr	254.36	254.36
Mu (mm ⁻¹)	0.078	0.078
F000	560.0	560.0
F000'	560.26	
h,k,lmax	7,12,26	7,12,26
Nref	2591[1526]	2591
Tmin,Tmax	0.981,0.988	0.975,0.988
Dx,g cm ⁻³	1.150	1.150
Z	4	4
Tmin'	0.965	

Correction method = # Reported T Limits: Tmin=0.975 Tmax=0.988

- AbsCorr = MULTI-SCAN
- Data completeness= 1.68/0.99 Theta(max)= 25.000
R(reflections)= 0.0687(2238) wR2(reflections)= 0.1236(2560); S = 1.204 Npar= 168

5A.5 Spectral Copies

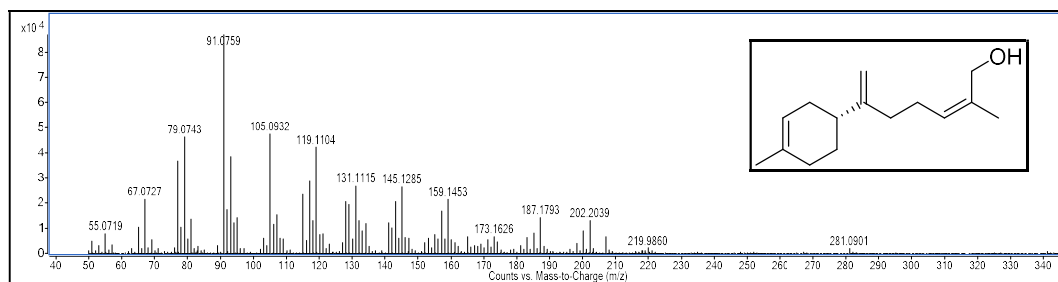
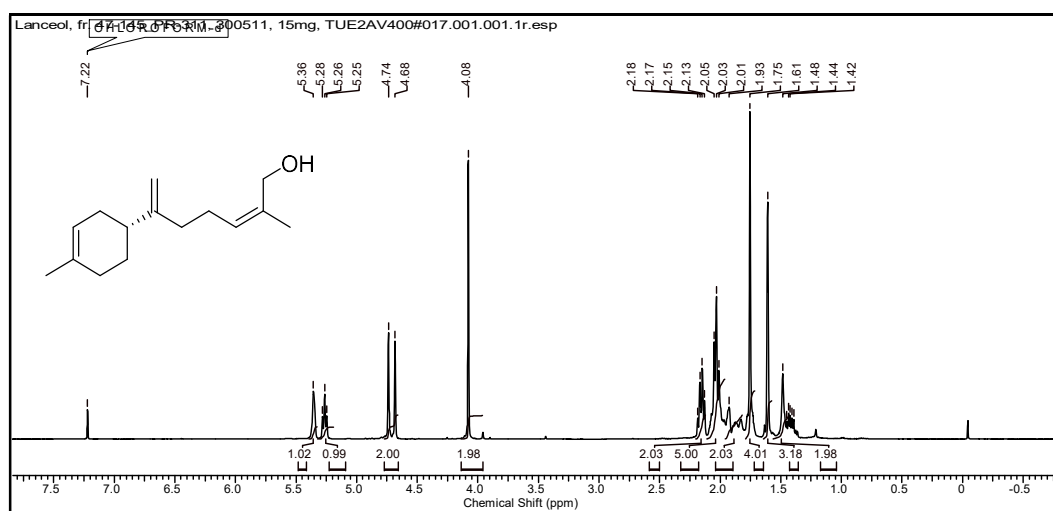
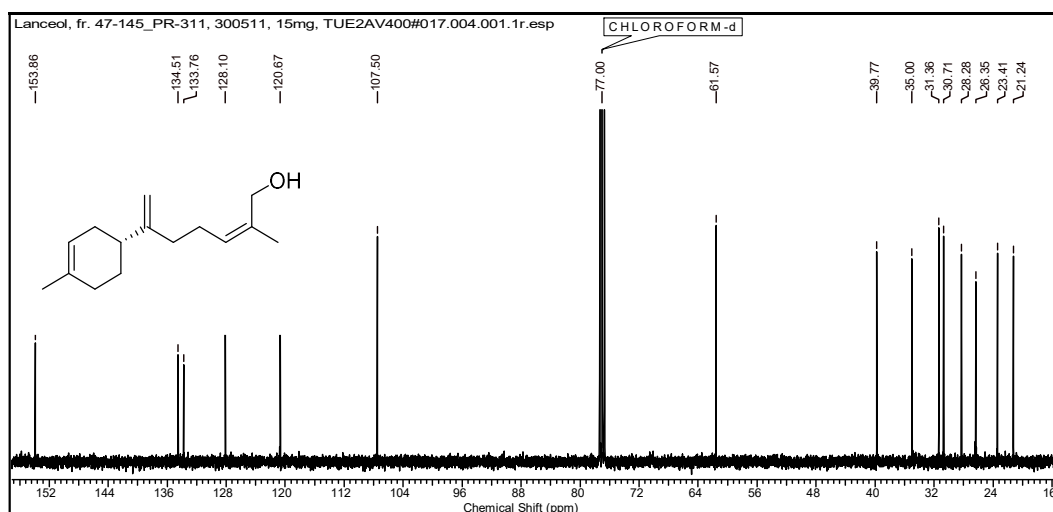


Figure 5C.3a. GC-EI-QToF-MS spectrum of lanceol

Figure 5C.3b. ^1H NMR spectrum of Lanceol in CDCl_3 Figure 5C.3c. ^{13}C NMR spectrum of lanceol in CDCl_3

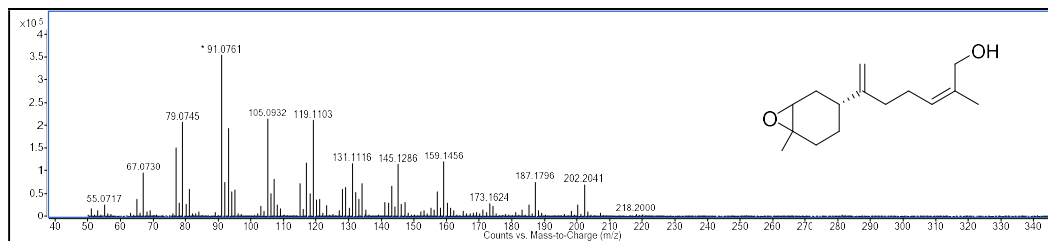
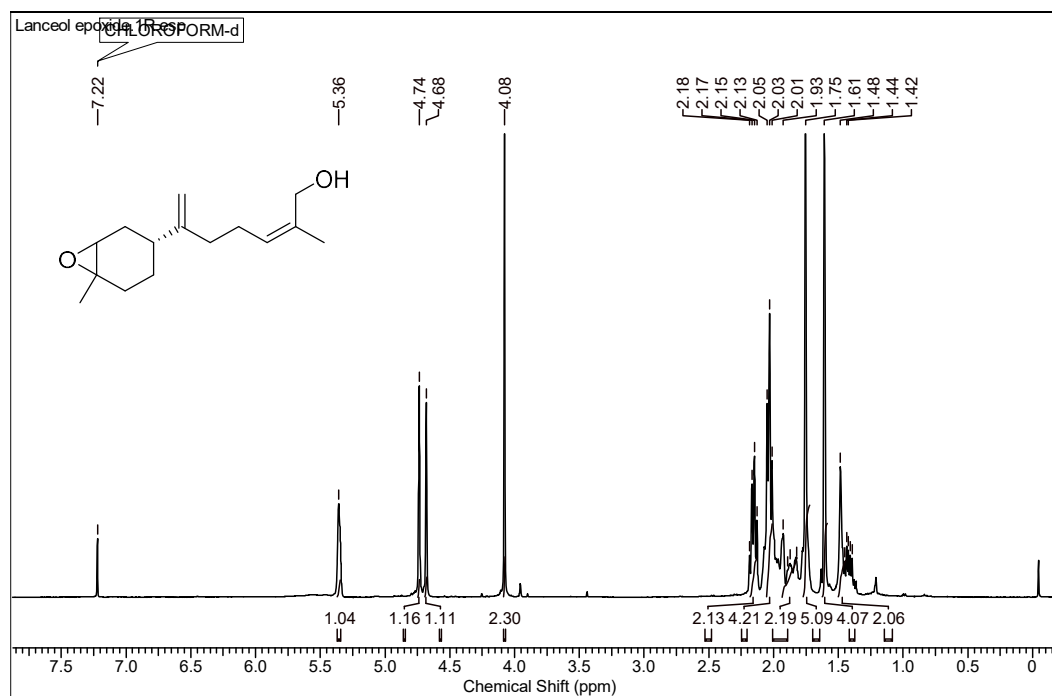
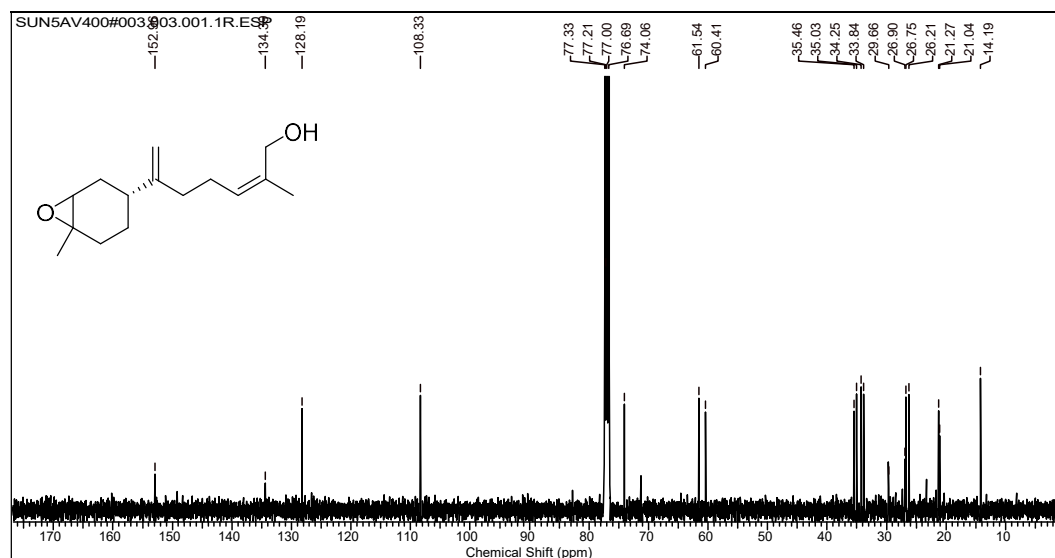


Figure 5C.4a. GC-EI-QToF-MS spectrum of lanceol epoxide

Figure 5C.4b. ^1H NMR spectrum of lanceol epoxide in CDCl_3 Figure 5C.4c. ^{13}C NMR spectrum of lanceolepoxide in CDCl_3

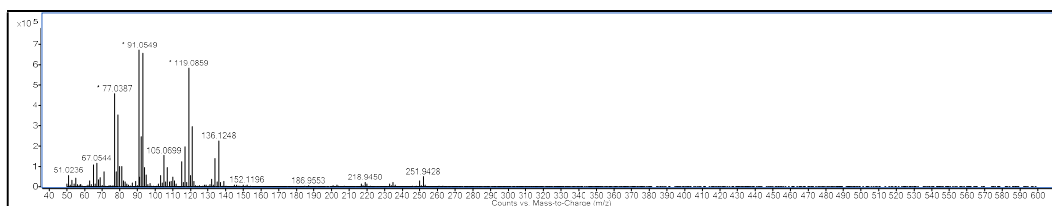
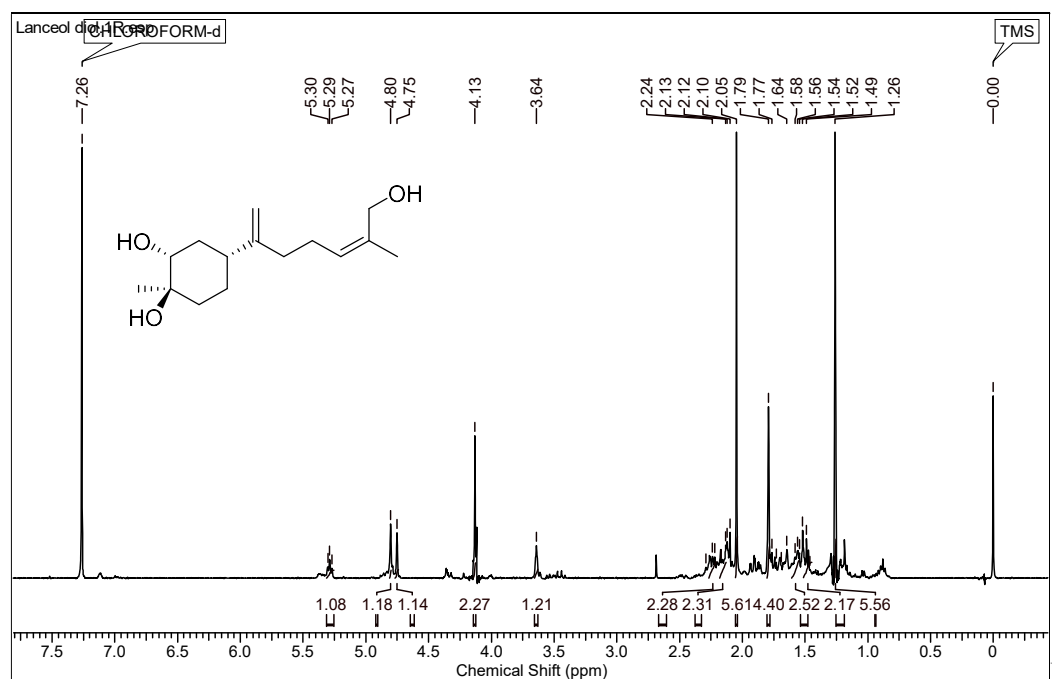
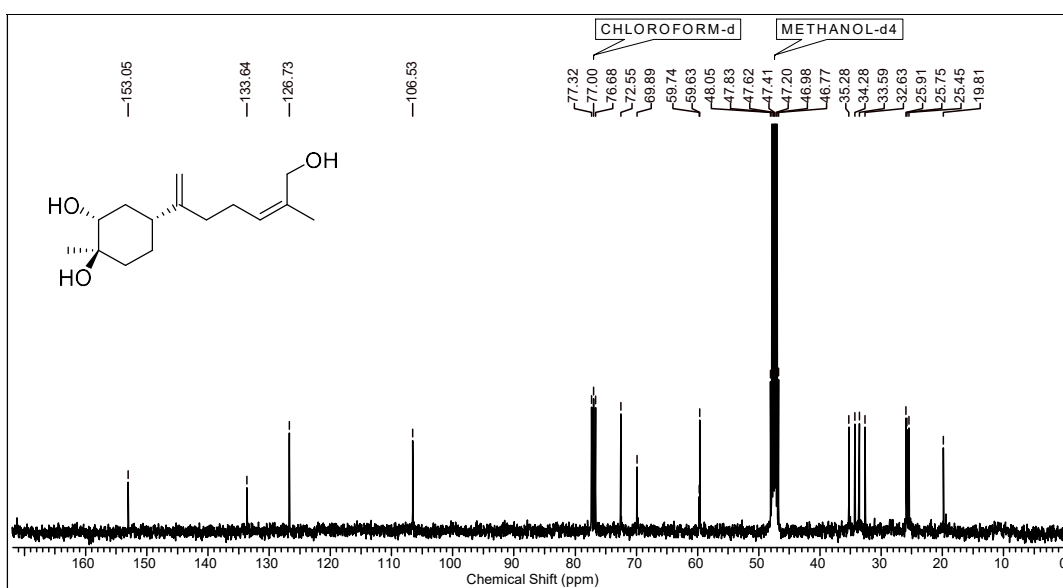


Figure 5C.5a. GC-EI-QToF-MS spectrum of lanceol diol

Figure 5C.5b. ^1H NMR spectrum of Lanceoldiol in CDCl_3 Figure 5C.5c. ^{13}C NMR spectrum of Lanceoldiol in CDCl_3

5D References

- 1 J. Rohloff, *J. Agric. Food Chem.*, 1999, **47**, 3782–3786.
- 2 R. Jaeger and E. Cuny, *Nat. Prod. Commun.*, 2016, **11**, 1373–1390.
- 3 G. P. P. Kamatou, I. Vermaak, A. M. Viljoen and B. M. Lawrence, *Phytochemistry*, 2013, **96**, 15–25.
- 4 D. N. Willis, B. Liu, M. A. Ha, S.-E. Jordt and J. B. Morris, *Faseb J.*, 2011, **25**, 4434–44.
- 5 K. Ahijevych and B. E. Garrett, *Nicotine Tob. Res.*, 2004, **6**, 17–28.
- 6 J. A. Farco and O. Grundmann, *Mini Rev. Med. Chem.*, 2013, **1**, 124–131.
- 7 J. W. Lee, J. Y. Lu, P. S. Low and P. L. Fuchs, *Bioorganic Med. Chem.*, 2002, **7**, 2397–414.
- 8 H. Khanam and Shamsuzzaman, *Eur. J. Med. Chem.*, 2015.
- 9 P. Thirumurugan, D. Matosiuk and K. Jozwiak, *Chem. Rev.*, 2013, **113**, 4905–4979.
- 10 I. Antonopoulou, S. Varriale, E. Topakas, U. Rova, P. Christakopoulos and V. Faraco, *Appl. Microbiol. Biotechnol.*, 2016, **100**, 6519–6543.
- 11 P. M. Wright, I. B. Seiple and A. G. Myers, *Angew. Chemie - Int. Ed.*, 2014, **34**, 8840–69.
- 12 L. Caputi, M. Rejzek, T. Louveau, E. C. O'Neill, L. Hill, A. Osbourn and R. A. Field, *Bioorganic Med. Chem.*, 2013, **21**, 4762–4767.
- 13 H. Hamada, Y. Miyamoto, N. Nakajima and T. Furuya, *J. Mol. Catal. - B Enzym.*, 1998, **5**, 187–189.
- 14 Y. Ghasemi, A. Mohagheghzadeh, Z. Ostovan, M. Moshavash, S. Rasoul-Amini and M. H. Morowvat, *Chem. Nat. Compd.*, 2010, **46**, 734–737.
- 15 J. Aleu, R. Hernández-Galán and I. G. Collado, *J. Mol. Catal. - B Enzym.*, 2002, **16**, 249–253.
- 16 H. S. Patil, D. D. Jadhav, A. Paul, F. A. Mulani, S. J. Karegaonkar and H. V. Thulasiram, *Bioorganic Med. Chem. Lett.*, 2018, **28**, 1332–1337.
- 17 S. S. Shankar, S. N. Benke, N. Nagendra, P. L. Srivastava, H. V. Thulasiram and H. N. Gopi, *J. Med. Chem.*, 2013, **56**, 8468–8474.
- 18 O. Sareer, S. Ahmad and S. Umar, *Nat. Prod. Res.*, 2014, **28**, 2081–2101.
- 19 Shirisha K and Mastan M, *Pharmacophore*, 2013, **4**, 212.
- 20 W. W. Chao, Y. H. Kuo and B. I. F. Lin, *J. Agric. Food Chem.*, 2010, **58**, 2505–2512.
- 21 A. Pawar, S. Rajalakshmi, P. Mehta, K. Shaikh and C. Bothiraja, *RSC Adv.*, 2016, **6**, 69282–69300.
- 22 S. Kumar, H. S. Patil, P. Sharma, D. Kumar, S. Dasari, V. G. Puranik, H. V. Thulasiram and G. C. Kundu, *Curr. Mol. Med.*, 2012, **12**, 952–966.
- 23 D. Chen, Y. Song, Y. Lu and X. Xue, *Bioorg. Med. Chem. Lett.*, 2013, **23**, 3166–3169.
- 24 H. W. Xu, G. Z. Liu, G. F. Dai, C. L. Wu and H. M. Liu, *Drug Discov. Ther.*, 2007, **1**, 73–7.
- 25 S. Giridhar, S. Kandanur, N. Rao and S. Nanduri, *Bioorg. Med. Chem. Lett.*, 2015, **25**, 5781–5786.
- 26 J. B. Atkhuu, K. H. Attori, F. T. Akano, S. F. Ushiya and K. O. Shiman, 2002, **25**, 1169–1174.
- 27 H. Xu, P. Jiang, W. Li, J. Wang and H. Liu, *Chinese J. Chem.*, 2011, **29**, 2114–2118.
- 28 M. Miyazawa, H. Kawazoe and M. Hyakumachi, *J. Chem. Technol. Biotechnol.*, 2003, **78**, 620–625.

-
- 29 P. Domínguez De María, C. Carboni-Oerlemans, B. Tuin, G. Bargeman, A. Van Der Meer and R. Van Gemert, *J. Mol. Catal. B Enzym.*, 2005, **37**, 36–46.
- 30 D. Sa, B. J. Zhang, C. Y. Wang, Y. Tian, J. H. Yao, L. An, S. S. Huang, J. Y. Peng, K. X. Liu and X. C. Ma, *Bioorganic Med. Chem. Lett.*, 2012, **22**, 1615–1618.
- 31 X. He, X. Zeng, H. Hu and Y. Wu, *J. Mol. Catal. B Enzym.*, 2010, **62**, 242–247.
- 32 A. E. Bradfield, E. M. Francis, A. R. Penfold and J. L. Simonsen, *J. Chem. Soc.*, 1936, **1**, 1619–1625.
- 33 A. T. Kreipl and W. A. König, *Phytochemistry*, 2004, **65**, 2045–2049.
- 34 H. S. Roh, J. Kim, E. S. Shin, D. W. Lee, H. Y. Choo and C. G. Park, *J. Pest Sci. (2004)*, 2015, **88**, 621–627.
- 35 T. Ochi, H. Shibata, T. Higuti, K. H. Kodama, T. Kusumi and Y. Takaishi, *J. Nat. Prod.*, 2005, **68**, 819–824.
- 36 P. P. Daramwar, P. L. Srivastava, S. P. Kolet and H. V. Thulasiram, *Org. Biomol. Chem.*, 2014, **12**, 1048–1051.
- 37 P. P. Daramwar, P. L. Srivastava, B. Priyadarshini and H. V. Thulasiram, *Analyst*, 2012, **137**, 4564–4570.
- 38 R. Batista, J. L. Humberto, E. Chiari and A. B. de Oliveira, *Bioorganic Med. Chem.*, 2007, **15**, 381–391.
- 39 R. M. da Costa, J. K. Bastos, M. C. A. Costa, M. M. C. Ferreira, C. S. Mizuno, G. F. Caramori, G. R. Nagurniak, M. R. Simão, R. A. dos Santos, R. C. S. Veneziani, S. R. Ambrósio and R. L. T. Parreira, *Phytochemistry*, 2018, **156**, 214–223.
- 40 H. J. Hocker, K. Cho, C. K. Chen, N. Rambahal and S. Rao, *Proc. Natl. Acad. Sci. U. S. A.*, 2013, **110**, 10201–10206.
- 41 H. S. Vieira, J. A. Takahashi, A. B. De Oliveira, E. Chiari and M. A. D. Boaventura, *J. Braz. Chem. Soc.*, 2002, **13**, 151–157.
- 42 S. Haldar, S. P. Kolet, D. S. Dandekar, B. S. Kale, R. G. Gonnade and H. V. Thulasiram, *RSC Adv.*, 2014, **4**, 27661–27664.
- 43 A. F. Barrero, J. E. Oltra, E. Cerdá-Olmedo, J. Ávalos and J. Justicia, *J. Nat. Prod.*, 2001, **64**, 222–225.
- 44 S. Pattnaik, V. R. Subramanyam, M. Bapaji and C. R. Kole, *Microbios*, 1997, **89**, 39–46.

Erratum

Erratum

Erratum